An Investigation into the Use of Bamboo as Reinforcement in Concrete

Abdullah Moh'd Abdullah Khatib

Department of Geography and Environmental Management
University of the West of England

A thesis submitted in partial fulfilment of the requirements for the degree of Doctor of Philosophy at the University of the West of England

May
2020

Abstract

The behaviour of bamboo reinforced concrete is not well understood and the methods proposed for its design suffers from problems that can result in an overly conservative design in some situations and unconservative designs in others. This investigation was carried using a combination of experimental testing and finite element modelling. It included flexural testing of bamboo reinforced beams and pull-out testing of bamboo splints. This research contributes to a limit state design method for bamboo reinforced concrete. It includes modelling bond, deflection, and cracking and it investigates how to model the flexural and shear capacities of bamboo reinforced concrete. In addition, this research investigates the credentials of bamboo as a low carbon footprint reinforcement of concrete.

Corrugation is presented as a solution for the bamboo weak bond with concrete. A model is developed that can estimate the bond of corrugated bamboo at short embedment lengths based on the shear strength of bamboo and the shear-friction of concrete. A model is developed that can estimate the bond of bamboo at any embedment length using the modulus of elasticity and reinforcement area as inputs. A deflection model is presented that takes into account the effect of low modulus of elasticity of bamboo reinforcement and its weaker bond with concrete in comparison with steel. The cracking of bamboo reinforced concrete is analysed and the results are used to validate established cracking models. Equivalent serviceability to up to 1% steel-reinforced concrete can be achieved using corrugated bundled bamboo reinforcement. At higher reinforcement percentage the use of bamboo becomes less practical due to the limitation of section workability.

Declaration of Originality

The candidate confirms that the work presented in this thesis is his own and was undertaken over the course of his PhD course at The University of the West of England. None of the work presented in this thesis has been submitted for another degree or qualification at any institute of education. A list of references is included to acknowledge and credit the work and information derived from the published work of others.

Abdullah Khatib

Table of Contents

ABSTRACT I

DECLARATION OF ORIGINALITY II

TABLE OF FIGURES VII

TABLE OF TABLES XI

NOTATION XII

1. INTRODUCTION 1

1.1 BACKGROUND 1

1.2 INTRODUCTION TO THE CURRENT RESEARCH 4

1.3 RESEARCH QUESTIONS 6

1.4 LIST OF PUBLICATIONS 7

1.5 THESIS STRUCTURE 7

2. LITERATURE REVIEW ON BAMBOO USE AS REINFORCEMENT IN CONCRETE 9

2.1 THE MECHANICAL BEHAVIOUR OF BAMBOO 9

2.1.1 Natural bamboo 10

2.1.2 Engineered bamboo 13

2.2 BAMBOO BOND TO CONCRETE 16

2.3 THE FLEXURAL CAPACITY OF BAMBOO REINFORCED CONCRETE 21

2.4 MODELLING FLEXURAL CAPACITY OF BAMBOO REINFORCED CONCRETE 24

2.5 MODELLING OF INDETERMINATE STRUCTURES 26

2.6 SHEAR STRENGTH OF BAMBOO REINFORCED CONCRETE ELEMENTS 28

2.7 SERVICEABILITY OF BAMBOO REINFORCED CONCRETE 29

2.8 CREEP BEHAVIOUR OF BAMBOO 30

2.9 DURABILITY OF BAMBOO 33

2.10 SUMMARY 37

3. METHODOLOGY 39

3.1 INTRODUCTION 39

3.2 GAPS IN THE LITERATURE THAT THIS RESEARCH FILLS AND THE METHODOLOGY STRUCTURE 39

3.3 BOND TESTING 42

3.3.1 Determination of sample size 43

3.3.2 The theoretical models for the bamboo bond at short and long embedment lengths 47

3.4 FLEXURAL TESTING OF BAMBOO REINFORCED BEAMS 49
3.5 STATISTICAL ANALYSIS 50
3.5.1 Analysis of Variance (ANOVA) *50*
3.5.2 Linear regression analysis *51*
3.5.3 Mixed linear models *53*
3.6 FE MODELLING OF BAMBOO REINFORCED CONCRETE 55
4. REVIEW OF REINFORCED CONCRETE FINITE ELEMENT MODELLING 58
4.1 INTRODUCTION 58
4.2 CONSTITUTIVE MODELS AND CHOOSING THE FE ELEMENTS 58
4.2.1 Linearity and Nonlinearity *61*
4.2.2 Nonlinear elastic, plastic, and the damage plasticity constitutive models *62*
4.3 CRACKING BEHAVIOUR OF CONCRETE 64
4.3.1 Discrete crack approach *65*
4.3.2 Smeared crack approach *65*
4.4 MODELLING THE BOND IN FE 70
4.5 SOLUTION METHODS AND CONVERGENCE 72
4.5.1 Newton-Raphson method *72*
4.5.2 Arc-length method *73*
4.5.3 Dynamic procedures *74*
4.6 THE PROPOSED FE MODEL FOR BAMBOO REINFORCED CONCRETE 75
4.6.1 The constitutive model used in the current research *75*
4.6.2 Mesh size in the current research *76*
4.6.3 Tensile strength and fracture energy *77*
4.6.4 Solution procedure *77*
4.7 DISCUSSION AND LIMITATIONS 78
5. BOND OF BAMBOO EMBEDDED INSIDE CONCRETE 79
5.1 INTRODUCTION 79
5.2 MATERIALS AND TESTING METHOD 80
5.3 RESULTS 81
5.4 STATISTICAL ANALYSIS 84
5.4.1 The two-way ANOVA analysis *84*

5.4.2 Linear regression of the bond results *85*

5.5 THEORETICAL MODELLING OF THE CORRUGATED BAMBOO BOND AT SHORT EMBEDMENT 90

5.6 STIFFNESS OF BOND AND THE BOND-SLIP MODEL 93

5.7 THEORETICAL BOND MODEL FOR BAMBOO IN UN-CRACKED CONCRETE AT HIGH EMBEDMENT LENGTH 96

5.8 VALIDATION OF THE THEORETICAL BOND MODEL FOR BAMBOO IN UN-CRACKED CONCRETE AT HIGH EMBEDMENT LENGTH 99

5.9 DISCUSSION 100

5.9.1 Discussion of the bond of corrugated bamboo *101*

5.9.2 Discussion of the bamboo bond at long embedment *102*

5.10 CONCLUSIONS 103

6. FLEXURAL BEHAVIOUR OF BAMBOO REINFORCED CONCRETE BEAMS 104

6.1 INTRODUCTION 104

6.2 REVIEW OF THE BENDING CAPACITY DESIGN METHOD FOR STEEL AND FRP REINFORCED CONCRETE 104

6.3 CONCRETE SHEAR STRENGTH IN BAMBOO REINFORCED CONCRETE 108

6.4 MATERIALS AND FLEXURAL TESTING ARRANGEMENT 110

6.5 RESULTS OF THE FLEXURAL TESTING OF BAMBOO REINFORCED CONCRETE BEAMS 113

6.5.1 Types of failure in the bamboo reinforced concrete beams *116*

6.5.2 The neutral axis in the beams *118*

6.6 STATISTICAL ANALYSIS OF THE BEAMS' LOAD-DEFLECTION BEHAVIOUR 120

6.7 VALIDATION OF THE FE MODEL 124

6.8 THE BOND FAILURE MODEL 126

6.9 VALIDATION OF BONDING, BENDING, AND SHEAR CAPACITY MODELS 132

6.10 COMPARING BAMBOO TENSILE TESTING METHODS 136

6.11 DISCUSSION 144

6.12 CONCLUSION 146

7. SERVICEABILITY OF BAMBOO REINFORCED CONCRETE BEAMS 147

7.1 INTRODUCTION 147

7.2 DEFLECTION 148

7.2.1 Deflection behaviour of steel-reinforced concrete *150*

7.2.2 Deflection behaviour of FRP reinforced concrete ... *151*
7.2.3 Modelling the deflection of bamboo reinforced concrete using existing models ... *153*
7.2.4 The proposed deflection model for bamboo reinforced concrete ... *161*
7.2.5 Validation of the proposed deflection model using experimental results ... *164*
7.3 Crack Control ... 170
7.3.1 Frosch (1999) method for the estimation of cracks ... *172*
7.3.2 CEB-FIB (1993) method for the estimation of cracks ... *175*
7.3.3 Strain comparison in different reinforcement for crack control ... *177*
7.4 Serviceability of bamboo, GFRP and steel-reinforced concrete ... 178
7.5 Sustainability credentials of bamboo reinforcement ... 182
7.6 Discussion ... 183
7.6.1 Discussion of serviceability of bamboo reinforced concrete ... *184*
7.6.2 Discussion of sustainability of bamboo reinforced concrete ... *185*
7.7 Conclusion ... 186
8. CONCLUSIONS & FUTURE WORK ... 187
8.1 The bond of bamboo to concrete ... 187
8.2 Flexural and shear capacities of bamboo reinforced concrete ... 188
8.3 Deflection and cracking estimation of bamboo reinforced concrete ... 188
8.4 Comparing bamboo reinforcement to steel and FRP ... 188
8.5 Limitations of using bamboo as reinforcement ... 189
8.6 Future work ... 190
References ... 192
Appendix A ... 208
Appendix B ... 212
Appendix C ... 218
Appendix D ... 220
Appendix E ... 227
Appendix F ... 229

Table of figures

Figure 2.1 Picture that shows the distribution of fibre within a Moso bamboo culm 14

Figure 2.2 Scatter plot of reinforcement percentage VS Experimental capacity /Theoretical plain concrete capacity (EC/TP) for all beams 24

Figure 2.3 Plot of the flexural moment in a three-span continuous beam 27

Figure 3.1 Diagram of the research methodology structure 41

Figure 3.2 Illustration of the general pattern of corrugation 43

Figure 3.3 Plot of the modified Bertero-Eligehausen-Popov bond-slip relationship (adapted from Focacci, Nanni and Bakis (2000)) 49

Figure 4.1 Illustration of a linear full integration quadrilateral element 60

Figure 4.2 Illustration of a non-linear higher-order quadrilateral element 60

Figure 4.3 Plot of the three stages of steel-reinforced concrete behaviour (adapted from Chen (2007)) 62

Figure 4.4 Plot of three concrete stress-strain models in uniaxial compression 64

Figure 4.5 Plot of the effect of mesh size on load resistance and crack energy (adapted from ACI Committee 446 (1991)) 67

Figure 4.6 Plot of fracture energy models (crack width VS stress) 69

Figure 4.7 Plot of the snap-through and the snapback behaviour 73

Figure 4.8 Snapshot of the mesh in the current research 77

Figure 5.1: Picture of a splint in the form with bitumen-based debonding compound 80

Figure 5.2 Picture of pull-out testing of a bamboo splint 81

Figure 5.3 Histogram of the average bond (Tr indicates that the specimen is treated with linseed oil, the first number indicates the projection, and the ratio is the B:A ratio) 82

Figure 5.4 Picture of the splitting of pull-out specimens 83

Figure 5.5 Picture of the bamboo-concrete surface after failure for linseed treated splint (Tr 2 mm 1:1.5) . 83

Figure 5.6 Picture of the bamboo-concrete surface after failure for linseed treated splint (Tr 2 mm 1:1) 84

Figure 5.7 Picture of the bamboo-concrete surface after failure for an untreated splint (2 mm 1:1) 84

Figure 5.8 Partial regression plot of interaction between linseed treatment, projection (mm), and thickness (mm) against load (N) 88

Figure 5.9 Partial regression plot of the pattern (B-A (mm) VS load (N)) 89

Figure 5.10 Scatter plot of the homoscedasticity of the linear regression residuals 90

Figure 5.11 Illustration of the internal stresses in bamboo and concrete 91

Figure 5.12 Illustration of concrete shear-friction surfaces with corrugated bamboo 91

Figure 5.13 Scatter plot of experimental bond results VS theoretical model 93

Figure 5.14 Plot of load-slip for a corrugated and non-corrugated specimen at free (FE) and loaded (LE) ends 93

Figure 5.15 Illustration of the bond stress along the embedment length inside the concrete 98

Figure 5.16 Plot of average bond VS embedment in Cox and McDonald (1970) experimental results and the proposed theoretical model 100

Figure 5.17 Plot of average bond VS embedment in the FE model and the proposed theoretical model for a corrugated splint with 13.9 GPa MOE and 140 mm2 section area 100

Figure 6.1 Illustration of the strain gradient and the equivalent Stress Block analysis (adapted from Nanni, De Luca and Jawaheri Zadeh (2014)) 105

Figure 6.2 Section of a concrete beam with bundled bamboo reinforcement 111

Figure 6.3 Plot of the flexural testing arrangement 112

Figure 6.4 Graph of load-deflection of beams with two non-corrugated splints 113
Figure 6.5 Graph of load-deflection of beams with two corrugated splints 113
Figure 6.6 Graph of load-deflection of beams with three corrugated splints 114
Figure 6.7 Graph of load-deflection of beams with four bundled corrugated splints 114
Figure 6.8 Graph of load-deflection of beams with two corrugated splints in tension and two corrugated splints in compression 115
Figure 6.9 Scatter plot of load results VS reinforcement area at different deflection (Def (mm)) levels 116
Figure 6.10 Picture showing compression failure of Beam 8 117
Figure 6.11 Picture showing the shear failure of Beam 7 117
Figure 6.12 Picture showing the bond failure of Beam 14 117
Figure 6.13 Picture of the strain Gauge protection material 117
Figure 6.14 Graph of the neutral axis depth VS reinforcement area in the experimental results and the transformed area predictions 119
Figure 6.15 Bar chart of the splints bond using equation 5.1 and the linear regression model 121
Figure 6.16 Scatter plot of the mixed linear model predicted values of load VS the experimental load results 122
Figure 6.17 Histogram of residuals 123
Figure 6.18 Histogram of the random variable 123
Figure 6.19 Graph of Finite element model (FE), Mixed Linear Model (MLM), and experimental results of Beam 15 (Exp) 125
Figure 6.20 Graph of Finite Element Model (FE), Mixed Linear Model (MLM), and experimental Results of Beam 8 (Exp) 125
Figure 6.21 Graph of Finite Element Model (FE), Mixed Linear Model (MLM), and experimental Results of Beam 6 (Exp) 125
Figure 6.22 Snapshot of cracking with low stiffness reinforcement at the maximum moment (ρ=1.06%, E=13.9 GPa) 126
Figure 6.23 Snapshot of cracking with stiff reinforcement at the maximum moment (ρ=8.47%, E=13.9 GPa) 126
Figure 6.24 Graph of model predictions VS maximum reinforcement stress result in the FE model at ρ=1.06% 129
Figure 6.25 Graph of model predictions VS maximum reinforcement stress result in the FE model at ρ=2.32% 129
Figure 6.26 Graph of model predictions VS maximum reinforcement stress result in the FE model at ρ=3.17% 130
Figure 6.27 Graph of model predictions VS maximum reinforcement stress result in the FE model at ρ=4.19% 130
Figure 6.28 Graph of model predictions VS maximum reinforcement stress result in the FE model at ρ=6.35% 131
Figure 6.29 Graph of model predictions VS maximum reinforcement stress result in the FE model at ρ=8.47% 131
Figure 6.30 Picture of a bamboo tensile specimen with the natural curvature 138
Figure 6.31 Picture of the use of tabs and epoxy for bamboo tensile test specimens 138
Figure 6.32 Picture of the tensile test arrangement 139
Figure 6.33 Picture of the tensile test's machine grip 139
Figure 6.34 Picture of typical failure of Moso 1:2 ratio (top view) 140
Figure 6.35 Picture of typical failure of Moso 1:2 ratio (side view) 140

Figure 6.36 Picture of typical failure of Moso 1:2 ratio + Aluminium tabs and epoxy (top view) 140

Figure 6.37 Picture of typical failure of Moso 1:2 ratio + Aluminium tabs and epoxy (side view)..... 140

Figure 6.38 Picture of typical failure of Moso 1:3 ratio (top view) 141

Figure 6.39 Picture of typical failure of Moso 1:3 ratio (side view) 141

Figure 6.40 Picture of typical failure of Moso with flattened ends, 1:2 ratio (top view) 141

Figure 6.41 Picture of typical failure of Moso with flattened ends, 1:2 ratio (side view)..... 141

Figure 6.42 Section in the bamboo tensile test..... 143

Figure 6.43 Illustration of a bamboo specimen and the loading grips..... 143

Figure 7.1 Plot of mid-span deflection VS total load using Branson and Metz (1963) model estimates using m=3 (m describes the transition from Ig to Icr)..... 154

Figure 7.2 Plot of mid-span deflection VS total load using Branson and Metz (1963) model estimates using m=4 154

Figure 7.3 Plot of mid-span deflection VS total load using European code deflection model estimates (CEB-FIB, 1993)..... 155

Figure 7.4 Plot of mid-span deflection VS total load using Masmoudi, Thériault and Benmokrane (1998) deflection model estimates..... 155

Figure 7.5 Plot of mid-span deflection VS total load using Bischoff (2005) deflection model estimates... 156

Figure 7.6 Plot of mid-span deflection VS total load using American Concrete Institute (2003) model estimates for deflection 156

Figure 7.7 Box plot of the normalised difference between the deflection models' estimates and the mixed linear model predictions..... 157

Figure 7.8 Plot of deflection VS normalized estimates of Branson and Metz (1963) using m=3 158

Figure 7.9 Plot of deflection VS normalized estimates of Branson and Metz (1963) using m=4 159

Figure 7.10 Plot of deflection VS normalized estimates of European code deflection model (CEB-FIB, 1993) 159

Figure 7.11 Plot of deflection VS normalized estimates of Masmoudi, Thériault and Benmokrane (1998)160

Figure 7.12 Plot of deflection VS normalized estimates of American Concrete Institute (2003) model estimates for deflection 160

Figure 7.13 Plot of deflection VS normalized estimates of Bischoff (2005) 161

Figure 7.14 Plot of FE model mid-span deflection VS Load at different longitudinal bond/area ratios using ρ = 8.5%..... 163

Figure 7.15 Plot of FE model mid-span deflection VS Load at different longitudinal bond/area ratios using ρ = 3.2%..... 163

Figure 7.16 Plot of the bond adjusted model and Biscoff's model deflection estimates for an FE beam with ρ = 8.5% and longitudinal bond of 0.125 MPa/mm 163

Figure 7.17 Plot of load-deflection of the proposed model and the experimental results of beam3 165

Figure 7.18 Plot of load-deflection of the proposed model and experimental results of beam 6 165

Figure 7.19 Plot of load-deflection of the proposed model and experimental results of beam 8 166

Figure 7.20 Plot of load-deflection of the proposed model and experimental results of beam 15 166

Figure 7.21 Plot of load-deflection of the proposed model and experimental results of YA by Yamaguchi Murakami and Takeda (2013)..... 167

Figure 7.22 Plot of load-deflection of the proposed model and experimental results of YB by Yamaguchi Murakami and Takeda (2013)..... 167

Figure 7.23 Plot of load-deflection of the proposed model and experimental results of CG6 by Cox and Geymayer (1969) 168

Figure 7.24 Plot of load-deflection of the proposed model and experimental results of CG17 by Cox and Geymayer (1969) 168

Figure 7.25 Plot of load-deflection of the proposed model and experimental results of CG18 by Cox and Geymayer (1969) 169

Figure 7.26 Plot of load-deflection of the proposed model and experimental results of CG19 by Cox and Geymayer (1969) 169

Figure 7.27 Plot of load-deflection of the proposed model and experimental results of CG20 by Cox and Geymayer (1969) 170

Figure 7.28 Plot of cracking in reinforced concrete 173

Figure 7.29 Scatter plot of Frosch (1999) model predictions for average crack width using $\Psi s = 3.2$ VS the experimental results 174

Figure 7.30 Scatter plot of Frosch (1999) model predictions for maximum crack width using $\Psi s = 4$ VS experimental results 174

Figure 7.31 Scatter plot of CEB-FIB (1993) model predictions for average crack width VS the experimental results 176

Figure 7.32 Scatter plot of CEB-FIB (1993) model predictions for maximum crack width VS the experimental results 177

Figure 7.33 Plot of the behaviour of bamboo reinforced concrete vs steel and GFRP (E_b =13.9 GPa) 179

Figure 7.34 Plot of the behaviour of bamboo reinforced concrete vs steel and GFRP (E_b = 20 GPa) 179

Figure 7.35 Plot of the behaviour of bamboo reinforced concrete vs steel and GFRP (E_b = 30 GPa) 180

Figure 7.36 Illustration of corrugated bundled bamboo reinforcement inside the concrete at $\rho = 8\%$ 182

Table of tables

Table 2.1 Strength and modulus of elasticity of natural material fibre 10
Table 2.2 Bamboo tensile strengths and modulus of elasticities in literature 11
Table 2.3 Bond of bamboo using different treatments in the literature 17
Table 2.4 Bending capacity of bamboo reinforced concrete beams in the literature 21
Table 3.1 The design of the bond study 47
Table 5.1 The bond results of corrugated and non-corrugated bamboo using the pull-out test 82
Table 5.2 ANOVA of the pull-out results 85
Table 5.3 Linear regression of maximum pull-out load using backward elimination 87
Table 5.4 Linear regression of the bond stiffness 95
Table 6.1 Details of the tested bamboo reinforced concrete beams 111
Table 6.2 The ultimate capacity results of the tested beams 117
Table 6.3 The beams' experimental and theoretical neutral axis 120
Table 6.4 Parameters variable using the mixed linear model in SPSS 122
Table 6.5 Normality test for the random variable 123
Table 6.6 The covariance structures in the mixed linear model 124
Table 6.7 Experimental and theoretical capacities of bamboo reinforced beams 132
Table 6.8 The average tensile strength of investigated bamboo specimens 140
Table 6.9 The univariate analysis of the bamboo tensile strength results 142
Table 7.1 Means and standard errors of the deflection models' normalised estimates 157

Notation

A_b: Area of bamboo reinforcement
A_{ce}: Area of concrete surrounding the reinforcement (effective concrete area)
C: Compressive force in the concrete
E: Modulus of elasticity
E_b: Modulus of elasticity of bamboo
E_c: Modulus of elasticity of concrete
E_{FRP}: Modulus of elasticity of fibre reinforced polymers
E_s: Modulus of elasticity of steel
G: Shear modulus
G_F: Fracture energy
I: Second moment of area
I_{cr}: The cracked second moment of area
I_e: Effective second moment of area
$I_{e,b}$: Effective second moment of area adjusted for bond
I_g: Gross second moment of area
M: Moment
M_a: Service moment
M_{cr}: Moment at first crack
M_n: Nominal moment capacity
M_u: Ultimate moment capacity
S_c: Spacing of cracks
$S_{c,A}$: Spacing of cracks in Frosch's formula
$S_{c,E}$: Spacing of cracks in the European code's formula
T: Tensile force in the reinforcement
W: Energy

b: Width of beam
d: Depth of reinforcement
d_a: Largest aggregate size
d_c: Reinforcement cover
c: Depth of neutral axis
c_e: Cement weight
c_b: Depth of neutral axis for a balanced section
f_b: Stress in bamboo reinforcement
f'_c: Compressive strength of concrete
f_{ctm}: Mean tensile strength of concrete
h: Height of beam
l: span
l_{cr}: The length of the cracked span from the support to mid-span
p: Total load applied to the beam
r: power parameter that controls the speed of shear resistance degradation
s: Reinforcement spacing
w: Water weight
$w_{c,A}$: Crack width based on Frosch's formula
$w_{c,E}$: Crack width based on the European code's formula

α_0: Factor for the type of aggregates
α_1: Factor that accounts for the strain gradient in the compression area of a beam
α_b: Factor that accounts for the effect of bond

β: Shear retention factor
β_1: Factor that accounts for the different area of the stress-strain diagram with concrete strength
β_A: Factor that accounts for the strain gradient in a beam's section
β_b: Reduction factor to account for bond and modulus of elasticity
β_E: Reduction factor for the concrete strain in the effective concrete area
y: Factor that accounts for moment function
ε: Strain
ε_o: Strain at the end of elastic behaviour
ε_b: Strain of the bamboo reinforcement at the crack
ε_{bm}: Mean strain of the bamboo reinforcement
ε_{cm}: Mean strain of the concrete surrounding the reinforcement
ε_{bu}: Strain of the bamboo reinforcement at ultimate tensile stress
ε^{cr}: Crack strain
ε_u^{cr}: Ultimate crack strain
ε_c: Concrete compressive strain
ε_{cu}: Strain of the concrete at ultimate compressive stress
ζ: Parameter that reflects the effect of the moment on the concrete stiffness
ν: Poisson's ratio
ρ: Geometrical percentage of reinforcement
ρ_b: Geometrical percentage of reinforcement that produces a balanced section
$\rho_{b,ef}$: Geometrical percentage of reinforcement in the effective concrete area
σ: Stress
σ_{bu}: Ultimate tensile stress of bamboo
σ_c: Compressive Stress
σ_{max}: The maximum tensile stress achieved in the reinforcement via bond
σ_{min}: The minimum tensile stress achieved in the reinforcement via bond
σ_τ: Stress in the reinforcement corresponding bond failure
τ_l: Longitudinal bond between the reinforcement and the concrete in short embedment
$\tau_{l,max}$: Maximum longitudinal bond stress
ψ: Concrete dilatation angle
ϕ: Safety factor

Δ: Deflection
θ: Deflection angle
Ψ: Curvature
Ψ_1: Curvature in an un-cracked section
Ψ_2: Curvature of a cracked section
Ψ_e: Effective curvature
Ψ_s: Spacing of cracks coefficient in Frosch's formula

Chapter 1

1. Introduction

1.1 Background

Steel reinforced concrete has been one of the most successful innovations in the structural industry since its inception in the 19th century. Concrete has remarkable properties that made it the most widely used construction material in the world. Concrete has exceptional compressive strength per unit cost and is durable with low maintenance requirements, and can be cast in a variety of shapes (McCormac and Brown, 2014). The more expensive of the two, steel, is used to compensate for the main weakness of concrete of low tensile strength. Another reason for the success of this combination is the relative affordability of steel in comparison with any metal. Iron, the main constituent of steel, ‘’is the least expensive and most widely used metal’’ (USGS, 2019). While Fibre Reinforced Polymers (FRP) can provide similar mechanical properties and superior durability to steel, it has a prohibitively higher cost (see Burgoyne and Balafas (2007)).

Despite steel excellent mechanical properties and its cost-effectiveness relative to other metals, there has been an interest in replacing steel with materials that are cheaper and more readily available in developing countries. The interest in replacing steel with bamboo to reinforce concrete is not new. In the early twentieth century, Chow (1914) carried the earliest study in MIT on the use of bamboo as reinforcement in concrete. His interest was sparked by the high tensile strength of bamboo and its availability in his home country of China. Reducing construction cost has been ever since one of the main arguments for the use of bamboo as reinforcement in concrete. The growing world

population is increasingly demanding more construction materials. This increase in demand comes with increased prices and pressure on the environment. The importance of cost-effective and environmentally sustainable materials can be emphasised by the fact that the construction industry consumes 50% of all raw materials (Pacheco-Torgal and Labrincha, 2013).

While the prices of bamboo can vary wildly, it is clear that bamboo is much cheaper relative to steel. Prices of bamboo vary greatly due to the shipping costs, quality of bamboo, size of culms, and species. In Laos, raw bamboo is sold for as little as $12 per ton (World Agroforestry Centre, 2006). Janssen (2000) estimated that an approximate price for bamboo is $105 US per cubic metre. A supplier in Canada made an estimate of $530 US per ton for wholesale prices in Canada. This translates to approximately $345 US per cubic metre assuming an average density of 650 Kg/m^3. The American geological survey estimates that hot rolled steel prices during 2014 were $621-765 US per ton (USGS, 2015), equivalent to $4720-5814 per cubic metre. The volumetric price comparison between steel and bamboo is more appropriate because strength is a product of section area and not weight. Furthermore, the density of steel is an order of magnitude larger relative to bamboo (7.6 ton/m^3 for steel VS 0.65 ton/m^3 for bamboo). Despite the difficulty of getting an accurate estimate of the price of bamboo, it is clear that bamboo is an order of magnitude less expensive relative to steel. In addition, bamboo exists mostly in developing countries, which makes it available in places where steel is not readily available (Ghavami, 1995; Sharma, 1990). Bamboo is mainly available in countries in South America, sub-Saharan Africa, India, China, and Indonesia while 95% of iron is mined in just twelve countries (USGS, 2019).

Another argument for bamboo use as reinforcement in concrete is it is sustainability and low carbon footprint relative to steel. Although iron is one of the most abundant elements

on earth, for the extraction to be considered economically viable, the deposit needs to contain at least 25% iron. It is possible that with advances in technology, and discoveries of new deposits that more iron is made available. For example, electric arc furnaces are replacing the less efficient basic oxygen furnaces (USGS, 2019). Nonetheless, as the most iron-rich deposits are depleted, the prices of iron and the energy required to process it will increase. Meaning, steel will have increasingly worse environmental credentials. Moreover, the demand for iron production is increasing. It increased from 274 million tonnes in 1950 to 1554 million tonnes in 2005. According to the U.S. Geological Survey (USGS, 2015), Iron ore production in 2014 was 3220 million tonnes. Yellishetty, Ranjith and Tharumarajah (2010) estimated that the currently viable worldwide reserves of 230 billion tonnes would last for about 50 years and that the global annual CO_2 emissions from the different manufacturing routes of steel will be 3169 million tonnes by 2020. In addition to the high environmental cost of mining and processing iron ore, its transport produces significant emissions. Some of the top steel-producing countries like Japan has no iron reserves of its own while Brazil exports 90% of its mined iron ore.

On the other hand, bamboo is rapidly renewable and has a low carbon footprint. Bamboo is harvested ideally at the age of three to four years while wood takes decades to mature. Bamboo improves the climate through photosynthesis (photosynthesis produces Oxygen and consumes CO_2) (Khatib, 2009), and sequesters more carbon per hectare relative to trees (see Lobovikov, Schoene and Yping (2012). Researchers have suggested that subsidising the cultivation of bamboo can help in greater carbon sequestration (see Wu *et al.* (2015)). In addition, cultivating bamboo can have additional localized benefits. For example, bamboo helps prevent erosion and flooding because of its root system (Khatib, 2009).

While bamboo can compensate for the weak tensile strength of concrete, concrete can potentially mitigate the drawbacks of bamboo. Bamboo is an anisotropic material. Meaning that, unlike steel, bamboo strength and modulus of elasticity depends on the direction of the load relative to the fibre direction. The MOE and strength are maximum in the direction of fibres. One of the problems in using bamboo as a construction material is its lack of fibre in the transverse and tangential directions which is the cause of its order of magnitude lower strength and modulus of elasticity (Archila *et al.*, 2018). In addition, the hollow section of bamboo complicates its use in its natural form and it complicates connecting members. Furthermore, the moment capacity and to a larger extent the shear capacity are negatively affected by the hollow section. Furthermore, the compressive strength of bamboo is significantly smaller to the tensile strength in the direction of fibres. Therefore, bamboo culms under flexure usually fail due to compression failure in the bamboo or due to shear flow failure. Using bamboo as reinforcement mitigates these weaknesses because tensile and shear reinforcement in concrete acts as unidirectional members in tension and the concrete can serve to resist compression, hold reinforcement in place, and carry part of the shear in the transverse direction of the beam.

1.2 Introduction to the current research

Since the research of Chow (1914), the interest in using bamboo as reinforcement in concrete came mainly from researchers in developing countries because of its wide availability. Notable among the exceptions are the research carried by Cox and Geymayer (1969). On the behest of the US army, Cox and Geymayer (1969) carried the largest research on the subject to date to provide expedient reinforcement in the field. Most of the studies carried since are small studies that made little progress in providing a design method for bamboo reinforced concrete. While some progress has been made on the improvement of the bond, little progress has been achieved on other aspects of using

bamboo as reinforcement. The current research investigates how to model the flexural and shear capacities of bamboo reinforced concrete according to limit state design.

Serviceability of bamboo reinforced concrete was often ignored by the researchers. There are currently no models that depict the deflection, cracking and bonding behaviour of bamboo reinforced concrete. Bamboo differs from steel in many ways but the most pertinent in its mechanical behaviour as reinforcement in concrete are weaker bond, lower modulus of elasticity, and lack of ductility. Archila *et al.* (2018) identified these problems in their comprehensive critique of the use of bamboo as reinforcement in concrete. The current research determines the severity and limits of these problems by developing models that depict the bonding, deflection and cracking behaviour of bamboo reinforced concrete. In addition, the current research investigates solutions to mitigate the problems of, bond, deflection, and cracking.

The current research will present a design method for bamboo reinforced concrete following the limit state design. It should be noted that other aspects of bamboo reinforced concrete such as durability and creep require further research. Some discussion on durability and creep is included in the current research to discourage premature adoption of bamboo as reinforcement and encourage further research.

1.3 Research questions

This research aims to contribute to the knowledge on bamboo reinforced concrete by answering the following questions:

1. Can corrugation improve bamboo's bond to concrete and what model can be used to estimate its bond at short embedment?
2. Can the bond of bamboo under large embedments in uncracked concrete be predicted using a theoretical model that is based on the stiffness of bamboo and its bond behaviour at short-embedment?
3. What theoretical models should be used to estimate the flexural and shear capacities of bamboo reinforced concrete according to the limit state design method?
4. Can the bond failure in bamboo reinforced concrete beams be predicted using a theoretical model that is based on the mechanical properties of bamboo and its bond behaviour at short-embedment?
5. Can the deflection behaviour of bamboo reinforced concrete be modelled using a theoretical model that accounts for bamboo unique mechanical properties and bond with concrete?
6. Is it possible to predict the cracking behaviour of bamboo reinforced concrete using models that account for the bond and stiffness of bamboo?
7. What reinforcement percentage of bamboo yields similar stiffness and cracking behaviour to GFRP (Glass Fibre Reinforced Polymers) and steel-reinforced concrete?
8. Is it possible to provide a lower carbon footprint using bamboo reinforcement relative to steel reinforcement?

1.4 List of Publications

During the research, the following papers were published:

1. Khatib, A. and Nounu, G. (2017) Corrugated bamboo as reinforcement in concrete. *Proceedings of the Institution of Civil Engineers*. 170 (4), pp. 311.
2. Khatib, A. and Nounu, G. (2016) State of the Art of the Use of Bamboo Sticks to Replace Steel Reinforcement in Reinforced Concrete. In: *The 9th International Concrete Conference*. 2016 Dundee, Scotland, UK: University of Dundee.

1.5 Thesis Structure

In this section, the structure of the thesis is presented to help guide the reader through the thesis. In addition, the research questions are linked to the chapters that answer the questions.

Chapter 2 - *Literature review on the use of bamboo as reinforcement in concrete*

This chapter presents a literature review on the use of bamboo as reinforcement in concrete that summarises previous research on the subject. This chapter identifies the limits of current knowledge on the use of bamboo as reinforcement and concrete. In addition, it serves to contextualize the contributions made in the current research.

Chapter 3 - *Methodology*

This chapter summarises the gaps in the literature and it presents the methodologies used in the current research. It includes a justification of the methods and it discusses alternative approaches.

Chapter 4 – *Review of Reinforced Concrete Finite Element Modelling*

This chapter reviews Finite element modelling of reinforced concrete. It provides the background for the choices made in developing an FE model for bamboo reinforced concrete and it presents the FE model suggested for bamboo reinforced concrete.

Chapter 5 - *Bond of Bamboo Embedded inside Concrete*

In this chapter, the first two questions are answered. The problem of bamboo bond with concrete is addressed. Corrugation is presented as a solution for the weak bond, and a model is created to estimate the bond of corrugated bamboo at short embedment lengths. In addition, a model is created to estimate the bond of bamboo at varying embedment lengths in uncracked concrete.

Chapter 6 - *Flexural capacity of Bamboo Reinforced Concrete Beams*

This chapter answers questions 3&4. It shows that the shear and flexural capacity of bamboo reinforced concrete are analogous to FRP reinforced concrete. Moreover, it presents a bond failure model for bamboo used as reinforcement in cracked concrete.

Chapter 7 - Serviceability of Bamboo Reinforced Concrete Beams

This chapter answers questions 5-8. It presents a deflection model for bamboo reinforced concrete. It validates two cracking models for bamboo reinforced concrete. It determines the percentage of bamboo that is needed to achieve the same cracking and deflection behaviour as GFRP and steel-reinforced concrete. In addition, it compares the carbon footprint of bamboo, GFRP, and steel-reinforced concrete.

Chapter 8 - *Conclusions & Future Work*

The main findings of the current research are summarised and recommendations are made to guide future work on the potential use of bamboo as reinforcement in concrete.

Chapter 2

2. Literature Review on Bamboo Use as Reinforcement in Concrete

This chapter provides a literature review on bamboo and its use as reinforcement in concrete. Section 2.1 reviews the bamboo mechanical properties most relevant to its use as reinforcement. Section 2.2 reviews the research on the treatment of bamboo for bond purposes. Section 2.3 reviews the flexural capacities achieved using bamboo reinforcement in literature. Section 2.4 reviews the approaches that have been followed in literature in the modelling of the flexural capacity of bamboo reinforced concrete and it discusses their deficiencies. Section 2.6 reviews and discusses the approaches that have been followed in the literature to model the shear capacity of concrete when reinforced with bamboo. Section 2.5 discusses the effect of bamboo brittleness on the modelling of indeterminate structures. Section 2.6 discusses serviceability limits and reviews the approaches that have been followed in the literature to address the serviceability of bamboo reinforced concrete. Section 2.8 discusses the creep of bamboo and review the literature available on the subject. Section 2.9 reviews the literature on bamboo durability. Finally, section 2.10 provides a summary of this chapter.

2.1 The mechanical behaviour of bamboo

The mechanical properties most important in a tensile reinforcement are the modulus of elasticity and the tensile strength. The tensile strength of the reinforcement is directly responsible for the moment capacity of reinforced concrete elements while the MOE is indirectly linked to the moment capacity. More importantly, the modulus of elasticity of reinforcement directly influences cracking and deflection in reinforced concrete. Relative

to other organic materials, bamboo fibres have a high modulus of elasticity and high tensile strength (see Table 2.1). The MOE of bamboo fibre is comparable to GFRP at 40 GPa; however, significantly smaller relative to steel at 200 GPa.

Table 2.1 Strength and modulus of elasticity of natural material fibre

Fibre	Ultimate tensile stress (MPa)	Modulus of elasticity, E (GPa)
Wood[1]	160	23
Bamboo[1]	550	36
Jute[1]	580	22
Cotton[1]	540	28
Wool[1]	170	5.9
Coir[1]	250	5.5
Asbestos[1]	1700	160

1: Vasiliev and Morozov (2013)

Bamboo can be potentially used in its natural form or as a composite material in engineered bamboo. The following two subsections review the properties of natural bamboo and engineered bamboo. In addition, their relative advantages and disadvantages are discussed.

2.1.1 Natural bamboo

Bamboo species are divided into two groups as follows: woody (lignified) stems bamboos (Arundinarieae (temperate) and Bambuseae (tropical) bamboo); and non-woody bamboo (Olyreae (temperate)) (Kelchner and Group, 2013). Woody bamboo has many uses in industry and can be potentially used as reinforcement. Table 2.2 shows the results of the tensile strength of a few bamboo species.

Table 2.2 Bamboo tensile strengths and modulus of elasticities in literature

Bamboo species	Age (year)	Thickness (mm)	Mean tensile strength / No node (MPa)	Modulus of Elasticity / No node (GPa)	Mean tensile strength / one node (MPa)	Mean modulus of Elasticity / one node (GPa)
Bambusa multiplex raeusch[1]	-	3.5	124.7	11.2	95.3	10.05
Bambusa tuldoidis[1]	-	6.0	119.5	11.93	104.00	9.27
Dendrocalamus Giganteus[1]	-	11.0	135.0	14.5	119.02	11.75
Bambusa vulgaris[1]	-	8.0	134.4	7.76	48.05	6.05
Bambusa vulgaris[2]	-		200	-	145	-
Phyllostachys edulis[3]	-	-	-	-	125.1	7.94
Bambusa vulgaris[4]	3	10–15	335	-	-	-
Dendrocalamus asper Backer[5]	3	-	224	-	-	-
Dendrocalamus giganteus[6]	-	-	277	23.75	-	-
Melocanna bambusoides[7]	3-5	-	-	-	185.9	24.5
Dendrocalamus strictus[8]	3	-	321	20	-	-

1. Ghavami (1995);
2. Sharma (1990);
3. Schneider, Pang and Gu (2014);
4. Adewuyi *et al.* (2015);
5. Leelatanon, Srivaro and Matan (2010);
6. Lima Jr *et al.* (2008);
7. Agarwal, Nanda and Maity (2014);
8. Kute and Wakchaure (2013)

It can be noticed from Table 2.2 that the data in the literature on bamboo tensile strength vary significantly for the same species. The results for Bambusa Vulgaris species ranged between 126-335 MPa. The following factors can explain this variation:

1. Natural materials have large variability in strength.
2. Bamboo tensile strength increases with height, and it increases towards the outer region of the culm cross-section (Verma, Chariar and Purohit, 2012).
3. Different moisture contents. The increase in moisture reduces the tensile strength and the modulus of elasticity. For example, Acha Navarro (2011) showed that the MOE of Dendrocalamus giganteus bamboo drops from 29 GPa to 17 GPa as moisture content increases from 2 to 23%.
4. Age at harvesting affects the tensile strength, bamboo strength peaks at the age of 3-4 years.
5. Different growing environment and quality of culms.

6. Use of different testing methods. Lima Jr *et al.* (2008), Agarwal, Nanda and Maity (2014), Schneider, Pang and Gu (2014) and Kute and Wakchaure (2013) used Aluminium tabs with epoxy to prevent the crushing of the splints ends. Adewuyi *et al.* (2015) and Kute and Wakchaure (2013) did not reduce the section in the gauge area. Lima Jr *et al.* (2008) reduced the section in the gauge area to 1:5 ratio (width in the gauge area : width in the grip area). In the current research, the methods used in literature are investigated to explore how effective they are in predicting the tensile strength of bamboo reinforcement inside the concrete.

Due to the remarkable strength of bamboo, some researchers were overly enthusiastic about its use. Bamboo is frequently compared favourably to steel in terms of cost-effectiveness, sustainability, and strength. Archila *et al.* (2018) rightly criticised the repeated claim that bamboo is ‘’the green steel’’. While the mean tensile strength of bamboo can be compared to mild steel, it is often not considered that bamboo characteristic strength is lower relative to the mean strength. This is due to the large variability of the natural bamboo material. The characteristic strength is the strength that 95% of the sample exceeds. In other words, the characteristic strength is the mean strength minus 1.64 the standard deviation of the material using the standard normal distribution (Z-distribution) (Montgomery, 2003). Another misleading comparison is comparing the strength of bamboo per weight compared to the strength of steel per weight to emphasise the great properties of bamboo. This comparison is misleading because the reinforcement is a small fraction of the weight in reinforced concrete. Another way that steel is superior to bamboo is its ductility. While bamboo failure is brittle, steel behaviour is ductile after it yields. This allows steel-reinforced concrete to provide ample warning before failure due to cracking and increased deflection.

Grading bamboo would serve to provide designers with predictable behaviour. As a natural material, similar to wood, suppliers would need to qualify there bamboo into grades for bamboo to be used in design (see British Standards Institution (2009)). Grading can be accomplished by experts' visual inspection; however, this typically yields conservative results. Another approach is by linking mechanical properties that can be measured non-destructively to the grading property. For example, Trujillo, Jangra and Gibson (2017) were able to establish a strong correlation between flexural capacity and flexural stiffness.

2.1.2 Engineered bamboo

Engineered bamboo is a composite material that includes bamboo fibre and a matrix of epoxy or resin. The purpose of engineered bamboo is to mitigate some of the problems of bamboo. Although engineered bamboo is relatively less sustainable and more expensive in comparison with the natural bamboo material, it has significant advantages over the natural bamboo as follows:

1. Higher tensile strength;
2. Higher modulus of elasticity;
3. Better mechanical properties in the transverse direction;
4. Lower variability in mechanical properties;
5. The ability to produce sections that are of a convenient shape;
6. Stronger bond with concrete.

Maximizing the modulus of elasticity (MOE) and tensile strength should be the priority in engineering bamboo for use as reinforcement in concrete. According to Janssen (2000), only 40% of the section bamboo made up of fibre, and the remainder is made of parenchyma (50%) and vascular bundles (10%). Meaning that the fibres high strength is

diluted in the bamboo's section. The fibre distribution in bamboo lends itself to the optimization of the engineered bamboo material by maximizing the fibre content. The fibre content in the bamboo culm increases cubically from the inner surface towards the outer surface (see Figure 2.1) (Li and Shen, 2011) and the fibre content increases with height (Verma, Chariar and Purohit, 2012). In addition, different species have different fibre contents. For example, Dendrocalamus giganteus bamboo has relatively high fibre content at 60%.

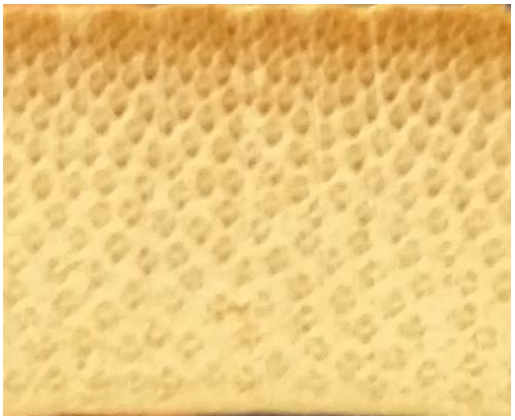

Figure 2.1 Picture that shows the distribution of fibre within a Moso bamboo culm

Engineering bamboo to produce a reinforcement for concrete is relatively a new field of study. Javadia*n et al*. (2016) were able to produce a composite bamboo material with a modulus of elasticity comparable to that of GFRP. The MOE was 37 GPa and the tensile strength was 295 MPa. Their process included boiling the bamboo to remove the starch to improve durability, processing the bamboo into strips, controlling the moisture content to below 10%, impregnating the strips with epoxy and hot pressing them in a mould for the desired shape. The density was equal to 1.22 g/cm^3, which is relatively low in comparison with the density of steel at over 7 g/cm^3. Ma *et al.*, (2018) made another attempt where they manufactured bamboo-laminated veneer lumber with a MOE of 24 GPa. Ma *et al.* (2018) manufacturing process included hot pressing bamboo strips using phenol-formaldehyde adhesive to achieve a density of 0.9 g/cm^3.

While engineered bamboo requires energy to manufacture and include the use of epoxy, engineered bamboo has significantly lower carbon footprint in comparison with steel. Lugt and Vogtländer (2015) assessed the carbon footprint of engineered bamboo and found that bamboo composites are carbon negative. Their assessment included processing, transport, and epoxy use. The negative carbon footprint is due to the storage of carbon in the material which offsets any carbon costs from epoxies and processing. However, it is not yet possible to determine whether engineered bamboo will be economically competitive with steel. Improvements in its manufacturing technology are going to reduce the cost. It is expected that any material that is still in the development stage would not be cost-effective. However, this does not mean that the costs will necessarily be competitive with steel. FRP prices were expected to become more competitive with steel as the technology improved and the market forces pushed to more efficiency; however, steel is still more economical than FRP as a reinforcement (see Burgoyne and Balafas (2007)). The current research will investigate how the superior stiffness of engineered bamboo relative to natural bamboo can affect deflection and cracking.

2.2 Bamboo bond to concrete

It is assumed in the design and analysis of steel-reinforced concrete that the bond between the reinforcement and the concrete is perfect. This assumption is justified by the strong bond achieved using deformed steel. Deformed steel can only lose bond due to failure in the surrounding concrete. For example, the bond with unconfined and confined C30 concrete is 11 MPa and 13.7 MPa, respectively (CEB-FIB, 1993). Untreated bamboo achieves an order of magnitude lower bond with concrete. Therefore, a fundamental problem in the use of bamboo as a reinforcement is bamboo's weak bond to concrete. A strong bond is critical in transferring the load between the reinforcement and the concrete. The weaker bond of bamboo makes the assumption of perfect bond in the design of bamboo reinforced concrete unrealistic. While there have been advances in improving the bond of bamboo (see Table 2.3), it is not clear how these advances would affect the behaviour of bamboo reinforced concrete. Agarwal, Nanda and Maity (2014), Cox and McDonald (1970), and Ghavami (2005) concluded that their beams failed under low loads due to bamboo's weak bond with the concrete. Cox and Geymayer (1969) and Ghavami (1995) attributed bamboo's weak bond to two reasons as follows:

1. When the concrete is cast, the bamboo splints absorb the water from the concrete leading to the expansion of the reinforcements inside the concrete. Upon loss of moisture, splints shrink and lose contact with the concrete;
2. Bamboo's smooth surface minimises friction and allows the reinforcements to slip without the development of a strong bond. Another possible cause of bamboo's weak bond is bond degradation due to the alkalinity of concrete. Altalmas, El Refai and Abed (2015) found that alkaline solutions can degrade the bond of GFRP and BFRP bars to concrete.

To improve the bond of bamboo with concrete a few researchers investigated waterproofing bamboo to limit the expansion and shrinkage due to changes in moisture. In addition, the researchers investigated roughening the surface of the bamboo to increase friction. These treatments resulted in a stronger bond in some cases, as shown in Table 2.3. However, epoxy treatments proved to be the most effective.

Table 2.3 Bond of bamboo using different treatments in the literature

Treatment	Average Bond (MPa)	Embedment Length (mm)	Concrete Compressive Strength (MPa)	Bond improvement relative to untreated (%)
Untreated[1]	0.73	150	20	-
Untreated node inside[1]	0.90	150	20	-
Untreated, notched, node inside[1]	0.92	150	20	2
Nailed[1]	0.90	150	20	23
Nailed node inside[1]	1.09	150	20	21
Binding wire wound[1]	1.06	150	20	45
Binding wire wound, node inside[1]	1.25	150	20	39
Oil painted[1]	0.48	150	20	-34
Oil painted, node inside[1]	0.69	150	20	-23
Oil painted, with zeolite powder[1]	0.71	150	20	-3
Oil painted, with zeolite powder, node inside[1]	0.93	150	20	3
Black Japan[1]	0.66	150	20	-10
Black Japan, node inside[1]	0.86	150	20	-4
Black Japan, with zeolite powder[1]	1.06	150	20	45
Black Japan, with zeolite powder, node inside[1]	1.19	150	20	32
Untreated[2]	0.127	100	20	-
Araldite[2]	0.232	100	20	83
Araldite with wire[2]	0.539	100	20	324
Tapecrete P 151[2]	0.315	100	20	148
Anti Corr RC[2]	0.159	100	20	25
Sikadur 32 Gel[2]	0.588	100	20	363
Untreated[3]	0.52	100	19[4]	-
Negrolin + fine sand[3]	0.73	100	19[4]	40
Negrolin + fine sand + wiring[3]	0.97	100	19[4]	87
Sikadur 32 Gel[5]	2.75	100	-	-
Untreated[6]	0.404	152	28	-
Untreated[6]	0.208	305	28	-
Untreated[6]	.202	457	28	-
Untreated[6]	0.195	610	28	-
No coating[7]	3.61*	200	20	-
Water-based epoxy coating[7]	3.47*	200	20	-3.9
Water-based epoxy coating with fine sand[7]	3.65*	200	20	1.1

Treatment	Average Bond (MPa)	Embedment Length (mm)	Concrete Compressive Strength (MPa)	Bond improvement relative to untreated (%)
Water-based epoxy coating with coarse Sand[7]	3.61*	200	20	0
TrueGrip EP[7]	3.30*	200	20	-8.6
TrueGrip EP with coarse Sand[7]	3.45*	200	20	-4
TrueGrip BP[7]	2.42	200	20	-33
TrueGrip BP with coarse Sand[7]	2.62	200	20	-27
Exaphen[7]	3.36*	200	20	-7
Exaphen with coarse Sand[7]	3.46*	200	20	-4
Enamel[7]	3.40*	200	20	-5

1: Kute and Wakchaure (2013)
2: Agarwal, Nanda and Maity (2014)
3: Ghavami (1995)
4: Lightweight concrete (17 KN/m^3)
5: Ghavami (2005)
6: Cox and McDonald (1970)
7: Javadian *et al.* (2016)
*: Bamboo tensile failure

The results presented by the different researchers varied significantly for untreated bamboo (see Table 2.3). This can be attributed to the following reasons:

1. Different bamboo species have different mechanical properties;
2. Different testing procedures: some researchers used an unbonded length near the loaded end (Ghavami, 1995)), whereas, in some research, there was not (Agarwal, Nanda and Maity, 2014);
3. Different embedment lengths;
4. Possibly different rates of pull-out as it wasn't reported by the researchers, except for Javadian *et al.* (2016);
5. Eccentricities in the alignments of splints: Agarwal, Nanda and Maity (2014) reported that some splints failed as a result of eccentricity in the experiment;
6. The use of different concrete mixes;
7. Reducing the thickness of bamboo: Agarwal, Nanda and Maity (2014) bond results were very low relative to other researchers. They tested splints with large widths of up to 44 mm, whereas thickness was as low as 3.13 mm. Reducing the

bamboo to 3 mm in thickness eliminates most of the friction and any mechanical interlock caused by the natural variation in section along the splint.

8. Javadian *et al.* (2016) tested the bond of engineered bamboo material. The material was impregnated with epoxy using a hot-press technology. Most of the composite bamboo splints failed in tension. Therefore, the bond is underestimated. Nonetheless, untreated composite bamboo specimens achieved surprisingly much stronger bond relative to raw bamboo with or without coatings. This may be due to the improved surface condition of the composite bamboo, the enhanced resistance to moisture change and shrinkage, and the superior mechanical properties of the bamboo material in the transverse direction.

Thus far, researchers found that epoxies are the best materials they investigated for enhancing natural bamboo's bond with concrete (Ghavami, 2005; Agarwal, Nanda and Maity, 2014). A bond equal to 2.75 MPa was achieved by treating bamboo with Sikadur 32 Gel epoxy (Table 2.3). Dey and Chetia (2018) reported surprisingly high bond strength of 9.71 MPa using an epoxy treatment and steel wire. However, they did not test untreated splints to provide control and they only tested one sample per treatment. In addition, they did not report the slippage at which this remarkable bond was achieved. However, epoxies are expensive, and the cheaper Oil and bitumen-based treatments were not found effective in treating bamboo. Although Oil and bitumen-based treatments can limit shrinkage due to change in moisture, they can hamper the bond between the bamboo and the concrete by decreasing friction and chemical adhesion. They can act as a lubricant between the bamboo and the concrete, especially when ample amounts are used. Oil painted, and Black Japan treated splints have 34% and 10% lower bond strengths relative to untreated splints, respectively (see Table 2.3). Drying oils such as Linseed oil can potentially prevent moisture absorption without causing lubrication and hampering the bond with concrete.

Since mechanical interlock is the main cause of steel's excellent bond to concrete (Arel and Yazici, 2012), it is intuitive to attempt to use mechanical interlock to improve the bond of bamboo to concrete. Limited mechanical interlock already exists in bamboo without corrugation due to the presence of nodes and it is the reason for the stronger bond achieved with splints that have nodes (Table 2.3). Utilising mechanical interlock by corrugating bamboo has the potential of improving the bond by utilising the shear strength of the bamboo in the fibre direction. Bamboo shear strength is much higher relative to the bond achieved in literature. Richard (2013) reported the shear strength of Moso bamboo at 14.2 MPa. Therefore, corrugating bamboo is a possible alternative to using epoxy. Corrugation utilises the shear strength of the bamboo by using mechanical interlock. Azadeh and Kazemi (2014) studied the bond of corrugated bamboo splints theoretically. They hypothesised that corrugating bamboo would increase mechanical interlock and would prevent splitting failure by limiting the concentration of load around the nodes. However, the mechanical interlock achieved through corrugation can be diminished by the swelling and shrinkage of the splints; therefore, treating bamboo with a water repellent may be necessary to protect the mechanical interlock. In the current research, corrugation with the use of linseed oil is investigated for improving the bond of bamboo with concrete. The purpose of the linseed oil treatment is to protect the mechanical interlock by preventing swelling and shrinkage while avoiding lubrication.

Another important aspect of the bond is the estimation of the bond at longer embedment lengths. Cox and McDonald (1970) found that the average bond decreases with increased embedment length. While different treatments have been investigated in the literature for improving bamboo bond with concrete, no attempts have been made to develop a mathematical model to estimate the bond at long embedment lengths. Furthermore, no attempts have been made to model the effect of bond on the flexural capacity, cracking, and the deflection behaviour in bamboo reinforced concrete beams. In the current

research, the bond at longer embedment lengths is analysed and a model is created to predict the bond at high embedment lengths. Moreover, the effect of bond on the deflection and cracking of bamboo reinforced concrete is included in modelling.

2.3 The flexural capacity of bamboo reinforced concrete

This section presents the result of bamboo reinforced concrete beams in literature and it argues that there is a need for a better model for the flexural capacity for bamboo reinforced concrete beams. While researchers have shown repeatedly that bamboo reinforcement improves the flexural capacity relative to plain concrete, there have been few attempts to provide a model for the flexural capacity for bamboo reinforced concrete. Table 2.4 shows a range of results for bamboo reinforced beams and it makes the comparison with the theoretical bending capacity of the plain concrete section.

Table 2.4 Bending capacity of bamboo reinforced concrete beams in the literature

Beam	ρ (%)	Ultimate tensile stress (σ_{bu}) (MPa)	Plain concrete flexural capacity (TP) (KN.M)	Experimental capacity (EC) (KN.M)	EC/TP %	Bond Treatment	Stirrups
A2[1]	3.36	200.00	3.53	18.75	531.3	Water glass	Steel
A3[1]	3.40	200.00	3.07	18.75	611.4	Bitumen + Sand	Steel
B4[1]	4.85	200.00	3.78	25.20	666.4	Water glass	Steel
B5[1]	4.96	200.00	3.53	30.00	850.0	Bitumen + Sand	Steel
C6[1]	5.19	200.00	3.14	15.00	477.5	Water glass	Bamboo
C7[1]	5.18	200.00	3.40	20.50	603.6	Bitumen + Sand	Bamboo
D8[1]	5.23	200.00	3.07	19.50	635.8	Water glass	Steel
D9[1]	5.21	200.00	3.21	18.00	560.1	Bitumen + Sand	Steel
BBR1[2]	6.94	126.72	1.26	4.20	332.7	Not treated	No stirrups
BBR2[2]	7.83	126.72	1.26	6.60	522.8	Not treated	Bamboo
BBR3[2]	7.22	126.72	1.26	7.20	570.3	Not treated	Steel
BBR4[2]	7.04	126.72	1.26	6.00	475.3	Not treated	Cane
BBR5[2]	6.46	126.72	2.47	6.00	243.0	Not treated	No stirrups
BBR6[2]	6.28	126.72	2.47	14.70	595.4	Not treated	Bamboo
BBR7[2]	5.49	126.72	2.47	15.30	619.7	Not treated	Steel
BBR8[2]	6.20	126.72	2.47	10.00	405.1	Not treated	Cane
BB1[2]	7.36	126.72	0.90	2.40	266.1	Not treated	No stirrups
BB2[2]	7.07	126.72	0.90	6.60	731.7	Not treated	Bamboo
BB3[2]	6.86	126.72	0.90	7.20	798.3	Not treated	Steel

Beam	ρ (%)	Ultimate tensile stress (σ_{bu}) (MPa)	Plain concrete flexural capacity (TP) (KN.M)	Experimental capacity (EC) (KN.M)	EC/TP %	Bond Treatment	Stirrups
BB4[2]	6.80	126.72	0.90	6.60	731.7	Not treated	Cane
BB5[2]	4.47	126.72	2.14	12.00	559.7	Not treated	No stirrups
BB6[2]	4.69	126.72	2.14	13.30	620.3	Not treated	Bamboo
BB7[2]	4.90	126.72	2.14	14.00	653.0	Not treated	Steel
BB8[2]	4.17	126.72	2.14	12.70	592.3	Not treated	Cane
YA[3]	3.86	136.00	4.38	31.00	612.3	Polymer cement mortar	Bamboo
YB[3]	3.86	116.00	4.38	27.00	603.1	Polymer cement mortar	Bamboo
CG1[4]	2.42	108.30	2.29	2.2	96.1	Not treated	No stirrups
CG2[4]	3.79	108.30	2.29	4.06	177.3	Not treated	No stirrups
CG3[4]	6.16	108.30	2.29	4.4	192.1	Not treated	No stirrups
CG4[4]	2.60	108.30	1.92	4	208.1	Not treated	No stirrups
CG5[4]	4.26	108.30	1.92	4.75	247.1	Not treated	No stirrups
CG6[4]	7.50	108.30	2.32	6.75	290.8	Not treated	No stirrups
CG7[4]	2.60	108.30	2.32	4.47	192.6	Not treated	No stirrups
CG8[4]	7.50	108.30	2.32	5.85	252.0	Not treated	No stirrups
CG9[4]	2.60	108.30	1.85	4.06	219.7	Not treated	No stirrups
CG10[4]	4.26	108.30	1.85	6.13	331.8	Not treated	No stirrups
CG11[4]	7.50	108.30	1.85	7.51	406.5	Not treated	No stirrups
CG12[4]	2.66	108.30	1.85	6.13	331.8	Whole culms ends	No stirrups
CG13[4]	2.60	108.30	2.10	4.74	226.0	Not treated	No stirrups
CG14[4]	4.26	108.30	2.10	6.82	325.1	Not treated	No stirrups
CG15[4]	7.50	108.30	2.10	8.2	390.9	Not treated	No stirrups
CG16[4]	5.27	108.30	1.99	8.2	411.2	Polyester and sand	No stirrups
CG17[4]	5.27	108.30	1.99	8.9	446.3	Epoxy and sand	No stirrups
CG18[4]	5.27	108.30	2.10	8.9	424.3	Epoxy and sand	No stirrups
CG19[4]	5.27	108.30	2.10	9.59	457.2	Polyester and sand	No stirrups
CG20[4]	5.27	108.30	2.41	9.59	397.9	Whole culms ends	No stirrups

1: Sharma (1990)
2: Adom-Asamoah and Russell (2011)
3: Yamaguchi, Murakami and Takeda (2013)
4: Cox and Geymayer (1969)

Some of the researchers used bond treatment for the bamboo splints and some used stirrups to reinforce against shear. As can be seen from Table 2.4, the efficacy of bamboo reinforcement varied significantly between the researchers. This variation is partly to the use of different shear reinforcements. In Sharma (1990), the beams average experimental is 617% of the theoretical strength plain concrete strength. The beams with steel stirrups averaged 643% of the plain concrete strength, and the beams treated with bamboo stirrups averaged 541% the plain concrete capacity. Similarly, in Adom-Asamoah and Russell (2011) test results varied widely due to the use of different shear reinforcement. The

beams averaged 545% of the theoretical plain concrete flexural capacity. Beams with steel stirrups averaged 660%, beams with no stirrups averaged 350%, beams with bamboo stirrups averaged 618%, and beams with cane stirrups averaged 551%. These results indicate that bamboo is an effective shear reinforcement; albeit, not as effective as steel shear reinforcement. Similarly, Yamaguchi, Murakami and Takeda (2013) tested beams with bamboo shear reinforcement and achieved 608% of the plain concrete flexural capacity.

Cox and Geymayer (1969) used no shear reinforcement and used different bond treatments. The beams reinforced with green whole culms (CG1-CG3) achieved the worst results at 155% of the theoretical plain concrete capacity. Split seasoned culms (CG4-CG5) achieved better results at 228% and the beams with pre-soaked split seasoned bamboo reinforcement (CG6-CG11) achieved 282%. The beams with green split pre-soaked culms (CG13-CG15) achieved similar values to the seasoned pre-soaked bamboo at 314%. Only two beams were reinforced with seasoned split bamboo culms where the ends consisted of a whole culm to provide mechanical interlock (CG12 and CG20) and the beam achieved 332% and 398% of the theoretical plain concrete bending capacity at 2.67% and 5.62% reinforcement area, respectively. Beams with reinforcement treated using epoxy and sand (CG17-CG18) or polyester and sand (CG16 and CG19) achieved similar results with an average moment to theoretical plain concrete moment at 435%. Based on Cox and Geymayer (1969) result, the improvement of bond improved the beams load capacity. However, it is not clear whether the improvement was due to the prevention of bond failure or to the narrower cracks and consequently the better shear strength of the concrete.

Figure 2.2 shows that the efficacy of using bamboo reinforcement was not diminished as the bamboo reinforcement percentage increased (Table 2.4 contains the data presented in

Figure 2.2). It should be noted that Sharma (1990) and Cox and Geymayer (1969) reported the reinforcement area fraction as a percentage of the gross section. In Table 2.4 it is reported as a percentage of the effective section as it is customary in reinforced concrete.

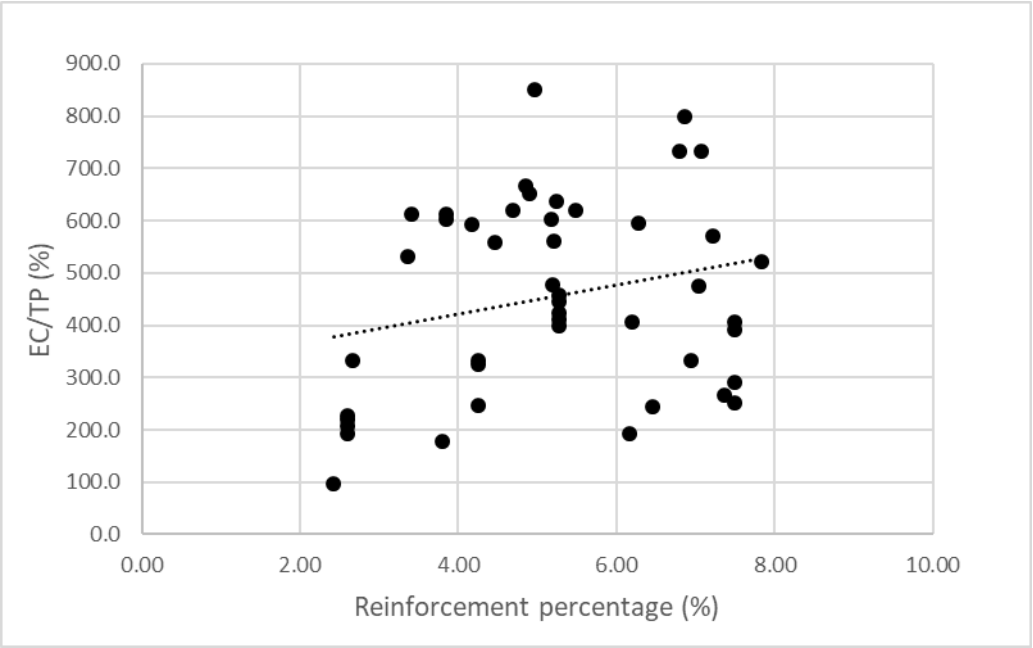

Figure 2.2 Scatter plot of reinforcement percentage VS Experimental capacity /Theoretical plain concrete capacity (EC/TP) for all beams

2.4 Modelling flexural capacity of bamboo reinforced concrete

There have been few attempts to model the flexural behaviour of bamboo reinforced concrete. The few researchers that presented models made some assumptions about bamboo reinforced concrete that does not necessarily apply to bamboo reinforced concrete beams with different bond conditions, reinforcement area, and MOE. The most important attempt to model bamboo reinforced concrete was carried by Cox and Geymayer (1969) and Cox and McDonald (1970). They carried one of the largest investigations of bamboo as reinforcement in concrete to date. They assumed that bamboo reinforced concrete is always under-reinforced because they assumed that bond failure would always take place between the bamboo and the concrete. Furthermore, they

assumed that the bond failure would allow the reinforcement to have pseudo-plastic behaviour. This assumption can be justified by their goal to provide expedient reinforcement with no bond treatment. The three methods Cox and McDonald (1970) suggested for the design of bamboo reinforced concrete are as follows:

1. Neglecting the bamboo reinforcement and assuming the ultimate load is equal to the cracking moment of the section. In this case, the bamboo only serves to provide a safety factor;
2. They proposed a method following the working stress method. They suggested allowable stress for the bamboo of 20.7 MPa;
3. Ultimate strength or limit state design. In this method, the researchers suggested that the tensile strength should not exceed 55.2 MPa. This limitation is based on the bond condition of untreated bamboo bond. However, since Cox and McDonald (1970) there have been advances in improving the bond of bamboo with concrete and considerably better treatment were found and much higher bond has been achieved since relative to the about 0.4 MPa achieved by Cox and Geymayer (1969). Therefore, the pseudo-plastic behaviour is not always valid and bond failure needs to be dealt with explicitly using a bonding model that can predict bond failure with the varying bond strengths that exist for bamboo. Moreover, this limitation does not take into account the deflection and cracking limitations which may result in non-conservative designs.

Brink and Rush (1966) made another attempt according to the working stress design method and using the results of the Clemson study and they suggested allowable tensile stress of bamboo of 27.6 MPa. Another attempt was made by Sharma (1990) where a perfect bond was assumed between the bamboo and the concrete. In addition, implicit in Sharma's (1990) analysis is that the section is always under-reinforced because the

bamboo fails in tension without bond failure and the moment level arm is equal to 0.75 of the reinforcement depth. This assumption was not justified by Sharma (1990). Similarly, Terai and Minami (2012) assumed that the bamboo would fail in tension but the moment level arm is equal to 0.9 of the reinforcement depth.

Bamboo reinforced concrete should not be; however, designed with a method analogous to steel. One of the drawbacks of bamboo relative to steel is its brittleness after it reaches the ultimate tensile stress. Similar to FRP, the brittleness of bamboo affects the moment capacity of bamboo reinforced concrete. After steel reaches the yielding point, it does not fail like bamboo and FRP. Steel undergoes a long plastic hardening phase allowing the neutral axis to become shallower reducing the area of concrete under compression. The reduction of concrete under compression allows the concrete to reach the ultimate compression stress before failure. The concrete reaches failure after providing ample warning due to excessive cracking and deflection. For this reason, the nominal capacity of steel over-reinforced beams is penalised by higher safety factors (American Concrete Institute, 2008; European Committee for Standardization, 2004). The current research investigates the design of bamboo reinforced concrete based on the FRP design approach. In addition, no method exists for the estimation of bond failure in bamboo reinforced concrete. In the current research, a method will be presented to estimate bond failure in bamboo reinforced concrete elements. The method is validated for use with bamboo reinforced concrete using the experimental results in the literature.

2.5 Modelling of indeterminate structures

While testing is usually carried on simply supported beams and slabs, for practical applications, it is often more economical to design beams and slabs as continuously supported. This serves to limit deflection and reduce the maximum moment resulting in a more economical design. One of the advantages of using steel over bamboo and FRP is

the moment redistribution in indeterminate structures (see Nanni, De Luca and Jawaheri Zadeh (2014) and American Concrete Institute (2015)). Moment redistribution allows flexural elements at points of the maximum negative or positive moment to become plastic hinges where the deflection angle increases with constant moment resistance. This can occur in steel under-reinforced beams due to the plasticity of the steel reinforcement. The result of the redistribution is reducing the maximum positive and negative moment at the cost of increasing moment at sections with a smaller moment resulting in a more efficient design (Figure 2.3). The benefit of moment redistribution is more important when multiple load cases are considered. Load cases are produced by manipulating the position of the live load along the spans to produce a moment envelope. This redistribution is, however, conservatively limited in design codes. American Concrete Institute (2008) limits the maximum moment redistribution to $1000\epsilon_s\% \leq 20\%$ of the maximum moment in steel under-reinforced beams (American Concrete Institute, 2008).

While there have been attempts to model moment redistribution in FRP reinforced beams, design codes conservatively do not permit moment redistribution in FRP reinforced concrete (El-Mogy, El-Ragaby and El-Salakawy, 2011; Gravina and Smith, 2008). Figure 2.3 shows how the negative moment is reduced in the beam due to moment redistribution. While the continuous beam can be designed as a series of simply supported beams, this would increase the moment at mid-span as shown in Figure 2.3.

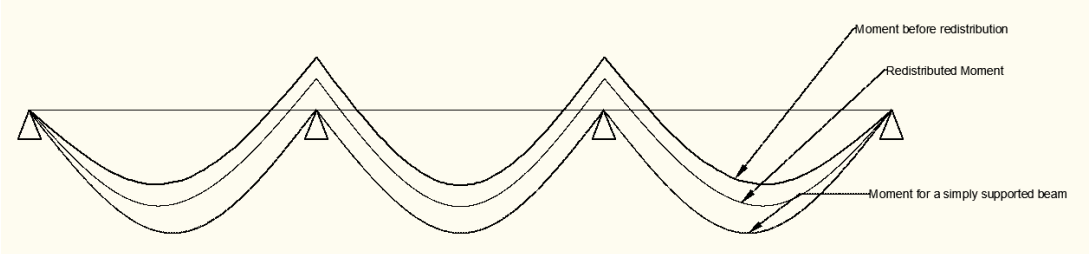

Figure 2.3 Plot of the flexural moment in a three-span continuous beam

The ductility of steel, in contrast with bamboo and FRP, allows for an overall larger margin of safety in the structure. The ductility of steel allows the redistribution of the moment when it exceeds the nominal capacity at a specific point. The formation of a plastic hinge due to the ductility of steel allows for the supports loads to be redistributed so the indeterminate structure can avoid failure. In the case of bamboo and FRP reinforced concrete failure at a specific point in the structure cannot be compensated for by moment redistribution.

An additional problem in continuous bamboo reinforced concrete is that there is no approximate method to estimate the moment along the beam. There are exact and approximate methods for determining the values of the maximum negative and positive moment along the spans of continuous flexural elements. The exact method is based on the elastic analysis of the element using the displacement method of analysis or the direct stiffness method. The same approximate method is used for FRP and steel-reinforced concrete (American Concrete Institute, 2015). While it is likely that the same approximate method can be applied to bamboo reinforced concrete, no experimental investigation exists on continuous bamboo reinforced concrete beams and slabs. Therefore, research is needed on the behaviour of indeterminate bamboo reinforced concrete beams and slabs.

2.6 Shear strength of bamboo reinforced concrete elements

The shear strength of bamboo reinforced concrete beams was modelled using assumptions that are analogous to steel reinforced concrete (see Sharma (1990), Cox and Geymayer (1969), Brink and Rush (1966), and Adom-Asamoah and Russell (2011)). In steel-reinforced concrete, the whole concrete section is assumed to transfer shear whether the concrete is cracked or not. The reason is that the cracks that develop in steel-reinforced concrete are narrow and significant mechanical interlock between the concrete at both sides of the crack exists. Similar to bamboo, with FRP reinforcement the cracks are wider;

therefore, only the uncracked concrete above the neutral axis should be assumed to transfer shear. Since the lower MOE of bamboo can result in wide cracks in comparison with steel-reinforced concrete, it is more accurate to think of the shear strength of bamboo reinforced concrete as analogous to FRP reinforced concrete where only the uncracked concrete can resist shear. The applicability of shear design analogous to FRP reinforced concrete is checked in the current research. In addition, a tentative method is made for estimating the strength of bamboo shear reinforcement.

2.7 Serviceability of bamboo reinforced concrete

Bamboo high tensile strength made it attractive to be investigated as reinforcement in concrete. The potential of replacing steel with a material that is cheap, rapidly renewable, and environmentally friendly excited researchers to carry studies on its use. However, the studies were focused on the ultimate load-carrying capacity of bamboo reinforced concrete and mostly ignored the serviceability limits. Reinforced concrete is now most commonly designed based on the limit states design method (American Concrete Institute, 2008; European Committee for Standardization, 2004). The limit state design method is based on ‘’states beyond which the structure no longer fulfils the relevant design criteria’’ (British Standards Institution, 2002). Limit states comprise of ultimate limit states and serviceability limit states. While ultimate limit states are concerned with states of collapse and failure, serviceability limit states are concerned with the service requirements of structures. British Standards Institution (2002) specifies these requirements as follows:

1. the functioning of the structure under regular use;
2. the appearance of the structure;
3. the comfort of the users.

Yamaguchi, Murakami and Takeda (2013) suggested that reducing the MOE of bamboo by 40% to account for the weaker bond of bamboo in deflection estimation. However, this approach ignores the large variability in bamboo bond properties. Brink and Rush (1966) dealt with deflection and cracking indirectly by adopting the conservative allowable stress design method. Brink and Rush (1966) recommended that the allowable stress in reinforcement should not exceed 27.6 MPa. This approach ignores the large variability of the bamboo bond. In addition, the allowable stress design method has been largely abandoned in the early sixties for the limit state design method because the latter produces more economical designs and it ‘’makes use of a more rational approach’’ (McCormac and Brown, 2014).

To design bamboo reinforced concrete according to limit states design method requires modelling deflection and cracking models. Deflection and crack control are dealt with explicitly in the limit state design method by using serviceability limits for deflection and cracking in steel and FRP reinforced concrete. Although Cox and Geymayer (1969) suggested a limit design method for bamboo reinforced concrete, they have not provided deflection and crack models. Similarly, Sharma (1990), Adom-Asamoah and Russell (2011), and Acha Navarro (2011) did not produce a method for the estimation of deflection or cracking. In the current research, a deflection model is presented that can estimate the deflection of bamboo reinforced concrete. In addition, two cracking models are validated for use in bamboo reinforced concrete.

2.8 Creep behaviour of bamboo

Creep is another long-term behaviour challenge in using bamboo as reinforcement. Creep is a permanent inelastic strain that occurs under sustained loading. If the load is large enough creep can cause the material to fail under significantly lower load relative to short-term strength. FRP reinforcement under sustained loading fails at only 30% of the short-

term strength (Nanni, De Luca and Jawaheri Zadeh, 2014). In the design of wood structures, there are methods based on abundant available data that can be used to estimate the strength at 10 or 50 years based on short-term tests (American Wood Council, 2018). The research on bamboo creep is scarce and no attempt has been carried so far to account for its effect on the long-term strength. Cox and McDonald (1970) found that the ultimate sustained tensile stress after one year is 50% of that observed in short-term tensile tests. In addition, they tested beams under sustained load and found that the beams where the reinforcement stress was up to 58 MPa survived. However, stressing the reinforcement to a higher sustained level caused failure. It should be noted that the failure might have been due to unstable creep or loss of bond through changes in moisture because the beams failed at a higher load when split culms are used relative to whole culms. In addition, Cox and McDonald (1970) believed that the crack pattern was indicative of shear failure and bond loss. The ultimate shear stress was supposed to be significantly higher based on their calculations; however, as discussed earlier in section 2.6, their shear estimation included a mistaken assumption about the shear strength of concrete when reinforced with bamboo.

In addition to strength, creep in the reinforcement can increase the deflection and cracking of the reinforced concrete. Cox and Geymayer (1969) found that the average creep factor (ratio of total strain to elastic strain) is 1.4. However, they made no attempts to control the moisture in the bamboo. Moisture content affects the creep of bamboo because, similar to wood, water acts as a plasticizer in bamboo fibre. Cox and Geymayer (1969) did not treat the bamboo against moisture and the bamboo was tested in an environment where the relative humidity varied between 24 and 75%. It should be noted, however, that Cox and Geymayer (1969) found that the creep at day 360 was not higher relative to the creep at 200 days. There are some data in the literature on bamboo creep behaviour under flexure which suggests stable secondary creep behaviour. Secondary creep is the stage at which the creep rate is minimal and minor increases in creep occur. Gottron, Harries and

Xu (2014) showed that bamboo specimens subjected to flexure show stable secondary creep behaviour where the average fractional deflection (the rate of deflection at day 90 of loading relative to instant deflection) of bamboo under flexure is equal to 1.29 (Gottron, Harries and Xu, 2014), which is significantly lower than 2.0 the maximum acceptable fractional deflection in wood (ASTM, 2015). Unlike Cox and Geymayer (1969), Gottron, Harries and Xu (2014) controlled the moisture content of the specimens at 12% during the test. It should be noted that Gottron, Harries and Xu (2014) argued that wood creep behaviour is worse compared to bamboo because its creep factor is 1.74 at 60 days compared to 1.29 for bamboo at 90 days.

While bamboo may have superior creep behaviour to wood, steel has negligible creep under normal temperatures. In addition, the creep factor for FRP is lower relative to bamboo at about 1.07 at 45 days of testing (Ascione, Berardi and D'Aponte, 2012). Similar to wood, the creep in bamboo is dependent on moisture content. Therefore, limiting the water content of bamboo is important for durability, strength, and stiffness in addition to controlling creep. Controlling the moisture content in engineered bamboo should be easier relative to natural bamboo because the bamboo is impregnated with hydrophobic epoxy materials.

In addition, choosing bamboo with high fibre volume fraction can help in limiting creep. Ma *et al.* (2016) found that creep in bamboo is strongly affected by fibre content. After 24 hours of testing the average fractional deflection was less than 1.14 for 50% fibre volume fraction compared to 1.3 at less than 30% fibre volume fraction. Ma *et al.* (2018) found that for bamboo-laminated veneer lumber exhibits 1.19 average fractional deflection when the specimens were loaded up to 50% of the maximum short-term load for 180 days. It should be noted that Ma *et al.* (2018) did not control the temperature or the relative humidity during the test; however, the bamboo was dried to 10% during the

manufacturing of the material. About 70% of the creep was recovered after the specimen was unloaded.

2.9 Durability of bamboo

While the long-term behaviour of bamboo reinforced concrete is outside the scope of this research, it was appropriate to include some discussion of long-term effects such as durability and creep to highlight the need for more research on the subject and to discourage any premature adoption of bamboo as reinforcement. Without adequate durability treatment and taking creep effects into account, the safety of the structure cannot be guaranteed in the long-term and cracking and deflection can exceed the values predicted for short-term behaviour. For common building structures, the design working life needs to be at least 50 years (British Standards Institution, 2002).

Both bamboo and wood rely on cellulose for their strength. Similar to bamboo, the biological decay of wood can be caused by fungi, insects, marine borers and bacteria (British Standards Institution, 2013). Wood is the oldest construction material. The durability of wood depends largely on the environment surrounding it. Under the right conditions, wood service life has been known to exceed 500 years (Bijen, 2003). However, bamboo have a higher starch content, which can make it more vulnerable to biological attack if not treated. According to Janssen (2000), bamboo lacks certain chemicals that make wood more durable. However, it should be noted that bamboo species vary in their durability against fungi. Wei, Schmidt and Liese (2013) tested six bamboo species following the European standards wood durability standards EN 350-1, EN 350-2, and EN 113. They investigated ten strains of fungi that belong to Brown-rot fungi, white-rot fungi, and soft-rot fungi. All the bamboo species that the researchers tested were durable against most of the strains. For most of the strains, the species were classified into class II (durable according to the European five-scale standard). For one

strain of soft-rot fungus the bamboo species were grouped into class II and class III (moderately durable), for another strain of white-rot the bamboo species were grouped into class II, class III, and class IV (little durable). Fungi require at least a water content of 22% to rot wood (Bijen, 2003). It is not known how low the moisture content needs to be to protect bamboo against fungi. In addition, it is not clear how embedment inside concrete affect the bamboo durability against fungi.

Protective finishes and coatings can improve bamboo durability against fungi by protecting it from moisture (Bijen, 2003). Heat treatment is another option for treatment against biological decay. Heat treatment improves bamboo durability against insects and fungi. Wahab *et al.* (2005) found that ninety minutes of heat treatment at 180^{o} and 220^{o} C reduced the weight loss due to biological attack from 48% to 11% and 5%, respectively. However, heat treatment affects the mechanical properties of bamboo negatively. Wahab *et al.* (2005) found that their heat treatment reduced the modulus of rupture from 174 MPa to 152 MPa and 132 MPa, respectively. Similarly, Bui, Grillet and Tran (2017) found that heat treatment at 180^{o} for 60-120 minutes improved the durability of bamboo against fungi by destroying the starch and protein content. It has been suggested that engineered bamboo can provide a solution for the problem of durability by limiting water absorption and protecting the bamboo fibre from the alkalinity of the concrete. Wood-plastic composites made from wood flour or bamboo flour and thermoplastic resins do degrade as a result of fungi attack. However, their degradation is assisted by abiotic factors such as UV light, moisture, Oxygen, freeze-thaw and soil (Feng *et al.*, 2017). The embedment of bamboo inside concrete can help mitigate these abiotic factors.

Biocides are the most effective in treating bamboo against fungi. Sun *et al.* (2012) tested the efficacy of the low-toxic preservative Chitosan-copper complex and organic fungicides for use on Moso bamboo splints with dimensions of 50 mm by 20 mm by

5mm. The treatment included dipping the bamboo in the fungicide for 30 minutes. The specimens were incubated in a temperature of 28^{o} and relative humidity of 90% for 28 days to accelerate the growth of fungi. Sun *et al.* (2012) found that the combination of Chitosan-copper complex and propiconazole was the most effective and significantly improved the resistance of bamboo against fungi. While the untreated bamboo specimens had over 75% of the surface area infected with the fungi after only 2 days, the treated bamboo specimens had less than 25% of the surface area infected after 28 days of incubation. Other biocides such as DCOIT and zinc pyrithione were found effective in treating bamboo-plastic composites against fungi. Feng *et al.* (2017) found that using these Biocides resulted in no weight loss due to fungi. More research is needed on the efficacy of biocides in resisting fungi in bamboo reinforcement under long-term conditions.

The use of bamboo as reinforcement in concrete presents an additional concern with regards to its durability against the alkalinity of the concrete. While the concrete may protect bamboo reinforcement against weathering, insects, and marine organisms if cracking is controlled, the alkalinity of concrete can degrade bamboo fibre. Ramakrishna and Sundararajan (2005) found that the tensile strength of vegetable fibres, i.e. Hibiscus cannabinus, coir, jute, and to a lesser extent Sisal fibre, was degraded by immersion in alkaline solutions (calcium hydroxide and sodium hydroxide). Similarly, Kriker *et al.* (2008) found that date palm fibre tensile resistance is degraded by the alkalinity of concrete. In addition, Tolêdo Filho *et al.* (2000) found that the tensile strength of coconut and sisal fibres are degraded by the immersion in alkaline solutions of calcium hydroxide and sodium hydroxide.

However, although organic fibres do degrade inside concrete, their surface area is much larger relative to its volume when compared to bamboo splints. For example, the diameter

of the fibre Tolêdo Filho *et al.* (2000) used is 0.08-0.30 and 0.11-0.53 mm for sisal and coconut fibre, respectively. Bamboo splints used as reinforcement in concrete have significantly larger dimensions (in the current research, the average splint thickness is 7.8 mm) which can mitigate the alkalinity problem. Lima Jr *et al.*, (2008) tested bamboo splints after it was immersed in a pH 12.8 solution of calcium hydroxide, and tested bamboo that was embedded in concrete prisms that were submerged in tap water. The bamboo was tested after 60 cycles of 24 hours. These extreme conditions were used to accelerate degradation and provide an indication of the behaviour in the long-term. The strength of bamboo was not affected by the severe conditions. Using scanning electron micrographs, Lima Jr *et al.*, (2008) found that only the fibres close to the splint surface showed some alteration due to calcium hydroxide deposition. Lima Jr *et al.*, (2008) attributed the resistance to alkalinity to the fact that the ‘’bamboo fibres are completely encased into the parenchyma and they are not directly exposed to the alkalinity of the cementitious matrix’’. Similarly, Terai and Minami (2012) found that bamboo tensile strength was not degraded by the alkalinity of the concrete after 84 days of exposure. Terai and Minami (2012) made tensile specimens from culms that were filled with concrete.

The Clemson study, as reported by Cox and Geymayer (1969), provides a rare case of building structures with bamboo as reinforcement. Their study can help shed light on the long-term durability of bamboo inside concrete. Three structures were built using Green, unseasoned, and seasoned bamboo. In the planer building, some of the structure failed and the failure was attributed to an error in weighing the concrete mix, the improper placing of the reinforcement, and faulty design. The press box structure was demolished after 15 years to enlarge the stadium. The press box was in ‘’excellent condition’’ after 15 years from building and the bamboo encased in concrete was in good condition (Cox and Geymayer, 1969). However, the bamboo that was subjected to air and moisture was

completely deteriorated. In the five-room residence ‘’all structural members, except the roof beam and girders, were performing satisfactorily’’ and ‘’the roof beam and girders required additional reinforcement with steel channels within 1 year’’ (Cox and Geymayer, 1969). This may be due to the week bond achieved by using whole culm bamboo, biological decay, or creep.

2.10 Summary

Bamboo has a remarkable tensile strength that made it attractive to be investigated as reinforcement in concrete. However, a grading system needs to be established for bamboo before it can be used in engineering applications. Engineered bamboo provides advantages over natural bamboo including a more uniform behaviour. However, it comes with increased cost and it is not clear whether it can be economically viable in the future.

The bond between bamboo and concrete is an important problem in the use of bamboo as reinforcement. Without a strong bond, there can be no transfer of stress between the bamboo and the concrete which renders the reinforcement ineffectual. Although there have been advances in treating bamboo for bond purposes, it is not clear how these advancements would translate into the improvement of bamboo reinforced concrete flexural capacity. While it has been shown repeatedly that bamboo can improve the flexural capacity in comparison with plain concrete, there are deficiencies in the modelling of bamboo reinforced concrete in flexure. The brittleness of bamboo has not been accounted for in modelling the flexural capacity. Similarly, the methods suggested for modelling the shear capacity of concrete in previous researches were analogous to steel-reinforced concrete and consequently, they can result in the overestimation of shear capacity in design. In addition, the brittleness can affect the effectiveness of bamboo as reinforcement in indeterminate structures where moment redistribution cannot be allowed. Furthermore, the brittleness of bamboo makes its use as reinforcement in

concrete in seismically active countries unadvisable. Ductility in the structure is needed to absorb the dynamic energy of lateral seismic loading.

For long term behaviour, creep and durability are the other two concerns that present themselves. Creep of bamboo is another mechanical behaviour concern that should be taken into consideration when designing bamboo reinforced concrete. More research is needed on bamboo creep under direct tensile load at different stress levels, moisture, and fibre contents. The durability of bamboo is an important non-mechanical long-term concern. More research is needed on effective treatments before it can be safely used in long-term applications.

Chapter 3

3. Methodology

3.1 Introduction

This chapter presents the methodology of the current research. Section 3.2 summarises the gaps which the current research fills. Section 3.3 presents the bond testing method used in the current research including an explanation of the sample size. Section 3.4 presents the flexural testing method of bamboo reinforced concrete beams. Section 3.5 presents the statistical methods used in the current research to analyse the results. Section 3.6 explains the use of the FE method in the current research.

3.2 Gaps in the literature that this research fills and the methodology structure

With regards to the use of bamboo as reinforcement in concrete, there are significant gaps in the literature. The gaps that the current research addresses and the methods used for filling the gaps are summarized as follows:

1. No experimental investigation exists on using mechanical interlock via corrugation to improve the bond of bamboo reinforcement to concrete. Pull-out testing is carried on corrugated bamboo specimens with different corrugation patterns with or without the use of linseed treatment to limit swelling and shrinkage. In addition, a theoretical model for the estimation of bond in corrugated bamboo under short-embedment lengths is created and validated using the experimental results. Statistical analysis is used to establish that corrugation and

water-proofing the bamboo using linseed oil significantly improves the bond of corrugated bamboo.

2. There are currently no bond failure models for bamboo reinforced concrete. Using the experimental results of the current research and the results from the literature, a method is validated for the estimation of bond failure.
3. The flexural capacity models in literature have deficiencies in modelling bamboo reinforced concrete. A method analogous to FRP reinforced concrete is proposed and validated using the experimental results in the literature and the current research.
4. It is not clear how the use of bamboo reinforcement can affect the shear strength of concrete. The experimental results in the literature are used to validate the assumption that only uncracked concrete can transfer shear similar in FRP reinforced concrete.
5. There are currently no models for the deflection behaviour of bamboo reinforced concrete. A theoretical model is created with the help of FE analysis results and the theoretical model is validated using the experimental results carried during this research and the experimental results in the literature.
6. There are currently no models for the cracking behaviour of bamboo reinforced concrete and there is no experimental data on crack widths in literature. Cracks are measured during the beams testing and the results are used to validate and adjust existing cracking models for use in bamboo reinforced concrete beams.

Figure 3.1 shows a diagram that reveals the structure of methods used in the current research to help the reader understand how the different methods interrelate to each other.

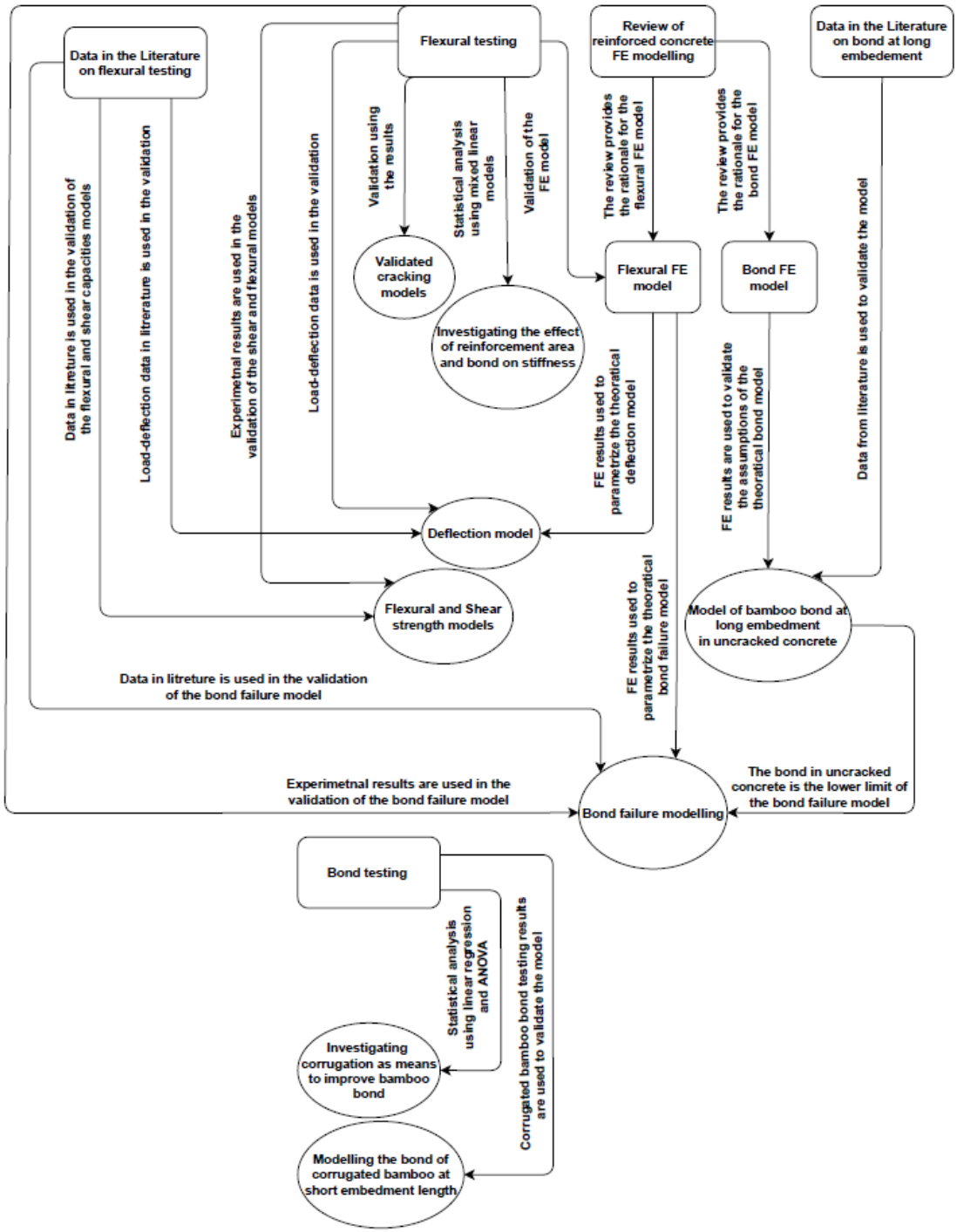

Figure 3.1 Diagram of the research methodology structure

3.3 Bond testing

The main purpose of this test is to investigate whether corrugation is effective in improving bamboo bond to concrete. The pull-out test was used in the current research to test the bond of corrugated and uncorrugated bamboo specimens. In addition, some of the splints were treated with linseed oil to reduce water absorption and protect mechanical interlock. The pull-out test is commonly used for testing the bond of steel and FRP (Fibre Reinforced Polymers) rebars to concrete (Wambeke and Shield, 2006; ASTM, 2014). The pull-out test does not accurately estimate the bond between the reinforcement and the concrete in structural elements because the embedment length of rebars inside the structural elements is much higher than the embedment lengths in the pull-out test. However, the pull-out test is useful for comparing the bond of different rebars and different treatments (Wambeke and Shield, 2006; ASTM, 2014).

In the current investigation, all the bamboo splints were taken from a single Moso bamboo culm to minimize variability due to different bamboo mechanical properties. The culm was 3-4 years old according to the supplier. All the concrete mixes had equal proportions to limit the number of variables that affect the results. Linseed oil treatment was investigated to waterproof corrugated and non-corrugated bamboo splints to limit shrinkage and improve the mechanical interlock. Linseed oil was investigated because it is a drying oil, not a lubricant; therefore, it would not hamper the friction between the bamboo and the concrete. Humar and Lesar (2013) found that linseed oil reduces short-term water uptake significantly. While waxes are superior to linseed in waterproofing wood (see Lozhechnikova *et al.* (2015), they were not investigated to avoid hampering the bond with the concrete. Furthermore, testing a waterproofing material against water submersion or exposure does not necessarily reflect the water uptake in fresh concrete. Water in concrete is partially bound to cement.

For a strong bond with concrete, the projection should be the least amount that provides adequate mechanical interlock. Determining this amount of projection theoretically is not simple. As the mechanical interlock can be diminished by the Poisson's effect due to tension in the reinforcement, shrinkage, and most importantly the normal forces from the concrete on the bamboo in the transverse direction to the fibre. Therefore, two levels of projection (P) are investigated, 1 and 2mm with or without linseed treatment. The notches were staggered to provide a more uniform bond transfer along the splint and to limit stress concentration in the bamboo (Figure 3.2). In addition, different ratios B:A were investigated to achieve failure in the concrete or the bamboo.

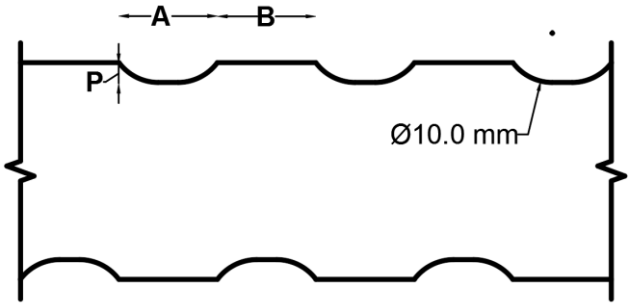

Figure 3.2 Illustration of the general pattern of corrugation

The next two subsections discuss how the sample size was determined and the modelling of bamboo bond with concrete.

3.3.1 Determination of sample size

A factorial study was designed to investigate the effect of corrugation on bamboo bond with concrete with or without the use of linseed treatment with two levels for the linseed treatment and three for the projection. Factorial design is a technique that enables the investigation of several independent variables main effects (at least two) and their interactions on the dependent variable. For each of the variables, two or more levels for the variable can be included in the investigation. The advantages of factorial designs over one factor at a time designs are that they are more efficient and can detect interactions

between the dependent variables. The minimum number of replicates in a factorial design is 2 (see chapter 14 in Montgomery (2003)). The limit of 2 is to get an estimate for variation within groups. In previous researches on bamboo bond with concrete, Kute and Wakchaure (2013), Dey and Chetia (2018), and Ghavami (1995) chose to carry unreplicated studies with one replicate for each treatment they tested. While testing with one replicate can indicate the effectiveness of a treatment relative to other treatments, it does not statistically prove that one treatment is better than the other. By contrast, Cox and Geymayer (1969) number of replicates varied between 1 and 10 for the bond treatments they tested. Agarwal, Nanda and Maity (2014) produced three replicates for every treatment they tested while Javadian *et al.* (2016) produced five replicates for every treatment they tested. In the pull-out testing of FRP reinforcement, it is common practice to test three pull-out samples for every treatment. Wang and Belarbi (2010) and Baena *et al.* (2009) used three replicates for every case they tested. Similarly, Rami Hamad, Megat Johari and Haddad (2017) tested three replicates of FRP reinforcement at different temperatures. On the other hand, Rolland *et al.* (2018) tested four samples for every FRP reinforcement type they tested while Li *et al.* (2018) tested two specimens for every case.

Moreover, determining the number of replicates in a study depends on the statistical power required in the investigation. Statistical power is the probability that a certain effect size can be detected using a specific number of samples. Bahçecitapar, Karadağ, and Aktas (2016) summarised the parameters that affect statistical power in a factorial study by the following:

1- standard deviation within groups;
2- the maximum difference between the means of the main effects;
3- number of replicates;
4- number of levels for factors;

5- and the significance level required (p-values of 0.01, 0.05, or 0.1).

As the maximum difference between the means of the main effects increases, the power of the statistical test increases and the probability that the effect is detectable increases. Higher values of the standard deviation within a group reduce the statistical power and more replicates are needed to prove significance. The effect size in a t-test can be found using equation 3.1. The effect size for an ANOVA (Analysis of variance) test can be found using equation 3.2 (Cohen, 1989). It should be noted that at the stage of study design, determining the values of the size effect and the standard deviation is not possible because no experimental data has been collected yet. Therefore, it is common practice to anticipate the size of the response to determine the size of the samples (Cohen, 1989).

$$d' = \frac{m_2 - m_1}{\sigma'} \qquad 3.1$$

$$f' = \frac{d'}{2}\sqrt{\frac{k+1}{3(k-1)}} \qquad 3.2$$

Where:
d' = the effect size in the t-tests
m_1 = minimum response
m_2 = maximum response
σ' = standard deviation within the group
f' = the effect size in the ANOVA tests
k = the number of levels

The bond results for corrugated bamboo can be roughly but conservatively anticipated at 2 MPa based solely on the shear strength of the bamboo at 14 MPa and no friction, B:A ratio of 1:1 (only half of the bamboo can be utilised in shear), and specimens with 8 mm thickness and 20 mm width ($14 \times \frac{8}{2}/(20+8) = 2$). Similarly, the standard deviation is not known. Therefore, the standard error based on the results provided by Cox and McDonald (1970) at 18.7% is used to roughly estimate the standard deviation. Taking the bond of non-corrugated bamboo at 1 MPa based conservatively on untreated bamboo in

previous research would yield d' result of 3.57 ($\frac{2-1}{0.187*1.5} = 3.57$) using equation 3.1. Taking the bond of non-corrugated bamboo at 1 MPa is conservative here because it minimizes d' and would result in a higher replicate number. Using the value of d' and equation 3.2 the value of f' can be evaluated at 1.46. After determining the effect size (f'), the number of samples required to prove significance can be found using the power tables provided by Cohen (1989) or by using a software package such as G*Power. It should be noted that the tables provided by Cohen (1989) go up to 0.8 effect size because the effect sizes encountered in behavioural sciences, which is the main focus of the book, are usually smaller than that here and in other engineering investigations. Therefore, using G*power software package, it was found that using three replicates would yield the statistical power of 85%. It should be noted that the statistical power of 85% is conventionally used. The statistical power simply means that there is an 85% probability that the effect is detectable at 0.05 p-value with three samples per case.

Therefore, three replicates are made for each case (P1-P18) (Table 3.1 presents the design of the pull-out study). Another dimension that has been investigated is the bamboo width to the concrete width (B:A ratio) using one variable at a time approach. To investigate the effect of pattern another 6 specimens were tested; three with B:A ratio of 1:1.5 and three with the 1.5:1 ratio.

Table 3.1 The design of the bond study

Specimen	Linseed treatment (Tr)	Projection	Pattern (B:A)
P1	-	0	-
P2	-	0	-
P3	-	0	-
P4	Tr	0	-
P5	Tr	0	-
P6	Tr	0	-
P7	-	1	1:1
P8	-	1	1:1
P9	-	1	1:1
P10	Tr	1	1:1
P11	Tr	1	1:1
P12	Tr	1	1:1
P13	-	2	1:1
P14	-	2	1:1
P15	-	2	1:1
P16	Tr	2	1:1
P17	Tr	2	1:1
P18	Tr	2	1:1
P19	Tr	2	1.5:1
P20	Tr	2	1.5:1
P21	Tr	2	1.5:1
P22	Tr	2	1:1.5
P23	Tr	2	1:1.5
P24	Tr	2	1:1.5

An alternative design to the study would have been to include pattern in the factorial study. This would have increased the total number of specimens to 36 specimens and the additional specimens would have had 1:1.5 and 1.5:1 ratio at 1 mm projection with and without linseed treatment. However, this was rejected because adding these specimens would have entailed adding 50% more specimens in the hope that 1 mm projection would be sufficient for mechanical interlock. In other words, if the projection of 1 mm was not sufficient for mechanical interlock to develop, the results from the additional specimens would have not been useful in establishing the effect of pattern on bond.

3.3.2 The theoretical models for the bamboo bond at short and long embedment lengths

The experimental results from the pull-out testing of corrugated bamboo are used to validate a theoretical model for the bond of corrugated bamboo at short embedment lengths (100 mm). The model is based on the assumption of perfect mechanical interlock.

It uses the shear strength of the bamboo and the shear friction of the concrete to estimate the bond of corrugated bamboo at short embedment lengths.

In addition, a theoretical model to estimate bond at higher embedment lengths is created and validated using the experimental results of Cox and Geymayer (1969) and the FE results. The lower modulus of elasticity of bamboo relative to that of steel can contribute to its weaker bond to concrete at longer embedment lengths. The data provided by Cox and McDonald (1970) show that the average bond decreases with the increase of bond. The bond of splints with 152 mm embedment is double the bond of reinforcements with 304 mm embedment. Similarly, the decrease in the average bond as embedment increases is observed in FRP reinforcement (Wambeke and Shield, 2006). In the pull-out test, FRP shows a relatively high discrepancy between the slip at the loaded end and the free-end compared to steel. This is attributed to the lower modulus of elasticity of FRP relative to steel (Focacci, Nanni and Bakis, 2000). Bamboo has a low modulus of elasticity relative to steel. Therefore, it is expected that bamboo would have a large difference between the slippage at the loaded end and the free-end. This effect is more pronounced with large embedment lengths. This is important because the bond at any point in the embedded length increases to a maximum value then decreases (see Figure 3.3). Varying slip along the embedded length causes consecutive debonding beginning at the loaded end and moving towards the free-end (Altalmas, El Refai and Abed, 2015). Consecutive debonding results in an overall lower average bond strength. With FRP reinforcement the bond is expressed as a function of bar diameter. However, a similar approach with bamboo reinforcement is not possible due to the large variability of geometry and mechanical properties in bamboo. Therefore, a theoretical model is developed that can account for the effect of MOE on bond at large embedment lengths in bamboo reinforced concrete.

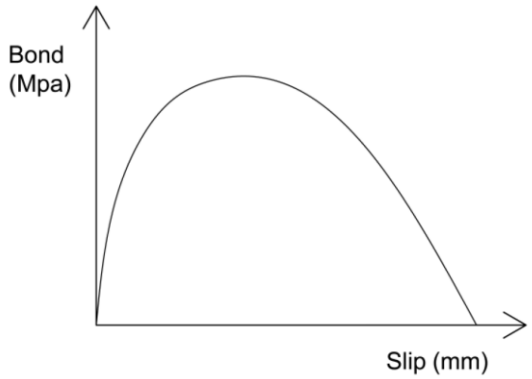

Figure 3.3 Plot of the modified Bertero-Eligehausen-Popov bond-slip relationship (adapted from Focacci, Nanni and Bakis (2000))

3.4 Flexural testing of bamboo reinforced beams

Flexural testing is carried in the current investigation to model the deflection of bamboo reinforced concrete at varying levels of reinforcement area and bond. In addition, the effect of bamboo compression reinforcement on stiffness is investigated. Moreover, the flexural testing was used to evaluate the flexural capacity of bamboo reinforced concrete without shear or bond failure. While some researchers used bond treatment for bamboo and steel stirrups before, none of the researchers tested beams with steel stirrups and adequate bond treatment simultaneously. Sharma (1990) used steel stirrups and treated the splints using water glass and bitumen; however, they did not test the bond. Therefore, it is not clear how strong the bond was between the splints and concrete and the cause of failure. Adom-Asamoah and Russell (2011) did not treat the splints for bond purposes. Yamaguchi, Murakami and Takeda (2013) used bamboo stirrups but did not treat the bamboo for the bond. By contrast, Cox and Geymayer (1969) treated the splints for the bond but did not use any stirrups.

This is an important gap because providing adequate bond and shear reinforcement allows the isolation of the bending behaviour and consequently it allows for the modelling of the flexural capacity of the section without shear and bond failures. In the current research,

the corrugation is used to prevent bond failure and steel stirrups are used to avoid shear failure. In addition, different levels of reinforcement areas were investigated where higher reinforcement areas were used to prove that compression failure can occur in bamboo reinforced concrete.

Another important gap in the literature is the lack of adequate data on cracks in bamboo reinforced concrete. Except for Adom-Asamoah and Russell (2011), none of the previous researches measured the crack widths in bamboo reinforced concrete. However, Adom-Asamoah and Russell (2011) did not report the loads at which the cracks were measured. In the current investigation, cracks were measured and the results were used to validate theoretical models for cracking.

3.5 Statistical analysis

In this section, the statistical models used in the current research are reviewed and their assumptions and limitations are discussed.

3.5.1 Analysis of Variance (ANOVA)

Two-way ANOVA is used to analyse the results of the bond testing. SPSS software package was used to perform the statistical test. The dependent variable is bond and the independent variables are projection and linseed treatment. Another one-way ANOVA test was used to analyse pattern. Unlike one-way ANOVA, two-way ANOVA can include more than one independent variable. Equation 3.3 presents the model for a general two-way design. In ANOVA, the residuals are assumed to be normally distributed. Therefore, this assumption is checked to ensure the validity of the model.

$$Y = \mu + \alpha + \beta + \alpha\beta + \varepsilon \qquad 3.3$$

Where:
Y = the dependent variable (bond)
α = main effect of corrugation
β = main effect of linseed treatment
$\alpha\beta$= the interaction of the main effects
ε = the residual

3.5.2 Linear regression analysis

In addition to two-way ANOVA, linear regression was used to determine the statistical significance of the different variables of corrugating bamboo using the SPSS software package. Since linear regression models covariates, it has an advantage here over ANOVA because it can delineate the different effects of thickness and width on bond in corrugated bamboo. In corrugated bamboo, thickness has a larger effect on the bond because corrugation is on the thickness side. Linear regression has been used in the estimation of bond in steel-reinforced concrete. Orangun, Jirsa and Breen (1977) regressed the normalised bond using the variables of the ratio of concrete cover to steel reinforcement diameter and the ratio of the reinforcement diameter to the splice length. Orangun, Jirsa and Breen (1977) regression became the basis for development length model recommended in the ACI code (American Concrete Institute, 2008). Dey and Chetia (2018) used linear regression to model the effects of the bond, curing period, and bar size on beams flexural strength.

Linear regression, as presented in equation 3.4, is used to determine the statistical significance of independent variables (x**)** on a dependent variable (Y**)**. In the current research, the dependent variable is load, and the independent variables are as follows:

1. Linseed treatment;
2. Width;
3. Thickness;
4. Projection;

5. Pattern.

$$Y = \beta_0 + x_1\beta_1 + \cdots + x_n\beta_n + \varepsilon \qquad 3.4$$

The least-squares method is used to determine the values of the parameters (β_n) that minimises the sum of squared errors. The least-squares method essentially draws a line of best fit. This line is defined as the line where the square sum of the difference between the dots and the line is minimised. Linear regression assumes that the errors (ε) (residuals) are normally distributed and statistically independent with mean equal to zero (Montgomery, 2003). In linear regression, the null hypothesis is that β_n is equal to zero. Meaning, it has no effect on the dependent variable. A larger value of β_n means that the independent variable has a more substantial impact on the dependent variable.

The t-test is used in the linear regression to test the probability that β_n is equal to zero (the null hypothesis) and safeguards against Type I error. Type I error occurs when an independent variable is mistakenly considered significant. A probability of less than 5% is considered to prove that the effect is significant. Unlike the z-distribution, the t-distribution have wider tails for smaller sample numbers (degrees of freedom). Meaning it is harder to prove significance when the sample number is lower. The t-test yields the same results as the z-test when the sample number becomes over 30.

The fit of the model to the data set is determined using R^2. It represents the percentage of variance that is explained by the model to the total variance and it has an upper value of one. When a large number of independent variables are used, R^2 can be overestimated due to overfitting the model. The adjusted R^2 value prevents the overfitting of the model by adjusting for the effect of the independent variable on the error. Meaning, the independent variable is only assumed to enhance the model if the residual mean square is reduced. Austin and Steyerberg (2015) suggested that the adjusted R^2 should be used

when SPV (Subjects per Variable) is low. The reason is that the R^2 can be biased when the SPV number is small; however, minimal bias is observed with the adjusted R^2 over the range of 2-50 SPV values. Austin and Steyerberg (2015) found that an SPV value as low as two was sufficient for accurate estimation of the regression coefficients, standard errors and confidence intervals in a linear model.

3.5.3 Mixed linear models

The purpose of this statistical analysis is to investigate the effect of reinforcement area, bond, compression reinforcement on beam stiffness. The mixed linear model was needed to analyse the load-deflection behaviour because repeated measurements were taken on every beam. Linear regression cannot be used because one of the assumptions of linear regression is violated. The repeated measurements at different deflection values are not independent and independence of measurements is assumed in linear regression (Landau and Everitt, 2003). Simply put, there is a correlation between the measurements for the same beam where if a beam achieved high result at one deflection level it is more likely that it will achieve high values at other deflection levels. Mixed linear models can be used in studies where multiple measurements are taken for each subject (Fox, 2016). Mixed linear models have random effects (μ) in addition to the fixed effects used in linear models (equation 3.5). The random variable represents the deviation for any particular member from the group mean.

$$Y = \beta_0 + \beta_1 Compression\ Group + \cdots + x_n\beta_n + \varepsilon + u \qquad 3.5$$

Another approach for dealing with repeated measures is to use the general linear model in SPSS and add a categorical factor where every beam has a unique categorical value. Unlike mixed linear models, this general linear model does not assume the distribution of the beams results around groups' mean. Although this procedure fixes the problem of

correlated errors between the random effects, this method is weaker and can result in a falsely insignificant result. Instead, the mixed linear model defines a random variable (u) around the group intercept to represent the dispersion of the intercepts of the beams around the group mean reducing the number of variables in the model. Finally, the assumptions of normality of the random variable and the residuals are checked to confirm the validity of the results.

There are different types of covariance structures that can be used with mixed linear models. The following covariance matrices were investigated and their applicability to the experimental results was checked:

1. scaled identity;
2. diagonal;
3. compound symmetry;
4. heterogeneous compound symmetry;
5. unstructured.

Scaled identity variance matrix assumes that all of the residual's variance is independent and that they are equal. This assumption, however, is very restrictive. Compound symmetry matrix assumes equal variance and constant correlation of variance along the different times. Unstructured matrix is the least restrictive and the most complex matrix and it makes no assumptions about variance and the correlation at different times; therefore, it should provide the best fit for the model. However, it has the largest number of parameters. Consequently, it is harder to prove significance. The compound symmetry and the heterogeneous compound symmetry both assume a constant correlation between the residuals at different times. But they differ in that the earlier one assumes homogeneous variance and the later assumes heterogeneous variance (see IBM Knowledge Center (2019)).

It should be noted that the purpose of the mixed linear model is not to provide a theoretical model for the estimation of deflection. The main purpose of the mixed linear model is to investigate the significance of the reinforcement area and bond on flexural stiffness. Additionally, the effect of bond and reinforcement area on flexural stiffness is shown by the FE model results.

3.6 FE modelling of bamboo reinforced concrete

In the current research, a finite element model is presented for bamboo reinforced concrete. The model is validated using the experimental results produced in the current research. Then the model is used to expand the scope of the research to different reinforcement areas and different bond conditions. A theoretical model for deflection is produced with the help of the FE results. In addition, the FE model is used to produce a theoretical model for bond failure in flexural elements. It should be noted that the theoretical models produced with the help of the FE model are then validated using the experimental results from the literature with wider range relative to the reinforcement areas used in the current research.

While extrapolation based solely on statistical modelling is not allowed, FE models are regularly used to extrapolate beyond the scope of the experimental data and to carry FE parametric studies. FE was developed to solve complex continuum problems. Discretization in FE serves to simplify the geometry by using simple elements where strain can be more easily related to nodal displacement. In addition, the complex material behaviour is approximated to relate the strain in the elements to stiffness. Therefore, the accuracy of an FE model is dependent on the accuracy of the material model and the accuracy of the elements used to represent the continuum structure. Since increasing or decreasing the bamboo in the section has no bearing on the accuracy of materials models or the accuracy of the elements, it is reasonable to extrapolate the area of bamboo beyond

the set of data that have been experimentally tested. The next chapter discusses the different FE elements and different concrete model that are used in reinforced concrete FE modelling. Statistical modelling has a completely different approach which makes extrapolation questionable. Extrapolating using a statistical model assumes that the trend observed on the range of the tested data does not change outside the range of measured data. However, this assumption can only be justified based on the physical nature of the problem.

Here three examples are cited from the FE literature on the use of FE models to carry parametric studies and extrapolate beyond the range of the experimental data as follows:

1. An (2015) carried a parametric study that investigated the influence of varying degrees of FRP stiffness, concrete strengths, and FRP-concrete width ratio on the fracture energy, slip at maximum bond, and maximum bond stress. An (2015) used the experimental results provided by Yao, Teng and Chen (2005) and expanded the scope of the research to parameter values significantly higher and lower relative to the experiments.
2. Tsavdaridis and Papadopoulos (2016) carried a parametric study to investigate the effect of reduced web sections on the stress distribution and performance in steel beams. The study included varying the distance of the first web opening and the spacing of openings. It should be noted that the FE model was validated using the experimental results of Maggi *et al.* (2005) which had no openings or reduction in the beams' sections.
3. Ziari and Kianoush (2014) validated their FE model using the experimental results of Kankam (1997). Using the FE model, Ziari and Kianoush (2014) carried a parametric study on the effect of the ratio of clear concrete cover to steel bar diameter on the longitudinal bond between the reinforcement and the concrete.

The study of Kankam (1997) included constant clear concrete cover to the steel bar diameter ratio and no confinement for the concrete. Nonetheless, Ziari and Kianoush (2014) varied the ratio of clear concrete cover to the steel bar diameter to investigate its effect on the longitudinal bond. Furthermore, they investigated the effect of confinement on the longitudinal bond.

A different approach would have been to test a large number of beams using different bonds and reinforcement areas and validate the theoretical model using only the experimental results. However, this approach is considerably labour intensive and it requires many hours of technical support. Furthermore, controlling the bond in experiments is difficult. However, it should be noted that the current experimental program is amongst the largest in the bamboo reinforced concrete literature.

Chapter 4

4. Review of Reinforced Concrete Finite Element Modelling

4.1 Introduction

In this chapter, Finite Element (FE) modelling is reviewed to provide the background and explain the rationale for the choices made in developing the FE model. Section 4.2 briefly reviews the commonly used constitutive models and FE elements for reinforced concrete beams. In addition, it discusses their relative advantages and disadvantages. Section 4.3 discusses the cracking behaviour of concrete and cracking models. Modelling the bond between the reinforcement and the concrete is reviewed in Section 4.4. The solution procedures of nonlinear finite element systems and the convergence issues are discussed in Section 4.5. Section 4.6 presents the FE model of bamboo reinforced concrete in the current research. Section 4.6.4 provides a discussion of the limitations of the suggested FE model.

4.2 Constitutive models and choosing the FE elements

The purpose of constitutive models is to approximate the complex behaviour of materials. Constitutive models are built with assumptions about the behaviour of the materials, and it is essential to understand these assumptions and their limitations to avoid inaccurate results. In addition, it is better to use the least complex constitutive model that provides accurate results for the practical purposes of the modelling. This is to reduce the computational cost of the model and avoid overcomplicating the problem needlessly. Similarly, the type of elements used to model the materials should not increase the

computational cost unnecessarily; therefore, elements with less computational cost are preferable if they can serve the purpose of the investigation.

In the case of reinforced concrete, there are two materials in question: the reinforcement and the concrete. Researchers usually model reinforcement using truss elements (see Appendix A) because reinforcement behaviour is mainly uniaxial. In addition, truss elements have less computational cost relative to the beam, plane, and 3D elements. For concrete, 2D and 3D elements have been used to model the concrete (see Appendix A). If there is no particular need, 2D elements are preferable. 3D elements are less commonly used unless there is a specific need, for example, to investigate the effect of reinforcement cover on beams' behaviour (Jason *et a.l*, 2013). Two-dimensional elements are more prevalent in modelling concrete beams because of three following reasons:

1. They have significantly less computational cost than three-dimensional elements;
2. The loads in beams are mainly biaxial;
3. Crack models work better with planer elements (ACI Committee 446.1R, 1991).

There are different types of planar elements. Triangular plane elements, used by Ngo and Scordelis (1967), are less popular than quadrilateral elements (Chen, Chen and Teng, 2012) because they have a shear-locking problem. The shear locking is unrealistic stiffness against bending due to the inability of the sides of the elements to bend. In addition, they have constant strain which can affect the accuracy of the results if used in large numbers.

Full integration quadrilateral elements (Figure 4.1) can have the shear-locking problem, but this can be mitigated by increasing the number of elements, using reduced integration, or by using higher-order elements (Logan, 2011). Higher-order elements have additional nodes introduced at the sides (see Figure 4.2). Therefore, they have higher strain variation

within the elements. Their use can accelerate convergence to the exact solution in situations where it is possible to use fewer elements (Logan, 2011). In addition, they are better at approximating curved shapes. However, their computational cost is significantly higher relative to the linear elements. Therefore, using linear elements can be more efficient depending on the mesh size and the particular problem. Using reduced integration elements (fewer integration points) reduces the computational cost significantly relative to full integration and higher-order elements. However, in some situations, they can be too flexible because they only have one Gauss point (integration point) located at the centre of the element. Bending causes one side of the element to increase in length and the opposite side to contract. However, in the middle of the element strain is constant in bending, which causes the element to have no bending resistance. Therefore, reduced integration elements produce highly inaccurate results if the mesh is too coarse or if they are used with contact problems.

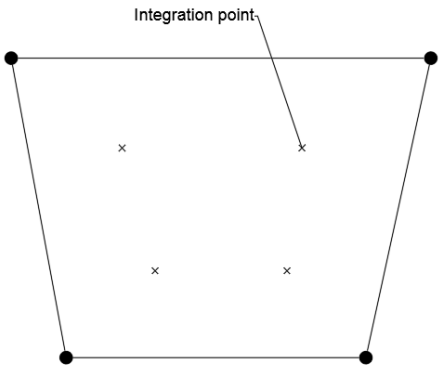

Figure 4.1 Illustration of a linear full integration quadrilateral element

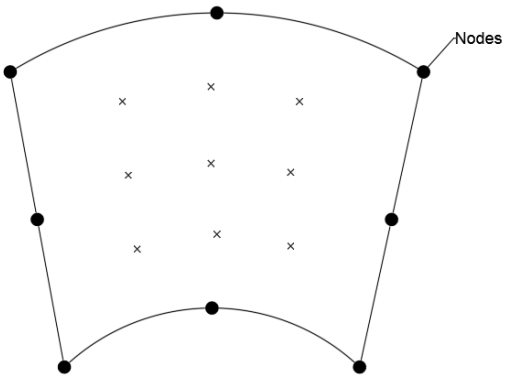

Figure 4.2 Illustration of a non-linear higher-order quadrilateral element

The following two subsections discuss the types of constitutive models used in FE modelling.

4.2.1 Linearity and Nonlinearity

Linear elastic constitutive models have much less computational cost, and they are much simpler than nonlinear constitutive models (Kim, 2014). However, they are not suitable for modelling the nonlinear behaviour of bamboo or steel-reinforced concrete under high load and deformation. In the case of steel-reinforced concrete, the reason is that both steel and concrete are highly nonlinear under large loads, especially with crack propagation. In the case of bamboo reinforced concrete, the bamboo shows linear brittle behaviour; however, it has a low modulus of elasticity relative to steel which results in significant deformations in the concrete and consequently in a highly nonlinear response in concrete which includes cracking and nonlinear compressive behaviour. Steel reinforced concrete elements have three stages in their load-displacement relationship as follows: elastic stage, crack propagation stage, and finally, the plastic stage (Figure 4.3). The load-displacement relationship is linear in the first stage and nonlinear in the second and the third stage. Chen and Saleeb (1994) and Chen (2007) attributed the nonlinearity to several causes as follows:

1. Cracking of the concrete;
2. The plasticity of the reinforcement (in the case of steel reinforcement) and of the concrete in compression;
3. Non-linear bond-slip between the reinforcement and the concrete;
4. Aggregate interlock of the cracked concrete;
5. Dowel action of the reinforcement;
6. Time-dependent effects (i.e. creep, shrinkage, temperature, and load history)) (Chen and Saleeb, 1994; Chen, 2007).

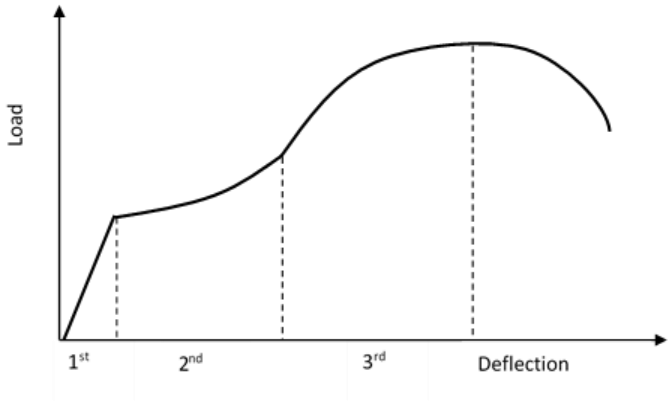

Figure 4.3 Plot of the three stages of steel-reinforced concrete behaviour (adapted from Chen (2007))

Nevertheless, there are several disadvantages to nonlinear systems. They are much more complicated than linear systems, their computational cost is much higher, and they have more complex modelling and solution procedures. Solving nonlinear systems is often accomplished by solving a sequence of linear analyses. Moreover, unlike linear systems, nonlinear systems do not always have a unique solution (Kim, 2014). Numerical methods are needed for linearizing the stiffness matrix and solving the nonlinear FE system. Unlike in a linear system, the stiffness matrix is not constant in a nonlinear system. Linearizing the stiffness matrix is the most complicated and computationally demanding step in solving a nonlinear system (Kim, 2014). Solving the system requires one of the numerical methods like the Newton-Raphson method or the arc-length method. More discussion on solution procedures is provided in section 4.5. Nonetheless, they are necessary for capturing the highly nonlinear behaviour of reinforced concrete.

4.2.2 Nonlinear elastic, plastic, and the damage plasticity constitutive models

Cauchy's nonlinear elastic formulation is the most straightforward nonlinear hyper-elastic formulation. Cauchy's nonlinear formulation produces stresses that are uniquely defined by the current state of strain (Chen, 2007). However, in materials that are not isotropic linear elastic, Cauchy's formulation results in strain-energy path dependency.

Therefore, restrictions are used to ensure that the laws of thermodynamics are not violated by the FE system (Chen, 2007). Green hyperplastic formulation satisfies the laws of thermodynamics by restricting Cauchy's formulation using the concept of internal energy. Both of Cauchy's and Green's hyper-elastic models are secant models, which means that the stiffness decreases with increasing strain to capture the convex behaviour of concrete beyond the linear elastic stage. However, hyper-elastic models do not capture the plastic flow part of the material behaviour that starts after the ultimate strength point is reached. In addition, hyper-elastic models do not capture the softening that follows the plastic flow.

Damaged plasticity models and plastic models are the most suitable to model bamboo reinforced concrete beams. The damaged plasticity model differs from the classic plastic model in that it has a softening after reaching maximum stress in compression and tension. In addition, the damaged plasticity model degrades the modulus of elasticity to model damage in cyclic loading. The usual procedure of treating problems with cracking behaviour was to use the plasticity theory in the compression zone and fracture mechanics in the zone where tensile stresses control the response. Lubliner *et al.* (1989) argued that this procedure has the following shortcomings:

1. the need for decoupling the behaviour along the principal axes;
2. the need to define random shear retention factors to allow shear transfer across the crack;
3. difficulties with cyclic loading pertaining to the opening and closing of cracks stress pathways;
4. challenges in modelling the combination of cracking and plasticity at damaged points.

Researchers use uniaxial concrete stress-strain empirical formulas as input data for the nonlinear constitutive models. Appendix A shows the different choices by researchers in literature. The empirical formulas enable the extrapolation of the limited stress-strain data to a complete set of data. FE models of reinforced concrete beams are not very sensitive to the concrete stress-strain models used as input data. Coronado and Lopez (2006) investigated the sensitivity of the damaged plasticity model to the three concrete stress-strain models shown in Figure 4.4. The simplest stress-strain model was a linear elastic-perfectly plastic with a sudden drop in stress to 10% of the ultimate strength. Although the three models have different stress-strain functions, they found that the three-concrete stress-strain functions yielded similar results. Meaning that the damaged plasticity model was not sensitive to different stress-strain models.

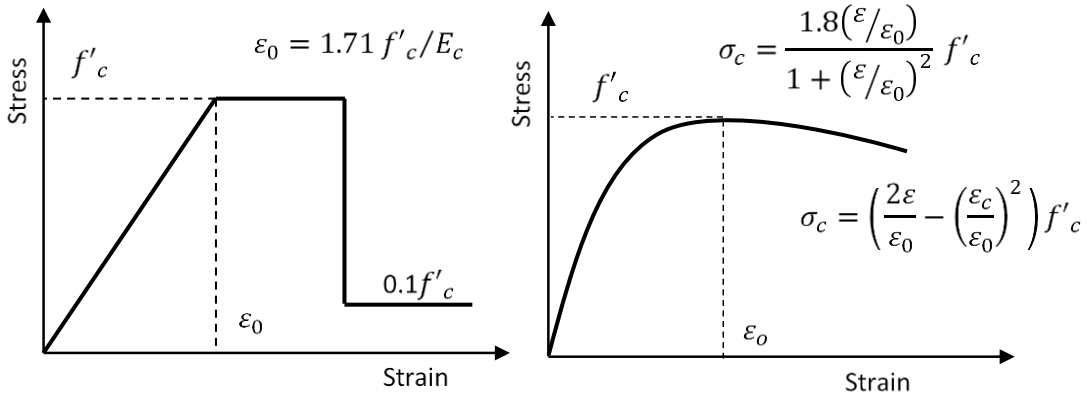

Figure 4.4 Plot of three concrete stress-strain models in uniaxial compression

4.3 Cracking Behaviour of Concrete

Besides aesthetics and durability concerns, cracks widths and spacing have an important influence on the stiffness of concrete beams. There are two main approaches for modelling cracks in FE: the discrete crack approach and the smeared crack approach. The discrete crack approach models cracks as geometrical discontinuities while the smeared crack approach considers cracks as continuum load resistance deterioration.

4.3.1 Discrete crack approach

Discrete cracks can be modelled using linear and nonlinear methods. The Linear Elastic Fracture Mechanics (LEFM) method is not suitable for normal size concrete structures as it has a large fracture process zones (ACI Committee 446.1R, 1991). Concrete has a large fracture process zone relative to metals and ductile metals because of the relative heterogeneity of concrete aggravated by the large size of aggregates (Bažant and Oh, 1983). The discrete crack approach is most useful when the local behaviour of a cracked area or the behaviour of a few predefined cracks is under investigation. Using the discrete crack model can cause mesh bias. This mesh bias is due to defining cracks along elements boundaries. To overcome this shortcoming, there have been attempts to produce FE codes with automatic re-meshing algorithms. Re-meshing techniques were introduced, so the cracks do not need to develop only through mesh boundaries. However, the continuous change of topology, due to crack propagation, causes computational difficulties (Bors*t et al.*, 2004). To overcome the shortcomings of discrete crack models, Hillerborg, Modéer and Petersson (1976) developed the fictitious crack model to capture the nonlinear softening behaviour of concrete under tension using the smeared crack approach.

4.3.2 Smeared crack approach

The smeared crack approach is most helpful when the load-deflection behaviour is the primary concern. The smeared crack approach can be used using the tension-stiffening model by relating stress to strain or using the fracture energy concept where stress is related to displacement. Utilising the tension stiffening approach leads to crack localisation and mesh dependency, especially when the reinforcement is not well distributed. Therefore, the fracture energy concept was introduced to the smeared crack approach (Chen, 2010).

The most basic smeared crack model uses zero in the stiffness matrix (D) for both stress across the crack and the shear transfer along the crack (equation 4.1). Introducing Rots' (1988) shear retention factor (β) reduces numerical difficulties and enhances accuracy by accounting for friction and aggregate interlocking along the crack (equation 4.2 and 4.3) (Bors*t et al.*, 2004). Chen (2010) found that any value for the parameter (r) within the range of 2-5 reasonably approximated the behaviour of their beams. The effect of shear deformation on the shear retention is insignificant in beams with large span-depth ratios. The reason is that in beams where shear tension failure occurs, shear deformation is small relative to the deformation in the tensile direction (Chen, Chen and Teng, 2012). Since in the current research, the span-depth ratio is much higher than the threshold of 2.5, the shear deformation effect on shear retention of bamboo reinforced concrete beams can be neglected.

$$D = \begin{bmatrix} 0 & 0 & 0 \\ 0 & E & 0 \\ 0 & 0 & 0 \end{bmatrix} \quad 4.1$$

$$\beta = \left[1 - \frac{\varepsilon^{cr}}{\varepsilon_u^{cr}}\right]^r \quad 4.2$$

$$D = \begin{bmatrix} 0 & 0 & 0 \\ 0 & E & 0 \\ 0 & 0 & \beta G \end{bmatrix} \quad 4.3$$

Where:
D = stifness matrix
E = modulus of elasticity (MPa)
β = shear retention factor
G = shear modulus (MPa)
ε^{cr} = crack strain (mm/mm)
ε_u^{cr} = ultimate crack strain (mm/mm)
r = a parameter that controls the degradation of shear resistance

It has been long known that the tensile resistance of concrete does not drop immediately to zero after reaching the ultimate tensile strength, but a gradual softening behaviour takes place. A tensile variable (μ) is introduced to the stiffness matrix to model the softening

(equation 4.4) that have an upper limit of one before the maximum tensile stress is reached and a lower limit of zero when the material is fully cracked. After cracking, modelling the stress softening behaviour of concrete is important for its effect on beams' stiffness.

$$D = \begin{bmatrix} \mu E & 0 & 0 \\ 0 & E & 0 \\ 0 & 0 & \beta G \end{bmatrix} \qquad 4.4$$

The major problem of the smeared crack approach is mesh sensitivity that is due to strain localisation (Crisfield, 1986). Strain localisation occurs because materials do not have the same mechanical properties at every point; therefore, strain-softening starts at the weakest point. The zone surrounding the weakest point is unloaded gradually during softening and stress redistribution takes place (Crisfield, 1986). Since the element strain energy is dependent on the mesh size, the crack energy is dependent on the mesh size. However, according to fracture mechanics, crack propagation energy is a material property. Figure 4.5 shows the relationship between crack length and load capacity for two mesh sizes; coarse and fine. The coarse mesh produces higher load resistance results relative to the fine mesh. The coarser mesh can overestimate the load capacity and required energy for the formation of a crack (ACI Committee 446, 1991). A coarse mesh can result in a smaller crack width in comparison with a fine mesh under the same load.

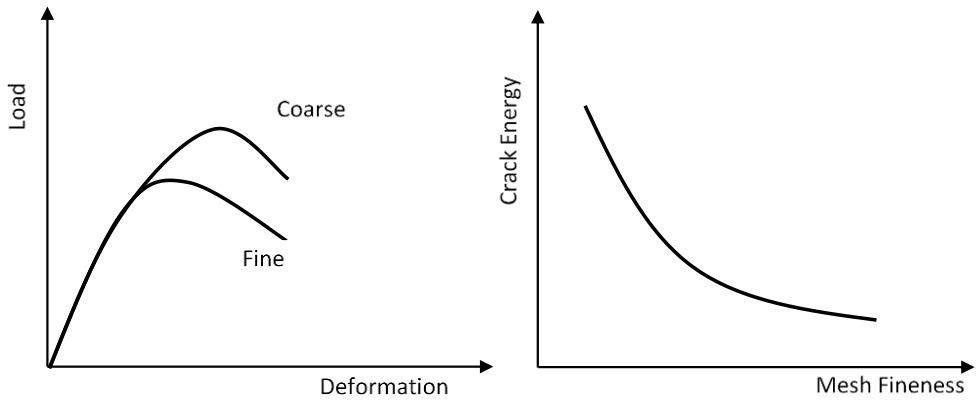

Figure 4.5 Plot of the effect of mesh size on load resistance and crack energy (adapted from ACI Committee 446 (1991))

The fracture energy concept is incorporated using localisation limiters to mitigate the mesh sensitivity problem. The crack band model is one of the successful localisation limiters. Bažant and Oh (1983) crack band model assumes uniform stress and strain within the crack band. The strain and stress inside the crack band are not uniform in reality; both decrease away from the centre of the crack. Therefore, other limiters were developed such as the non-local continuum model and the gradient model that makes stress and strain-dependent on the location relative to the centre of crack (American Concrete Institute, 1997). Nonetheless, the crack band model yields accurate results for stiffness and cracks widths in reinforced concrete (Chen, Chen, and Teng, 2012).

Hillerborg, Modéer and Petersson (1976) were the first to relate the stress in the concrete to crack width. This relation became the fictitious crack model. The assumption is that cracks start to propagate when the tensile strength of concrete is reached. Their model assumes that the stress drops linearly from the tensile strength of the concrete at zero crack width to zero stress at a value of the order 0.01-0.02 mm. The real softening behaviour of concrete reaches zero asymptotically. Since the development of the fictitious crack model, researchers have used different concrete softening models (Appendix A). Figure 4.6 shows the two softening models that Coronado and Lopez (2006) investigated. Although the two models are different, the researchers found that the two models yielded similar results.

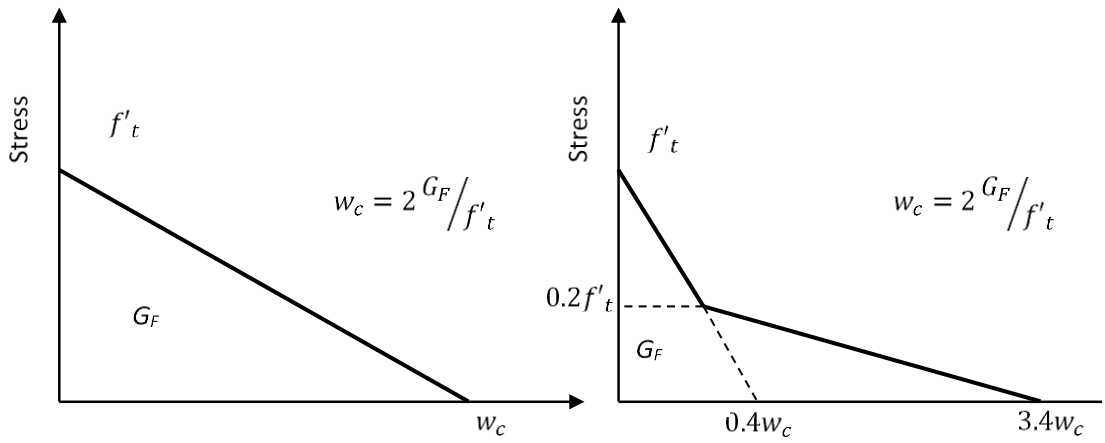

Figure 4.6 Plot of fracture energy models (crack width VS stress)

In the case of FRP strengthened concrete beams, the assumed tensile strength of the concrete does not change the outcome significantly. Coronado and Lopez (2006) studied the sensitivity of the numerical solution to tensile strength (f'_t). The tensile strength was varied between 0.5-2 f'_t. The variation in the load-deflection graph was negligible with the higher tensile strength yielding slightly stiffer results. However, using the FRP reinforcement may have been the cause of this insensitivity. In the case of bamboo reinforced concrete beams, this may be different as the bamboo reinforcement has little effect on the initial behaviour due to its low modulus of elasticity. The initial response is dominated by the tensile strength and the fracture energy (softening behaviour) of the concrete.

Higher fracture energy increases the stiffness of the beam after crack propagation and limits crack size. Coronado and Lopez (2006) found that the sensitivity of their model due to the change of the fracture energy G_f is dependent on the failure mode. Beam failure by concrete crushing in compression is insensitive to altering G_f. Plate debonding failure was highly sensitive to the change of G_f. The higher G_f results in delaying plate debonding in comparison with smaller values because it limits cracking that initiate debonding. In

the case of bamboo reinforced concrete, only stiffness is expected to be affected by the fracture energy.

4.4 Modelling the bond in FE

In steel-reinforced concrete, modelling the bond is essential for accurate cracks width and spacing. However, modelling the bond is not necessary for accurate stiffness against deflection. Ngo and Scordelis (1967) found no significant difference in load-deflection results between the assumption of perfect bond and modelling the bond using spring elements. However, their model predefined the discrete cracks and did not predict the cracking pattern. Therefore, they assumed that the bond does not affect cracks number and spacing. Conversely, Chen, Chen and Teng (2012) found that modelling the bond results in fewer cracks that are wider while assuming perfect bond results in more distributed cracks that are narrower. Since shear retention is dependent on crack width, stiffer bond-slip results in higher cracked concrete shear strength. Chen (2010) compared FE models with different steel reinforcement bond models. The first model assumed a perfect bond, the second model used a bond-slip model, and the third model approximated the bond by using the tension-stiffening model of Bentz (2005). All of the three models produced acceptable load-deflection results with the bond-slip dependent model being the most accurate and the tension-stiffening model being the stiffest. The load capacity was significantly different amongst the three models with the slip dependent bond model producing the most accurate results. The other two models overestimated the load capacity and the maximum deflection. The cracks sizes and spacing found using the bond-slip model agreed more closely with the test result. In the other two models, the cracks were smaller and more smeared. Chen (2010) claimed that inaccurate crack estimation in literature is due to the assumption of a perfect bond.

Similarly, Jason *et al.* (2013) found that using a slip-dependent bond model or assuming perfect bond produced similar results in terms of load-deflection behaviour but unacceptable crack prediction results. Concerning modelling the cracks, the model incorporating a slip-dependent bond model achieved excellent results in all loading stages. The model with perfect bond assumption underestimated the number of cracks in the first stage (load under 20 KN), and in the second stage (25 KN) the model overestimated the number of cracks; however, in the remaining stages of loading the model predicted the number of cracks accurately. Underestimating the width of cracks in the case of perfect bond assumption resulted in a lower estimated maximum stress in the reinforcement. The researchers compared the cumulative crack openings in the FE models and the experiment. In addition, the researchers compared the maximum crack opening in the FE models and the experiment. Jason *et al.* (2013) concluded that the FE model with the slip-dependent bond model is better at estimating crack opening, although, both simulations produced good results.

In the case of bamboo reinforcement, the bond is weaker relative to steel which makes the assumption of perfect bond not realistic in modelling deflection, crack widths, and spacing of cracks. The bond of deformed steel is significantly higher and stiffer relative to the bond of bamboo reinforcement and closer to the perfect bond assumption. Therefore, while assuming a perfect bond of steel-reinforced concrete may yield acceptable results, especially for deflection, assuming perfect bond in bamboo reinforced concrete can result in underestimating the deflection. The current research will determine the bond at which the perfect bond assumption in bamboo reinforced concrete becomes reasonable.

4.5 Solution methods and Convergence

Convergence difficulties arise in modelling reinforced concrete beams due to the combined effect of bond and cracking behaviour. There are a few methods for solving nonlinear models. This section explores the main techniques commonly used with reinforced concrete. These methods are the Newton-Raphson method, the arc-length method and the dynamic method.

4.5.1 Newton-Raphson method

Newton-Raphson method solves finite element problems using an iterative process because the stiffness of the elements is dependent on the displacement. In the Newton-Raphson method, the load is divided into steps and the stiffness is estimated at a certain displacement, and the loads consequently found. Then this internal load is compared to the external loads. If the difference is within a given tolerance, the assumed displacement is accepted as real. If not, the difference is used as an input load, and the displacement is estimated, and the result is added to the previous displacement to find the displacement at the end of the 2nd iteration. The modified Newton-Raphson method uses the initial stiffness in all iterations, which means it requires less computational cost; however, more iterations are needed to reach convergence. The Newton-Raphson method is faster relative to the Secant method in terms of the number of iterations required. However, the cost of a secant iteration is much lower than a Newton-Raphson iteration because there is no need to estimate the Jacobian matrix at every iteration (Kim, 2014). The Jacobian matrix serves to translate changes in the global coordinate system to the element local coordinates. Smaller time steps help the program converge; however, it increases the computational cost. The number of iterations used to finish a time step is used to know if the time step or load step is of the right size. If the Newton-Raphson method is used, the time step is considered of acceptable size if it requires 5-6 iterations to converge. If the

number of iterations is less than that, the time step should be increased. If the number of iterations is higher than 10, the time step should be decreased (Kim, 2014).

4.5.2 Arc-length method

Convergence can be hard to achieve when snap-through and snap-back behaviour occur using the Newton-Raphson method because the structure can lose some of its stiffness temporarily. Crisfield (1986) showed that snap-through and snap-back behaviour could occur in concrete elements due to concrete cracking (Figure 4.7). Snap-through results in a sudden jump of displacement under the same load, and it prevents the model from converging if the test is load controlled. Snap-back results in a sudden decrease in load under the same displacement and it causes problems when the test is load or displacement controlled. To solve these problems without using a dynamic procedure, Crisfield (1986) suggested the use of the spherical arc-length method coupled with line searches.

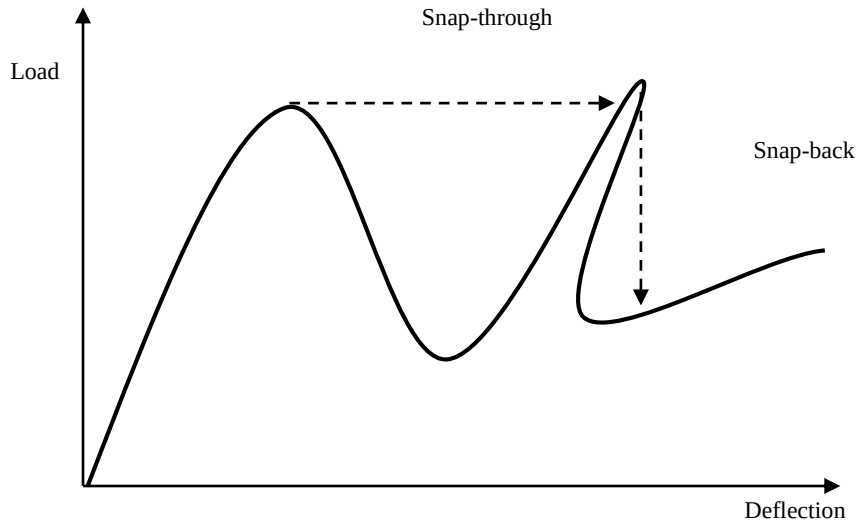

Figure 4.7 Plot of the snap-through and the snapback behaviour

The way that the arc-length method differs from the Newton-Raphson method is that rather than defining a load limit, a surface is defined that include all the possible load-displacement points using a fixed incremental length (Crisfield, 1981). Then the slope at

the starting point is found and the point at which the slope intersects the surface constitutes the result from the first iteration. Consequently, the actual load result is found at the same displacement of the iteration and the difference between the two loads is calculated. The difference is used to find the displacement, using the slope at the first point, and both results are added to the previous iteration to constitute the new iteration.

The main problem with the arc-length method is the solution evolution in snap-back behaviour. ABAQUS, for example, uses forward solution evolution. When the solution is carried, there are two sets of intersection points. If the forward solution used, like in ABAQUS, the set with the largest displacement is used; however, when there is a snap-back behaviour the two sets, have negative displacement relative to the last convergence point (Crisfield, 1981).

4.5.3 Dynamic procedures

Dynamic solution procedures can be used to solve quasi-static nonlinear systems. Mercan, Stolarski and Schultz (2016) found that the arc-length method was computationally less expensive relative to the dynamic procedure, especially for coarser meshes. However, unlike static procedures, dynamic procedures can absorb any instabilities in the system into dynamic energy. Therefore, they can converge where the static procedures (Newton-Raphson method and the arc-length method) cannot. In addition, unlike static procedures, the dynamic approach can capture the local dynamic behaviour of cracking (Chen, 2010). Chen, Chen and Teng (2012) and Chen (2010) were able to reach convergence only by using the implicit dynamic procedure. They encountered numerical difficulties with using the arc-length method within the static procedure and the dynamic method was more robust. The arc-length method was only able to reach convergence with the fracture energy tension-stiffening model. The implicit dynamic method reached convergence regardless. Mercan, Stolarski and Schultz (2016)

found that the arc-length method was less sensitive to mesh refinement and compared more closely to the experimental results. However, both methods provided good results and the arc-length method did not always converge with finer meshes.

4.6 The proposed FE Model for bamboo reinforced concrete

Based on the review of FE models of reinforced concrete a model was created to model bamboo reinforced concrete. ABAQUS finite element software package was used to carry the FE tests. Saenz's model was calibrated to the experimental compression test data to determine the input data for the concrete material as required by the constitutive model (see Chen (2007) for Saenz's model). Bamboo's mechanical behaviour depends on the direction of loading; however, the reinforcement inside concrete acts primarily as uniaxial truss element, therefore, a simple tension test is sufficient for modelling the bamboo. Quadrilateral elements (CPE4) were used to model the concrete. The bamboo reinforcement and the stirrups were modelled using truss elements (T2D2). The bond between the bamboo reinforcement and the concrete was modelled using a bilinear bond. For stirrups, the bond is assumed to be perfect between the stirrups and the concrete. Assuming a perfect bond for stirrups is reasonable because the stirrups encircle the concrete, and the stirrups are deformed.

The following subsections present the different choices made in developing the FE model.

4.6.1 The constitutive model used in the current research

The concrete damaged plasticity model was used in the present study. The damaged plasticity model was used because it is capable of modelling effects like hardening and consequent softening of concrete in compression, softening of concrete in tension, and cracking. In addition, the plastic smeared crack model available in ABAQUS was harder to solve, and convergence problems occurred regularly. The difficulty can be attributed

to the fact that the only stress-displacement function available within the smeared crack model is linear softening, while in the concrete damage plasticity model the bilinear softening of CEB-FIB (1993) model can be used. The more gradual softening in the bilinear model helps the model converge to the solution.

The damaged plasticity model requires defining the angle of dilatancy (Ψ). A value of 30^o was used in the current research. The angel of dilatancy is usually taken as 30^o for concrete (Appendix A). Coronado and Lopez (2006) investigated the sensitivity of their model to the angle of dilatancy (Ψ). Coronado and Lopez (2006) found that the sensitivity of the results to varying Ψ from 20^o to 40^o was dependent on the failure mode. Concrete crushing failure mode was insensitive to different Ψ unlike the debonding failure mode. Higher values of Ψ overestimates the load at the onset of debonding. However, setting Ψ to 30^o yielded good results. In the current research, it was observed that higher values for the angel of dilatancy results in stiffer beam behaviour.

4.6.2 Mesh size in the current research

The concrete in the beam is modelled using 20 mm elements, as shown in Figure 4.8. To determine if the mesh size is appropriate. Chen (2010) found that reducing the maximum element size to less than 20 mm is not necessary. Mias *et al.* (2015) investigated the mesh size sensitivity of their model. All the mesh sizes that the researcher investigated produced similar results. Mias *et al.* (2015) investigated the following meshes: 6X23, 6X46, and 12X46. The beam size was 200X150X2300 mm; however, symmetry was used so only half of the beam was modelled. Similarly, in the current research by using symmetry only half of the beam need to be modelled.

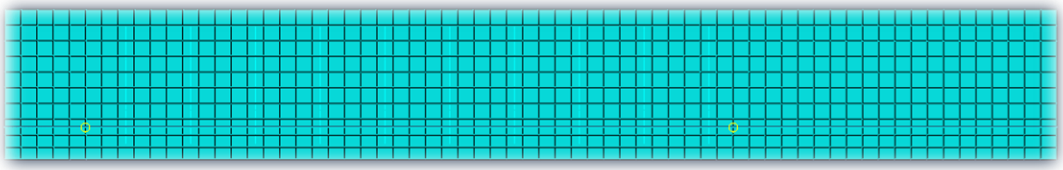

Figure 4.8 Snapshot of the mesh in the current research

4.6.3 Tensile strength and fracture energy

The fracture energy of concrete was calculated using equation 4.5 of Bažant and Becq-Giraudon (2002). Concerning the tensile strength, it should be noted that the tensile strength of concrete is very variable and that there are various methods to estimate its value based on the compressive strength. Chen (2007) estimated that the tensile strength is equal to 0.085-0.11 of the compressive strength (f'_c.), Coronado and Lopez (2006) used the American Concrete Institute (2008) model of 0.6 $f'^{0.5}_c$, Wight and MacGregor (2012) estimated the tensile strength to be 0.08-0.15 f'_c. In the current research, the tensile strength was calculated using the American Concrete Institute (2008) model and estimated at 3.23 MPa for 30 MPa concrete characteristic compressive strength.

$$G_F = 2.5\alpha_0 \left(\frac{f'_c}{0.051}\right)^{0.46} \left(1 + \frac{d_a}{11.27}\right)^{0.22} \left(\frac{w}{c_e}\right)^{-0.3} \qquad 4.5$$

Where:
G_F = fracture energy of concrete (N.mm)
α_0 = type of aggregates factor
f'_c = characteristic compressive strength of concrete (MPa)
d_a = the size of aggregates (mm)
$\frac{w}{c_e}$ = water to cement ratio (%)

4.6.4 Solution procedure

A few options were investigated to solve the nonlinear problem. The Newton-Raphson method and the arc-length method were not able to converge, and the model crashed soon after the simulation started. The implicit dynamic method was the only successful method in completing the simulation. The reason for the difficulty of convergence is attributed to

the problems of cracking and bond interaction between the reinforcement and the concrete.

4.7 Discussion and limitations

This chapter reviewed the finite element analysis of reinforced concrete to justify the choices made in developing an FE model for bamboo reinforced concrete. This is the first attempt to develop an FE model for bamboo reinforced concrete beams. A limitation is that by using symmetry the developed FE model forces the beam to develop an even number of cracks along the full span. However, the validation using the experimental results will show whether this can significantly affect the accuracy of the FE model predictions. Another limitation is that the model approximates the geometry using two-dimensional elements for concrete and one-dimensional elements for the bamboo reinforcement. However, as it was discussed in this chapter these elements are the most commonly used in FE modelling of reinforced concrete because they are more efficient modelling relative to models with three-dimensional elements. In addition, the validity of the model will be checked against the experimental results. With regards to modelling the bond interaction between the bamboo and the concrete, the software package used in the current investigation limits the choices available in modelling the bond-slip to a bilinear model with hardening and softening of the bond. While this limitation is restrictive, the next chapter investigates whether these assumptions can produce reasonable results in bond modelling.

Chapter 5

5. Bond of Bamboo Embedded inside Concrete

5.1 Introduction

This chapter presents the results of the pull-out testing of corrugated and non-corrugated bamboo. Section 5.2 presents the materials and the testing method used in testing the bond of bamboo with concrete. 5.3 presents the results of the pull-out testing. In section 5.4, the results are statistically analysed to investigate the effect of corrugation on the bond and to investigate the role of waterproofing bamboo in protecting mechanical interlock. In section 5.5, a model is developed that can estimate the bond of bamboo at short embedment lengths based on the shear strength of bamboo and the shear-friction behaviour of concrete. The experimental results are used to validate the model for the corrugated bamboo bond at short embedment lengths assuming perfect mechanical interlock. Section 5.6 discusses the stiffness of bamboo bond and it suggests a bilinear bond-slip model for the bamboo bond. Section5.7 develops a theoretical model for the bond of bamboo at long embedment length inside uncracked concrete. The theoretical model uses the bilinear bond-slip model, modulus of elasticity, and reinforcement area as inputs to predict the average bond. Section 5.8 validates for the theoretical bond at long embedment using experimental results from the literature. Section 5.9 presents a discussion on the work carried during this chapter and its limitation. Finally, the chapter is concluded in section 5.10.

5.2 Materials and testing method

All of the bamboo splints were taken from a single Moso bamboo culm to limit variation. No nodes were included in the bond experiment because of the large variability encountered in nodes spacing and sizes in bamboo; therefore, ignoring the effect of nodes yields more conservative and reliable results. The widths and the thicknesses of the splints were determined by taking the average of three measurements. The measurements were taken using a digital calibre with 0.01 mm precision. 18 out of the 24 splints were waterproofed with linseed oil. Three coats were applied with 24 hours between applications. All of the samples had a total embedment length of 200 mm. Half of which was debonded to prevent splitting failure in the concrete at the loaded end. A bitumen-based debonding compound was used for debonding the splints (Figure 5.1).

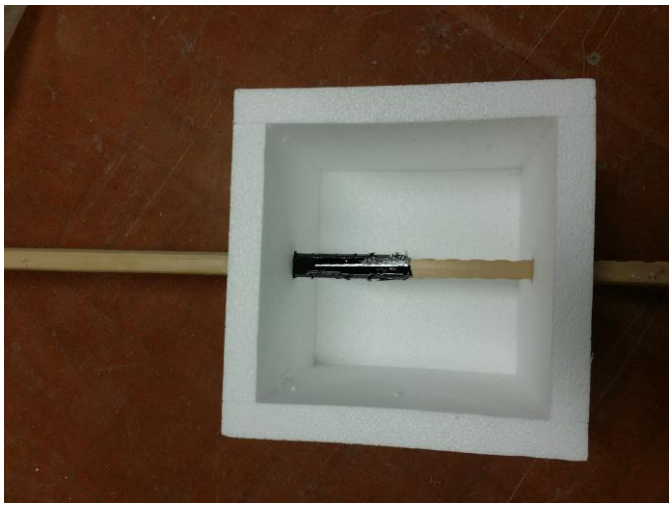

Figure 5.1: Picture of a splint in the form with bitumen-based debonding compound

The concrete mix used in this experiment was 1: 1.7: 3 (cement: fine aggregates: coarse aggregates) by weight with a water-cement ratio of 0.5. The aggregates are crushed river aggregates. The compressive strength of the concrete cubes on the day of testing, 28 days after casting, ranged between 40-48 MPa. This is equivalent to a cylindrical compressive strength of 32-38 MPa (Cylinder compressive strength = 0.8*cube compressive strength (McCormac and Brown, 2014). The concrete was cast in the forms in three layers of equal

thickness and was vibrated after the casting of each layer. The concrete is cast into 200 mm cube shape. Slump tests were performed to ensure that the slump was about 75 mm.

The pull-out test was performed using the Instron 8033 servo-hydraulic fatigue testing machine (which can be used for quasi-static tests). The machine has a capacity of 250 KN. The experiments were carried out at a rate of 1 mm/min. Two LVDTs (linear variable displacement transducer) were used to measure the displacements at the loaded and the free-ends (Figure 5.2).

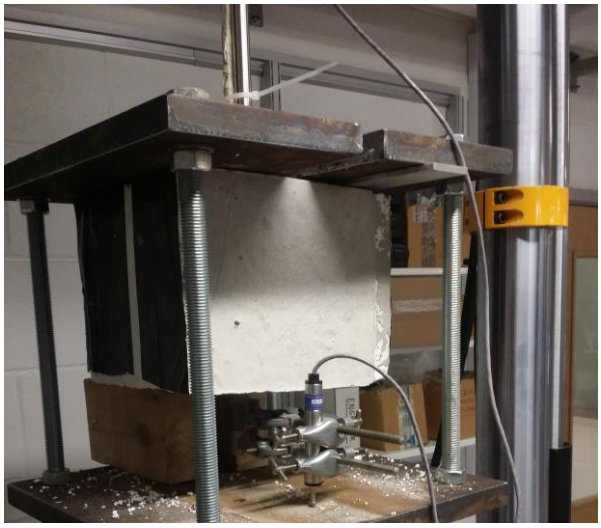

Figure 5.2 Picture of pull-out testing of a bamboo splint

5.3 Results

Corrugated and linseed treated bamboo splints achieved the strongest bond (Figure 5.3). The specimens with the 1:1.5 ratio achieved on average a bond equal to 2.92 MPa. This result is comparable to the bond achieved using Sikadur 32 Gel at 2.75 MPa (Table 5.1). All the corrugated splints achieved better results in comparison with the non-corrugated ones. Splints with a 1:1.5 ratio achieved on average 37% and 5% higher results relative to splints with 1.5:1 and 1:1 ratios, respectively.

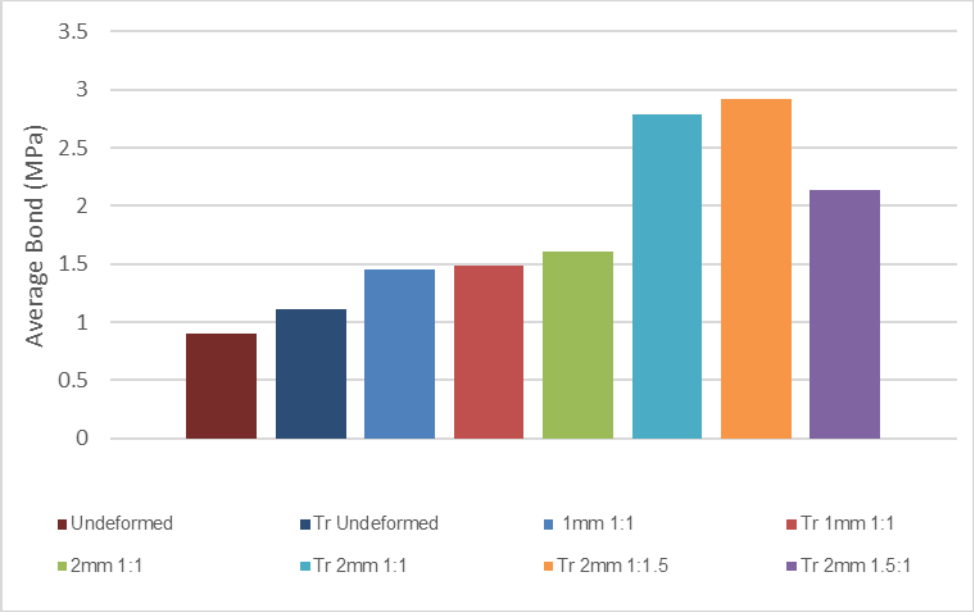

Figure 5.3 Histogram of the average bond (Tr indicates that the specimen is treated with linseed oil, the first number indicates the projection, and the ratio is the B:A ratio)

Linseed oil-treated splints with 2 mm projection and 1:1 ratio achieved on average 88% higher bond relative to Linseed oil-treated splints with 1mm projection and 1:1 ratio (Table 5.1). Untreated splints with 2 mm projection and 1:1 ratio achieved 19% stronger bond relative to untreated splints with 1 mm projection and 1:1 ratio. Linseed oil improved the bond of the non-corrugated splints by 26% and improved the bond of the corrugated splints with 2 mm projection and 1:1 ratio by 73%. Appendix B presents the full results for all of the pull-out tests presented in graphs.

Table 5.1 The bond results of corrugated and non-corrugated bamboo using the pull-out test

Treatment	Without Linseed oil * (A)	With Linseed oil*	Without Linseed oil	With Linseed oil	Without Linseed oil	With Linseed oil	With Linseed oil	With Linseed oil
B:A ratio	-	-	1:1	1:1	1:1	1:1	1:1.5	1.5:1
Projection (mm)	-	-	1	1	2	2	2	2
Average Bond (MPa) (B)	0.90	1.11	1.35	1.48	1.61	2.79	2.92	2.14
Standard deviation (MPa)	0.14	0.43	0.25	0.52	0.49	0.29	0.38	0.41
Standard error (%)	16	39	18	35	30	10	13	19
Number of specimens	2**	3	2****	3	3	2***	3	3
SD (MPA)	0.14	0.43	0.25	0.52	0.49	0.29	0.38	0.41
Bond improvement relative to A (%)	-	26	50	69	84	220	235	145

*: Non-corrugated.

**: One specimen was ignored as a result of a technical error: setting the rate of pull-out to 10mm/min instead of 1 mm/min.

***: One specimen was ignored because the splint failed in tension.

****: One specimen was ignored because the maximum load occurred at an exceedingly high slippage

To investigate the type of bond failure, pull-out specimens were split as shown in Figure 5.4. Only linseed oil treated bamboo splints with 2 mm projection and the 1:1.5 pattern had a shear failure in the bamboo. Figure 5.5 shows the surface of linseed treated 2 mm 1:1.5 splint after failure, where the bamboo lugs were completely sheared off. Figure 5.6 shows the surface of a treated 2 mm 1:1 splint. The damage in the bamboo is more pronounced in the area adjacent to the loaded end. Figure 5.7 shows the surface of a 2mm 1:1 splint without linseed treatment. The bamboo splint is not damaged. The shrinkage of the bamboo splint resulted in the loss of the mechanical interlock.

Figure 5.4 Picture of the splitting of pull-out specimens

Figure 5.5 Picture of the bamboo-concrete surface after failure for linseed treated splint (Tr 2 mm 1:1.5)

Figure 5.6 Picture of the bamboo-concrete surface after failure for linseed treated splint (Tr 2 mm 1:1)

Figure 5.7 Picture of the bamboo-concrete surface after failure for an untreated splint (2 mm 1:1)

5.4 Statistical Analysis

Two statistical models were used to analyse the results of the pull-out test. Two-way ANOVA and linear regression.

5.4.1 The two-way ANOVA analysis

In Khatib and Nounu (2017) two-way ANOVA was used to analyse the effects of corrugation and linseed treatment on bond. It was found that projection significantly improves the bond of bamboo but the effect of linseed treatment was not statistically significant. Table 5.2 shows that the p-value for projection is less than 0.05 while the p-value for linseed treatment is higher than 0.05 and therefore not statistically significant. It should be noted that having a p-value of higher than 0.05 (0.094 for linseed treatment) does not mean that the linseed treatment does not affect the bond. It only means that the effect cannot be proven with 95% confidence (1 - p-value). To check the assumption of

homogeneity of variance in ANOVA, Levene's test was carried and the result was 0.627 which is higher than 0.05. Therefore, the homogeneity of variance assumption was not violated.

Table 5.2 ANOVA of the pull-out results

Source	Type III Sum of Squares	df	Mean Square	F	Sig.
Corrected Model	4.589[a]	5	.918	3.450	.051
Intercept	34.099	1	34.099	128.190	.000
Linseed	.929	1	.929	3.494	.094
projection	3.544	2	1.772	6.661	.017
Linseed * projection	.814	2	.407	1.530	.268
Error	2.394	9	.266		
Total	41.231	15			
Corrected Total	6.983	14			

a. R Squared = .657 (Adjusted R Squared = .467)
Dependent Variable:Bond

One drawback of using ANOVA is that it required making bond the dependent variable because two-way ANOVA can only model categorical independent variables. Therefore, the ANOVA model assumed that the effect of width and thickness are equal on bond. However, the corrugation is only on the thickness side of splints and higher bond values can be achieved if the thickness was in higher proportion to the width. In addition, the contribution of thickness in corrugated bamboo to shear is different from the contribution of thickness in non-corrugated bamboo. In the latter, the contribution is due to friction only while in the former the contribution is mostly due to mechanical interlock. Therefore, a more accurate approach is to include width and thickness in the model as covariates. This can be accomplished via linear regression.

5.4.2 Linear regression of the bond results

In the linear regression, the pull-out force is the dependent variable and the width and thickness are included as covariates. Table 5.3 shows the independent variables used in the model. Backward elimination was used to eliminate the variables that are not significant. Backward elimination starts with all the independent variable and eliminates the least significant predictor in every step. A few combinations of independent variables

were entered into the backward elimination process, and the one that contains the model with the highest adjusted R^2 value is selected. In Table 5.3 Variance Inflation Factors (VIF) are used to evaluate the severity of collinearity. Simply put, collinearity means that the independent variables (predictors) are correlated. Values larger than 10 indicates that there is a collinearity problem (Montgomery, 2003). Collinearity makes it harder to prove the significance of the independent variables, and it makes it harder to disentangle the effects of the different independent variables on the dependent variable (Montgomery, 2003).

Except for pattern, all the variables were found statistically significant at $p = 0.05$ (Table 5.3). The p-value for the pattern is slightly higher than 0.05. Testing with more specimens may prove the significance of the pattern. The interaction between corrugated thickness, projection, linseed treatment was found significant. Similarly, the effect of the uncorrugated width and thickness is significant. While in the two-way ANOVA analysis the effect of linseed treatment was not statistically significant, in linear regression it was found that its interaction with thickness and projection is statistically significant. This is due to separating the effects of width and thickness in the linear regression model.

Table 5.3 Linear regression of maximum pull-out load using backward elimination

		Unstandardized Coefficients				Collinearity Statistics
	Model	β	Std. Error	t	Sig.	VIF
1	L*P*T	270.040	108.415	2.491	.025	25.964
	Pattern	-322.392	196.628	-1.640	.122	1.020
	Width + noncorrugated thickness	248.785	104.886	2.372	.032	14.137
	Linseed (L)	-728.281	1595.766	-.456	.655	28.216
	Projection (P)	-690.222	1906.936	-.362	.722	31.339
	Corrugated Thickness (T)	182.738	278.698	.656	.522	17.007
2	L*P*T	241.089	71.172	3.387	.004	11.832
	Pattern	-331.544	189.627	-1.748	.100	1.003
	Width + noncorrugated thickness	229.701	88.173	2.605	.019	10.564
	Linseed (L)	-432.159	1332.364	-.324	.750	20.800
	Corrugated Thickness (T)	111.963	193.122	.580	.570	8.635
3	L*P*T	226.880	54.596	4.156	.001	7.349
	Pattern	-334.651	184.333	-1.815	.087	1.001
	Width + noncorrugated thickness	203.919	37.144	5.490	.000	1.979
	Corrugated Thickness (T)	115.111	187.733	.613	.548	8.613
4	L*P*T	256.274	25.670	9.983	.000	1.683
	Pattern	-334.331	181.109	-1.846	.081	1.001
	Width + un-corrugated thickness	212.735	33.649	6.322	.000	1.682

The effect of corrugated thickness is dependent on the projection because small projection value makes the effect of thickness more similar to that in non-corrugated bamboo. The effect of projection is dependent on the linseed oil treatment as it protects the mechanical interlock. For interaction, a value of 2 is used for specimens treated with linseed oil (L) and a value of 1 for non-treated specimens. These values are chosen to reflect the interaction between linseed treatment and projection and thickness. Table 5.3 shows that the backward elimination deemed this variable significant. In addition, Figure 5.8 shows that the interaction between linseed treatment, projection, and thickness is the strongest predictor relative to the other predictors. Figure 5.8 shows the partial regression plot of the independent variable Linseed*Projection*Thickness. As can be seen from the plot, the relationship is linear, and the correlation is strong.

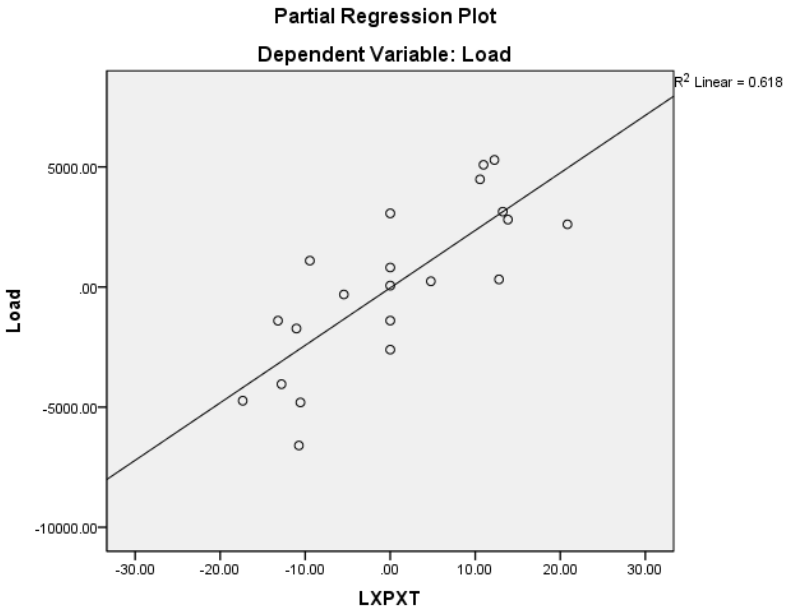

Figure 5.8 Partial regression plot of interaction between linseed treatment, projection (mm), and thickness (mm) against load (N)

Although the pattern is not statistically significant, Figure 5.9 indicates that there is a negative linear relationship between bamboo width relative to concrete width (B-A) and load. There is an inflexion point, however, when the shear failure changes from concrete to bamboo. This inflexion point is in the interval between 0 and -5, where the failure changes from concrete to bamboo shear failure. This is confirmed by the inspection of the bamboo splints after the pull-out testing. It should be noted that the X-axis is not the observed values; it is the residual of regressing the (B-A) (The difference in width between the bamboo and the concrete in the corrugation pattern) variable against all the other variables. The Y-axis represents the residuals from regressing the load over all variables except for the B-A variable. The residuals are used in partial plots to remove the effect of correlation between the B-A variable and the other independent variables. If there were no correlation at all, all of the observations would have the same measured values (-5, 0, and 5). However, this correlation is not large enough to violate the conditions of the linear regression, as shown by the VIF values.

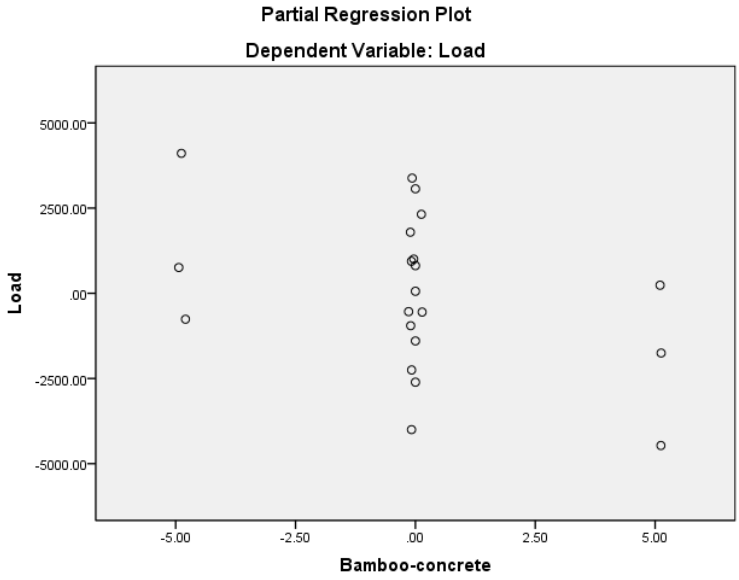

Figure 5.9 Partial regression plot of the pattern (B-A (mm) VS load (N))

Here the assumptions of linear regression are checked to ensure the validity of the model. One of the assumptions of linear regression is the homogeneity of variance (homoscedasticity) over the interval of predicted values. Homoscedasticity of the residuals can be assessed using a scatter plot of the studentized residuals (the residual divided by its standard deviation) against the standardised predicted values as shown in Landau and Everitt (2003). Figure 5.10 shows that the homoscedasticity assumption is not violated because the variance has no trend over the interval of the standardized predicted values. In addition, there are no outliers, and no observations fall outside the interval -2 to 2. Therefore, none of the observations needs to be excluded from the regression.

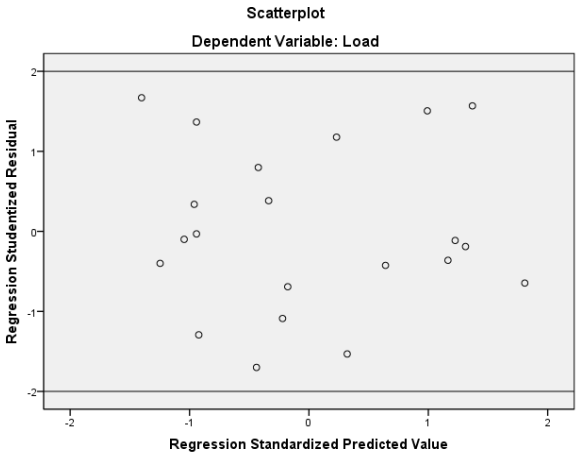

Figure 5.10 Scatter plot of the homoscedasticity of the linear regression residuals

5.5 Theoretical modelling of the corrugated bamboo bond at short embedment

In this section, a theoretical model is presented for the bond of corrugated bamboo at short embedment lengths and the experimental results are used to validate the theoretical model. The theoretical model assumes that there is sufficient mechanical interlock to induce shearing in the bamboo or the concrete. Therefore, only the results from the specimens 2 mm projection and linseed oil treatment are used here to validate the theoretical model.

The failure between the corrugated bamboo and the concrete can be caused by the shearing of the bamboo lugs, the failure of the concrete between bamboo lugs, the degradation of the mechanical interlock due to shrinkage, and the diminishing of the mechanical interlock due to the weak mechanical properties of bamboo in the direction perpendicular to fibre. Azadeh and Kazemi (2014) determined the internal stresses in the bamboo and the concrete, as shown in Figure 5.11. However, in addition to the concrete shear surface determined by Azadeh and Kazemi (2014), two concrete shearing surfaces contribute to the shear strength (Figure 5.12). These two surfaces are parallel to the plane shown in Figure 5.11, with a width equal to the projection and length equal to A (Figure 5.12). Khatib and Nounu (2017) presented equation 5.1 based on the stresses shown in

Figure 5.11 in addition to the stresses in the concrete surfaces parallel to the plane (Figure 5.12).

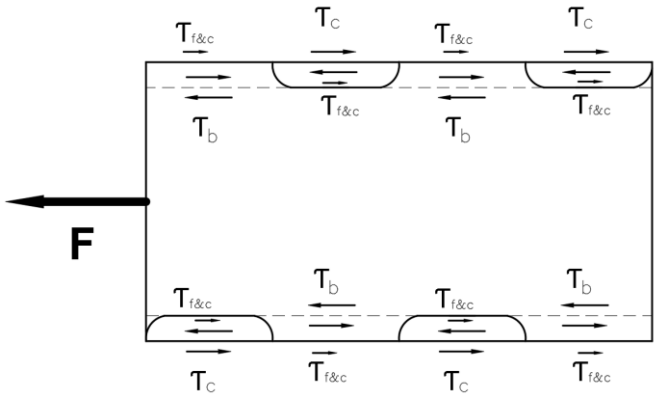

Figure 5.11 Illustration of the internal stresses in bamboo and concrete

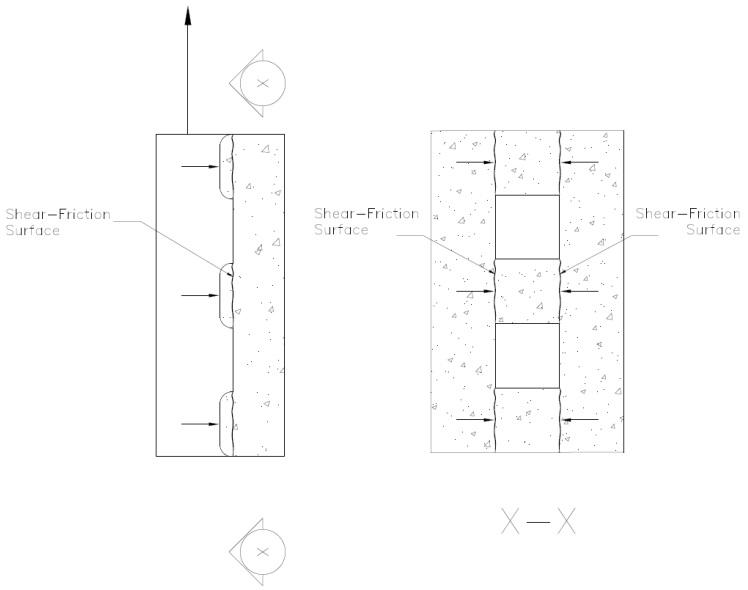

Figure 5.12 Illustration of concrete shear-friction surfaces with corrugated bamboo

$$\tau = \frac{\tau_b \times T' \times B}{(A+B) \times (W+T')} + \tau_{f\&c} \times \frac{W}{W+T'} \leq \frac{\tau_c A(T'+2P)}{(A+B) \times (W+T')} + \tau_{f\&c} \times \frac{W}{W+T'} \quad 5.1$$

$$\tau_c = 0.2f'_c \leq 3.31+0.08f'_c \leq 11 \qquad 5.2$$

Where:

τ = average bond (MPa)
τ_b = bamboo longitudinal shear strength (MPa)
τ_c = concrete shear-friction (MPa)
$\tau_{f\&c}$ = friction and chemical adhesion bond (MPa)
T' = splint thickness (mm)
A = the width of corrugation where τ_b (mm)
B = the width of concrete between the lugs where τ_c is active (mm)
W = splint width (mm)
P = the splint projection (mm)
f'_c = concrete compressive strength (MPa)

τ_c can be found using equation 5.2 (American Concrete Institute, 2008)). Concrete shear-friction (τ_c) develops when the concrete at the opposite sides of a crack is prevented from moving apart (McCormac and Brown, 2014). The concrete between the lugs is held in place by the bamboo on one side and the concrete in the opposite side. The theoretical model expressed in equation 5.1 is in general form to accommodate for different concrete grades and different bamboo shear strengths.

To validate the theoretical bond model (equation 5.1), the experimental results are compared to the estimates of the theoretical model. Richard (2013) and Jiang *et al.*, (2012) reported the average shear strength in the longitudinal direction in Moso bamboo at 14.2 and 16 MPa, respectively. Using an average value for longitudinal shear strength at 15 MPa (τ_b) and by evaluating τ_c using equation 5.2, the theoretical bond is found as shown in Figure 5.13. There is a strong correlation between the estimates of the theoretical model and the experimental results. It should be noted that the theoretical model assumes perfect mechanical interlock between the bamboo and the concrete. Therefore, it cannot be used with a projection of less than 2 mm and without linseed treatment.

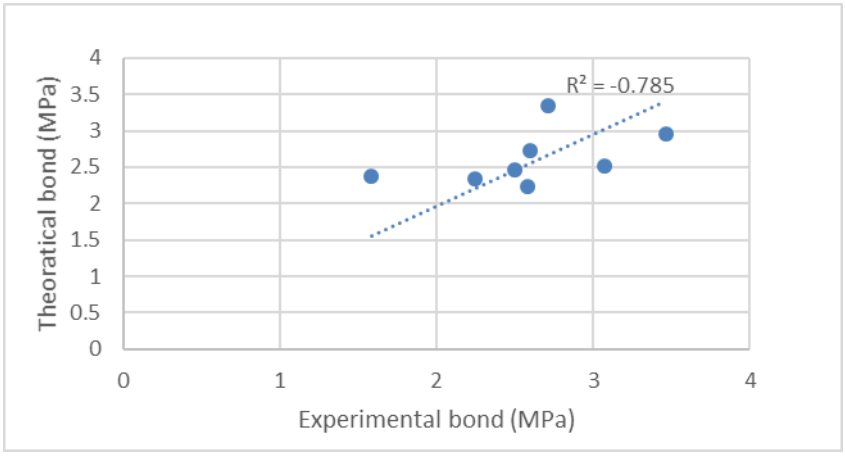

Figure 5.13 Scatter plot of experimental bond results VS theoretical model

5.6 Stiffness of bond and the bond-slip model

Figure 5.14 presents the bond-slip behaviour of one corrugated and non-corrugated specimens. Appendix B presents the full load-slip graphs for all the pull-out tests. The difference between the slippage readings at the loaded and free-ends is due to the elongation of the bamboo inside concrete under stress. The difference is more considerable in corrugated bamboo due to the larger load and smaller section caused by corrugation. In corrugated bamboo, the load drops after reaching the maximum more gradually relative to non-corrugated bamboo.

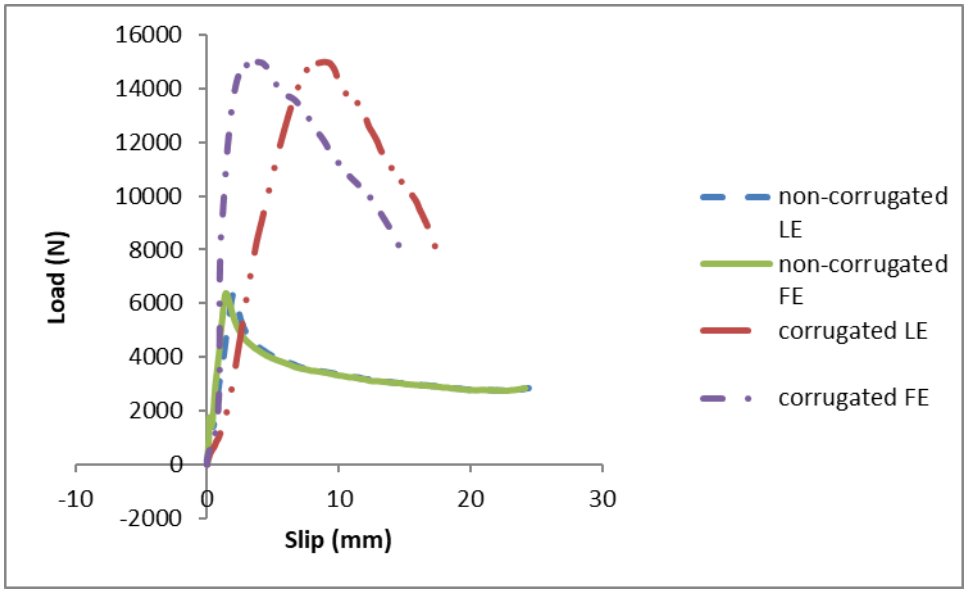

Figure 5.14 Plot of load-slip for a corrugated and non-corrugated specimen at free (FE) and loaded (LE) ends

The bond-slip behaviour of bamboo inside concrete can be conservatively approximated using a bilinear model. The ascending branch is more linear relative to the bond-slip models of steel and FRP reinforced concrete. The descending branch is significantly more variable than the ascending one. In addition, the corrugation affects the bond-slip relationship. Therefore, a conservative approach is taken where the descending branch is linear and reaches zero-bond at twice the slippage corresponding maximum bond. The slippage corresponding 80% and 20% of the maximum load is used to determine the slope of the ascending branch. This approach eliminates the effect of any errors in slippage measurement due to any gaps between the concrete and the loading plate at the start of the test.

Linear regression is used here to determine the variables that significantly affect the stiffness of bond. The linear regression included the following variables: 80% of maximum load, the linseed treatment, projection, width, thickness, and pattern. None of these had a significant effect on the stiffness except for the load. Table 5.4 shows the coefficients of a linear regression where all the independent variables are entered, and backward elimination is carried. A few different combinations of the independent variables were introduced in the backward elimination process to reach the best model. Model 5 is moderately correlated with the data. The model accounts for 63.7% of the variance.

Table 5.4 Linear regression of the bond stiffness

	Model	β	Std. Error	t	Sig.	VIF
	80% of maximum load	1.008	0.28	3.597	0.004	24.306
	Corrugated Thickness	222.496	168.371	1.321	0.211	8.581
	Pattern	-8.129	192.037	-0.042	0.967	1.415
	L*P	-981.212	624.516	-1.571	0.142	15.559
1	Width + Non-corrugated Thickness	7.154	55.347	0.129	0.899	5.517
	80% of maximum load	1.002	0.23	4.365	0.001	17.663
	Corrugated Thickness	223.068	161.256	1.383	0.19	8.526
	L*P	-969.654	539.667	-1.797	0.096	12.584
2	Width + Non-corrugated Thickness	8.091	48.735	0.166	0.871	4.633
	80% of maximum load	1.031	0.146	7.074	0	7.646
	Corrugated Thickness	225.643	154.834	1.457	0.167	8.447
3	L*P	-1014.2	451.701	-2.245	0.041	9.474
	80% of maximum load	1.112	0.139	7.975	0	6.517
4	L*P	-646.453	388.423	-1.664	0.117	6.517
5	80% of maximum load	0.899	0.058	15.611	0	1

Based on the regression, the stiffness is directly dependent on the load and the slippage at the maximum bond can be considered constant. Equation 5.3 is based on the linear model. Based on the equation, the free-end displacement at 80% of the maximum load can be considered constant at 1.11 mm. These results are consistent with the values observed for slippage in Kute and Wakchaure (2013) and Acha Navarro (2011). The slippage results for bamboo at maximum load are slightly higher relative to steel reinforcement. Steel reinforcement reaches maximum bond at 1 mm slippage for confined concrete (CEB-FIB, 1993). The higher slippage with bamboo reinforcement can be explained by the different mechanical properties of bamboo and the lower shear modulus of the bamboo relative to steel. While the slippage at maximum bond is similar to steel reinforcement, the stiffness of bond is significantly lower relative to steel because the maximum bond of bamboo is significantly lower. Deformed steel can only lose bond due to failure in the surrounding concrete at a bond of 11 MPa and 13.7 MPa for unconfined and confined C30 concrete, respectively (CEB-FIB, 1993).

$$Stiffness = 0.8 \times 0.899 \times Load_{max} \quad 5.3$$

5.7 Theoretical bond model for bamboo in un-cracked concrete at high embedment length

The low modulus of elasticity (MOE) of bamboo relative to steel contribute to its weaker bond, especially at higher embedment lengths. A smaller MOE means that the reinforcement elongates more inside the concrete. Thereby producing higher variability of slippage along the embedded length. As discussed in the previous section, the bond is a function of slip. Therefore, the loaded end reaches the slip corresponding maximum shear earlier relative to the free end. The load transfer between reinforcement and concrete does not increase linearly with increasing embedment length. Only a reinforcement material with an infinite modulus of elasticity (MOE) can have a linear increase of load transfer with longer embedded length. This is because a material with an infinite MOE has the same slippage at all points along the embedment. Since bamboo has a lower MOE relative to steel, the bamboo bond is more sensitive to the length of the embedment. Therefore, a model is needed that can predict the bonding behaviour of bamboo at varying embedment lengths. This section presents an approach to estimate the bond at different embedment lengths with the reinforcement's MOE and area as factors.

Equations 5.4-5.7 represent the relationships between load, slip, and longitudinal bond stress. The load is an integral function of slip (equation 5.4) and slip is an integral function of load (equation 5.5). To solve this problem, the strain can be assumed to increase linearly over the embedment with a starting value equals to zero and a maximum value at the loaded end (equation 5.6). Any continuous differentiable bond-slip function can be solved using these assumptions. If it is not possible to get a closed-form integration, a numerical integration technique can be used. The first step is to replace $\tau_l(S)$ with a

function $\tau_l(l, \varepsilon, S_{FE})$ and integrate over L (equation 5.7). Since ε increases linearly over L, it can be assumed equal to $l * c'$ where c' is a constant. After the integration, c' is substituted for $\frac{\varepsilon}{L}$.

$$F = \int_0^L \tau_l(S) \, . \, dl \tag{5.4}$$

$$S = \int_0^L \varepsilon \, . \, dl = \int_0^L \frac{F}{EA} \, . \, dl \tag{5.5}$$

$$S = \frac{1}{2}\varepsilon L + S_{FE} \tag{5.6}$$

$$F = \int_0^L \tau_l(l, S_{FE}) . \, dl \tag{5.7}$$

Where:

F = pull-out load (N)
S = slippage between the reinforcement and the concrete (mm)
τ_l = the longitudinal bond stress equalvilant to the bond of 1 mm embedment (N/mm)
ε = strain in the reinforcement (mm/mm)
L = the embedment length (mm)
S_{FE} = slippage at the free-end (mm)

The bond-slip model suggested here for bamboo is a bilinear bond-slip model and therefore not differentiable over the maximum bond stress. The bond increases linearly with slip to a maximum value at 1.11/0.8 =1.383 mm slip (S_{max}) and drops linearly to zero at 2.766 mm slip (S_0). Since this function is not differentiable, the method is slightly changed. With the bilinear model, the maximum active embedment needs to be divided into two lengths because there is no continuous function over the full length (Figure 5.15). The maximum active embedment is the maximum embedment at which there is a transfer of shear between the reinforcement and the concrete. The first part of the embedment length (L_1) can be estimated using equation 5.8 and the second part (L_2) using equation 5.10. Equation 5.8 is derived by substituting F in equation 5.5 for F_1 in equation 5.9 and integrating over L_1 (Figure 5.15). Equation 5.10 is derived by substituting F for $F_1 +$

$\tau_{l,max} l_2 (1 - \frac{l_2}{L_2})$ in equation 5.5. Here $\tau_{l,max} l_2 (1 - \frac{l_2}{L_2})$ is a function that depicts the decending of τ_l to zero over L_2. The difference between L_2 and l_2 is that the former is a constant number where the latter is a variable. By performing the integration and solving for L_2, equation 5.10 is created. It should be noted that the integration constant is equal to S_{max}. After finding the value of L_2, F_2 can be found as shown in equation 5.11.

$$L_1 = \sqrt{S_{max} * 4EA/\tau_{l,max}} \quad 5.8$$

$$F_1 = \frac{1}{2}\tau_{l,max} L_1 \quad 5.9$$

$$L_2 = \sqrt{3((S_0 - S_{max})EA - F_1 L_2)/\tau_{l,max}} \quad 5.10$$

$$F_2 = \frac{1}{2}\tau_{l,max} L_2 \quad 5.11$$

$$F_{total} = F_1 + F_2 \quad 5.12$$

Where:

L_1 = first part of the embedment (mm)
S_{max} = slippage corresponding maximum bond stress (mm)
A = reinforcement area (mm^2)
$\tau_{l,max}$ = maximum longitudinal bond (N/mm)
F_1 = force produced by the bond in the first part of the maximum embedment (N)
L_2 = second part of the embedment (mm)
S_0 = slippage corresponding zero bond (mm)
F_2 = force produced by the bond in the second part of the maximum embedment (N)

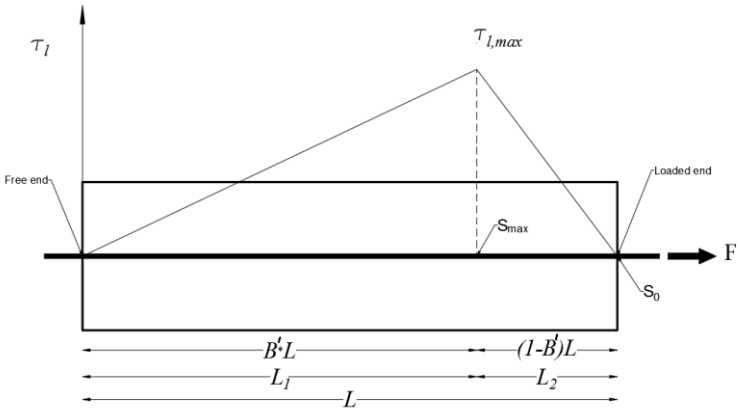

Figure 5.15 Illustration of the bond stress along the embedment length inside the concrete

Equations 5.13 and 5.14 can be used to estimate the load when the actual embedment length is smaller relative to L. B' designates the location of the maximum shear stress point along the embedment with a value equal to zero at the free-end and one at the loaded end. Maximum load is always achieved with B greater than 0.5 because L_1 is always greater than L_2 in a bilinear model where $S_0 = 2S_{max}$. With increasing embedment lengths, the value of B' at maximum load also increases. To determine the value of B' that translates into the maximum bond load, MATLAB or an Excel sheet can be used where B' is varied between 0.5-1 and the value corresponding the maximum bond resistance is chosen. Alternatively, a value of 0.70 provides a reasonable and conservative approximation for B'.

$$f_1 = \tau_{l,max} B' l (1 - B' \frac{l}{2L_1}) \quad 5.13$$

$$f_2 = \tau_{l,max} (1 - B')(l - (1 - B') \frac{l^2}{2L_2}) \quad 5.14$$

Where:
l = actual embedment length (mm)
f_1 = force produced by the bond in the first part of the embedment (N)
f_2 = force produced by the bond in the second part of the embedment (N)
B' = factor that designates S_{max} along the embedment

5.8 Validation of the theoretical bond model for bamboo in un-cracked concrete at high embedment length

To validate the equations 5.8-5.14, they were compared to the experimental results of Geymayer and Cox (1970) (Figure 5.16) and the predictions of the FE model (Figure 5.17). As it can be seen from Figure 5.17 the mathematical model agrees closely with the FE model results. Although the value of slippage at maximum load in Geymayer and Cox (1970) was not reported, the theoretical model using the bilinear bond-slip model provides reasonable estimations of the experimental results (see Figure 5.17). An example

is provided in appendix B to help the reader understand how the theoretical model can be applied.

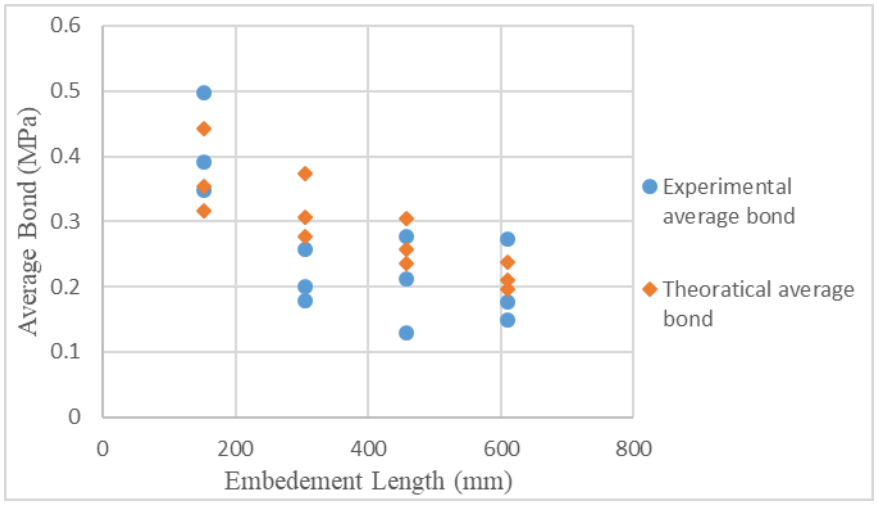

Figure 5.16 Plot of average bond VS embedment in Cox and McDonald (1970) experimental results and the proposed theoretical model

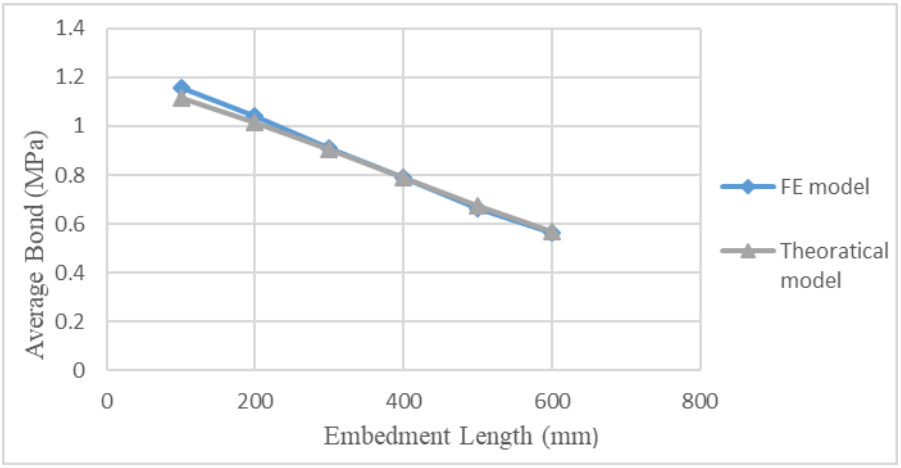

Figure 5.17 Plot of average bond VS embedment in the FE model and the proposed theoretical model for a corrugated splint with 13.9 GPa MOE and 140 mm2 section area

5.9 Discussion

In this chapter, the first two research questions are answered. It was shown that corrugation can improve the bond of bamboo with concrete. In addition, a theoretical model was presented for the estimation of the corrugated bamboo bond at short embedment lengths. A theoretical model for bamboo at long embedment length was presented.

5.9.1 Discussion of the bond of corrugated bamboo

Two statistical models were used to analyse the results; two-way ANOVA, and linear regression. Both models show that corrugation can improve the bond. 2mm corrugation is more effective in improving the bond relative to 1 mm corrugation. However, only the linear regression model shows that the interaction between the corrugation and linseed treatment is effective. This discrepancy is attributed to the better fit of the linear model to the data. The two-way ANOVA assumes that width and the thickness affect the bond similarly. However, the corrugation being on the thickness side means that the thickness should have a larger effect on bond. The linear model provides a better fit because it can disentangle the effects of thickness and width on bond.

Deformed steel can achieve strong mechanical interlock with lower protrusions at its surface relative to corrugated bamboo because bamboo is more easily compressible in the transverse direction. The projection should be equal to the lowest projection that develops a full mechanical interlock to achieve optimum behaviour. Waterproofing bamboo prevents the diminishing of the mechanical interlock due to shrinkage. Higher projections can prevent degradation of the mechanical interlock due to the compressibility of bamboo in the direction perpendicular to fibre. However, using high projections reduces the tensile strength of splints. If other waterproofing treatments prove more effective than linseed oil, it is possible that a smaller projection can provide adequate mechanical interlock. In addition, to avoid premature shear failure in the bamboo or in the concrete, the B:A ratio (width of bamboo to concrete) should be such that the shear strength of the bamboo lugs and the shear-friction of concrete between the lugs are equal.

5.9.2 Discussion of the bamboo bond at long embedment

A model is created and validated for the bond of bamboo under large embedment lengths in bamboo reinforced concrete. The model is validated using the experimental results provided by Cox and McDonald (1970) and the FE model. Cox and McDonald (1970) only provided the maximum bond, Therefore, it was assumed that the slippage corresponding maximum bond is equal to that observed to the current research. Nonetheless, the results show that the model provides reasonable estimates of the experimental results. For the FE model, only the inputs of the reinforcement area, MOE, and bond-slip model at short embedment were used in common for the theoretical model and the FE model. The average bond at longer embedment lengths is then used to show that the theoretical model yields similar results to the FE model. The purpose of the comparison between the FE model and the proposed theoretical model is to show that the assumptions of the theoretical model are robust.

The simple development length approach used in steel and FRP reinforced concrete where the development length is a function of the bar diameter and concrete cover is not applicable for bamboo reinforcement. An important distinction between bamboo on one hand and steel and FRP on the other is the relative uniformity of behaviour in steel and FRP. Bamboo mechanical properties and section geometry vary widely. A practical limitation of the proposed approach is the relatively complex method in estimating bond in comparison with steel and FRP reinforced concrete. A simpler model may be created as more research becomes available. In addition, the suggested bilinear model for bond-slip is conservative in that it assumes that the bond drops linearly to zero as the slip increase to double the value corresponding maximum bond. The bond-slip model can be refined and replaced with a more accurate model as more data becomes available.

Nonetheless, this research makes the first attempt to link the bond at long embedment to the mechanical properties of bamboo.

It should be noted that the proposed theoretical is limited to uncracked concrete. It can be conceived of a beam under flexure as two pull-out tests that co-occur where the loaded end is at midspan. This assumption can be overly conservative because it assumes that only one cracks develop. In the next chapter, a bond model is developed for beams at high embedment lengths where the concrete is cracked.

5.10 Conclusions

This chapter investigated the use of corrugation to bamboo's bond to concrete. Corrugating bamboo was found effective in improving bamboo's bond to concrete. Stronger bond contributes to a higher bending capacity of bamboo reinforced concrete beams. In addition, stronger bond helps to limit the deflection of bamboo reinforced concrete beams. This chapter shows that achieving a strong bond does not require expensive epoxy materials and can be replaced by corrugation. A theoretical model is presented for the estimation of the corrugated bamboo bond at short embedment lengths (100 mm) based on the shear strength of bamboo and the shear-friction behaviour of concrete. A mathematical model is presented that can predict the average bond in uncracked concrete at high embedment lengths based on the reinforcement mechanical properties.

Chapter 6

6. Flexural Behaviour of Bamboo Reinforced Concrete Beams

6.1 Introduction

This chapter investigates the bending, bonding, and shear capacities of bamboo reinforced concrete. Section 6.26.3 reviews the methods used in literature for the estimation of concrete shear capacity when reinforced with bamboo and highlights their deficiencies. Section 6.4 presents the materials and the testing method used to test the flexural capacity of bamboo reinforced concrete. Section 6.5 presents the results of the experimental testing of the bamboo reinforced concrete beams. Section 6.66.7 validate the proposed FE model using the experimental results of the flexural testing. Section 6.86.9, the experimental results from the current and previous investigations are used to validate the flexural, shear, and bond failure models suggested in this chapter.6.10 explores the underestimation of the bamboo reinforcement tensile strength by the tensile testing as shown by the flexural testing results. Section 6.11 provides a discussion on the work carried in this chapter and its limitations. Finally, section 6.12 presents the conclusion of this chapter.

6.2 Review of the bending capacity design method for steel and FRP reinforced concrete

This section reviews steel and FRP flexural design assumptions to explain the rationale for bamboo reinforced concrete design. In the design of FRP reinforced concrete under flexure the following assumption are made: the strain in the concrete and the reinforcement is proportional to the distance from the neutral axis, a maximum compressive strain in the concrete (taken usually as 0.003 mm/mm), the tensile strength

of the concrete is ignored due to cracking, the reinforcement is linear elastic and perfect bond exists between the reinforcement and the concrete (Nanni, De Luca and Jawaheri Zadeh, 2014; American Concrete Institute, 2015). The same assumptions apply to steel reinforced concrete except that the reinforcement exhibits a plastic behaviour which allows the neutral axis to become shallower and achieve compression failure in the concrete after ample warning due to excessive deflection and cracking.

Similar to steel, determining the flexural capacity of FRP reinforced beams and slabs require first determining whether the section is under or over-reinforced. The section is considered under-reinforced if the failure is caused by the tensile failure of the reinforcement and over-reinforced if the failure is the result of concrete crushing. For steel and FRP reinforced concrete, if the section is over-reinforced the ultimate capacity can be found by assuming concrete compression failure using the stress-block analysis (Figure 6.1). The difference in estimating the moment capacity between steel reinforcement on one hand and bamboo and FRP reinforcement on the other exists when the section is under-reinforced. This difference arises from the ductility of steel and the brittle behaviour of FRP and bamboo.

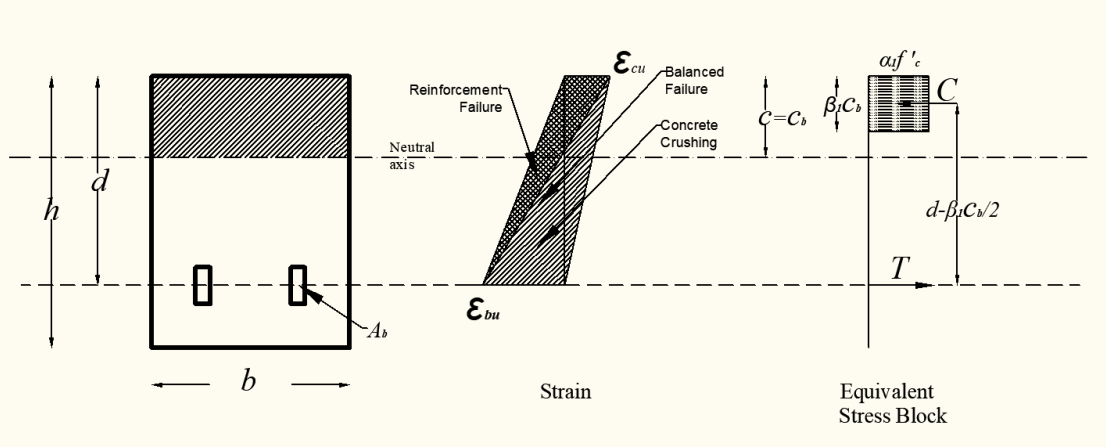

Figure 6.1 Illustration of the strain gradient and the equivalent Stress Block analysis (adapted from Nanni, De Luca and Jawaheri Zadeh (2014))

Determining whether the section is under-reinforced or over-reinforced can be achieved by finding the balanced section. The balanced section is the line between an under-reinforced and an over-reinforced section (Figure 6.1). A balanced section is achieved in steel-reinforced concrete when the reinforcement yields and the concrete reaches the strain corresponding maximum stress (ε_{cu}) at the same time. American Concrete Institute (2008) suggests that the strain in the steel reinforcement needs to be at least 0.005 mm/mm for the section to be considered ductile and under-reinforced. This strain limit is conservative because steel yields at a strain of 0.0025 mm/mm for 500MPa steel strength. With FRP reinforced beams, the FRP reinforcement does not yield. Therefore, the balanced section is achieved when the reinforcement and the concrete reach failure simultaneously. The balanced section for bamboo reinforced concrete can be found using the same method applied for FRP and steel reinforcement with substituting bamboo strain at failure in equation 6.1. If the neutral axis (c) is lower relative to the balanced neutral axis (c_b), the member is considered under-reinforced.

$$c = \frac{\varepsilon_{cu}}{\varepsilon_{cu} + \varepsilon_b} d \geq c_b = \frac{\varepsilon_{cu}}{\varepsilon_{cu} + \varepsilon_{bu}} d \qquad 6.1$$

Where:
c = depth of the neutral axis (mm)
c_b = depth of the neutral axis in a balanced section (mm)
ε_{cu} = ultimate compressive strain in the concrete (mm/mm)
ε_{bu} = ultimate strain in the bamboo reinforcement (mm/mm)
ε_b = strain in the bamboo reinforcement (mm/mm)
d = depth of the reinforcement (mm)

Calculating the theoretical strength for under-reinforced FRP or bamboo sections is not simple because the stress block analysis is not applicable. The stress block analysis is not applicable because the stress distribution in the concrete cannot be approximated using the parabolic distribution if the concrete has not reached the ultimate compressive strain. For FRP under-reinforced beams, American Concrete Institute (2015) suggests using c_b as the neutral axis for simplicity. This approach is on the conservative side and a more

rigorous approach like that suggested by Nanni, De Luca and Jawaheri Zadeh (2014) may produce a slightly more economical section. However, the difference is small because it only marginally affects the moment lever-arm. In addition, with bamboo reinforced concrete the main concerns are deflection and crack control. Therefore, the simpler approach is preferable.

Equations 6.2 and 6.3 can be used to calculate the tensile (T) and the compressive forces (C) in a beam's section (Nanni, De Luca and Jawaheri Zadeh, 2014). The tensile force should be equal to the compressive force, and strain compatibility should be enforced. Therefore, an iterative process is needed to estimate c. If the section is under reinforced then only the tensile force in the reinforcement is calculated and the lever arm is found using $d - \frac{c_b}{2}$. Then the nominal moment capacity can be found using equation 6.4.

$$C = \alpha_1 f'_c \beta_1 b c \tag{6.2}$$

$$\alpha_1 = 0.85, \beta_1 = 0.85 - 0.008\left(f'_c - 30\right) \geq 0.65$$

$$T = A_b \varepsilon_b E_b \tag{6.3}$$

$$M_n = A_b \varepsilon_b E_b \left(d - \frac{\beta_1 c_b}{2}\right) \tag{6.4}$$

Where:

C = compressive load in the concrete (N)
α_1 = a factor that accounts for the strain gradient in the compression area
β_1 = factor that accounts for the different shapes of the stress-strain diagram relative to concrete strength
b = width of the concrete beam (mm)
T = tensile force in the reinforcement (N)
A_b = reinforcement area (mm^2)
E_b = reinforcement modulus of elasticity (MPa)
M_n = nominal moment of capacity (N.mm)

Since FRP reinforcement is not ductile, the American Concrete Institute (2015) penalises FRP under-reinforced sections and prescribes a lower safety factor for FRP rupture

(equations 6.5 and 6.6). It is appropriate to apply the safety factor in formula 6.6 for bamboo reinforced concrete because, similar to FRP, bamboo is a brittle material. In equation 6.6, the safety factor ϕ is equal to 0.65 for $\rho \geq 1.4\rho_b$. The transition in equation 6.6 for the safety factor is to ensure compressive failure in the concrete. CEB-FIB (2007) draws upon the 2006 version of American Concrete Institute (2015) and recommends a similar method where some of the constants are changed.

$$M_u = \phi M_n \tag{6.5}$$

$$0.55 \geq \phi = 0.65 - 0.25 \times (\rho - \rho_b)/\rho_b \geq 0.65 \tag{6.6}$$

Where:
M_u = ultimate moment of capacity (N.mm)
ϕ = safety factor
ρ = reinforcement area fraction (%)
ρ_b = reinforcement area fraction in a balanced section (%)

6.3 Concrete shear strength in bamboo reinforced concrete

Cox and Geymayer (1969) suggested that the shear strength of bamboo reinforced concrete can be designed according to the conservative working stress method using equation 6.7. Equation 6.7 is based on the shear strength of concrete in steel-reinforced concrete and is based on a working stress method. Cox and Geymayer (1969) found that some of the beams they tested failed in shear at loads much lower than estimated using equation 6.7. In addition, the model used in limit state design for steel-reinforced concrete is less conservative as shown in equation 6.8.

$$V_c = 0.292\sqrt{f'_c/10}bh \tag{6.7}$$

$$V_c = \frac{1}{6}\sqrt{f'_c}bd \tag{6.8}$$

Where:
V_c = concrete shear capacity (N)
b = the beam width (mm)
h = the beam height (mm)

d = the effective depth of the reinforcement (mm)

However, equations developed for the shear capacity of steel-reinforced concrete should not be applied to bamboo reinforced concrete. With bamboo reinforcement, similar to FRP, lower shear capacity is expected due to the low MOE of the reinforcement in comparison with steel reinforced sections. In steel-reinforced concrete the whole section transfer shear. The transfer of shear in steel-reinforced concrete is caused by the uncracked concrete in the compression zone, the aggregates mechanical interlock, dowel action, and residual tension in the reinforcement (Tureyen and Frosch, 2002). However, the low MOE of FRP and bamboo reinforcement results in wider cracks and a shallower neutral axis. The shallower neutral axis reduces the amount of concrete under compression and the wider cracks reduce the mechanical interlock between the concrete aggregates resulting in lower shear capacity relative to steel-reinforced concrete.

Therefore, American Concrete Institute (2015) makes the conservative assumption that the cracked concrete in FRP reinforced concrete carries no shear and only the concrete above the neutral axis (c) can transfer shear. Since the moment and shear both assume maximum values at the loading points when the beam is loaded at third point, it is expected that shear failure would occur at the load point. With a uniformly distributed load, moment do not assume maximal values at the same point and shear failure is more likely to occur near the support. For FRP reinforcement, American Concrete Institute (2015) suggests using equation 6.9 to estimate the shear resistance in the concrete. In this chapter, equation 6.9 is validated for use with bamboo reinforced concrete using the experimental results in the current research and literature.

$$V_c = 0.4\sqrt{f'_c}bc \qquad 6.9$$

6.4 Materials and flexural testing arrangement

The concrete mix used for all the beams was 1: 1.7: 3 (cement: fine aggregates: coarse aggregates) with a water-cement ratio of 0.5 and the aggregates were crushed river aggregates (the same mix in the pull-out test). The compressive strength was tested using three 100 mm cube specimens for every beam. The cube specimens were cured with the same conditions as the beams. The compressive strength of the concrete cubes on the day of testing, 28 days after casting, ranged between 36.6 and 51.2 MPa with an average cube strength of 47 MPa. The beams were cast in three layers of equal thickness, and the concrete was vibrated after the casting of each layer.

All of the bamboo splints were fabricated from eight Moso poles. Moso was chosen because it is a widespread species, easier to procure, and there are many studies on its properties. The splints were treated using linseed oil. The average splint had a width of 25 mm and a thickness of 8mm. Table 6.1 shows the details of the beams. For three of the beams, the splints were not corrugated. For 12 beams, different percentages of corrugated splints were used as reinforcement. Bundling the bamboo splints allows the use of a higher percentage of bamboo reinforcement (see Figure 6.2). All of the tested beams had the same dimensions as follows: 135X185X2600 mm (width X depth X length). These dimensions were chosen because they are within the span depth ratios (span depth ratio of about 16 was used in the current study) encountered in the common structural application and because it fits the moulds available in the concrete laboratory. The clear concrete cover is 20 mm for all beams. The beams were reinforced for shear with steel stirrups to ensure bending failure (10 mm shear stirrup per 80 mm in the shear span). Steel stirrups were used instead of bamboo stirrups to isolate the effect of bamboo as tensile reinforcement in concrete and to investigate whether compression failure can be achieved in the concrete before shear failure.

Table 6.1 Details of the tested bamboo reinforced concrete beams

Beam	Area of tensile reinforcement (mm^2)	Number of splints	Compression reinforcement (CR)	Bundled (B)	Corrugated (C)
B1	419	2	-	-	-
B2	416	2	-	-	-
B3	441	2	-	-	-
B4	628	3	-	-	C
B5	660	3	-	-	C
B6	680	3	-	-	C
B7	743	4	-	B	C
B8	792	4	-	B	C
B9	743	4	-	B	C
B10	388	2	CR	-	C
B11	393	2	CR	-	C
B12	371	2	CR	-	C
B13	478	2	-	-	C
B14	449	2	-	-	C
B15	441	2	-	-	C

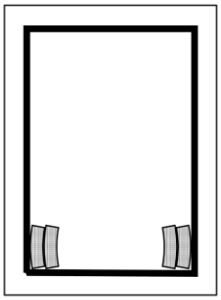

Figure 6.2 Section of a concrete beam with bundled bamboo reinforcement

Figure 6.3 shows the general arrangement of the bending test. The beams were tested under bending at third points (similar to most investigations in bamboo reinforced concrete) which means there is no shear in the middle third of the span.

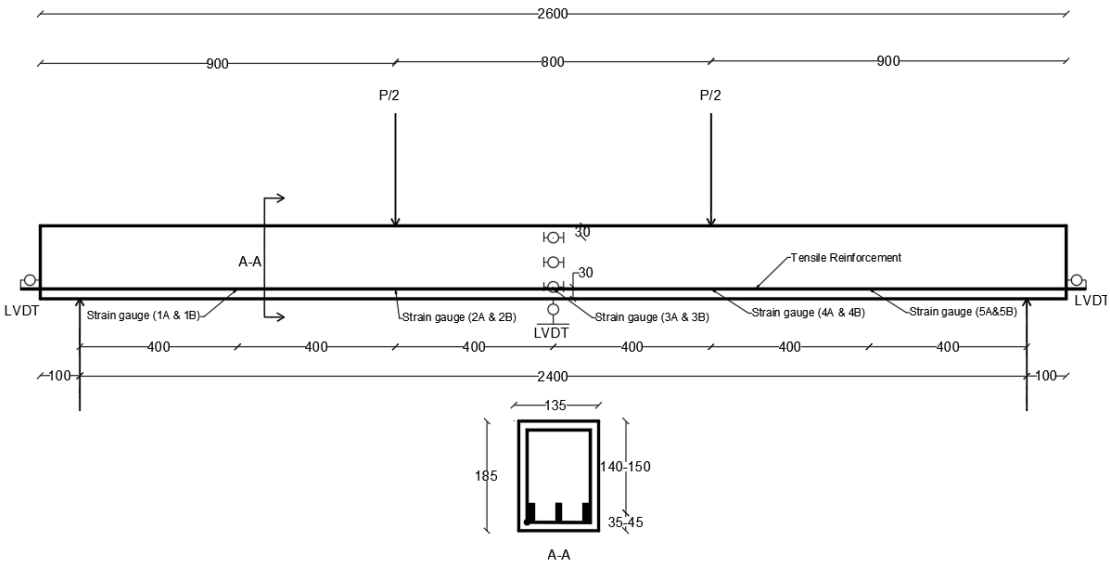

Figure 6.3 Plot of the flexural testing arrangement

The test was displacement controlled at 2 mm/min. Load and corresponding deflection were recorded. The reinforcement protruded 50 mm outside the concrete at each end to measure any possible slippage. LVDTs at the two ends were used to measure the slippage between the reinforcement and concrete. Three LVDTs were used to measure the strain in the concrete in mid-span at three levels. The first one is in the tension area (30 mm from the bottom fibres of the tension side); the second one is in the middle of the beam's depth, and the third one is in the compression area (30 mm from the top fibre of the compression side). The LVDTs strain points were 280 mm apart at the start of the test. Another LVDT measured the deflection at mid-span. For three of the beams (B13-B15), the strains in the reinforcement were measured. The strain was measured at 5 points for each reinforcing splint using electrical strain gauges.

6.5 Results of the flexural testing of bamboo reinforced concrete beams

Figure 6.4 to Figure 6.8 show load-deflection results for the tested bamboo reinforced beams. As it can be noticed from the figures, once the beams cracked there is a significant reduction in stiffness.

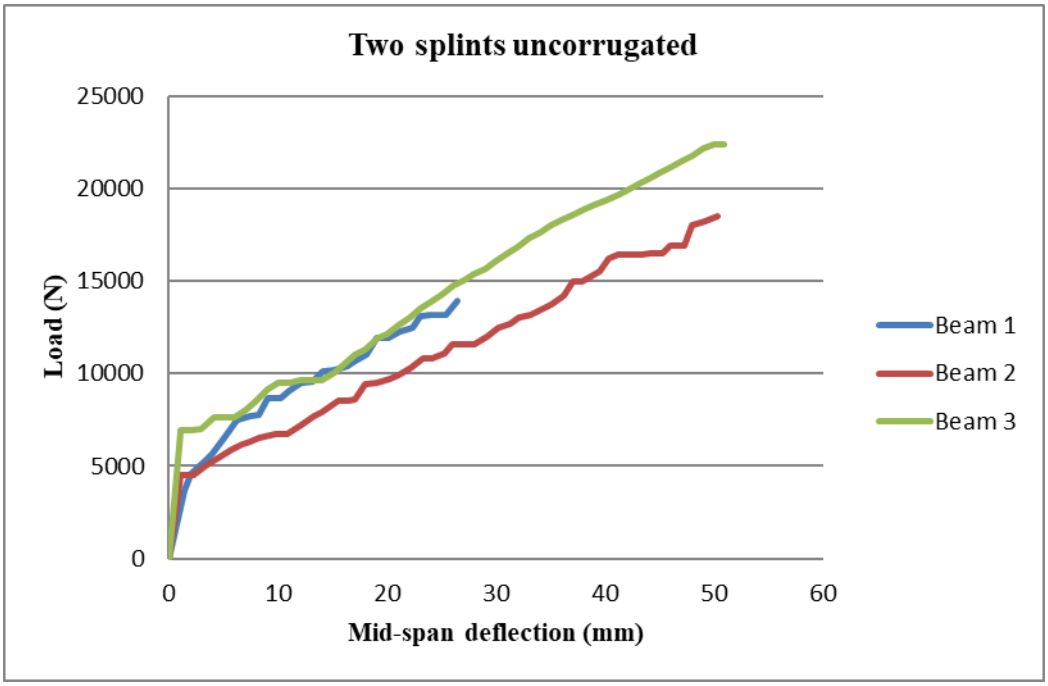

Figure 6.4 Graph of load-deflection of beams with two non-corrugated splints

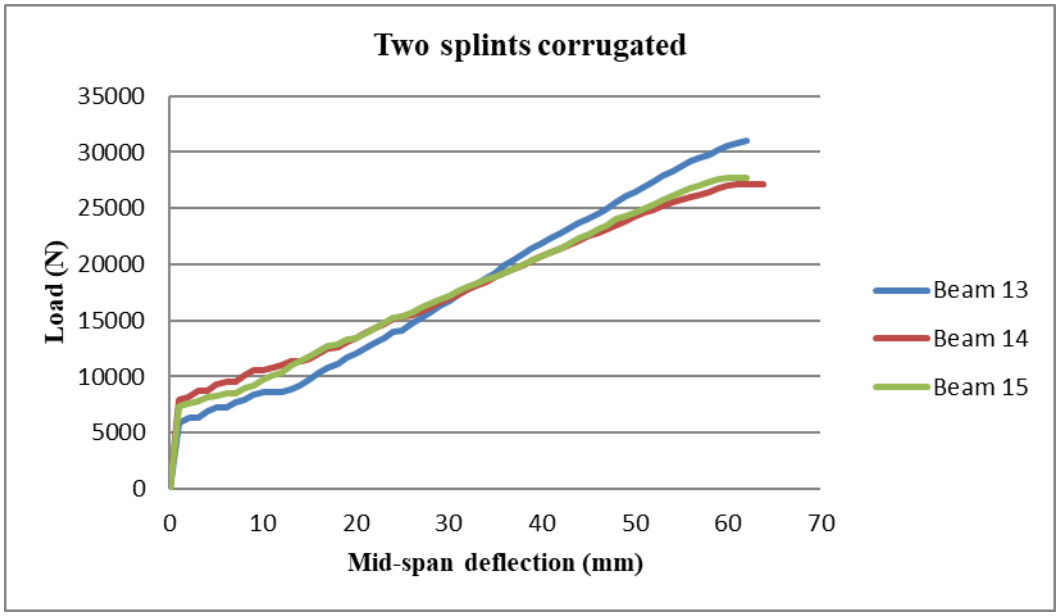

Figure 6.5 Graph of load-deflection of beams with two corrugated splints

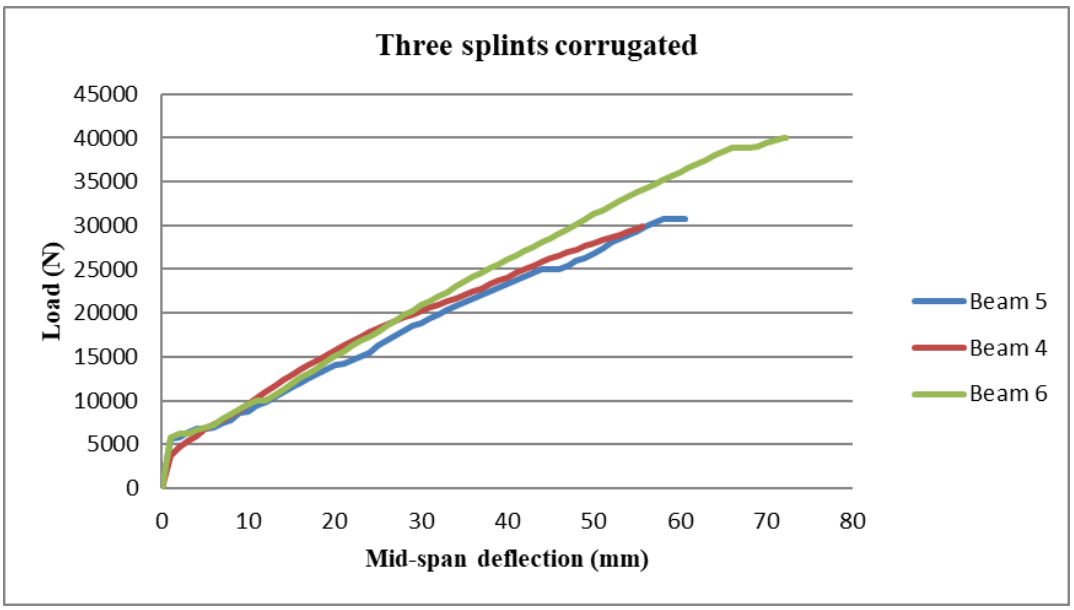

Figure 6.6 Graph of load-deflection of beams with three corrugated splints

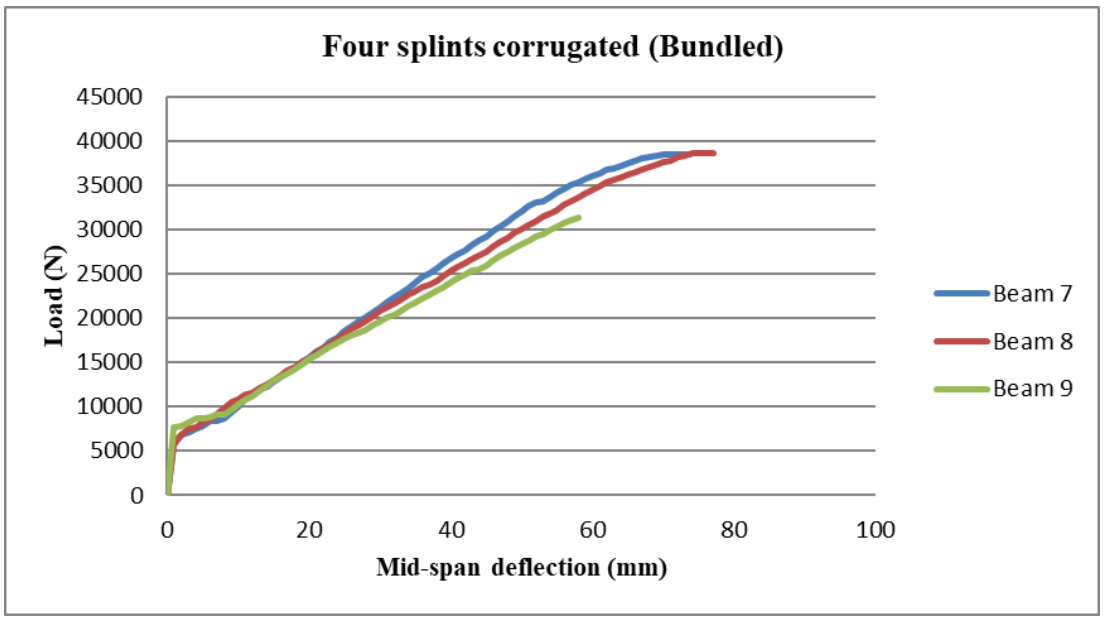

Figure 6.7 Graph of load-deflection of beams with four bundled corrugated splints

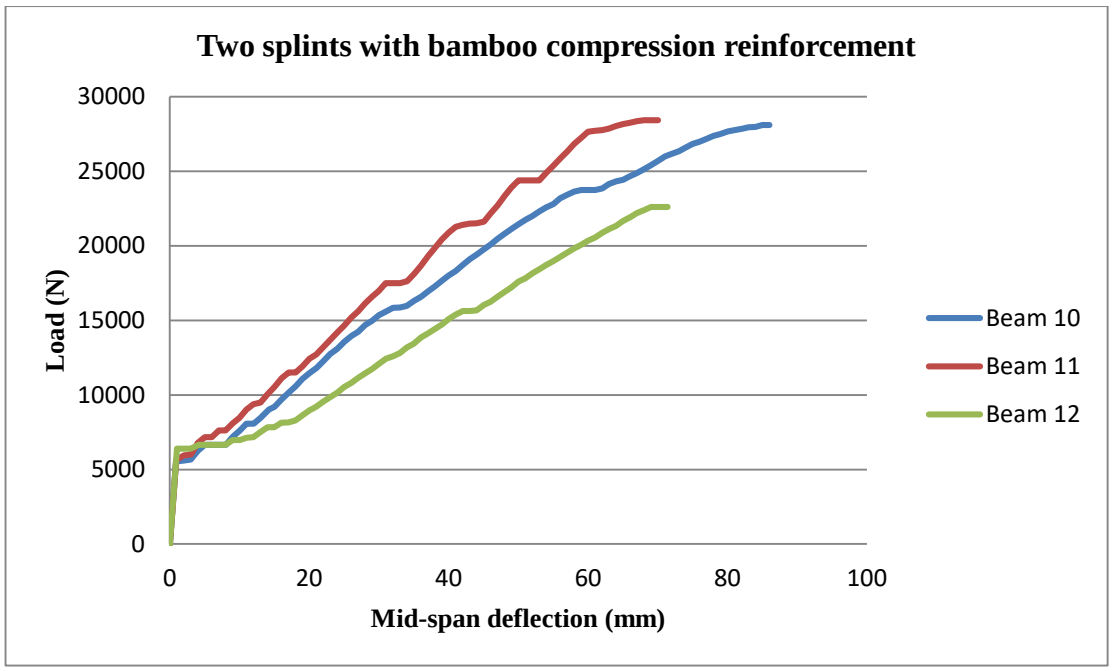

Figure 6.8 Graph of load-deflection of beams with two corrugated splints in tension and two corrugated splints in compression

Figure 6.9 shows the load VS reinforcement area at different levels of deflection where every point represents load resistance of one beam at a specific deflection. As can be seen from Figure 6.9, the effect of increasing the area of reinforcement on load is dependent on the deflection level because the slope of the linear fit increases with increasing deflection (Figure 6.9). This is expected because increasing the reinforcement increases the section stiffness. In addition, R^2, the fit of the trend line improves at higher deflection levels. The steeper fit line means that the effect of a larger reinforcement area is amplified at higher deflection values. The slope at 1 mm deflection is close to zero, and the correlation between the reinforcement area and load is very weak ($R^2 = 0.04$). As the deflection increases, the slope increases and the correlation improves. Indicating that the main effect of reinforcement on load resistance is not strong; however, the effect of the interaction between deflection and reinforcement area is strong. Interaction means that the effect of one independent variable on the dependent variable is modulated by the value of another independent variable.

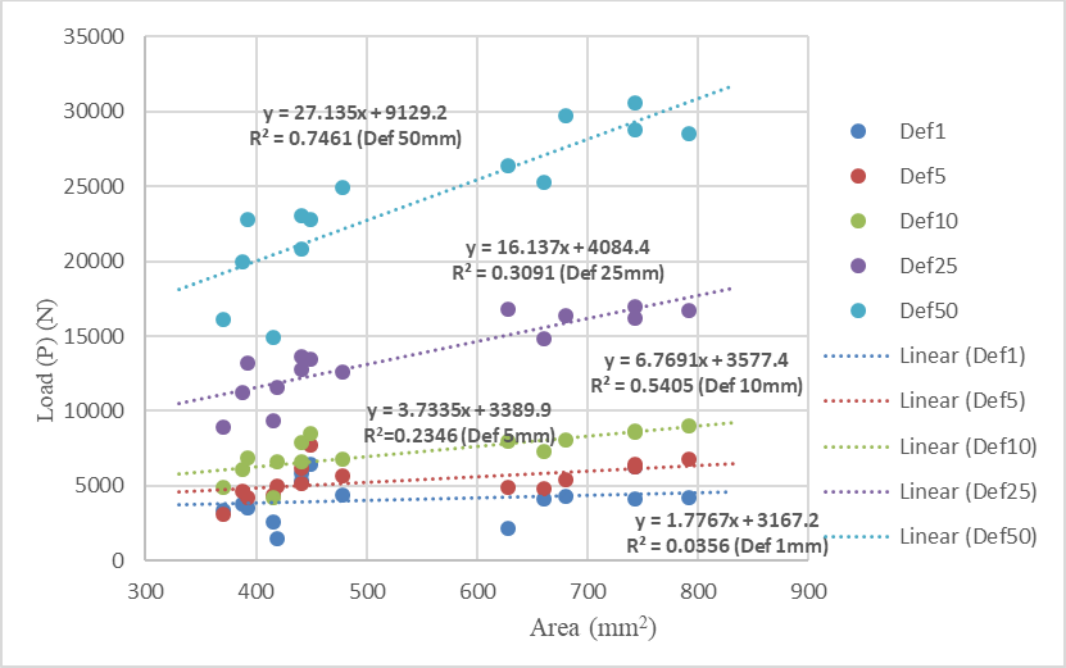

Figure 6.9 Scatter plot of load results VS reinforcement area at different deflection (Def (mm)) levels

6.5.1 Types of failure in the bamboo reinforced concrete beams

Beams 6-15 were tested to failure (Table 6.2). Two of the beams with bundled reinforcement (Beams 8 & 9) failed due to concrete compressive failure (see Figure 6.10) and the third due to combined shear flexural failure near the loading point (Beam 7, see Figure 6.11). The angle of crack was larger than 45^{o}, which enabled the crack to circumvent the shear reinforcement. The wide crack reduced the uncracked concrete, increased the compressive stress in the reinforcement, and lowered the shear capacity of the concrete. Beams 13-15 failed due to bond failure in the reinforcement; the splints were intact (see Figure 6.12). However, the width of the crack at the failure point increased rapidly at failure. The bond failure may be due to the effect of strain gauges protection material on bond in beams 13-15 (Figure 6.13). The protecting material (YM-COAT JA-1 Kit Polysulfide made by Vishay Precision Group Micro Measurements division) is soft to the touch and can hamper the bond. Bamboo reinforcement of B10-12 failed suddenly in tension.

Figure 6.10 Picture showing compression failure of Beam 8

Figure 6.11 Picture showing the shear failure of Beam 7

Figure 6.12 Picture showing the bond failure of Beam 14

Figure 6.13 Picture of the strain Gauge protection material

Table 6.2 The ultimate capacity results of the tested beams

Beam	Area of reinforcement (mm^2)	Failure	Ultimate moment capacity (KN.M)	Deflection corresponding maximum moment (mm)
B6	680	Shear/moment	16.0	71.7
B7	743	Shear/moment	15.4	71.0
B8	792	Compressive	15.4	73.9
B9	743	Compressive	12.6	57.8
B10	388	Tensile	11.2	86.3
B11	393	Tensile	11.4	67.3
B12	371	Tensile	9.0	68.9
B13	478	Bond	12.5	62.3
B14	449	Bond	10.9	61.0
B15	441	Bond	11.1	60.0

6.5.2 The neutral axis in the beams

Locating the neutral axis is necessary for the estimation of deflection. The location of the neutral axis affects the cracked second moment of area (I_{cr}). The transformed area method is used in the estimation of I_{cr} for steel and FRP reinforced beams (McCormac and Brown, 2014; Nanni, De Luca and Jawaheri Zadeh, 2014). In this approach, the reinforcement is replaced by an area of concrete with the same centroid as the reinforcement. However, the transformed area is equal to the product of the reinforcement area and $n = E_s/E_c$. The nonlinearity of concrete means that the MOE decreases with increasing stress, therefore, in American Concrete Institute (2008) the modulus is equal to $0.45f'_c$ divided by the corresponding strain. European Committee for Standarization (2004) takes advantage of the transformed area method; although, it suggests a slightly higher MOE for the concrete by using $0.40f'_c$ and the corresponding strain. The location of the neutral axis shifts as the deflection of the beam and strain in the reinforcement increase. Therefore, there are different methods used to locate the neutral axis depending on the objective. For deflection estimation purposes, the transformed area method is used where the concrete and the reinforcement are assumed linear elastic.

The transformed area method assumes a uniform neutral axis location along the cracked span. This assumption is more accurate when the reinforcement is stiff enough and have a strong bond with the concrete to limit crack localisation. Low reinforcement stiffness due to small reinforcement area or small reinforcement MOE, results in wider more localised cracking and consequently less uniform neutral axis along the span.

According to the transformed area method, the neutral axis should be deeper with higher reinforcement (Table 6.3). However, with bamboo reinforced concrete, increasing reinforcement area correlated with a shallower neutral axis (Figure 6.14). The experimental neutral axis is found based on the results of the Three LVDT gauges. These

results, however, represent only 280 mm of the span. In between the cracks, the strain in the reinforcement decreases due to tension stiffening and the neutral axis becomes deeper. The scatter in Figure 6.14 is due to the location of cracks relative to the strain gauge area. Limited cracking within the gauge area would result in an ostensibly deep neutral axis. As the reinforcement area increases, the experimental results converge with the theoretical values. It appears that there is a bias for cracking outside the strain gauge area for more lightly reinforced sections. This bias is due to the bond behaviour of bamboo reinforcement producing non-uniform cracking. A stiffer reinforcement and a stronger bond serve to arrest these cracks and provide more a uniform cracking along the section.

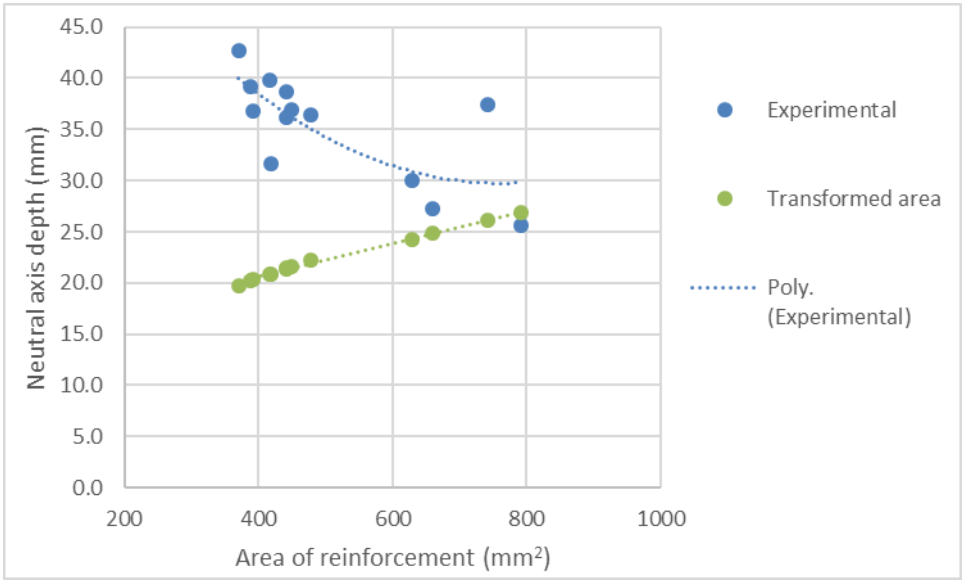

Figure 6.14 Graph of the neutral axis depth VS reinforcement area in the experimental results and the transformed area predictions

Table 6.3 The beams' experimental and theoretical neutral axis

Beam	Reinforcement Area (mm^2)	Experimental Neutral axis (mm)	Transformed area Neutral axis (mm)
B1	419	31.7	20.9
B2	416	39.8	20.9
B3	441	38.7	21.4
B4	628	30.0	24.3
B5	660	27.2	24.8
B7	743	31.5	26.2
B8	792	25.6	26.9
B9	743	37.2	26.2
B10	388	39.1	20.2
B11	393	36.8	20.3
B12	371	42.6	19.8
B13	479	36.5	22.2
B14	449	37.0	21.6
B15	441	36.1	21.4

6.6 Statistical analysis of the beams' load-deflection behaviour

The mixed linear model is used here to investigate the effects of reinforcement area, bond, and compression reinforcement on flexural stiffness. The longitudinal bond is the total shear force per unit length of the splint (τ_l) (N/mm). Longitudinal bond/area is used here to eliminate the collinearity between the splint area and the bond. This serves to better disentangle the effect of bond and the effect of the reinforcement area on the load-deflection behaviour. Longitudinal bond/area is found by dividing the longitudinal bond by the splint's area. The longitudinal bond of the splints was evaluated using the bond theoretical model developed in chapter 5. The purpose of this evaluation is to analyse the effect of bond on deflection using the mixed linear model. Equation 5.1 is used to evaluate the longitudinal bond of the bamboo splits used as reinforcement. It should be noted, as can be seen from Figure 6.15, that the linear regression model created in chapter 5 and the theoretical model of equation 5.1 are in close agreement.

Figure 6.15 Bar chart of the splints bond using equation 5.1 and the linear regression model

Table 6.4 shows that the main effects of the longitudinal bond/area (τ_l/A_b) and the area of bamboo reinforcement and compression reinforcement on load-deflection behaviour are not significant. Meaning, that the cracking of the concrete is not affected by the reinforcement area or the strength of the bond. However, their interaction with deflection is statistically significant. Meaning that increasing the reinforcement area and the longitudinal bond, improves the stiffness while bamboo compression reinforcement reduces the stiffness of the beams. The compression reinforcement reduces the stiffness because it displaces some of the concrete in compression which has higher compression MOE relative to bamboo.

Table 6.4 Parameters variable using the mixed linear model in SPSS

Parameter	Estimate	Std. Error	Degree of freedom	t	Sig.
Intercept	3934.880523	2305.623630	14.822	1.707	.109
Deflection	84.057831	30.381442	127.988	2.767	.007
Compression	-161.860271	1399.572045	13.276	-.116	.910
Longitudinal bond/Area	715.190451	3903.781704	14.144	.183	.857
Deflection * Compression	-54.346191	13.622353	143.504	-3.989	.000
Deflection * Longitudinal bond/Area	195.008015	45.996985	142.270	4.240	.000
Area	2.069202	3.419997	13.336	.605	.555
Deflection * Area	.389311	.034019	148.490	11.444	.000

Figure 6.16 presents a scatter plot of the predicted load VS the experimental load results at equal deflection for all the beams. The correlation is strong, with an R^2 value of 0.973. The high R^2 value means that the model explains most of the variability of the results.

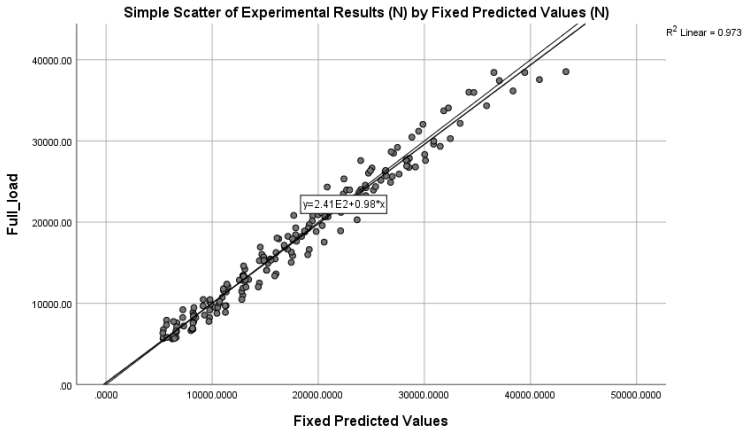

Figure 6.16 Scatter plot of the mixed linear model predicted values of load VS the experimental load results

To check normality, standard tests like Kolmogorov-Smirnov test and Shapiro-Wilk test are not recommended for sample sizes larger than 50 because they are too sensitive with larger samples (See D'Agostino (1971) and Ghasemi and Zahediasl (2012)). Meaning, that even a small deviation from a normal distribution can be significant with large sample sizes. Therefore, for the residuals, a visual test is carried to check for any departure from normality. Figure 6.17 shows that the residuals do not deviate much from a normal distribution. Figure 6.18 shows the distribution of the random variable and Table 6.5 presents the results for the normality tests for the random variable. The results indicate

that there is little deviation from the normal distribution for the random variable. Shapiro-Wilk and Kolmogorov-Smirnova are two different tests for normality. The Shapiro-Wilk test is considered to have more statistical power relative to the Kolmogorov-Smirnova test and it is better able to ‘’ detect whether a sample comes from a non-normal distribution’’ Ghasemi and Zahediasl (2012).

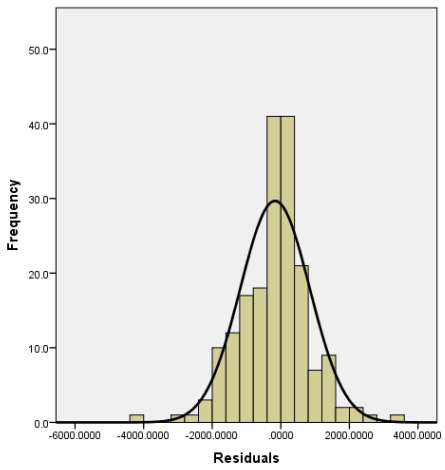

Figure 6.17 Histogram of residuals

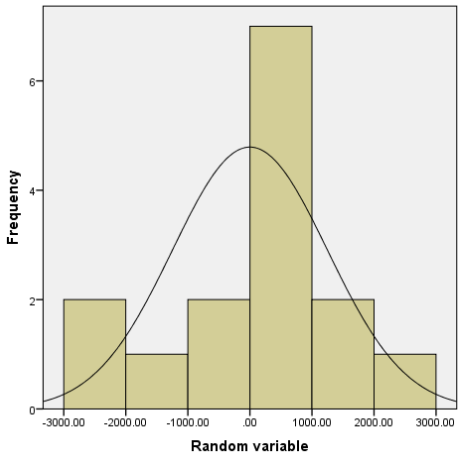

Figure 6.18 Histogram of the random variable

Table 6.5 Normality test for the random variable

	Kolmogorov-Smirnova[a]			Shapiro-Wilk		
	Statistic	df	Sig.	Statistic	df	Sig.
Random variable	0.193	15	0.138	0.960	15	0.690

a. Lilliefors Significance Correction

Different covariance matrices are used in mixed linear models to structure the variance at different levels. Table 6.6 offers a summary of the model’s likelihood and the number of parameters. In addition, it shows the significance of the change in likelihood. The diagonal variance matrix provides a significantly better fit to the data relative to the homogeneous compound symmetry matrix. Moreover, the diagonal matrix is not significantly different from the unstructured model.

Table 6.6 The covariance structures in the mixed linear model

Covariance Matrix	Restricted Log-Likelihood	Parameters	Comparisons	Sig.
a- Scaled identity	3095.49	10	Scaled identity VS Diagonal	0.000
b- Compound Symmetry	3095.49	11	Diagonal VS Unstructured	1.000
c- Diagonal	3017.038	26		
d- Compound Symmetry: Heterogeneous	3061.636	27		
e- Unstructured	2947.852	162		

6.7 Validation of the FE model

In this section, the FE model is validated and in the next section, the FE model is used to parameterise the bond failure model. The FE model is validated based on the experimental results produced in the current investigation. The validation is carried using the experimental results and the mixed linear model to avoid any outlier bias. Before validating the FE model, the longitudinal bond of the bamboo splints needs to be estimated.

Figure 6.19 to Figure 6.21 show the experimental and the mixed linear model results for the beams 6, 8, and 15. Beam 6 and beam 15 have 3 and 2 splints, respectively; while beam 8 has 4 bundled splints. The mid-span deflection is plotted against the total load applied at third points. As can be seen from the figures, the FE model agrees with the experimental results and the mixed linear model. The flat part of the FE line is the temporary softening due to cracking. The flattening is shorter in the experiments because there is micro cracking that makes the behaviour change between hardening and softening more often. Nonetheless, what is important is that the FE model approximates well the overall load-deflection of the beams.

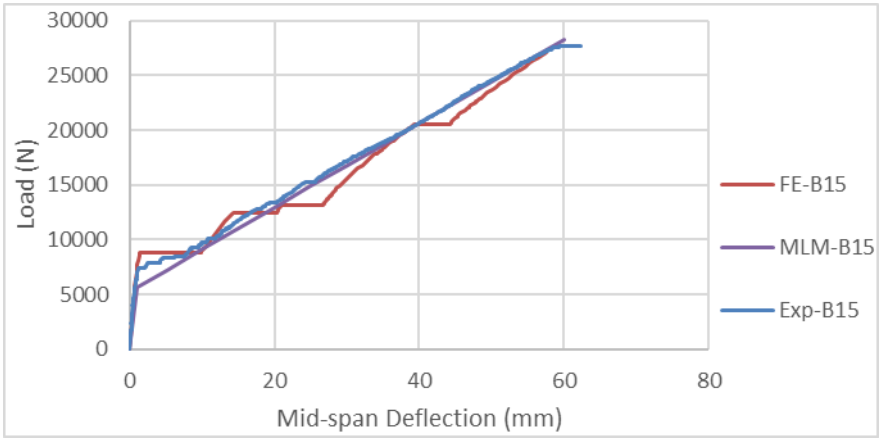

Figure 6.19 Graph of Finite element model (FE), Mixed Linear Model (MLM), and experimental results of Beam 15 (Exp)

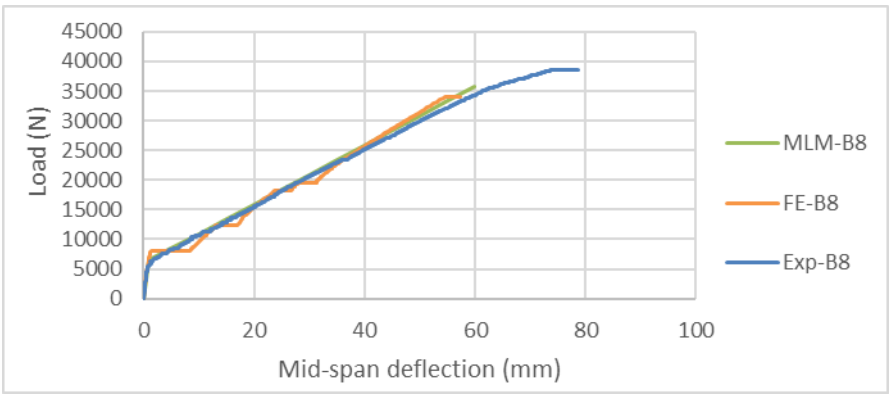

Figure 6.20 Graph of Finite Element Model (FE), Mixed Linear Model (MLM), and experimental Results of Beam 8 (Exp)

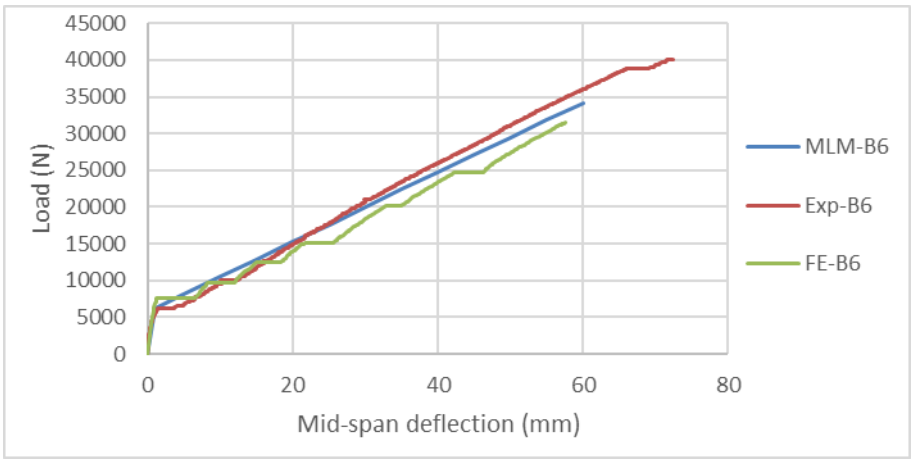

Figure 6.21 Graph of Finite Element Model (FE), Mixed Linear Model (MLM), and experimental Results of Beam 6 (Exp)

6.8 The bond failure model

In bamboo reinforced concrete, the assumption that the strain in the concrete and the reinforcement is proportional to the distance from the neutral axis can be violated due to bond failure. Therefore, a method will be presented in this chapter for the estimation of bond failure. In chapter 5, a model was developed for the estimation of the bond at high embedment lengths. The expression is, however, limited to cases where one crack develops in the span. These cases occur with lightly reinforced beams or in cases where the bond between the reinforcement and the concrete is weak. A stiffer reinforcement and a stronger bond force more cracks to develop and the cracking becomes more uniform along the span. Figure 6.22 and Figure 6.23 show the cracking in the FE model with low and high reinforcement, respectively.

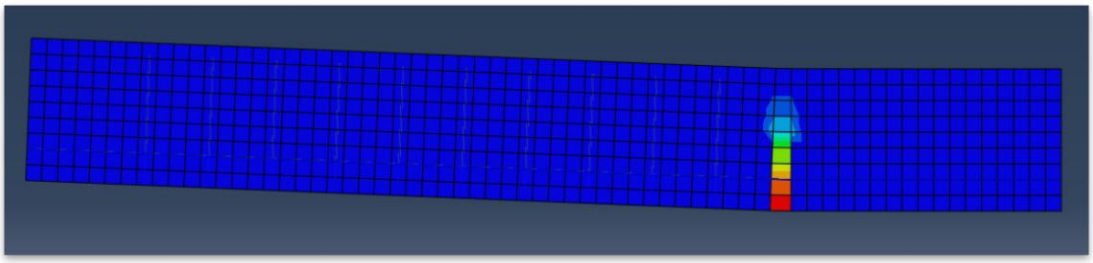

Figure 6.22 Snapshot of cracking with low stiffness reinforcement at the maximum moment (ρ=1.06%, E=13.9 GPa)

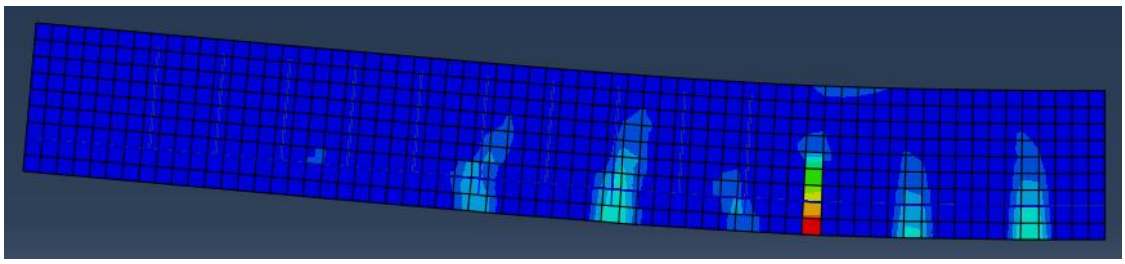

Figure 6.23 Snapshot of cracking with stiff reinforcement at the maximum moment (ρ=8.47%, E=13.9 GPa)

A theoretical model is proposed here that can estimate the tensile strength of the reinforcement at bond failure (σ_τ) with varying reinforcement levels and bond strengths (equation 6.12). The rationale for the theoretical model is that there is an upper limit and a minimum limit for the bond developed between the reinforcement and concrete depending on the stiffness of reinforcement. For the upper limit, a certain percentage of the maximum longitudinal bond can be achieved for the full cracked section due to the development of multiple cracks. The lower limit is based on the development of one crack and can be found using the model developed in Chapter 5 for the bond in uncracked concrete. There is a transition from the lower to the upper limit as the reinforcement area and MOE increases.

Nonlinear regression is used to determine the percentage of the maximum longitudinal bond can be utilised in equation 6.10 and the transition power in equation 6.12. The FE model results were used as inputs for the nonlinear regression. 31 FE beam models were used at varying degrees of bond and reinforcement. The reinforcement area was varied between 200 mm^2 and 1600 mm^2, 1.1-8.5% of the effective section, respectively. Two variables were used in the nonlinear regression, where through an iterative procedure, the values that best correlate the model to the FE results are chosen. The values were 0.654 in equation 6.11 and 1.246 in equation 6.12. The model has a strong correlation with the FE results; the model achieved an R^2 value of 0.956.

An upper limit for the proposed model is σ_{max} at which some percentage of the longitudinal bond ($\tau_{l,max}$) can be achieved for the cracked span (l_{cr}) from the support to the point of the maximum moment (equation 6.11). In equation 6.11, the cracked length can be found by determining the cracking moment (M_{cr}) and the support reaction under service load (p/2); while l is the span length between the supports. σ_{min} is the lower limit for the proposed model and it is based on the one crack assumption and can be found

using equation 6.10 where $F_1 + F_2$ are found using equations 5.8-5.14. In appendix D an example is provided to help the reader understand how the model can be applied.

$$\sigma_{min} = \frac{F_1 + F_2}{A_b} \quad 6.10$$

$$\sigma_{max} = 0.654 \times \tau_{l,max} l_{cr} / A_b \quad 6.11$$

$$\sigma_\tau = \left(\frac{\rho E_b}{1177}\right)^{1.246} \times \sigma_{max} + \left[1 - \left(\frac{\rho E_b}{1177}\right)^{1.246}\right] \times \sigma_{min} \leq \sigma_{max} \quad 6.12$$

Where:

σ_{min} = minimum stress in the reinforcement at bond failure (MPa)
σ_{max} = maximum stress in the reinforcement at bond failure (MPa)
l_{cr} = length of the cracked span from the support to the point of the maximum Moment (mm)
$\tau_{l,max}$ = maximum longitudinal bond (N/mm)
σ_τ = model prediction for the stress of the reinforcement at bond failure (MPa)

Figure 6.24 to Figure 6.29 show the FE results and predictions of the proposed theoretical model. In addition, The minimum estimate (σ_{min}) based on the bond in uncracked concrete model and the maximum estimate (σ_{max}) based on maximum bond model are included in the figures to show how the FE results transition from σ_{min} to σ_{max} as the reinforcement area and bond/area increase. The maximum stress in the reinforcement in bond critical sections is closer to σ_{min} when the reinforcement is less stiff. As the reinforcement stiffness increases, the behaviour approaches σ_{max}. If the tensile strength of bamboo is lower than that produced by the maximum embedment inside the concrete, then the full tensile strength of the bamboo can be utilized. Otherwise, bond failure would occur and there is no development length. Meaning, that the bamboo can never reach its tensile strength via its bond with concrete. In that case, the beam failure under flexure can be pseudo ductile due to the weak bond as assumed by Cox and McDonald (1970). However, the moment capacity is lower relative to that achieved with a stronger bond, and the stiffness of the beam is reduced.

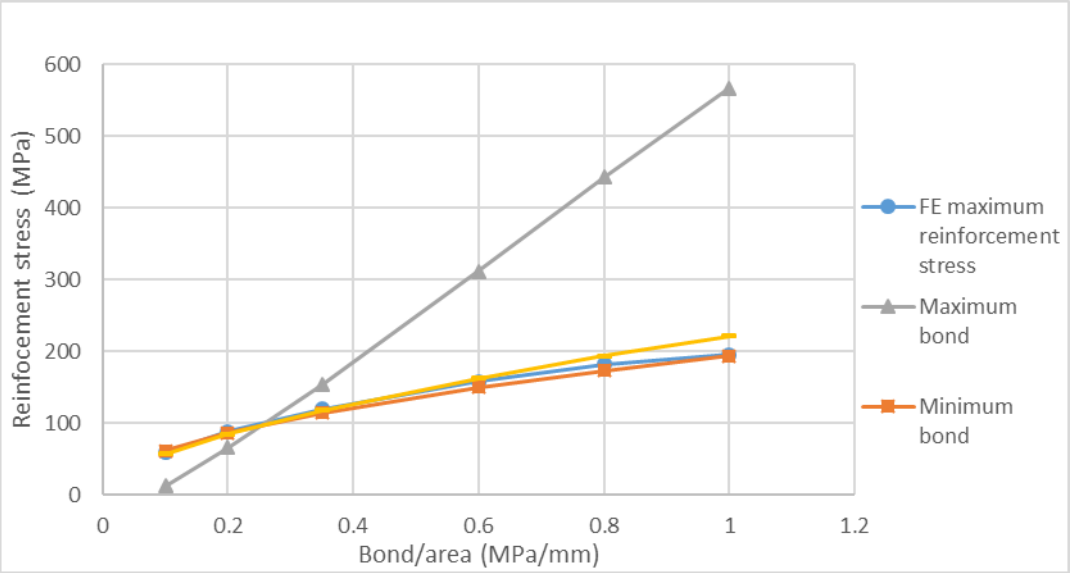

Figure 6.24 Graph of model predictions VS maximum reinforcement stress result in the FE model at ρ=1.06%

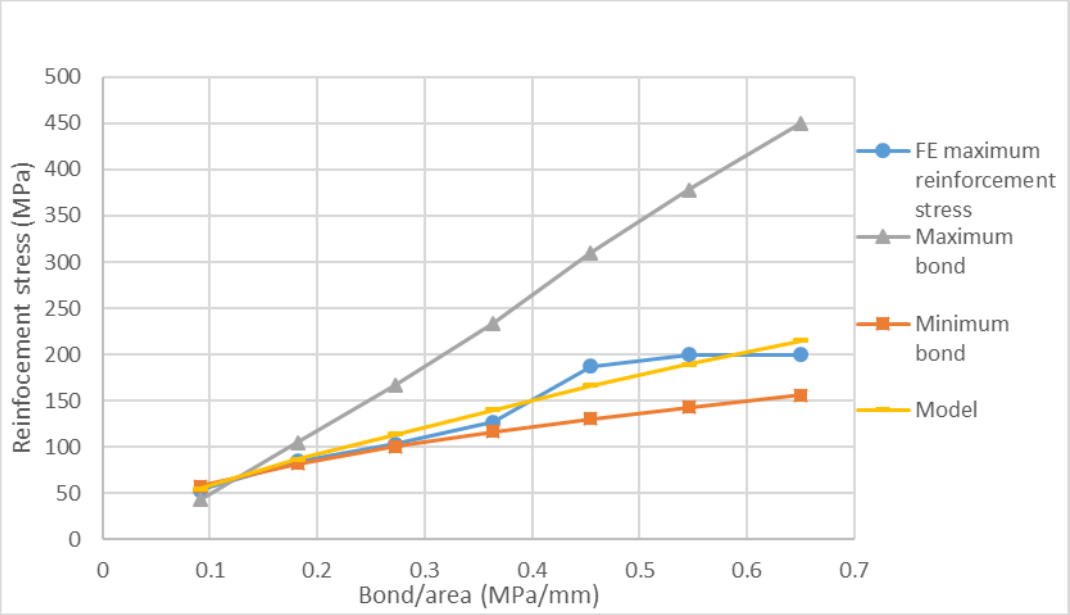

Figure 6.25 Graph of model predictions VS maximum reinforcement stress result in the FE model at ρ=2.32%

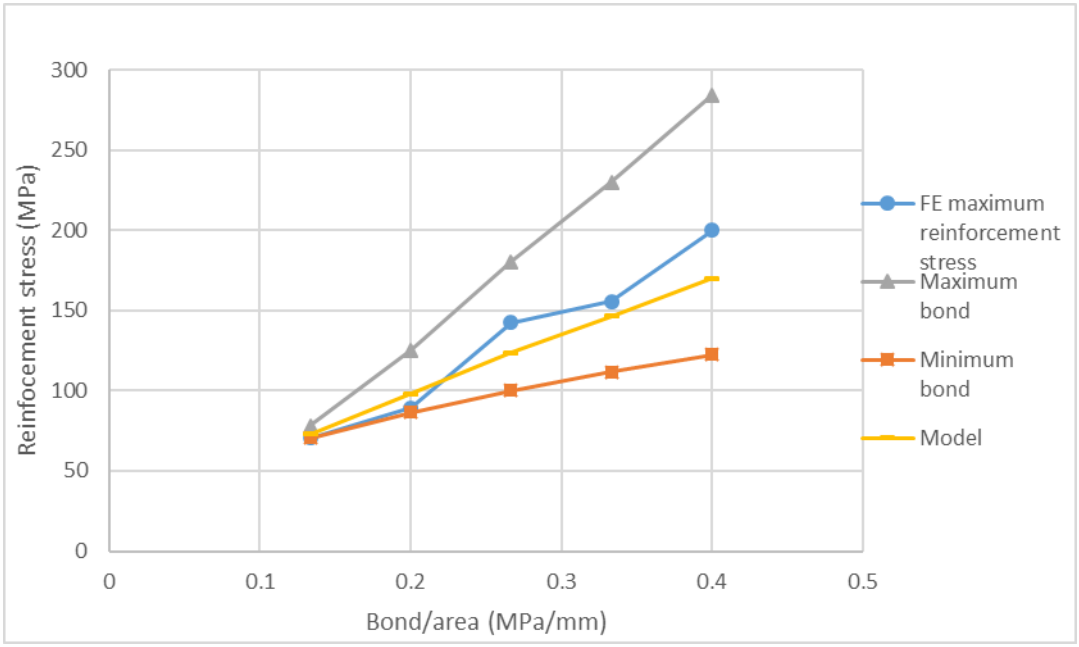

Figure 6.26 Graph of model predictions VS maximum reinforcement stress result in the FE model at ρ=3.17%

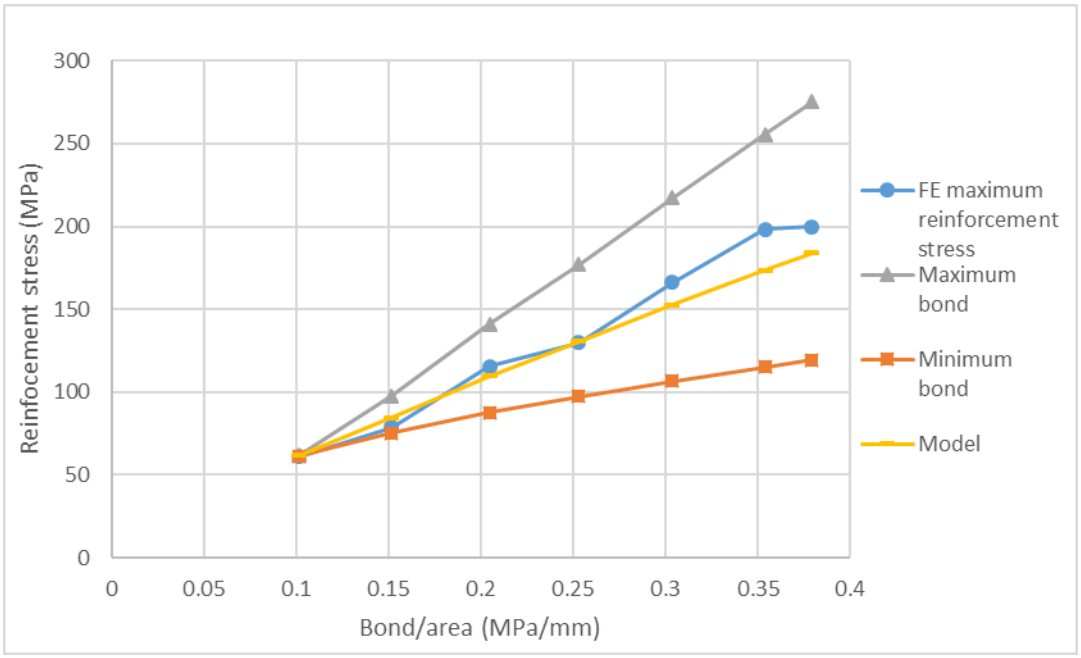

Figure 6.27 Graph of model predictions VS maximum reinforcement stress result in the FE model at ρ=4.19%

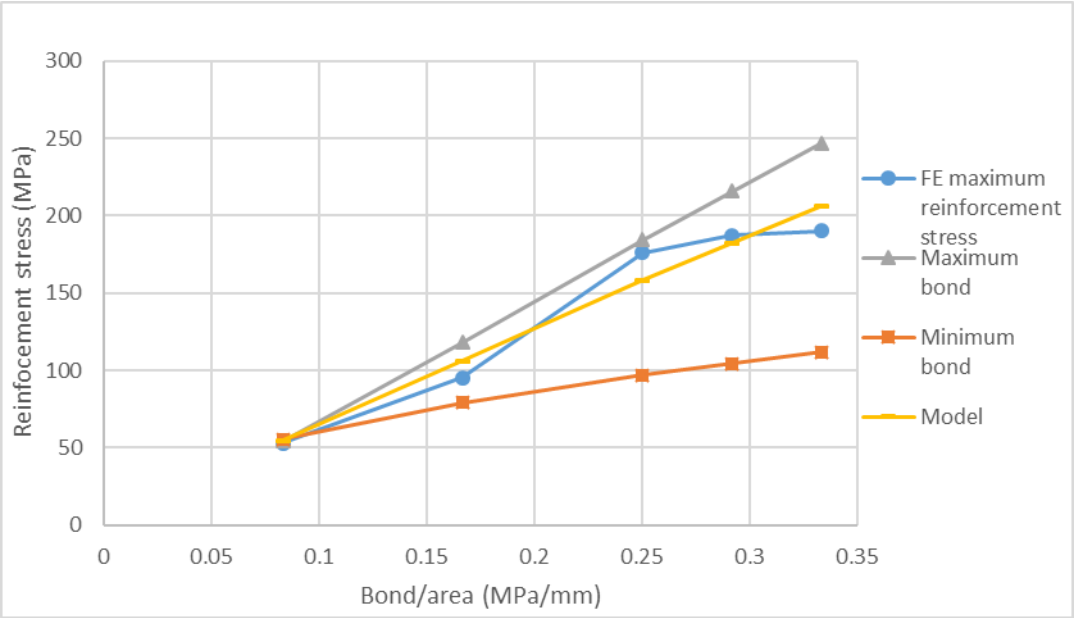

Figure 6.28 Graph of model predictions VS maximum reinforcement stress result in the FE model at ρ=6.35%

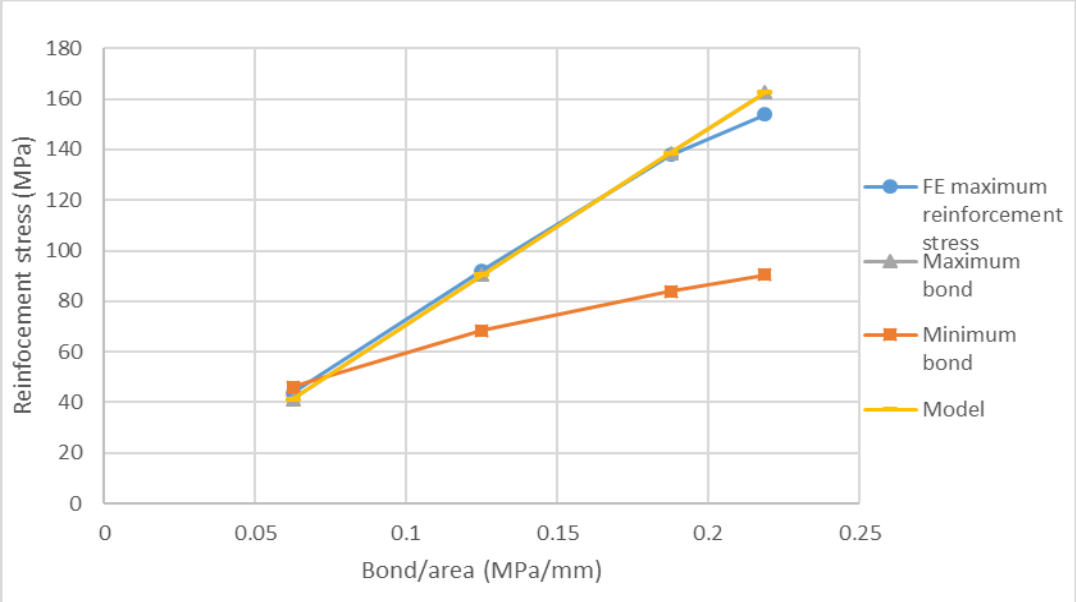

Figure 6.29 Graph of model predictions VS maximum reinforcement stress result in the FE model at ρ=8.47%

6.9 Validation of bonding, bending, and shear capacity models

In this section, the suggested models for bonding, bending, and shear are compared to the experimental results from literature and the experimental results carried during the current research. Table 6.7 shows the theoretical moment capacities based on the flexural, shear, and bond models suggested in the current research. Moment corresponding shear and bond failure are reported in Table 6.7 to provide an easier comparison with the experimental results. Appendix D provides the details of the beams. In addition, solution examples are provided to help the reader understand how the bond, shear, and flexural models are applied. It should be noted that the theoretical results reported here are the nominal capacities without the inclusion of safety factors. For shear, a 0.75 safety factor is required for steel and FRP reinforced concrete (American Concrete Institute, 2015). Similarly, for FRP reinforced concrete under flexure more conservative safety factors are used of 0.55 and 0.65 for under-reinforced concrete and over-reinforced concrete, respectively. In addition, the mean prism compressive strength is used for concrete strength in the calculation. For design purposes, the characteristic strength should be used which would result in more conservative estimates.

Table 6.7 Experimental and theoretical capacities of bamboo reinforced beams

Beam	ρ (%)	Ultimate experimental moment[a] (KN.M) (EC)	Theoretical moment based on perfect bond (KN.M)	Theoretical moment capacity based on bond (KN.M)	Theoretical moment based on shear failure (KN.M)	Critical Moment (CM)	EC/CM (%)	Stirrup
CG1[1]	2.42	2.20	7.16	2.43	4.33	2.43	90.5	-
CG2[1]	3.79	4.06	9.87	3.95	5.10	3.95	102.8	-
CG3[1]	6.16	4.40	12.80	5.57	5.90	5.57	79.0	-
CG4[1]	2.60	4.00	6.04	3.02	4.02	3.02	132.3	-
CG5[1]	4.26	4.75	7.41	4.12	4.59	4.12	115.3	-
CG6[1]	7.50	6.75	8.06	5.66	5.28	5.28	127.8	-
CG7[1]	2.60	4.47	6.08	3.73	4.18	3.73	119.9	-
CG8[1]	7.50	5.85	8.06	5.66	5.28	5.28	110.8	-
CG9[1]	2.60	4.06	6.03	4.18	3.99	3.99	101.7	-
CG10[1]	4.26	6.13	7.38	5.61	4.56	4.56	134.6	-
CG11[1]	7.50	7.51	7.66	5.75	5.00	5.00	150.3	-

Beam	ρ (%)	Ultimate experimental moment[a] (KN.M) (EC)	Theoretical moment based on perfect bond (KN.M)	Theoretical moment capacity based on bond (KN.M)	Theoretical moment based on shear failure (KN.M)	Critical Moment (CM)	EC/CM (%)	Stirrup
CG12[1]	2.66	6.13	6.10	6.10	4.02	4.02	152.5	-
CG13[1]	2.60	4.74	6.06	3.95	4.08	3.95	120.0	-
CG14[1]	4.26	6.82	7.48	5.44	4.67	4.67	146.1	-
CG15[1]	7.50	8.20	7.90	5.73	5.14	5.14	159.6	-
CG16[1]	5.27	8.20	7.79	7.79	4.71	4.71	174.0	-
CG17[1]	5.27	8.90	7.79	7.79	4.73	4.73	188.3	-
CG18[1]	5.27	8.90	7.84	7.84	4.91	4.91	181.3	-
CG19[1]	5.27	9.59	7.84	7.84	4.74	4.74	202.2	-
CG20[1]	5.27	9.59	7.96	7.96	5.43	5.43	176.5	-
A2[2]	3.36	18.75	20.00	-	10.58	10.58	177.2	steel
A3[2]	3.40	18.75	17.27	-	10.20	10.20	183.9	steel
B4[2]	4.85	25.20	24.50	-	11.95	11.95	210.9	steel
B5[2]	4.96	30.00	23.14	-	11.80	11.80	254.2	steel
C6[2]	5.19	15.00	20.53	-	8.35	8.35	179.7	bamboo
C7[2]	5.18	20.50	22.69	-	8.68	8.68	236.2	bamboo
D8[2]	5.23	19.50	20.14	-	11.46	11.46	170.2	steel
D9[2]	5.21	18.00	21.00	-	11.58	11.58	155.4	steel
BBR1[3]	6.94	4.20	9.50	-	4.86	4.86	86.3	-
BBR5[3]	6.46	6.00	20.80	-	7.50	7.50	80.0	-
BB1[3]	7.36	2.40	7.20	-	3.97	3.97	60.4	-
BB5[3]	4.47	12.00	16.20	-	5.44	5.44	220.6	-
BBR2[3]	7.83	6.60	9.90	-	6.38	6.38	103.4	bamboo
BBR6[3]	6.28	14.70	20.60	-	10.08	10.08	145.9	bamboo
BB2[3]	7.07	6.60	7.10	-	5.16	5.16	127.8	bamboo
BB6[3]	4.69	13.30	16.50	-	8.59	8.59	154.8	bamboo
BBR3[3]	7.22	7.20	9.60	-	16.77	9.60	75.0	steel
BBR7[3]	5.49	15.30	19.70	-	25.65	19.70	77.7	steel
BB3[3]	6.86	7.20	7.10	-	15.71	7.10	101.4	steel
BB7[3]	4.90	14.00	16.70	-	24.69	16.70	83.8	steel
BBR4[3]	7.04	6.00	9.50	-	7.07	7.07	84.8	cane
BBR8[3]	6.20	10.00	20.50	-	11.40	11.40	87.7	cane
BB4[3]	6.80	6.60	7.10	-	6.05	6.05	109.1	cane
BB8[3]	4.17	12.70	15.80	-	9.76	9.76	130.1	cane
YA[4]	3.86	26.80	27.30	13.00	13.25	13.00	206.2	bamboo
YB[4]	3.86	26.40	27.30	13.00	16.06	13.00	203.1	bamboo
1.5SCC 150[5]	1.50	1.35	2.87	-	0.90	0.90	150.5	-
1.5VC1 50[5]	1.50	1.80	2.87	-	0.93	0.93	194.4	-
3.0SCC 150[5]	3.00	2.03	5.74	-	1.22	1.22	165.4	-
3.0VC1 50[5]	3.00	2.03	5.74	-	1.27	1.27	159.8	-
1.5SCC 250[5]	1.50	4.05	9.31	-	2.91	2.91	139.4	-
1.5VC2 50[5]	1.50	4.46	9.31	-	3.00	3.00	148.5	-

Beam	ρ (%)	Ultimate experimental moment[a] (KN.M) (EC)	Theoretical moment based on perfect bond (KN.M)	Theoretical moment capacity based on bond (KN.M)	Theoretical moment based on shear failure (KN.M)	Critical Moment (CM)	EC/CM (%)	Stirrup
3.0SCC 250[5]	3.00	5.67	18.61	-	3.97	3.97	142.9	-
3.0VC2 50[5]	3.00	6.48	18.61	-	4.11	4.11	157.8	-
1.5SCC 275[5]	1.50	5.85	11.49	-	3.59	3.59	163.0	-
1.5VC2 75[5]	1.50	6.30	11.49	-	3.70	3.70	170.1	-
3.0SCC 275[5]	3.00	7.20	22.98	-	4.90	4.90	147.0	-
3.0VC2 75[5]	3.00	8.55	22.98	-	5.07	5.07	168.6	-
B6[6]	3.47	16.00	10.63	10.63	41.72	13.47	150.6	steel
B7[6]	3.80	15.40	11.62	11.62	41.99	13.95	132.5	steel
B8[6]	4.05	15.40	12.38	12.38	42.18	14.30	124.4	steel
B9[6]	3.79	12.60	11.61	11.61	41.98	13.94	108.5	steel
B10[6]	1.98	11.20	6.07	6.07	40.24	9.60	184.5	steel
B11[6]	2.01	11.40	6.14	6.14	40.26	9.71	185.6	steel
B12[6]	1.89	9.00	5.80	5.80	40.13	9.17	155.3	steel
B13[6]	2.44	12.50	7.48	7.48	40.75	11.69	167.1	steel
B14[6]	2.29	10.90	7.02	7.02	40.59	11.11	155.2	steel
B15[6]	2.25	11.10	6.89	6.89	40.54	10.90	161.0	steel

1: Cox and Geymayer (1969)
2: Sharma (1990)
3: Adom-Asamoah and Russell (2011)
4: Yamaguchi, Murakami and Takeda (2013)
5: Adom-Asamoah and Banahene Osei (2018)
6: Carried during the current research
a: Including the dead weight of concrete

It can be seen from Table 6.7 that for all the beams tested by Cox and Geymayer (1969), shear failure and bond failure are the critical limits. While the model used by Cox and Geymayer (1969) found that the shear strength was overestimated for some beams, the shear model suggested by American Concrete Institute (2015) for FRP reinforced beams yielded reasonable and conservative results. Beams with good bond due to the use of polyester and sand (CG16 and CG19), epoxy and sand (CG18 and CG19) had larger shear capacity than predicted by the model. Similarly, CG12 and C20 had larger shear capacity than predicted by the model due to the use of whole culms at the ends. The use of ends that consisted of whole culms improved the bond due to mechanical interlock. The higher than expected shear capacity is due to the relatively high reinforcement area and the strong bond that push the concrete shear behaviour towards that in steel-reinforced

concrete. Nonetheless, the American Concrete Institute (2015) formula yields more conservative and more reliable results relative to the method used by Cox and Geymayer (1969). The capacity of beams CG1 and CG3 were marginally overestimated; however, Cox and Geymayer (1969) reported that CG1and CG3 beams had longitudinal cracks due to the expansion through water absorption of the whole culms reinforcement.

Some of Adom-Asamoah and Russell (2011) beams failed at a lower load than expected. Similar to Sharma (1990), Adom-Asamoah and Russell (2011) did not test the bond of the bamboo reinforcement. However, unlike Sharma (1990), Adom-Asamoah and Russell (2011) did not use any treatment for bond purposes. Therefore, the theoretical bond failure is not estimated which can explain the overestimation of capacity. In addition, the spacing of the steel stirrups was too large for some beams which can enable the shear failure to develop without the resistance of stirrups. American Concrete Institute (2015) recommend that the spacing of stirrups is no larger than half the effective depth. The beams tested by Yamaguchi, Murakami and Takeda (2013) failed at a higher load than expected from their bond and shear capacity. The beams tested by Adom-Asamoah and Osei (2018) had not any shear reinforcement and as a result, their beam failed due to shear or possibly bond as they did not test the bond of their reinforcement.

The beams tested in the current research had steel reinforcement and the reinforcement was corrugated to achieve a strong bond with the concrete. As a result, it was possible to achieve compression failure in the concrete. The strong bond achieved using corrugated bamboo and the use of steel stirrups with d/2 spacing forced the section to fail due to compression failure for beams with high reinforcement. The beams tested in the current research achieved results that underestimate the flexural capacity. Table 6.7 shows that the beams achieved experimental bending capacities higher to the theoretical capacities based on the perfect bond assumption. The reason for this is possible due to the

underestimation of the tensile strength of the reinforcement at 121 MPa. Based on the moment achieved in the section the tensile stress in the reinforcement at failure ranged between 134 MPa in beam 9 where the failure was due to compression failure in the concrete, and 207 MPa in beams 10 &11 where the failure was due to tensile failure in the reinforcement. The next section explores the reason why the tensile strength was underestimated by the tensile test.

For the beams reinforced with bamboo stirrups, it was found that limiting the strain in the reinforcement to 30 MPa yielded reasonable results as it can be seen from the results of Adom-Asamoah and Russell (2011), Yamaguchi, Murakami and Takeda (2013), and Sharma (1990) (Table 6.7). Adom-Asamoah and Russell (2011) assumed that similar to steel, the full tensile strength of the bamboo shear reinforcement can be utilised. However, this assumption is invalid because, similar to FRP, the lower MOE of bamboo limits the amount of shear that the bamboo can carry. American Concrete Institute (2015) and ISIS Canada (2007) limit the strain in the shear reinforcement to 0.004 and 0.002, respectively. Limiting the strain in the bamboo to 0.002 with an average MOE of 15 GPa would result in a bamboo reinforcement tensile stress of 30 MPa.

To summaries, the models used in the current research to estimate bond, shear, and flexural capacities of bamboo reinforced concrete provided reasonable and conservative estimates. Researchers should be careful to test the bond of their reinforcement and provide adequate shear reinforcement in future research and more research is needed on bamboo shear reinforcement.

6.10 Comparing bamboo tensile testing methods

This section aims to investigate the reason why bamboo reinforcement achieved a higher tensile strength when used as reinforcement relative to the tensile test. Different methods

have been followed in the literature to test the tensile strength of bamboo while preventing failure at the grip. The International Organization for Standardization (2004) produced a standard for testing bamboo physical and mechanical properties that have since been withdrawn; the standard requires the end of specimens to be shaped in a way to ensure the failure in the gauge area; however, it does not specify how. The standard requires that a minimum specimen width does not fall below 10 mm and that the thickness should not be reduced. However, these limits would result in underestimating the tensile strength for thicker bamboo specimens. In addition, for lower bamboo culm diameter, the acute curvature limits the width of the specimen at the grip. The curved shape can result in a longitudinal split in the bamboo specimen. Lima Jr *et al.* (2008), Agarwal, Nanda and Maity (2014), Schneider, Pang and Gu (2014) and Kute and Wakchaure (2013) used Aluminium tabs with epoxy (Figure 6.31). The tabs (1-3 mm thick) were glued to the specimens in the grip area using the epoxy. The researchers explained that the taps with the epoxy could prevent the splints from being crushed by distributing the load: the epoxy fills the gaps that result from the curvature of the specimen (Figure 6.30). This allows the epoxy to transfer some of the compressive load to the specimen in the area where there is no direct contact with the tabs. Adewuyi *et al.* (2015) and Kute and Wakchaure (2013) did not reduce the section in the gauge area. Lima Jr *et al.* (2008) reduced the section in the gauge area to 1:5 ratio (width in the gauge area : width in the grip area).

Figure 6.30 Picture of a bamboo tensile specimen with the natural curvature

Figure 6.31 Picture of the use of tabs and epoxy for bamboo tensile test specimens

The efficacy of using aluminium tabs with epoxy and flattening bamboo ends to reduce gaps with the machine's grip id investigated here. The effect of the gauge width relative to the grip width on the failure is investigated. In addition, an explanation for the observed type of failure is presented. An extensometer was mounted to the sides of specimens to measure strain. The crosshead speed was fixed at 0.01 mm/second. Figure 6.32 and Figure 6.33 show the general testing arrangement and the machine's grip. The width of the section in the gauge area was about 10 mm for all 1:2 specimens. The full thickness of the culm was used in all samples. The grip of the machine can fit a width of up to 25 mm. In addition, there was a need to keep the section of the specimen as flat as possible. Therefore, the grip width was limited to 25 mm. The testing included two species of bamboo: Moso bamboo and Guadua Bamboo. These species are chosen because they are widespread species in East Asia and South America, respectively. After investigating the best way to do the testing with the node free specimens, three specimens with nodes from each species were tested. This is because node free specimens fail at a higher load and therefore more likely to fail due to the grip effect.

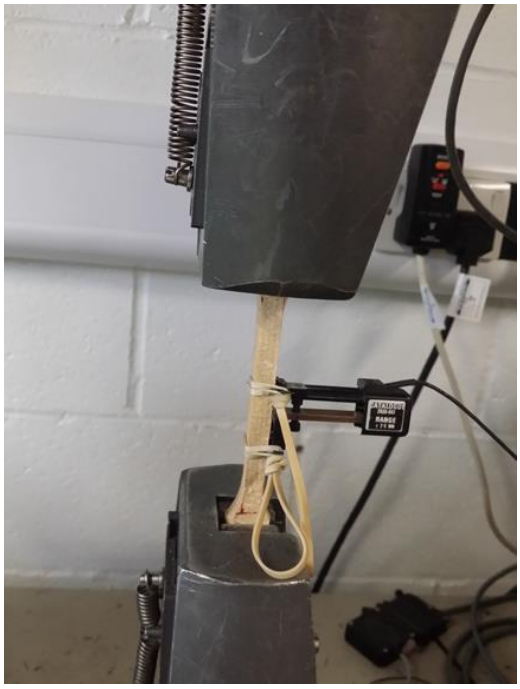

Figure 6.32 Picture of the tensile test arrangement

Figure 6.33 Picture of the tensile test's machine grip

Table 6.8 presents the results from the tensile test. Appendix C presents the full results for all of the specimens. All of the specimens with a gauge width to grip width ratio of 1:2 failed at the grip end (see Figure 6.34 and Figure 6.35). The Moso and Guadua bamboo specimens with a 1:3 ratio failed at higher average stress relative to Moso and Guadua bamboo specimens with the 1:2 ratio. In addition, the failure occurred in the gauge area (see Figure 6.38 and Figure 6.39). For the specimens with Aluminium tabs samples or flattened ends, the failure was at the grip (Figure 6.36 - Figure 6.41) and the tensile strength results were lower relative to the specimens with 1:3 ratio. While the tensile strength of Guadua and Moso bamboo was similar for the same gauge width to grip width ratio, the MOE of Guadua was significantly higher. Therefore, Guadua can deliver better deflection behaviour in bamboo reinforced concrete and should be investigated in future research.

Table 6.8 The average tensile strength of investigated bamboo specimens

Specimen ends treatment	Node	Species	Number of specimens	Grip width : Gauge width ratio	Mean tensile strength (Standard deviation) (MPa)	MOE (Standard deviation) (GPa)
-	-	Moso	3	1:2	133 (3.7)	13.8 (0.44)
-	-	Moso	3	1:3	170 (6.2)	12.4 (1.9)
Aluminium tabs + epoxy	-	Moso	3	1:2	127 (12.2)	12.5 (0.87)
Flattened	-	Moso	3	1:2	136 (21.4)	11.1 (0.91)
-	1	Moso	3	1:3	130 (5.9)	13.4 (1.1)
-	-	Guadua	3	1:2	139 (9.8)	21.2 (1.4)
-	-	Guadua	3	1:3	166 (6.8)	19.4 (2.2)
-	-	Guadua	3	1:4	165 (5.9)	21.5 (1.7)
-	1	Guadua	3	1:4	126 (14.9)	24.4 (1.6)

Figure 6.34 Picture of typical failure of Moso 1:2 ratio (top view)

Figure 6.35 Picture of typical failure of Moso 1:2 ratio (side view)

Figure 6.36 Picture of typical failure of Moso 1:2 ratio + Aluminium tabs and epoxy (top view)

Figure 6.37 Picture of typical failure of Moso 1:2 ratio + Aluminium tabs and epoxy (side view)

Figure 6.38 Picture of typical failure of Moso 1:3 ratio (top view)

Figure 6.39 Picture of typical failure of Moso 1:3 ratio (side view)

Figure 6.40 Picture of typical failure of Moso with flattened ends, 1:2 ratio (top view)

Figure 6.41 Picture of typical failure of Moso with flattened ends, 1:2 ratio (side view)

The univariate general linear model in SPSS is used to examine the results. The univariate general linear model is used because it combines linear regression (covariates) and categorical variables (factors). The investigated independent variables are species, test method, and the ratios of gauge width : grip width. Type III Sum of Squares is used in because of the unbalanced model (unequal number of observations between groups within the independent variable). The mean square is found by dividing the Sum of Squares by the number of degree of freedoms. The F-value is found by dividing the mean sum of squares for the factor by the mean error. shows that the effect of species is insignificant. Meaning, Moso and Guadua bamboo specimens had equal tensile strength. In addition,

there was no benefit in the use of Aluminium tabs or flattening the ends of the bamboo specimens.

Similar to the Moso bamboo specimens, Guadua bamboo specimens achieved higher tensile strength results at 1:3 and 1:4 in comparison with the 1:2 ratios. However, there was no difference between the 1:3 and 1:4 ratios (Table 6.9). Table 6.9 shows that specimens without nodes failed at higher tensile stress compared with specimens with nodes and that the average difference is 36.9 MPa.

Table 6.9 The univariate analysis of the bamboo tensile strength results

Parameter	β	Std. Error	t	Sig.	95% Confidence Interval	
					Lower Bound	Upper Bound
Intercept	99.104	8.930	11.098	.000	80.477	117.732
[species=1.00]	-4.284	6.204	-.691	.498	-17.227	8.658
[species=2.00]	0[a]	.	.	.	.	.
[1:2 ratio]	2.376	8.455	.281	.782	-15.262	20.013
[1:3 ratio]	29.893	8.124	3.680	.001	12.948	46.839
[1:4 ratio]	32.016	10.999	2.911	.009	9.071	54.960
[1:2 ratio + Aluminium tabs]	-8.733	9.082	-.962	.348	-27.679	10.212
[1:2 ratio + flattened ends]	0[a]	.	.	.	.	.
[Node=.00]	36.862	6.204	5.941	.000	23.920	49.805
[Node=1.00]	0[a]	.	.	.	.	.

a. This parameter is set to zero because it is redundant

The univariate general linear model assumes homogeneity of variance among the groups, and that the residuals (ε_{ijkl}) are normally distributed. Levene's test for homogeneity of variance is used to check the assumptions of the general linear model. The test significance value is 0.317, which means that the homogeneity assumption is not violated. In addition, the normality of the residuals is tested using Shapiro-Wilk and Kolmogorov-Smirnov normality tests. Both of which were not significant with values of 0.765 and 0.200, respectively.

In a tensile test, the machine grip applies a compressive force on the bamboo specimen proportional to the tensile force (F) to prevent the sample from slipping away (see Figure 6.42 and Figure 6.43). Bamboo specimens can be crushed under the testing machine grip before it reaches ultimate tensile strength because of bamboo's low compressive strength perpendicular to the grain. The reduction of the specimen width in the gauge area relative to the grip area reduces the compression on the specimen ends significantly. A reduction to a ratio of 1:3 (gauge width : grip width) reduces the compressive force from the machine by a factor of 3 for the same tensile stress.

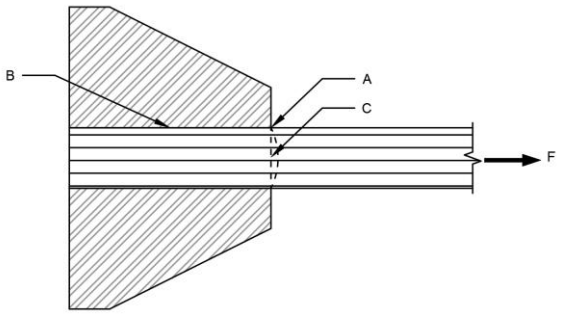

Figure 6.42 Section in the bamboo tensile test

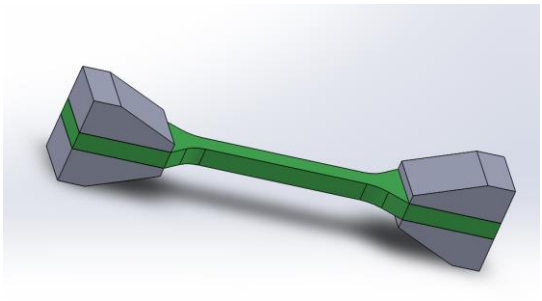

Figure 6.43 Illustration of a bamboo specimen and the loading grips

The stiff machine grip precipitates an additional problem in testing the tensile strength of bamboo. Bamboo is less rigid relative to the steel of the grip. Therefore, this prevents the bamboo form elongating within the grip length (in the direction of F) resulting in an abrupt increase in strain near the end of the machine grip (A). The strain at point B in Figure 6.42 is negligible assuming no slippage between the bamboo and the grip. Moreover, as a result of bamboo shear strain between the bamboo layers, the strain of the bamboo layer closest to the grip at point A is greater in comparison to the strain at point C. The grip transfers the tensile load (-F) to the bamboo immediately adjacent to it at point A through friction. The bamboo layer adjacent to the grip transfers the tensile load through shear to the layers beneath. Since bamboo is a brittle material, the failure is

initiated at point A before the bamboo at point C reaches the full tensile strength. Furthermore, the sharp increase of strain at grip end (A) reduces the area of shear flow. The force F at failure should be reduced by reducing the width of the bamboo in the gauge area to ensure tensile failure in the gauge area. Another solution is to reduce the thickness of the bamboo specimen; this would simultaneously reduce the force F at failure and limit the variation of strain between the centre of the bamboo specimen at point C and the grip at point A.

6.11 Discussion

This chapter answered research questions 3&4. It is shown that the flexural and shear capacities of bamboo reinforced concrete are analogous to FRP reinforced concrete. A model is provided for the bond failure of bamboo reinforced beams and validated using the experimental results.

In the proposed bond model, it is implicitly assumed that the failure is due to the degradation of the bamboo concrete surface. The splitting failure of the concrete is assumed to be unlikely because of the weaker bamboo bond relative to steel and FRP. However, with stronger bond treatment splitting in the concrete should be taken into consideration. It is expected that bamboo bond with concrete would require smaller cover in comparison with steel and FRP which can potentially relax the cover requirements advised for bamboo reinforced concrete. Reducing the cover would help in providing a higher percentage of bamboo reinforcement in the section and increase the depth of the reinforcement. It should be noted, however, that the requirements of concrete cover for the reinforcement have other purposes in addition to bond. The cover requirements include concerns such as durability and protection against fire. It is advised that the minimum requirements for cover for steel and FRP reinforcement are followed until more research becomes available.

More research is needed on the shear strength of bamboo reinforced concrete. The shear model can yield very conservative results, especially, when high reinforcement area and strong bond are provided. It is possible to link the concrete shear capacity of the concrete to the stiffness of the reinforcement and the strength of the bond. This would allow a more economical design. In addition, limited data is available on the use of bamboo as shear reinforcement. Therefore, it was tentatively proposed that the strain in the reinforcement should be considered not to exceed 0.002 mm/mm. In the literature, some researchers failed to report the bond and the MOE of their reinforcement (Adom-Asamoah and Russell, 2011; Sharma, 1990). In addition, researchers should be careful to report the bond of the reinforcement and the slippage corresponding maximum bond.

Based on bending capacity, it may be argued that using bamboo reinforcement is an attractive alternative to steel reinforcements, especially if higher reinforcement percentage is used and adequate bond is provided. However, as it will be shown in the next chapter serviceability limits of cracking and deflection are the critical concerns in the design of bamboo reinforced concrete.

6.12 Conclusion

Similar to FRP reinforced concrete, beams reinforced with bamboo should be designed to fail in compression. Since bamboo and FRP are brittle materials in comparison with steel, the bending capacity of bamboo reinforced concrete should be designed with a method analogous to the design method of FRP reinforced concrete. Similarly, shear in bamboo reinforced concrete is analogous to shear in FRP reinforced concrete where only the uncracked concrete can transfer shear. A method was presented for predicting bond failure in reinforced concrete beams and slabs. Increasing bamboo reinforcement area improves the stiffness of the section. Similarly, a stronger bond enhances stiffness. Corrugating bamboo to achieve a stronger bond is recommended to improve the stiffness of bamboo reinforced beams and slabs. Compression bamboo reinforcement negatively affects the stiffness of bamboo reinforced concrete. Bundling the reinforcement can be used to increase the reinforcement area in the section and achieve better deflection behaviour.

Chapter 7

7. Serviceability of Bamboo Reinforced Concrete Beams

7.1 Introduction

This chapter deals with two serviceability limit states of bamboo reinforced concrete. Section 7.2 deals with deflection where a deflection model is presented that can be used in the design of bamboo reinforced beams and slabs. The model can predict deflection with different bond conditions. Section 7.3 deals with cracking limits and validates two cracking models for use with bamboo reinforced concrete. Section 7.4 discusses the serviceability of bamboo reinforced concrete in comparison with steel and GFRP reinforced concrete. It shows that the critical design criteria of bamboo reinforced concrete is deflection and crack control. Section 7.5, provides a comparison between the carbon footprint of bamboo and steel-reinforced concrete. Section 7.6 discusses the work carried in this chapter and its limitations. Finally, section 7.7 provides the conclusion of this chapter.

7.2 Deflection

Design codes control deflection by suggesting a maximum span/depth ratio or by limiting deflection to specific values (American Concrete Institute, 2008; CEB-FIB, 1993). Deflection is controlled for the functionality of the structure and to avoid the perception of risk. Deflection can be estimated using Mohr's moment-area theorem where the curvature (Ψ) is inversely proportional to the second moment of area and the MOE (equation 7.1). The change of angle is equal to the integration of curvature over the span length (equation 7.2) and deflection (Δ) is equal to the integration of θ over the span length (equation 7.3).

$$\Psi = \frac{M}{EI} \tag{7.1}$$

$$\theta = \int_0^x \frac{M}{EI}.dx \tag{7.2}$$

$$\Delta = \iint_0^x \frac{M}{EI}.dx \tag{7.3}$$

Where:
Ψ = curvature
M = moment
I = second moment of area
θ = deflection angle
Δ = deflection

However, Mohr's moment-area theorem is not immediately applicable to reinforced concrete because it assumes linear elastic behaviour and does not account for cracking. In reinforced concrete, as the moment increases beyond the cracking moment, cracks develop and the second moment of area is reduced. The second moment of area assumes a minimal value at cracks and a maximal value at un-cracked sections. Cracking and deflection are intertwined phenomenon in reinforced concrete. Since cracks propagate at a low tensile strain in concrete, almost all of the curvature in the beam occurs at cracks.

Stiff reinforcement and a strong bond with concrete cause the cracks to be uniform, narrower, and more distributed. Less stiff reinforcement results in more localised cracking. However, it is difficult to predict the locations and the number of cracks due to the inherent variability of the concrete cracking behaviour. Therefore, design codes rely on empirical formulas and abandon a first-principles approach. The empirical formulas used in the design codes are based on experimental results of steel-reinforced beams and utilises the concept of an effective second moment of area (American Concrete Institute, 2008) or an effective curvature (European Committee for Standardization, 2004). Therefore, these empirical formulas are not necessarily valid in beams that have reinforcement with different mechanical properties and bond behaviour such as bamboo.

The effect of reinforcement on the stiffness of the non-cracked reinforced element is limited. However, after cracking, the beam's stiffness is strongly dependent on the stiffness of the reinforcement. In addition, the cracked concrete contributes to the overall stiffness due to tension stiffening. Tension stiffening is caused by the concrete surrounding the reinforcement. The cracked concrete surrounding the reinforcement is considered to increase the reinforcement stiffness artificially in between the cracks by reducing its strain. While the role of tension-stiffening in bending capacity is negligible, it has a significant effect on deflection behaviour. The tension stiffening effect is dependent on the bond between the reinforcement and the concrete, and the reinforcement stiffness. Weak bond and low reinforcement stiffness diminish the tension stiffening effect. In addition, as the moment increases the effect of tension stiffening decreases.

This section develops a method for the estimation of bamboo reinforced concrete deflection. Subsection 7.2.1 reviews the methods used to model the deflection in steel-reinforced concrete; while, subsection 7.2.2 reviews the methods used to model the deflection of FRP reinforced concrete. In subsection 7.2.3 the models discussed in 7.2.1

and 7.2.2 are used to model the deflection behaviour of bamboo reinforced concrete. The proposed model for bamboo deflection is presented in subsection 7.2.4. Subsection 7.2.5 validates the proposed deflection model.

7.2.1 Deflection behaviour of steel-reinforced concrete

The European code assumes a quadratic transition (ζ) for curvature from a non-cracked section curvature (Ψ_1) to a fully cracked section curvature (Ψ_2) as the service moment (M_a) exceeds the cracking moment (M_{cr}) (equations 7.4-7.7) (European Committee for Standardization, 2004). The curvature needs to be estimated at different sections along the span, and then deflection is estimated by double integration of the curvature over the span length. Boundary conditions are enforced to solve the integration constants.

$$\Psi_e = \zeta\Psi_2 + (1-\zeta)\Psi_1 \quad (7.4)$$

$$\Psi_1 = \frac{M_a}{E_c I_g} \quad (7.5)$$

$$\Psi_2 = \frac{M_a}{E_c I_{cr}} \quad (7.6)$$

$$\zeta = 1 - \left(\frac{M_{cr}}{M_a}\right)^2 \quad (7.7)$$

Where:

ψ_e = effective curvature
ζ = curvature trarnsition function
Ψ_1 = curvature in an uncracked section
Ψ_2 = curvature in a fully cracked section
I_g = gross second moment of area (mm^4)
I_{cr} = cracked second moment of area (mm^4)
M_a = service moment (N.mm)
M_{cr} = cracking moment (N.mm)
E_c = concrete modulus of elasticity (MPa)

The ACI code uses Branson and Metz (1963) equation to estimate an effective second moment of area (I_e) that represents the full span. In this approach, stiffness is considered uniform along the span and the integration is carried using this one simple value (equation 7.8). Power m designates the transition from the gross (I_g) to the cracked second moment of area (I_{cr}) and higher values accelerate this transition resulting in a more conservative estimate of stiffness. American Concrete Institute (2008) recommends a value of 3 for steel-reinforced concrete. This value accounts for the concrete tension stiffening along the cracked span and for the un-cracked portion of the span. Setting the value of m to 4 is considered to account only for the tension stiffening (Bischoff, 2005).

$$I_e = \left(\frac{M_{cr}}{M_a}\right)^m I_g + \left[1 - \left(\frac{M_{cr}}{M_a}\right)^m\right] I_{cr} \leq I_g \qquad 7.8$$

7.2.2 Deflection behaviour of FRP reinforced concrete

In this section, the methods used for the estimation of deflection are used to shed light on the deflection behaviour of bamboo reinforced concrete. With the onset of FRP reinforcement, it was found that models developed originally for steel do not always yield accurate results for FRP reinforced concrete. Methods used for steel had to be modified for the application in FRP reinforced concrete because FRP reinforcement has a much lower MOE relative to steel. Bischoff (2005) showed that Branson and Metzs' (1963) model should not be used for FRP reinforced concrete because Branson and Metzs' (1963) model was developed for beams with lower I_g/I_{cr} than that encountered for most FRP reinforced beams and therefore can overestimate the stiffness. Branson and Metzs' (1963) equation was developed using the result of beams with I_g/I_{cr} ratio of about 2.2 (Bischoff, 2005). Similarly, in bamboo reinforced the I_g/I_{cr} ratio is higher relative to steel reinforced concrete as a result of the lower MOE.

There have been several attempts to account for the difference in deflection between Steel and FRP reinforced concrete. Masmoudi, Thériault and Benmokrane (1998) suggested using a reduction factor (β_b) to reduce I_g by 40% in the case of GFRP (equation 7.9). American Concrete Institute (2003) used this reduction factor; however, it made it dependent on the reinforcement MOE and bond condition (α_b) (equation 7.10). A value of 0.5 for (α_b) was suggested until more research is done on the bond effect. In American Concrete Institute (2015), the previous model is substituted for Bischoff's (2005) model (equations 7.11&7.12).

$$I_e = \left(\frac{M_{cr}}{M_a}\right)^m I_g \beta_b + \left[1 - \left(\frac{M_{cr}}{M_a}\right)^m\right] I_{cr} \leq I_g \tag{7.9}$$

$$\beta_b = \alpha_b \left(\frac{E_{FRP}}{E_s} + 1\right) \tag{7.10}$$

$$I_e = \frac{I_{cr}}{1 - y\left(\frac{M_{cr}}{M_a}\right)^2 \left(1 - \frac{I_{cr}}{I_g}\right)} \leq I_g \tag{7.11}$$

$$y = 1.72 - 0.72\left(\frac{M_{cr}}{M_a}\right) \tag{7.12}$$

Bischoff's (2005) model is based on the observation that the largest curvature difference between a fully cracked beam and an un-cracked beam is at the point where the beam just started cracking. Increasing the moment closes the gap between the two beams. The difference in curvature between a fully cracked beam and a beam with some concrete tension stiffening decreases asymptotically to zero as moment increases.

7.2.3 Modelling the deflection of bamboo reinforced concrete using existing models

In this section, six models that were proposed for steel and FRP reinforced concrete are compared to the results in the current investigation. It should be noted that the results from the mixed linear model are used in this comparison to avoid comparison with outliers. In addition, as it was shown in section 6.7, the mixed linear model (MLM) agrees closely with the experimental results. The investigated models are as follows:

1. Branson and Metz (1963) deflection model for steel-reinforced concrete using m=3 (BR3);
2. Branson and Metz (1963) deflection model for steel-reinforced concrete using m=4 (BR4);
3. European code deflection model for steel-reinforced concrete (CEB-FIB, 1993) (EN);
4. Masmoudi, Thériault and Benmokrane (1998) deflection model for FRP reinforced concrete (Mas);
5. Bischoff (2005) deflection model for FRP reinforced concrete (BI);
6. American Concrete Institute (2003) deflection model for FRP reinforced concrete (ACI-03).

Figure 7.1 to Figure 7.6 show the estimates of the different models and the MLM results for three beams B6, B8, and B15. The beams chosen had three different levels of reinforcement. B15, B8, and B6 have 2, 4, and 3 bamboo splints, respectively. Figure 7.1 to Figure 7.6 show that all of the models provide reasonable estimations of deflection.

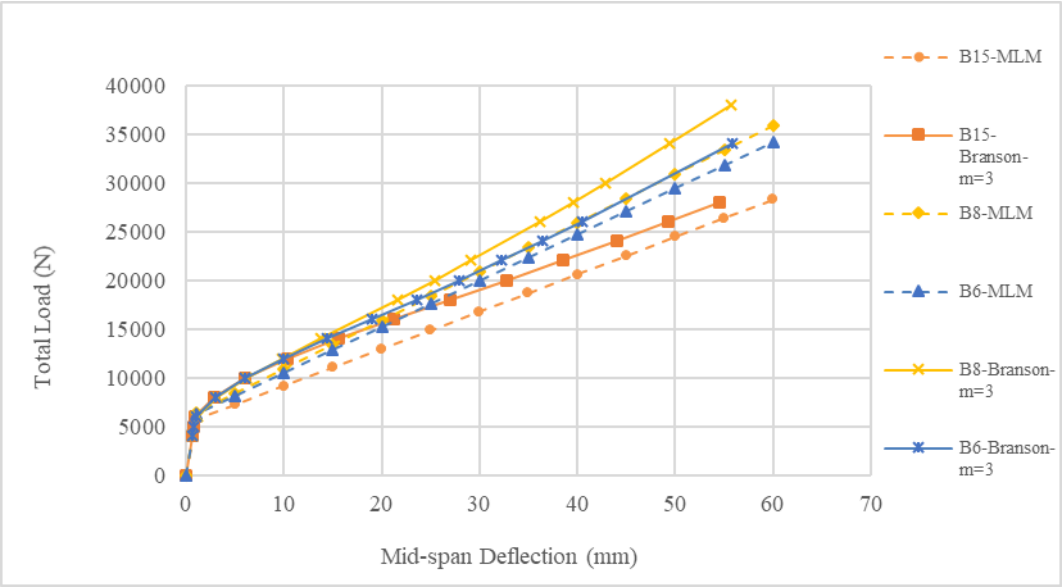

Figure 7.1 Plot of mid-span deflection VS total load using Branson and Metz (1963) model estimates using m=3 (m describes the transition from I_g to I_{cr})

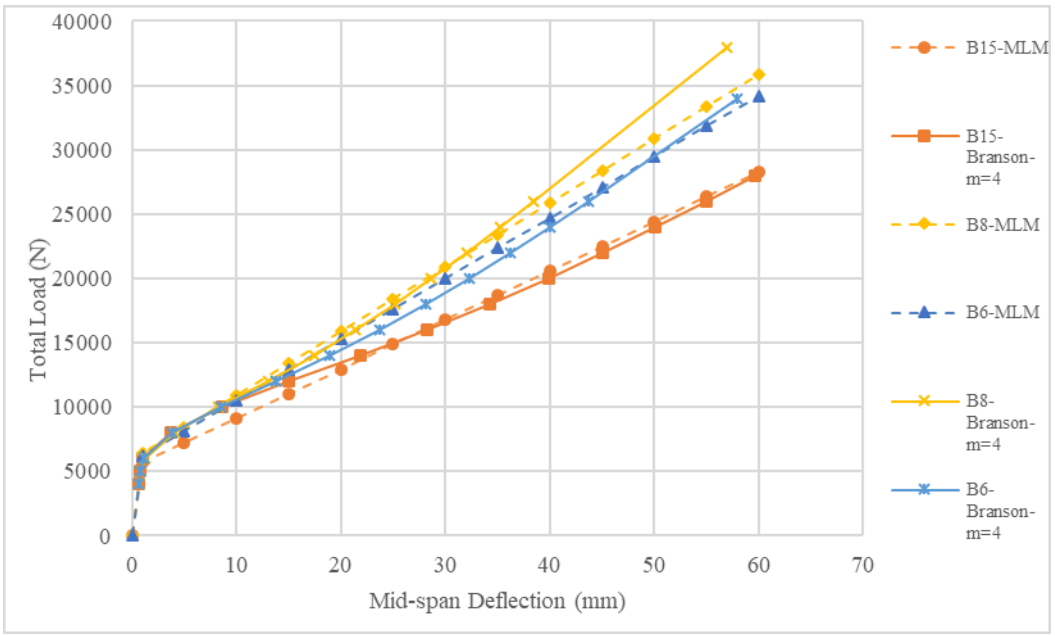

Figure 7.2 Plot of mid-span deflection VS total load using Branson and Metz (1963) model estimates using m=4

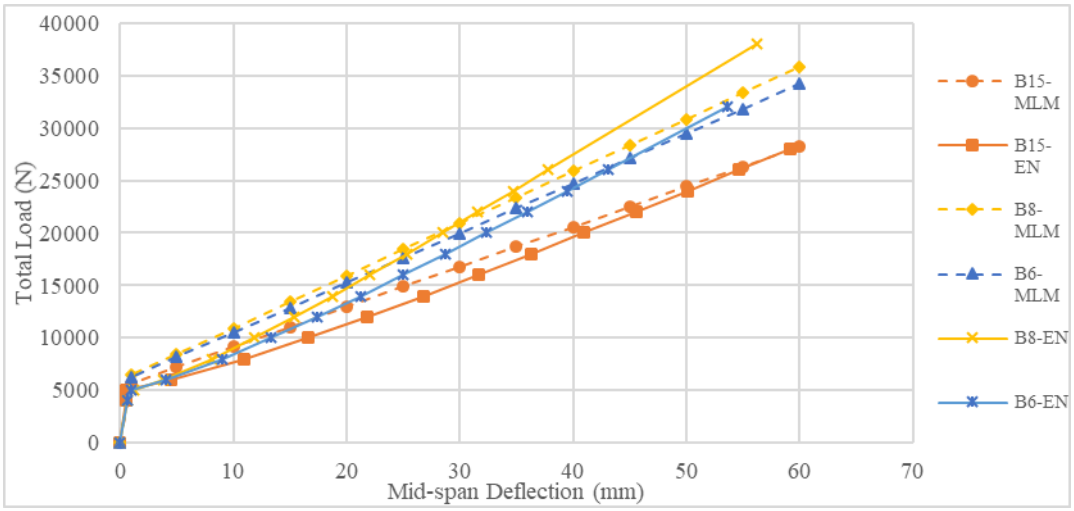

Figure 7.3 Plot of mid-span deflection VS total load using European code deflection model estimates (CEB-FIB, 1993)

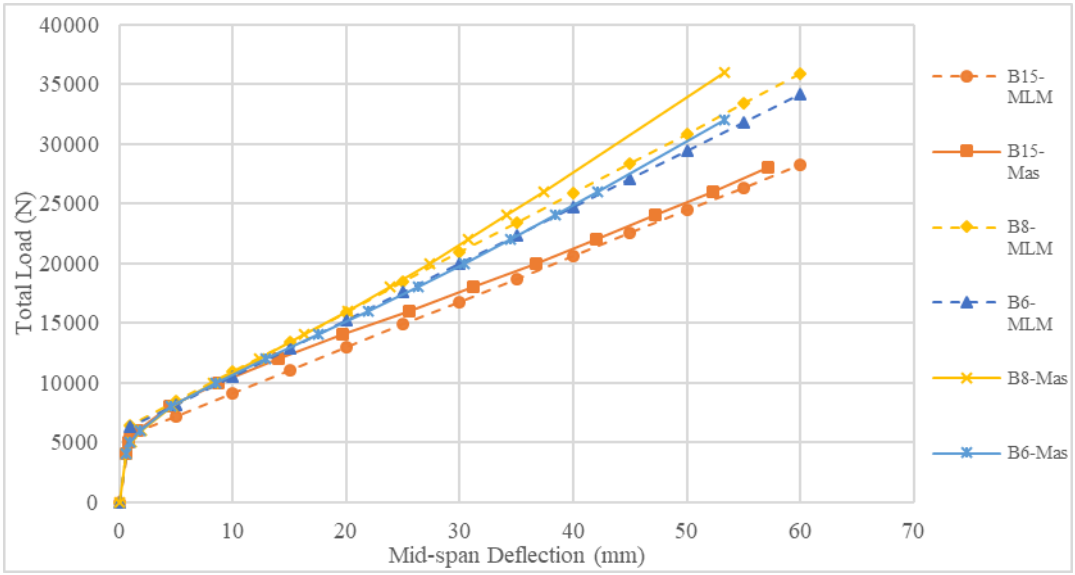

Figure 7.4 Plot of mid-span deflection VS total load using Masmoudi, Thériault and Benmokrane (1998) deflection model estimates

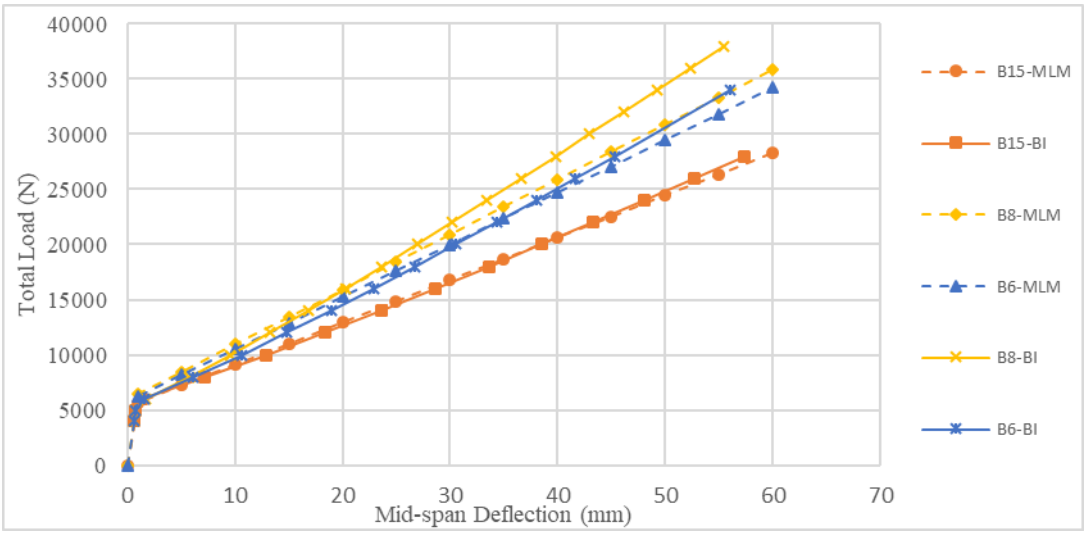

Figure 7.5 Plot of mid-span deflection VS total load using Bischoff (2005) deflection model estimates

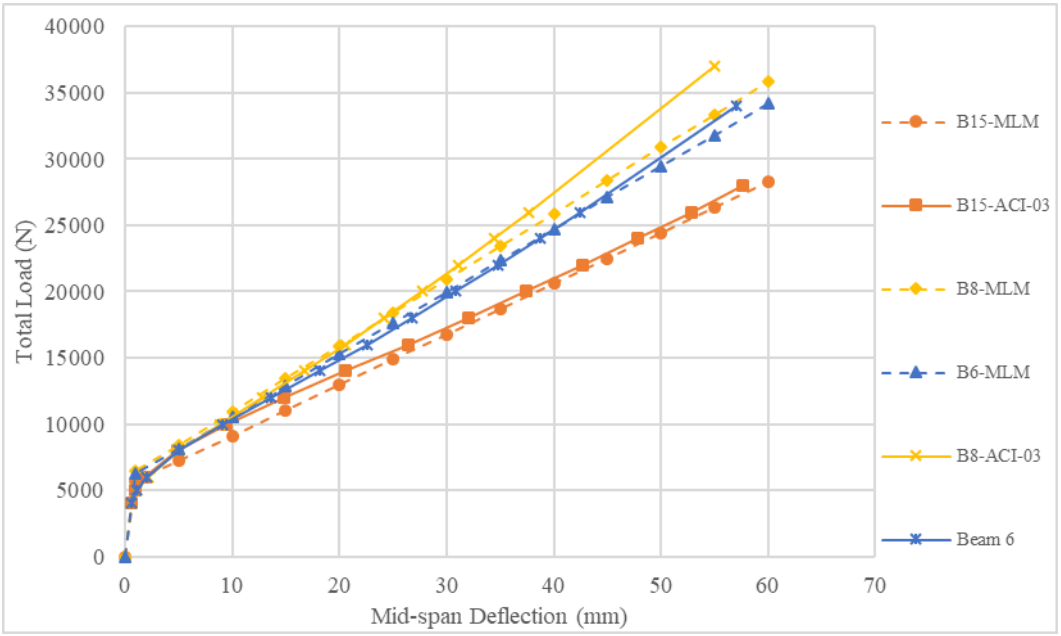

Figure 7.6 Plot of mid-span deflection VS total load using American Concrete Institute (2003) model estimates for deflection

Table 7.1 and Figure 7.7 show the deviation of the estimates from the mixed linear model estimates. The mean of the normalised difference between the models' estimates and the mixed linear model result. Using m=3 in the Branson and Metz (1963) resulted in the highest stiffness overestimation. However, using m=4 resulted in a more accurate estimate on average and a smaller standard deviation. Bischoff's (2005) model provided the most accurate overall deflection estimate. The model suggested by CEB-FIB (1993), and European Committee for Standardization (2004) is the most conservative, and on average, it underestimates the stiffness of the beams and results in the highest standard error. However, the underestimation is a result of the conservative tensile strength suggested by the code which reduces the beam cracking moment.

Table 7.1 Means and standard errors of the deflection models' normalised estimates

	BR3	BR4	EN	Mas	AIC-03	BI
Mean of (model estimate-MLM)/MLM (%)	9.75	0.38	-7.33	2.76	1.31	-0.32
Standard deviation (%)	8.03	6.12	9.46	5.98	5.67	5.87

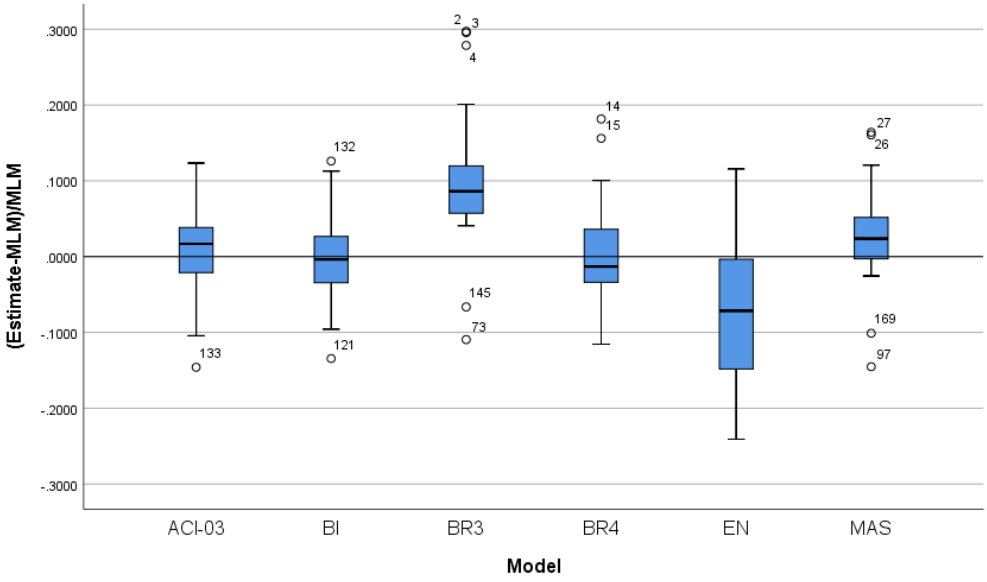

Figure 7.7 Box plot of the normalised difference between the deflection models' estimates and the mixed linear model predictions

Figure 7.8 to Figure 7.13 were produced to investigate the tendency of the models to overestimate or underestimate the stiffness relative to the deflection level. Figure 7.8 to Figure 7.13 show the normalised difference between estimates and the mixed linear model at different deflection levels. All of the investigated models overestimate the stiffness at higher deflection; especially, the highly reinforced beams (beams 6&8). The stiffness of Beam 8 at high deflection is even slightly smaller relative to the cracked stiffness. The overestimation at the higher moment can be explained by the fact that the models assume that the concrete is elastic. However, with increasing load, the concrete's MOE decreases; therefore, decreasing the stiffness of the section. Another cause of the overestimation of stiffness is the reduced bond/Area for B8 compared with B6 and B15. Branson and Metz's (1963), Masmoudi, Thériault and Benmokrane (1998), and American Concrete Institute (2003) models overestimate the stiffness at low deflection for the lightly reinforced beam 15. Bischoff's (2005) model underestimates stiffness at lower deflection; albeit to a lesser extent compared to the European code model (CEB-FIB, 1993).

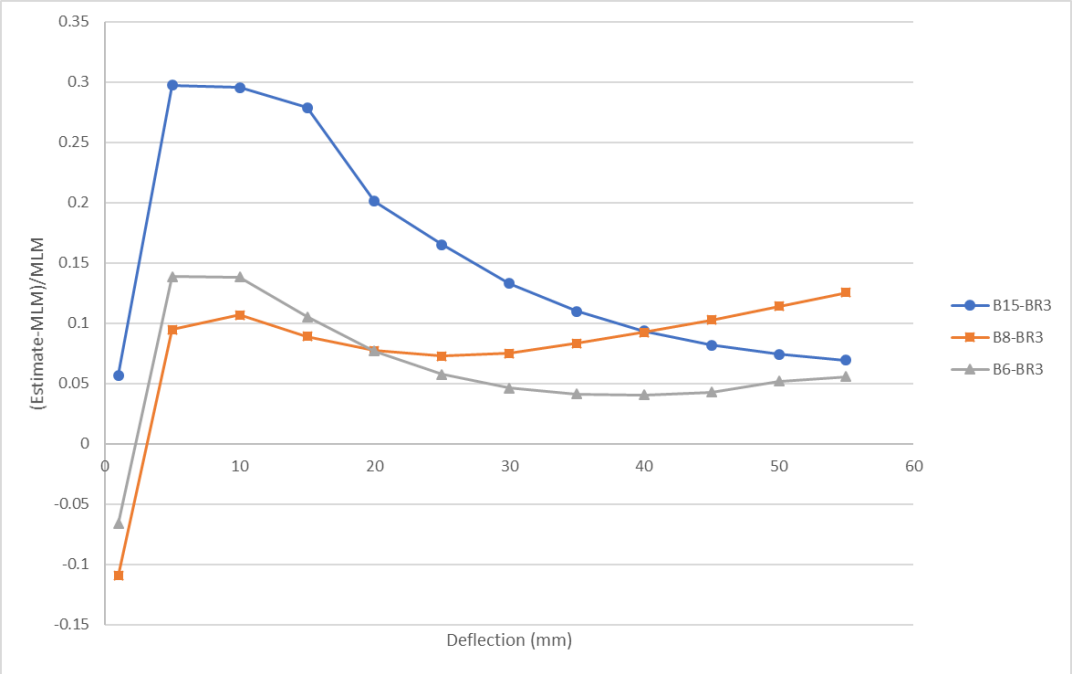

Figure 7.8 Plot of deflection VS normalized estimates of Branson and Metz (1963) using m=3

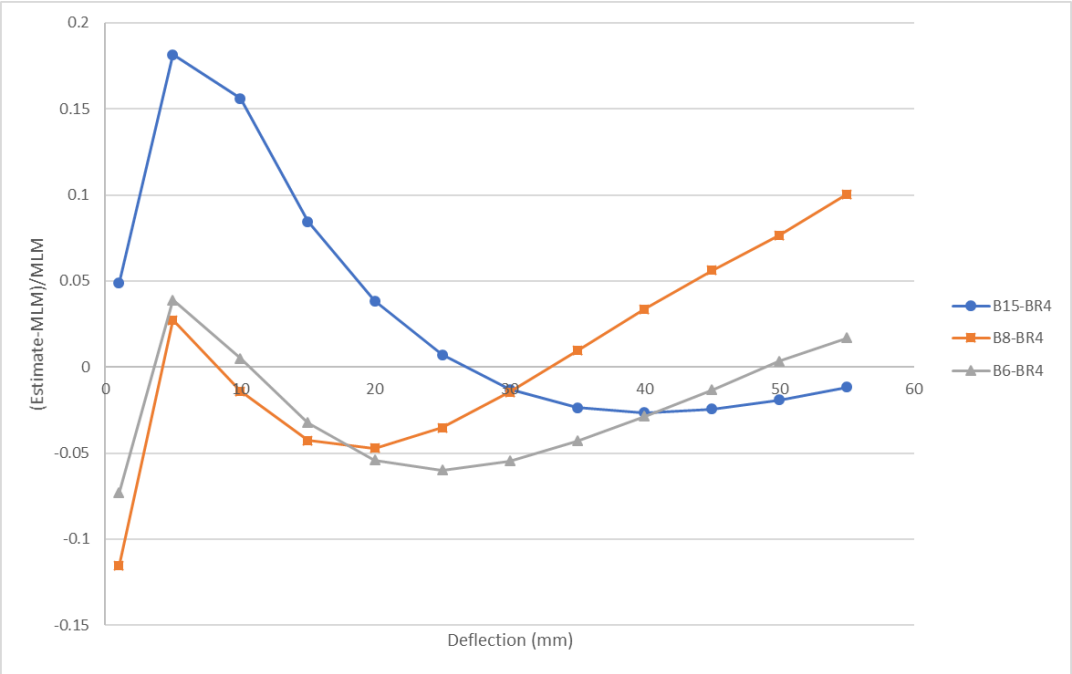

Figure 7.9 Plot of deflection VS normalized estimates of Branson and Metz (1963) using m=4

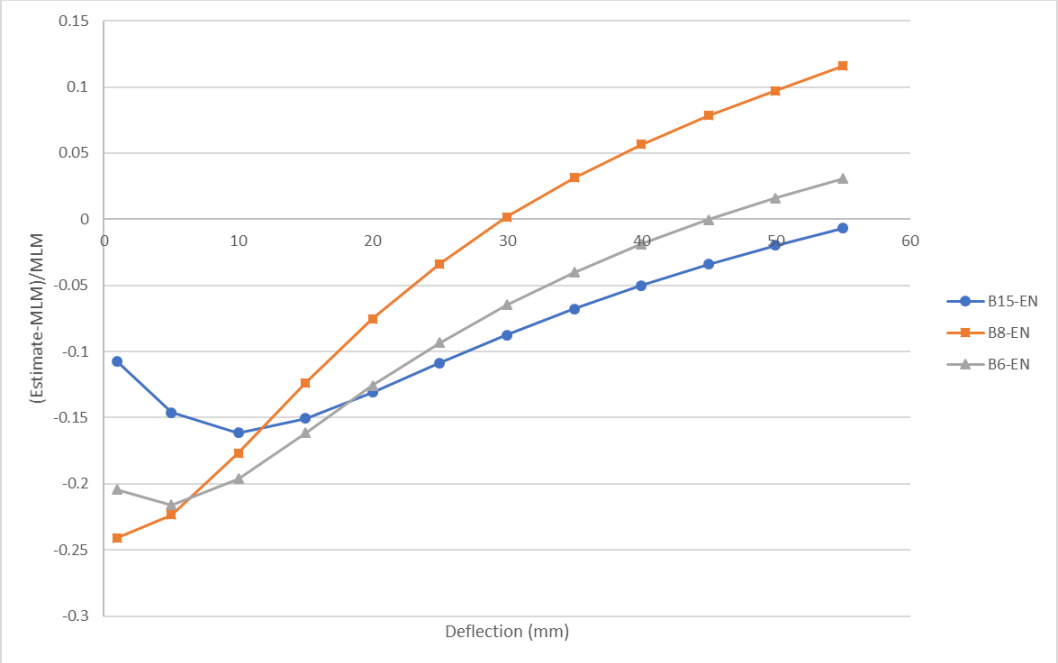

Figure 7.10 Plot of deflection VS normalized estimates of European code deflection model (CEB-FIB, 1993)

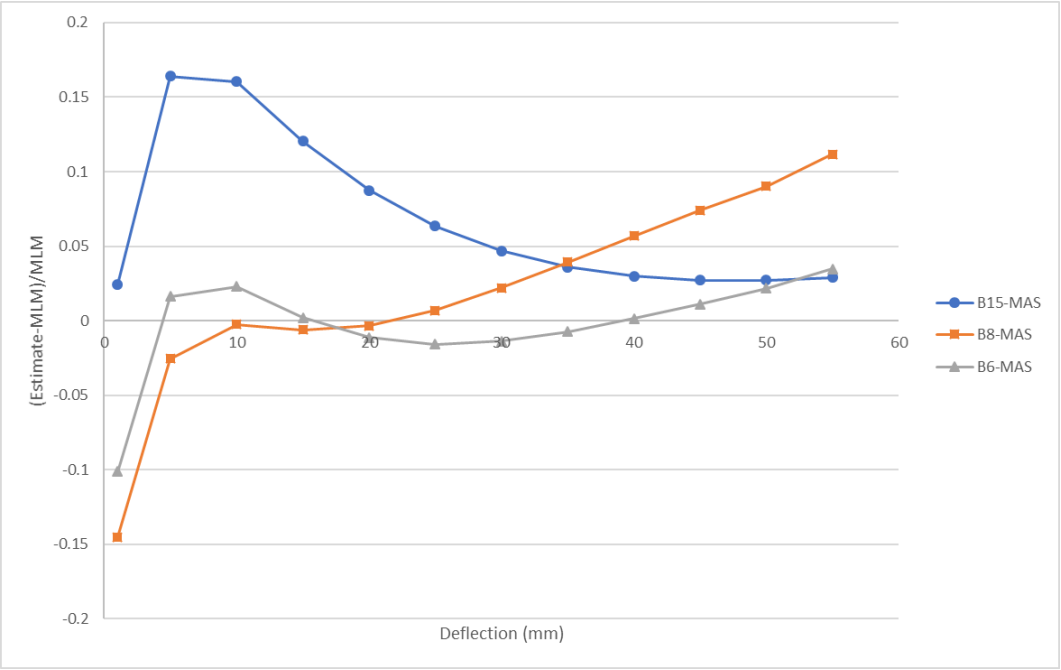

Figure 7.11 Plot of deflection VS normalized estimates of Masmoudi, Thériault and Benmokrane (1998)

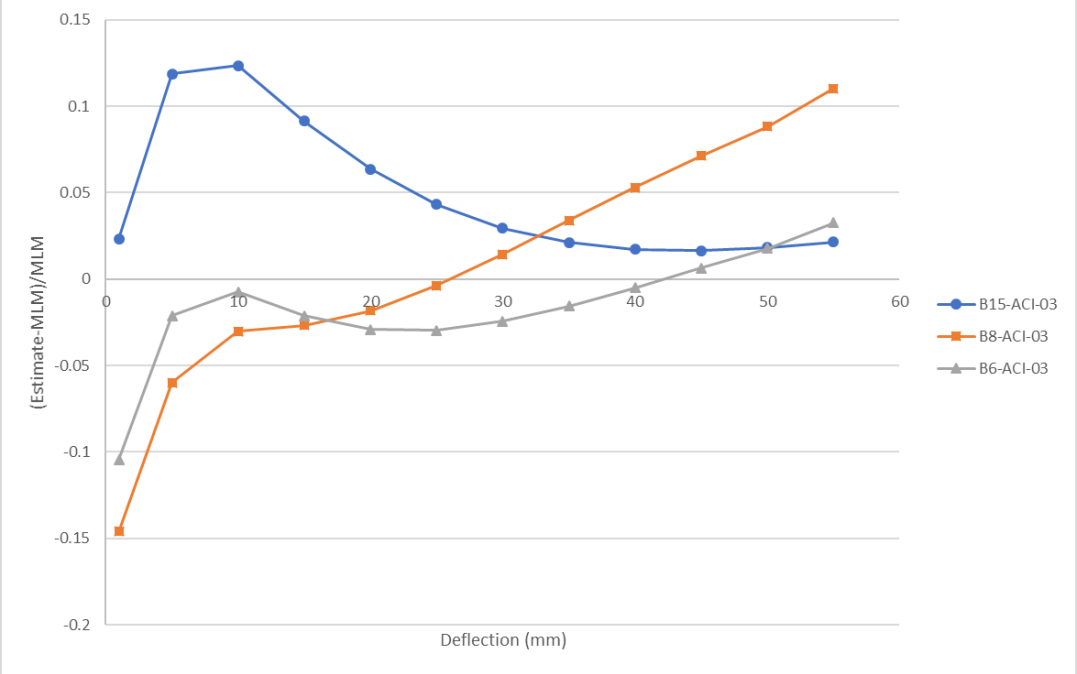

Figure 7.12 Plot of deflection VS normalized estimates of American Concrete Institute (2003) model estimates for deflection

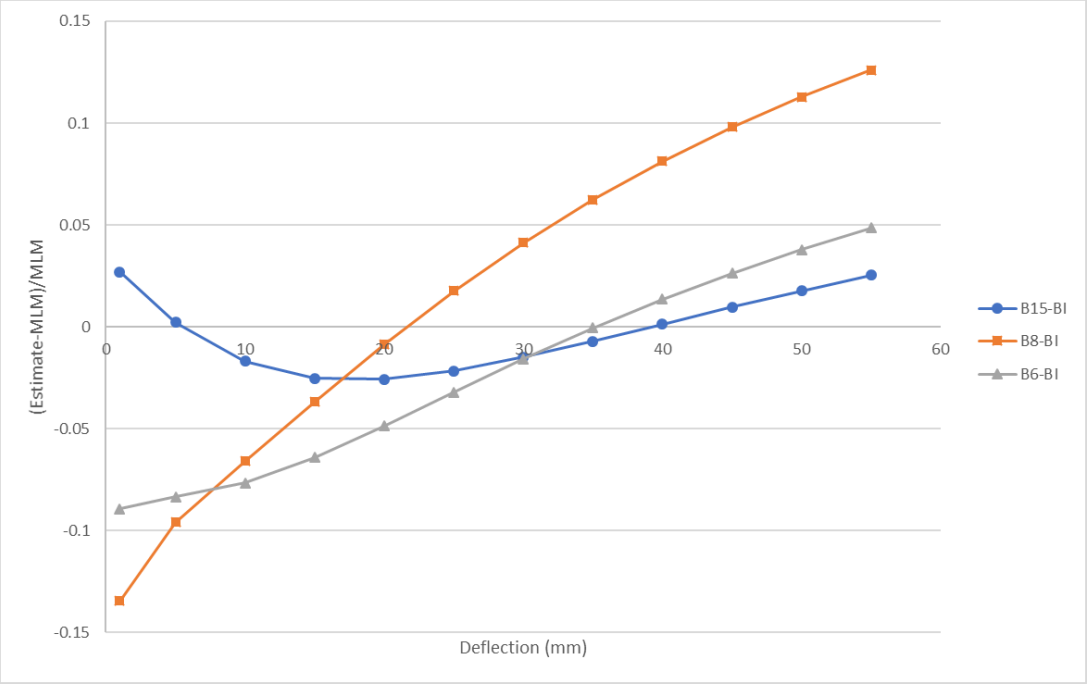

Figure 7.13 Plot of deflection VS normalized estimates of Bischoff (2005)

7.2.4 The proposed deflection model for bamboo reinforced concrete

While both bamboo and FRP has lower MOE relative to steel, bamboo additionally can have much lower bond strength. Since the bond is the conduit for tension stiffening, a strong bond is needed to fully utilise the concrete tension stiffening. Section 7.2.3 showed that Bischoff's (2005) model yields reasonable results for beams with corrugated reinforcement. However, it would not necessarily yield accurate results for beams with a weaker bond because the model assumes a perfect bond with concrete. The large variability of bond in bamboo reinforced concrete underlies the need for a deflection model that explicitly accounts for the effect of bond on the deflection. The variability in bond arises from the natural variability in bamboo, the different treatments, and the different surface to section area ratios. For example, using a splint with a smaller section yields a better bond/section area ratio due to the small reinforcement section. Simply put, a splint section area increases more rapidly relative to the surface area with increasing dimensions.

The effect of bond on stiffness should include both cracked and un-cracked stiffness. The American Concrete Institute (2003) code model reduces un-cracked stiffness to account for the bond behaviour of FRP reinforcement with concrete. However, the MLM shows that for bamboo reinforced concrete the effect of bond on stiffness does not decrease with increased deflection. In other words, a weak bond reduces the stiffness of the beams more severely at higher deflection relative to lower deflection. In equation 7.13, a modification is made to Bischoff's (2005) model. A power function of bond/area is used to reduce the second moment of area. A power function is chosen since it has diminishing returns similar to the effect of bond on stiffness where E_b is the reinforcement MOE in GPa, A_b is the reinforcement area in mm^2, and $\tau_{l,max}$ is the maximum longitudinal bond. SPSS nonlinear regression is used to regress the FE data to determine the power value (0.096) in equation 7.13.

$$I_{e,b} = \frac{I_{cr}}{1 - y\left(\frac{M_{cr}}{M_a}\right)^2\left(1 - \frac{I_{cr}}{I_g}\right)} \times \left(\frac{13.9\tau_{l,max}}{E_b A_b}\right)^{0.096} \leq I_e \qquad 7.13$$

The FE model data encompassed varying reinforcement stiffness and bond strength. Then the theoretical model is validated using the experimental results produced in the current investigation and the experimental results found literature. The results from the 31 FE beam models are used to regress equation 7.13 The reinforcement percentages used in the analysis were 1.1, 2.3, 3.2, 4.2, 6.3, and 8.5%. The longitudinal bond/area ratio ($\frac{\tau_{l,max}}{A_b}$) was varied between 0.08 and 1 MPa/mm. Figure 7.14 and Figure 7.15 show the effect of the bond/area ratio on deflection behaviour. As the bond increases the stiffness of the beam improves. At 1 MPa/mm bond/area ratio, the response approximates that with the perfect bond for bamboo reinforcement with 13.9 GPa MOE. Figure 7.16 shows how the bond adjustment in equation 7.13 provides better deflection estimation in comparison with Bischoff's (2005) model in beams with a weaker bond.

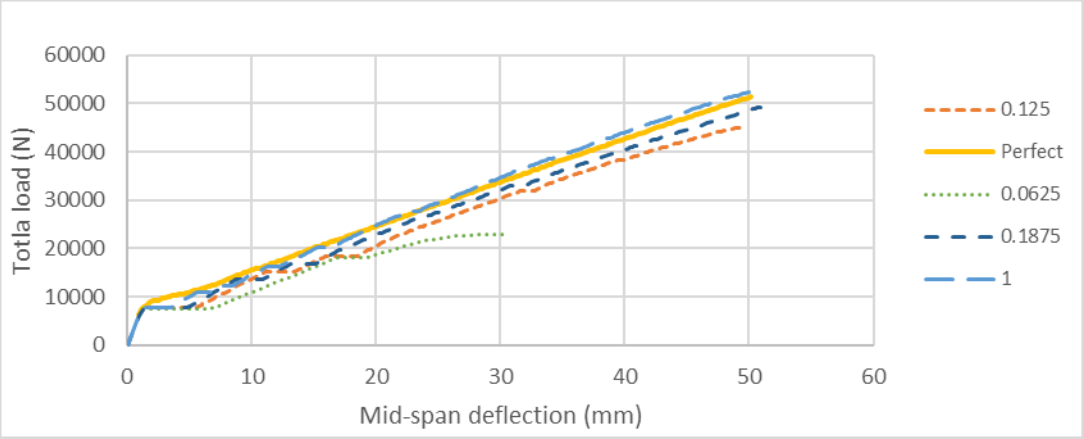

Figure 7.14 Plot of FE model mid-span deflection VS Load at different longitudinal bond/area ratios using ρ = 8.5%

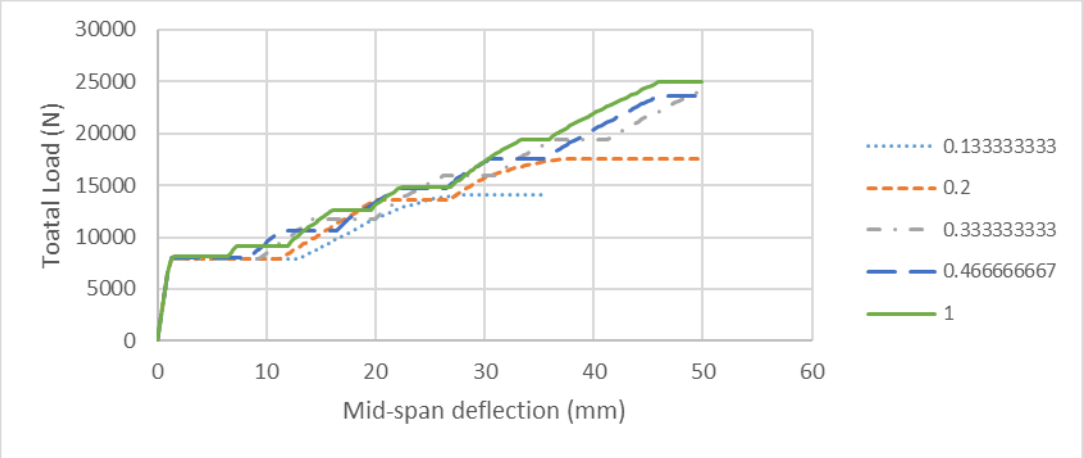

Figure 7.15 Plot of FE model mid-span deflection VS Load at different longitudinal bond/area ratios using ρ = 3.2%

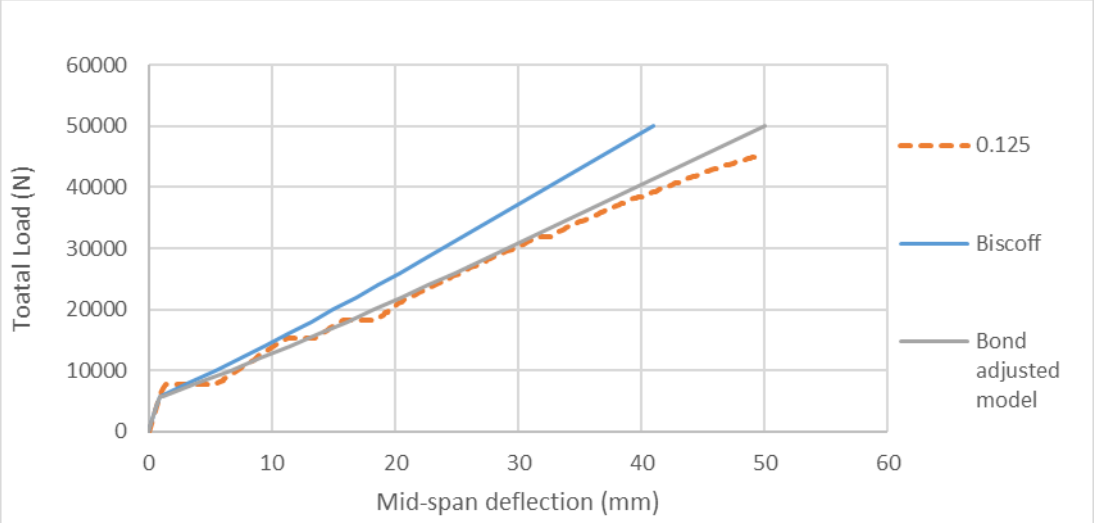

Figure 7.16 Plot of the bond adjusted model and Biscoff's model deflection estimates for an FE beam with ρ = 8.5% and longitudinal bond of 0.125 MPa/mm

7.2.5 Validation of the proposed deflection model using experimental results

In this section, the proposed deflection model (equation 7.13) is validated using the experimental results produced during the current investigation and the experimental results in the literature. An example is provided in appendix E to help the reader understand how the model is applied. Four beams are used from the current research. These beams had two un-corrugated splints (Beam 3), two corrugated splints (Beam 15), three corrugated splints (Beam 6), and four corrugated bundled splints (Beam 8). In addition, the two beams by Yamaguchi, Murakami and Takeda (2013) are modelled where they used bundled un-corrugated Moso bamboo splints as reinforcement. Five of Cox and Geymayer (1969) beams were used here. One of the beams (CG6) was predicted to have bond failure and the other four did not fail due to bond.

The theoretical model agrees with the result of beams tested in the current research (Figure 7.17 - Figure 7.20). Similarly, the model agrees with the beams tested by Yamaguchi, Murakami and Takeda (2013) (Figure 7.21-Figure 7.22). Cox and Geymayer's (1969) beams had larger variability in their load-deflection behaviour due to bond failure in some beams. In beams where bond capacity is lower relative to the flexural capacity assuming perfect bond (results were presented in Table 6.7), the deflection cannot be reliably predicted. The deflection model provides reasonable estimations of deflection in beams CG17-CG20 (Figure 7.24-Figure 7.27). However, for beams with lower bond capacity than that required to achieve the full flexural strength of the beam as in CG6 (Figure 7.23), the model overestimates the stiffness of the beams. The model works well for accounting for the effect of bond on tension stiffening effect and consequently deflection. However, a different mechanism occurs with bond failure where not only tension stiffening is eliminated but the apparent stiffness of the reinforcement is

diminished due to the loss of bond between the reinforcement and the concrete. In bond failure, there can be some hardening in the behaviour such as in beam CG6, pseudo-plastic behaviour where the deflection increases under a constant load or softening with increasing deflection. Therefore, to accurately estimate the deflection, the beams should be designed to avoid bond failure.

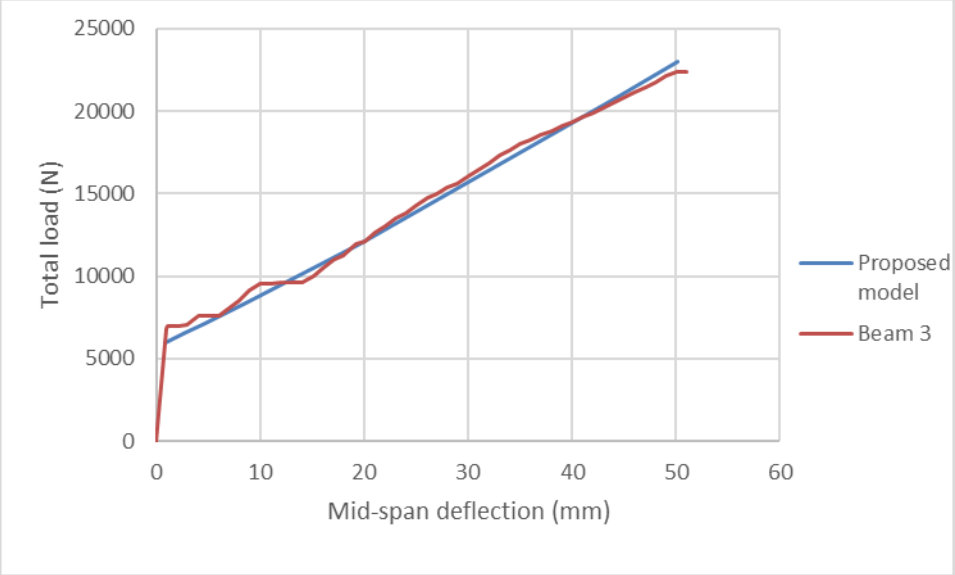

Figure 7.17 Plot of load-deflection of the proposed model and the experimental results of beam3

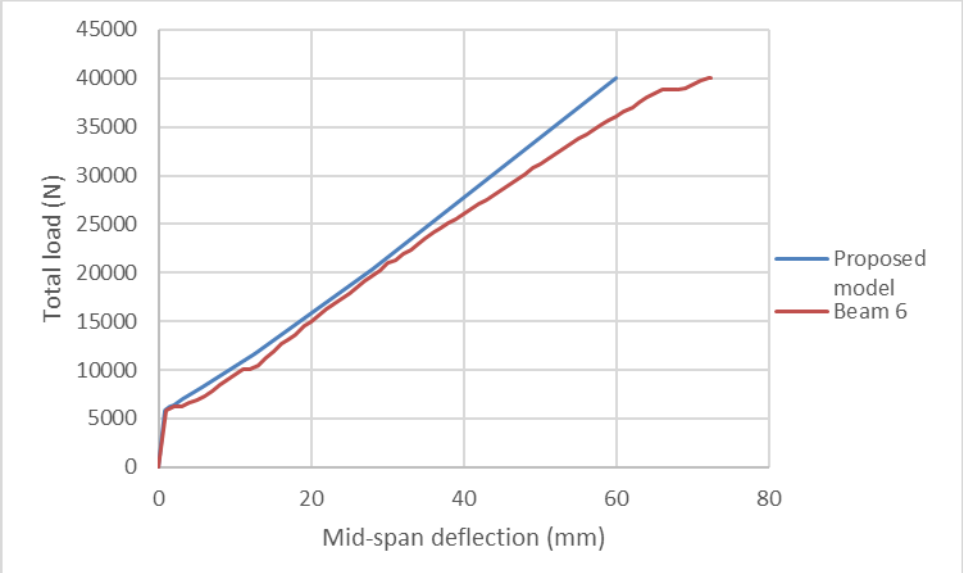

Figure 7.18 Plot of load-deflection of the proposed model and experimental results of beam 6

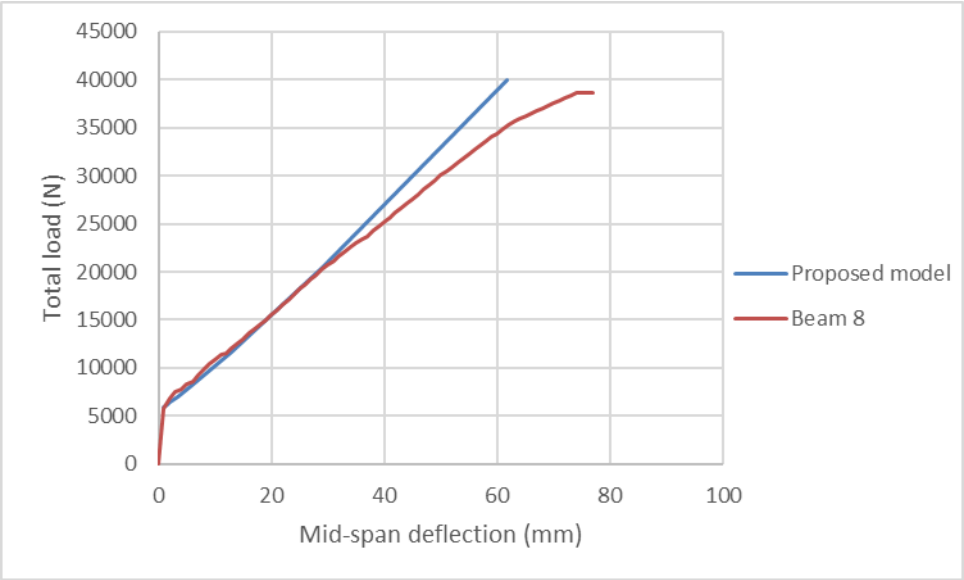

Figure 7.19 Plot of load-deflection of the proposed model and experimental results of beam 8

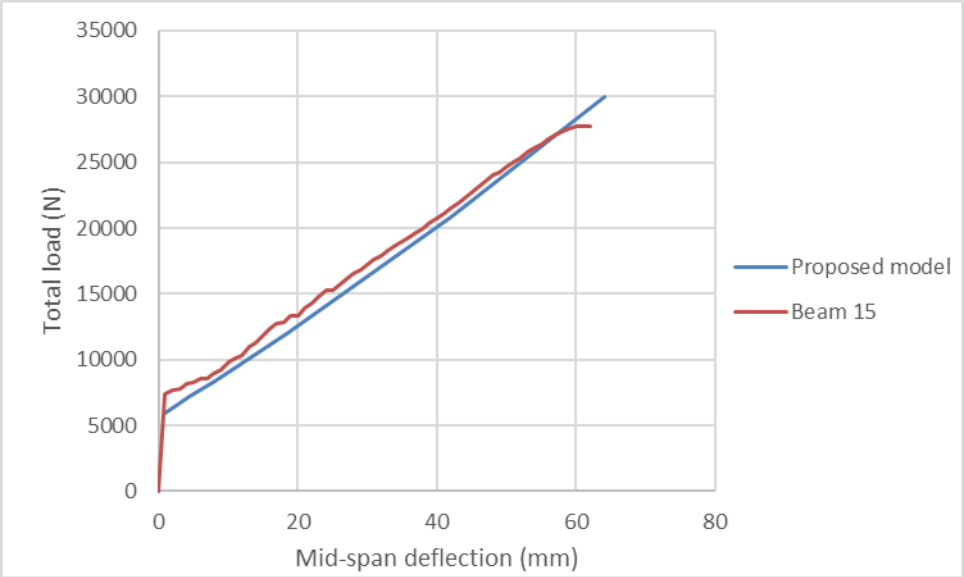

Figure 7.20 Plot of load-deflection of the proposed model and experimental results of beam 15

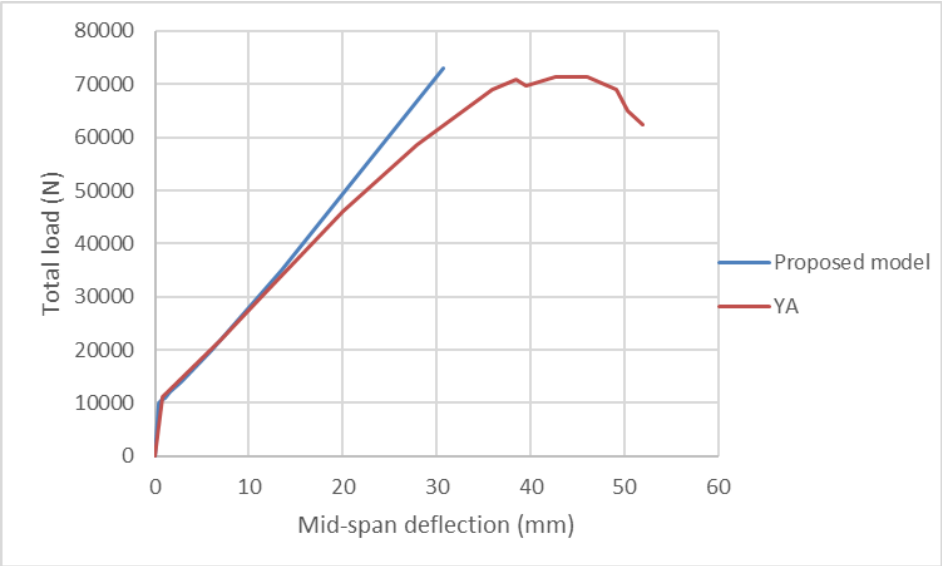

Figure 7.21 Plot of load-deflection of the proposed model and experimental results of YA by Yamaguchi Murakami and Takeda (2013)

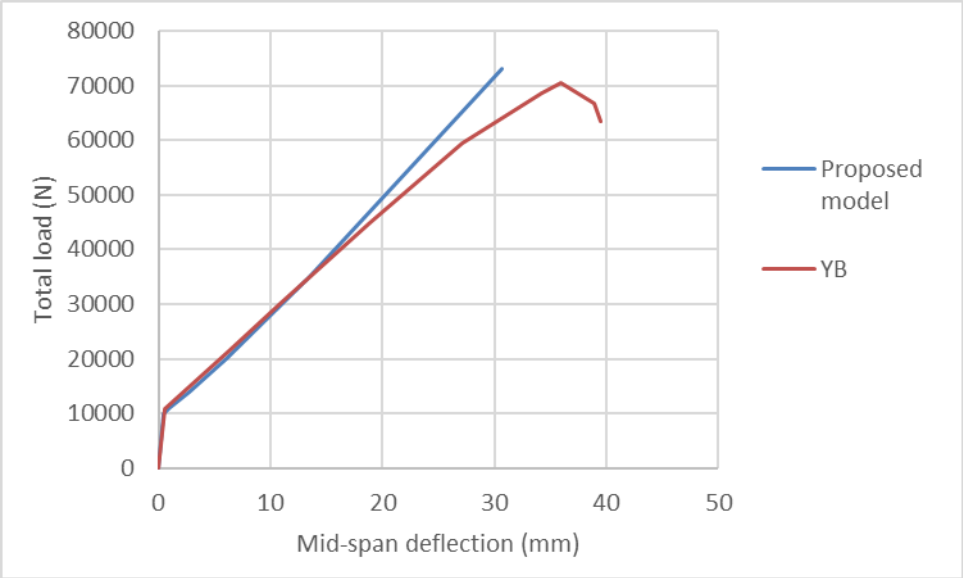

Figure 7.22 Plot of load-deflection of the proposed model and experimental results of YB by Yamaguchi Murakami and Takeda (2013)

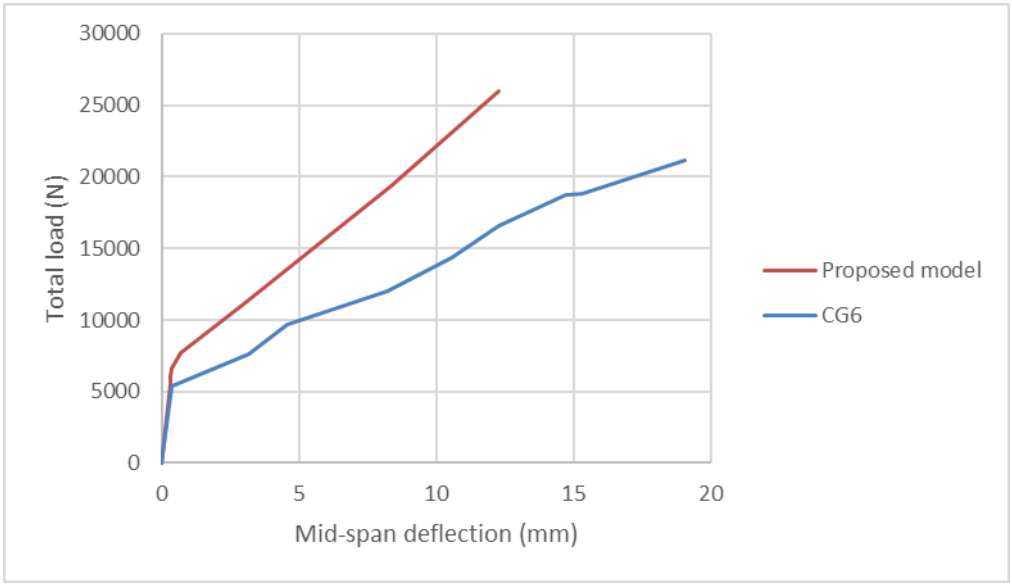

Figure 7.23 Plot of load-deflection of the proposed model and experimental results of CG6 by Cox and Geymayer (1969)

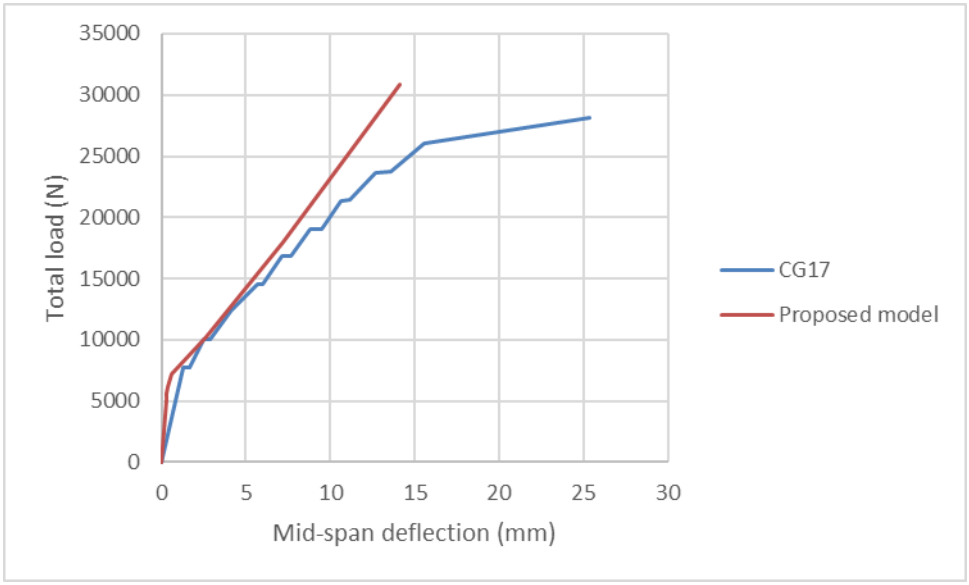

Figure 7.24 Plot of load-deflection of the proposed model and experimental results of CG17 by Cox and Geymayer (1969)

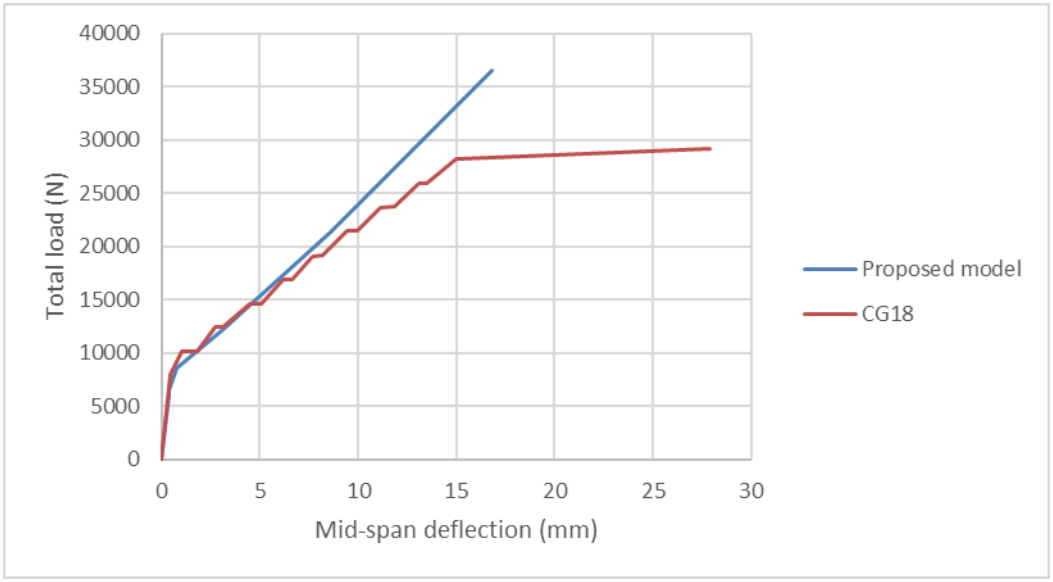

Figure 7.25 Plot of load-deflection of the proposed model and experimental results of CG18 by Cox and Geymayer (1969)

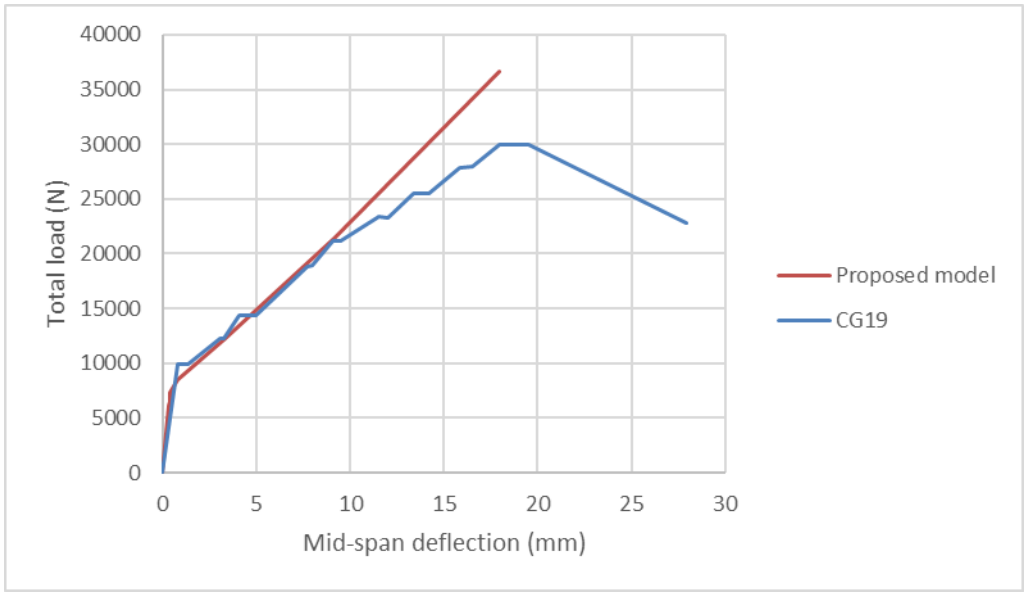

Figure 7.26 Plot of load-deflection of the proposed model and experimental results of CG19 by Cox and Geymayer (1969)

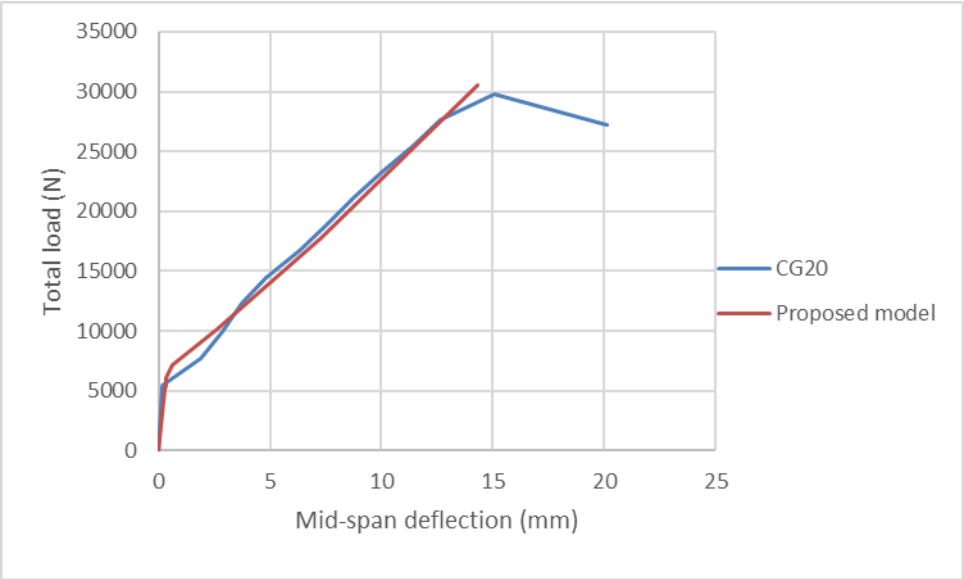

Figure 7.27 Plot of load-deflection of the proposed model and experimental results of CG20 by Cox and Geymayer (1969)

7.3 Crack Control

Cracks are controlled within certain widths for durability and appearance purposes. There are currently no deflection and cracking models that have been validated for use with bamboo reinforced concrete. In this section two crack models are validated for bamboo reinforced concrete.

Cracks develop in reinforced concrete as a result of the brittleness of concrete in tension. It is desirable to achieve uniform cracking and limit the spacing and widths of cracks. While European Committee for Standardization (2004) maintains that cracking is normal in reinforced concrete, it mandates that cracking should be limited so that it does not impair ‘’the proper functioning or durability of the structure or cause its appearance to be unacceptable’’. However, it allows for uncontrolled cracking when they do not impair the functioning of the structure. Bamboo lower modulus of elasticity (MOE) can lead to excessive deflection and cracking.

CEB-FIB (1993) requires that crack width in steel-reinforced concrete to be less than 0.3 mm for durability and appearance purposes. European Committee for Standardization (2004) allows cracking in dry environments for durability and appearance purposes for up to 0.4 mm. However, the code does allow for uncontrolled cracks' widths ''provided they do not impair the functioning of the structure''. American Concrete Institute (2015) puts an upper limit for crack width for FRP reinforced concrete at 0.7 mm. This limit is for aesthetic reasons as excessive cracking may give the impression that the structure is not safe. Lower limits are required in situations where water tightness is required or if there is a corrosion risk. American Concrete Institute (2015) accepts that the evidence on the effect of crack width on corrosion is mixed in steel-reinforced concrete. Nonetheless, the crack width limit was relaxed with FRP reinforcement because the degradation risk is lower relative to steel.

Archila *et al.* (2018) suggested that cracks wider than 0.8 mm may expose bamboo to termite attack. Plastering may be useful in mitigating the risk of termites and in improving the concrete appearance. In addition, Archila *et al.* (2018) pointed out that while steel reinforcement when corroded gives a visual warning by the staining and spalling of the concrete cover. Bamboo degradation can occur without warning. Sudden failure can occur if the reinforcement is loaded close to the ultimate capacity of the reinforcement. However, the serviceability limits of bamboo reinforced concrete are much lower relative to the ultimate limit states. In addition, degradation of the bamboo would result in excessive deflection and increased cracking before failure; thereby providing a warning. No attempts have been made so far for the estimation of cracks spacing and size in bamboo reinforced concrete and no data is provided in the literature. In addition, it is not clear what the effect of crack control the durability of bamboo reinforced concrete.

During the current investigations, cracks were measured using a digital calibre (data is presented in appendix F) and the machine time was recorded at the time of measurement to know the corresponding moment. In reinforced concrete, cracking behaviour depends on the following:

1. the bond between the reinforcement and the concrete, a stronger bond reduces the widths and spacing of cracks;
2. the concrete area surrounding the reinforcement, a more substantial area due to large concrete cover or wider reinforcement spacing result in wider crack spacing and width;
3. the tensile strength of the concrete, a higher tensile strength yields wider cracks and crack spacing;
4. stiff reinforcement decreases the cracks spacing and widths.

In this section, two cracking models, i.e. Frosch (1999) and CEB-FIB (1993), are validated for use with bamboo reinforced concrete using the experimental results.

7.3.1 Frosch (1999) method for the estimation of cracks

Crack width has inherently large scatter; however, Frosch (1999) was able to produce a simple empirical formula (equation 7.15) for the estimation of crack width in steel-reinforced concrete. In this model, the width of a crack is the product of crack spacing and reinforcement strain. Cracks spacing ($S_{c,A}$) is dependent on the cover and the reinforcement spacing (equation 7.14). The effect of the bond on cracking is dealt with indirectly. With deformed steel reinforcement, Ψ_s values of 2 and 1.5 are used for maximum and average crack spacing, respectively. These values are specific for the bonding behaviour of deformed reinforcement. Frosch (1999) advised Ψ_s value of 4 for maximum crack spacing for coated reinforcement due to its weaker bond. Therefore, an

appropriate Ψ_s value is need to be found for bamboo reinforced concrete because bamboo bond with concrete is weaker relative to deformed steel. In addition, the lower MOE of bamboo increases the cracks spacing and it increases the length at which the reinforcement is elongating inside the concrete.

$$S_{c,A} = \Psi_s \sqrt{d_c + \left(\frac{s}{2}\right)^2} \tag{7.14}$$

$$w_{c,A} = S_{c,A} \frac{f_b}{E_b} \beta_A = \Psi_s \frac{f_b}{E_b} \beta_A \sqrt{d_c + \left(\frac{s}{2}\right)^2} \tag{7.15}$$

$$\beta_A = \frac{h - c}{d - c} \tag{7.16}$$

Where:

$S_{c,A}$ = cracks spacing in Frosch's model (mm)
Ψ_s = factor that accounts for bond
d_c = reinforcement cover (mm)
s = reinforcement spacing (mm)
$w_{c,A}$ = crack width (mm)
f_b = stress in the reinforcement (MPa)
β_A = factor to account for the strain gradient

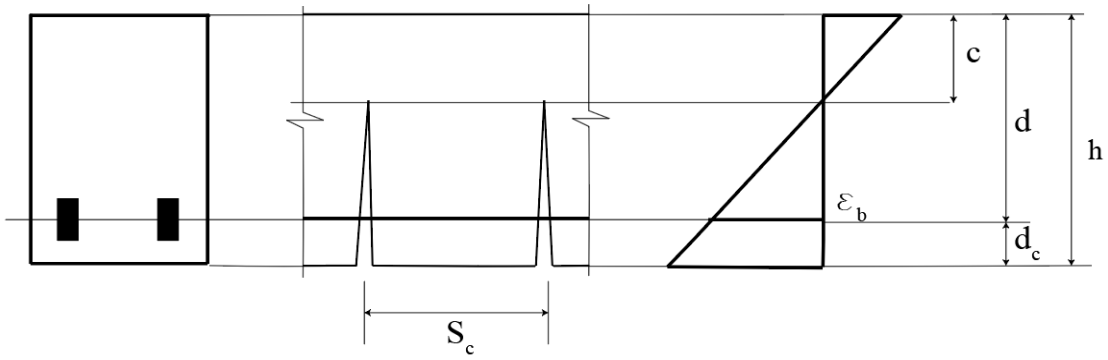

Figure 7.28 Plot of cracking in reinforced concrete

Equation 7.15 was regressed using the experimental results and it was found that and Ψ_s is equal to 3.21 for average crack width (see Figure 7.29). As for the maximum crack, Figure 7.30 shows that using $\Psi_s = 4$ predicts the maximum crack wideth. There are fewer

data points in Figure 7.30 relative to Figure 7.29 because Figure 7.30 includes only the crack with the maximum width at a given point in time.

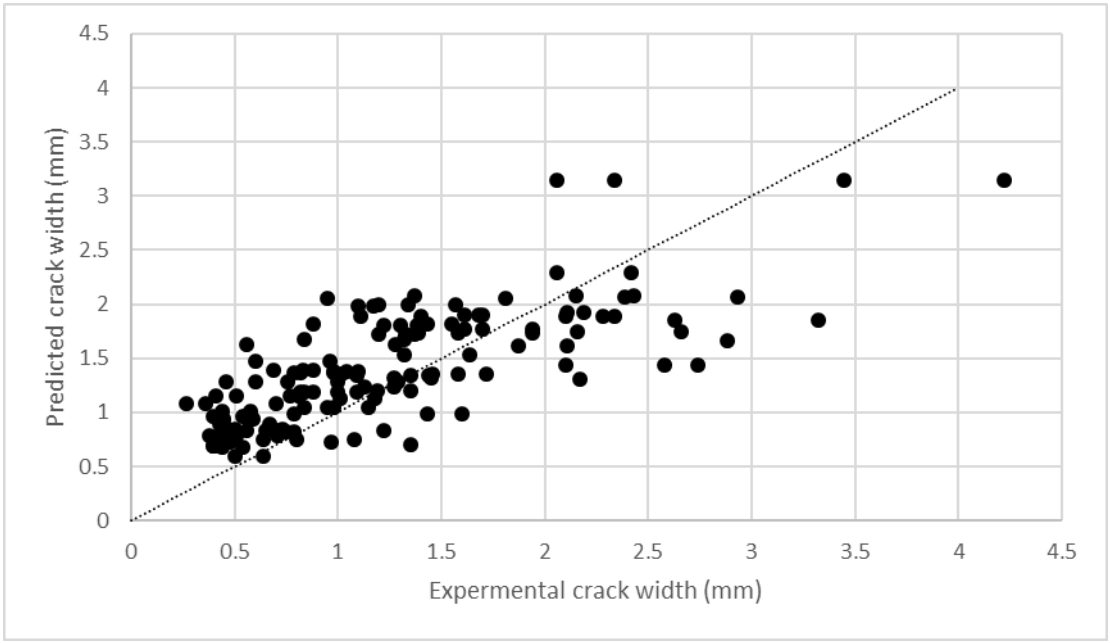

Figure 7.29 Scatter plot of Frosch (1999) model predictions for average crack width using $\Psi_s = 3.2$ VS the experimental results

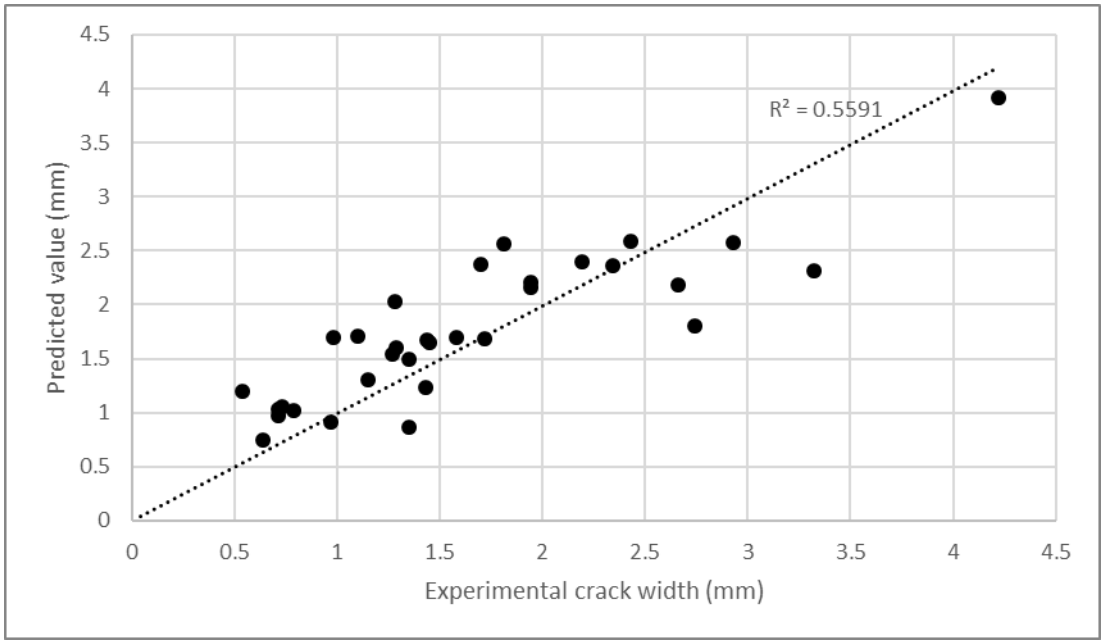

Figure 7.30 Scatter plot of Frosch (1999) model predictions for maximum crack width using $\Psi_s = 4$ VS experimental results

7.3.2 CEB-FIB (1993) method for the estimation of cracks

CEB-FIB (1993) recommends a more direct; albeit, a more involved approach. Unlike Frosch (1999), It deals explicitly with the effect of bond on cracking. The maximum crack spacing ($S_{c,E}$) is found using the difference in the reinforcement stress at the crack and the zero-slip point divided by the bond/length ($\tau_{l,max}$) of the reinforcement. This difference is assumed to equal the product of the mean tensile strength of the concrete (f_{ctm}) and the effective concrete area surrounding the reinforcement (A_{ce}). Equation 7.17 is based on CEB-FIB (1993) crack estimation method. To find the crack width ($w_{c,E}$), the maximum crack spacing ($S_{c,E}$) is multiplied by the mean difference in strain between the concrete and the reinforcement. The model assumes the mean difference in strain equal to the maximum steel strain at the crack with the subtraction of the reduction in strain in the embedded length from the crack to the point of zero slippage due to tension stiffening. The transfer of the full tensile strength of the concrete in the effective area from the reinforcement reduces the reinforcement strain. The code assigns a lower value for β_E in repeated and long-term loading. A value of 0.6 yielded good results for bamboo reinforcement with short-term loading. Research on long-term behaviour is needed to determine the value for repeated and long-term loading behaviour in bamboo reinforced concrete.

$$S_{c,E} = 2\frac{f_{ctm}A_{ce}}{0.667\tau_{l,max}} \qquad 7.17$$

$$\varepsilon_{bm} - \varepsilon_{cm} = \varepsilon_b - \beta_E \frac{f_{ctm}}{\rho_{b,ef}E_b} \qquad 7.18$$

$$w_{c,E} = S_{c,E}(\varepsilon_b - \beta_E \frac{f_{ctm}}{\rho_{b,ef}E_b}) \qquad 7.19$$

Where:

$S_{c,E}$ = maximum crack spacing (mm)

f_{ctm} = mean tensile strength of the concrete (MPa)
A_{ce} = effective concrete area surrounding the reinforcement (mm^2)
ε_{bm} = mean strain in the bamboo (mm/mm)
ε_{cm} = mean strain in the concrete (mm/mm)
ε_b = strain in the reinforcement at the crack (mm/mm)
β_E = factor used to find the average strain reduction
$\rho_{b,ef}$ = area fraction of the reinforcement as a percentage of the concrete surrounding area (%)
$w_{c,E}$ = crack width (mm)

The models of Frosch (1999) and CEB-FIB (1993) produced similar correlation strength with the experiments. The Frosch (1999) model achieved an R^2 value of 0.559, while the CEB-FIB (1993) achieved 0.513. The dispersion within the CEB-FIB (1993) model about the identity line is slightly larger than that of the Frosch (1999) model (Figure 7.32 and Figure 7.34Figure 7.30, respectively). However, since CEB-FIB (1993) deals with the effect of bond on cracking more explicitly, it is more appropriate for use with a material like bamboo that exhibits large variability in bond behaviour.

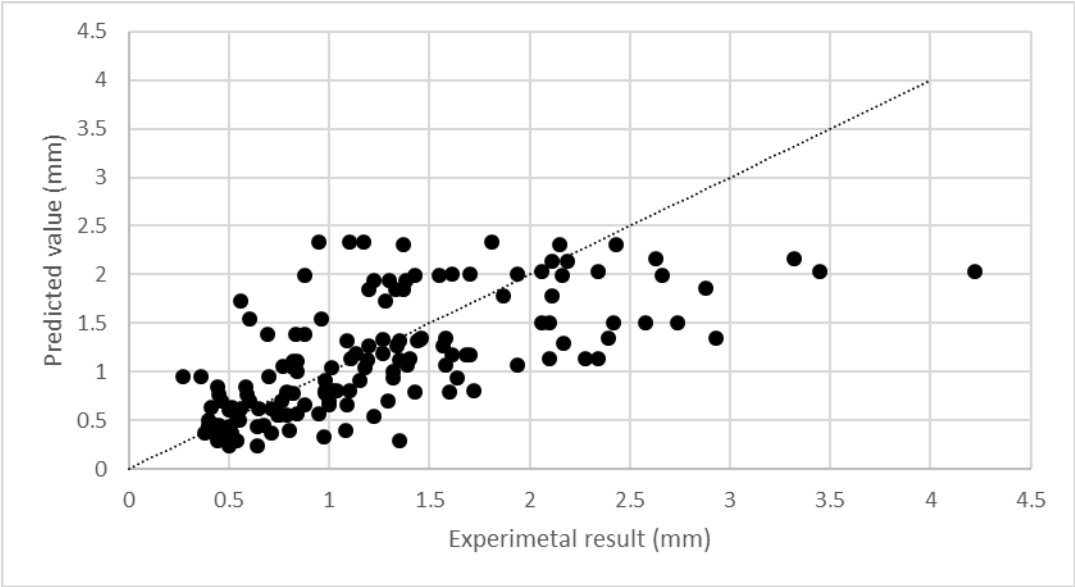

Figure 7.31 Scatter plot of CEB-FIB (1993) model predictions for average crack width VS the experimental results

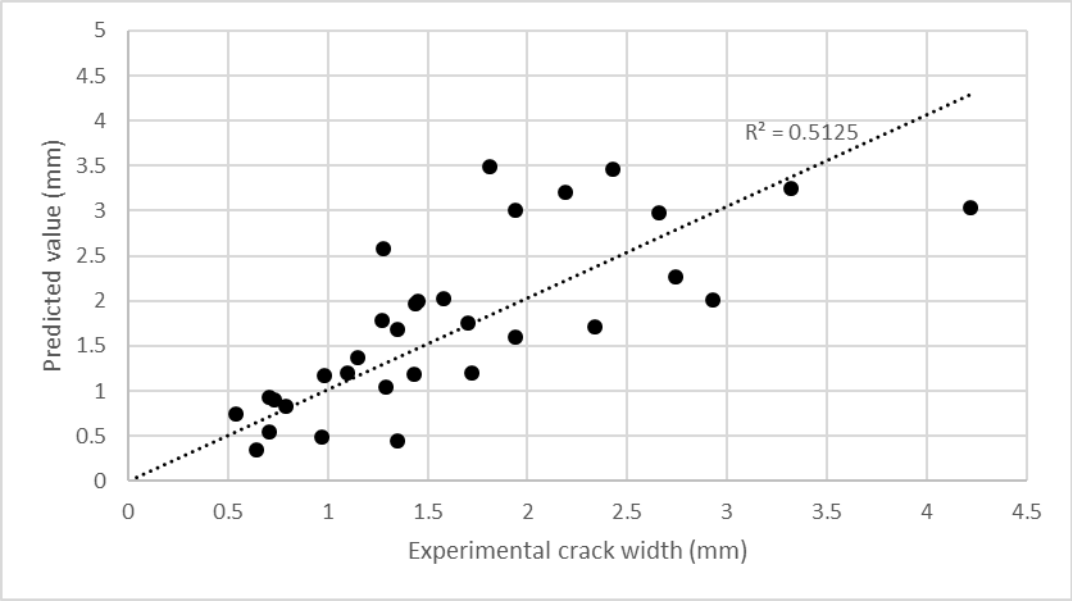

Figure 7.32 Scatter plot of CEB-FIB (1993) model predictions for maximum crack width VS the experimental results

7.3.3 Strain comparison in different reinforcement for crack control

At 0.7 mm crack limit and using Frosch (1999) model, the maximum strain in the reinforcement for the beams tested in the current research should not exceed 2370 με corresponding to 32.9 MPa at 13.9 GPa MOE. This result is comparable to the one recommended by ISIS Canada (2007) for FRP reinforcement of 2000 με and the corresponding working stress of 27.8 MPa at E_b = 13.9 GPa. For controlling crack in steel-reinforced concrete ISIS Canada (2007) recommends 1200 με working strain for steel reinforcement. This conservative value is due to the corrosion risk of steel reinforcement. Using these strain limits, the working stress of the bamboo reinforcement is significantly smaller than that of steel at 240 MPa and FRP at 80 MPa for GFRP. In the case of bamboo reinforced concrete, it is not yet clear whether cracks can affect durability. Therefore, more research on the durability of bamboo inside concrete is needed. It should be noted that the limit state design method of Cox and McDonald (1970) where the

reinforcement stress is 55 MPa is not conservative and it would result in cracks that are too wide.

7.4 Serviceability of bamboo, GFRP and steel-reinforced concrete

In this section, the deflection and cracking behaviour of bamboo reinforced beams are compared with steel and GFRP reinforced concrete. The comparison is based on a limit design approach where deflection and cracking are explicitly controlled. The comparison uses equal amounts of concrete. The reinforced section stiffness is estimated using the modified expression in equation 7.13. The bond/area ratio is assumed to equal 0.5MPa/mm which can be achieved using corrugation. The same amount of concrete is used in all sections by increasing the depth of the beam to account for the reinforcement-displaced concrete and to limit the comparison to the reinforcement. It should be noted, however, that the width of the beam is kept constant throughout. In addition, this serves to flatten any differences in other structural components due to weight differences. Increasing the weight would increase the load on the columns and the foundation. In the current study three different MOE levels are investigated because of the variability of bamboo MOE as follows:

1. 30 GPa, in engineered bamboo;
2. 20 GPa, some bamboo species have higher MOE like Guadua;
3. 13.9 GPa, the value achieved by Moso bamboo in the current research.

Figure 7.33 to Figure 7.35 show the stiffness behaviour of bamboo, GFRP, and steel-reinforced concrete. I_{cs} represent the second moment of area of the solid concrete section without reinforcement while I_{cs} is the estimated second moment of area using the proposed deflection model The dotted line in Figure 7.33 to Figure 7.35, indicates the

behaviour beyond the cracking limit. The line is stopped at the point where the ratio of service moment to crack moment (M_a/M_{cr}) reach the value of 6 or at the point at which the reinforcement reaches the ultimate tensile strength. The ultimate tensile stress is considered for steel, GFRP, and bamboo equal to 420, 600, and 150 MPa, respectively.

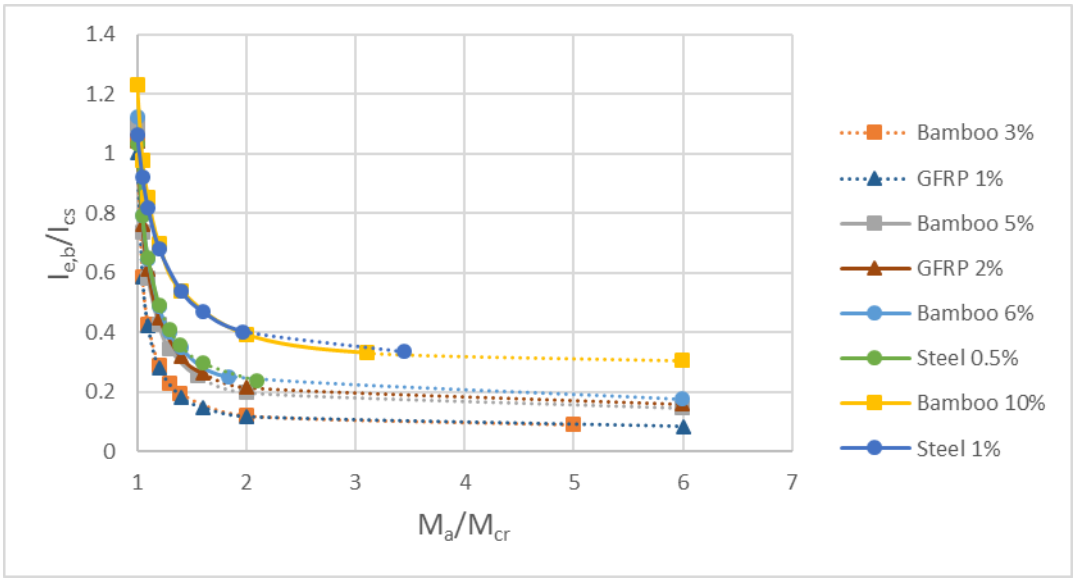

Figure 7.33 Plot of the behaviour of bamboo reinforced concrete vs steel and GFRP (E_b =13.9 GPa)

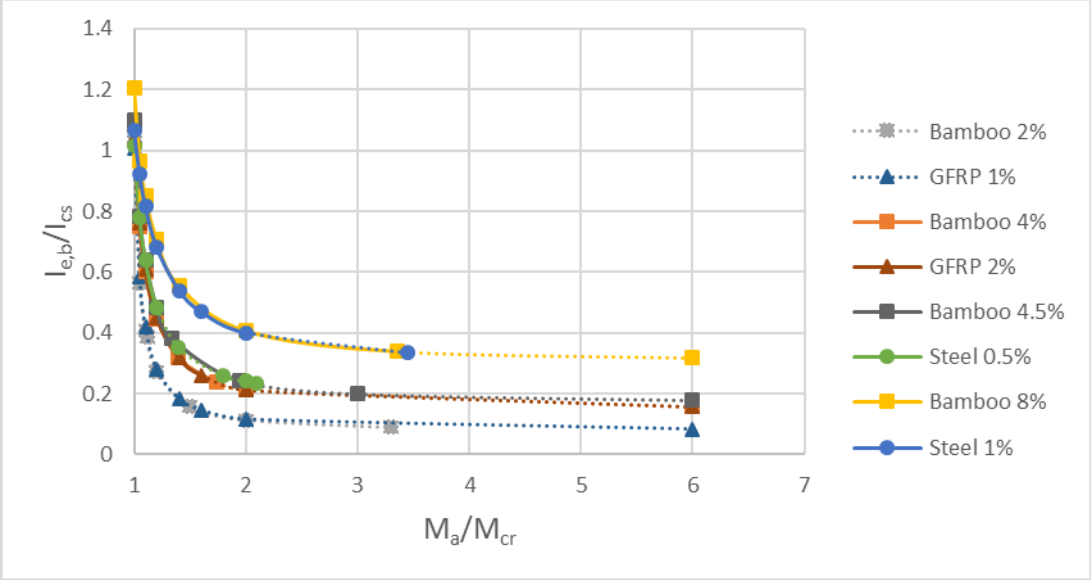

Figure 7.34 Plot of the behaviour of bamboo reinforced concrete vs steel and GFRP (E_b = 20 GPa)

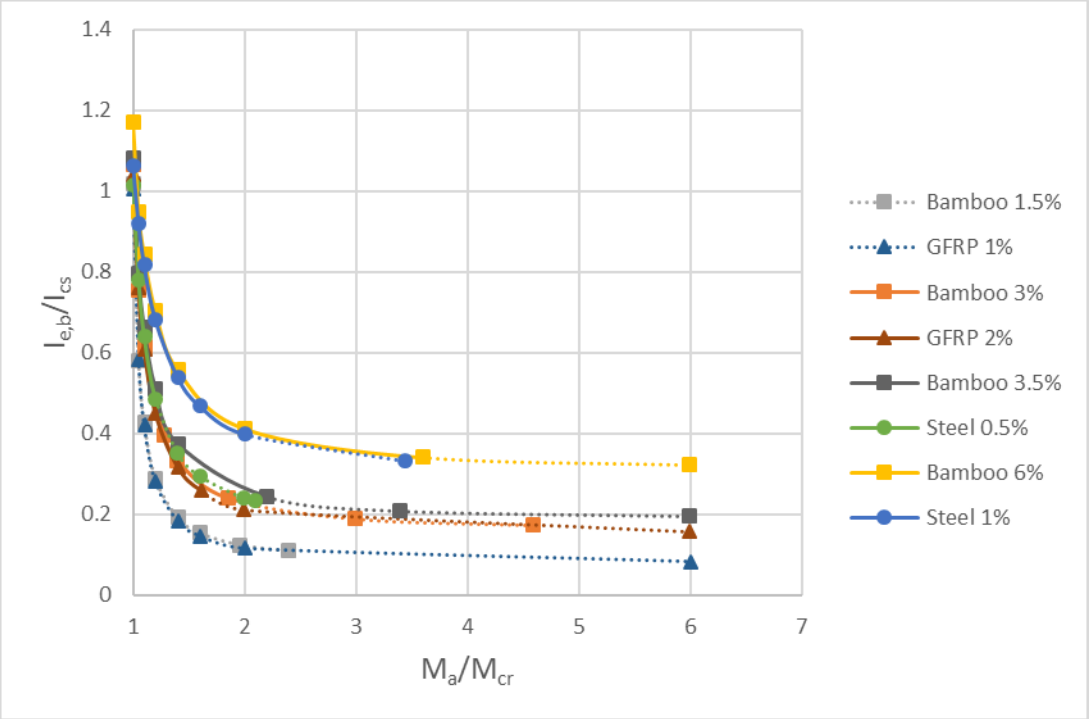

Figure 7.35 Plot of the behaviour of bamboo reinforced concrete vs steel and GFRP (E_b = 30 GPa)

As it can be seen from the figures, steel reaches the ultimate tensile strength under smaller service moment relative to GFRP and bamboo for equal section stiffness. This is due to the larger disparity in MOE relative to tensile strength between bamboo and steel. In other words, for beams with equal stiffness, bamboo reinforced beams have higher bending capacity relative to steel reinforced beams. Therefore, deflection and crack control are more critical in bamboo reinforced concrete relative to steel-reinforced concrete. As it can be seen from Figure 7.33 to Figure 7.35, for equal section stiffness ($I_{e,b}$), bamboo and GFRP reach the ISIS Canada (2007) cracking strain limit of 2000 με at the same service moment (M_a). In addition, for equal section stiffness steel reaches the acceptable cracking limit at a lower moment (M_a) which suggests that stiffness is more critical in bamboo reinforced concrete relative to cracking in comparison with steel reinforced concrete.

As the MOE of bamboo increases, the percentage area of bamboo needed to achieve a similar deflection and cracking behaviour to steel and GFRP decreases. Bundling of the

reinforcement is an adequate solution to achieve a stiffness similar to that achieved using GFRP reinforcement. At E_b = 13.9 GPa, 3 and 5% bamboo reinforcement percentages are needed to achieve the same stiffness as 1 and 2% GFRP reinforcement. At E_b = 20 GPa the required bamboo reinforcement decreases to 2 and 4%, respectively. At E_b = 30 GPa it decreases to 1.5 and 3% respectively. Significantly higher bamboo reinforcement percentages are needed to achieve the same stiffness as steel-reinforced concrete. At E_b=13.9 GPa, 6 and 10% bamboo reinforcement percentages are needed to achieve the same stiffness as 0.5 and 1% steel reinforcement, respectively. At E_b=20 GPa the bamboo reinforcement required decreases to 4.5 and 8%, respectively. At E_b=30 GPa it further decreases to 3.5 and 6% respectively.

However, the 10% reinforcement area can be practically too difficult to achieve especially at the lower MOE of bamboo reinforcement and 1% steel. Relatively high reinforcement areas of up to 7.5% of the effective section have been used by Cox and Geymayer (1969). However, they were forced to use multiple reinforcement layers which decrease the effective depth of the reinforcement and reduces the cracked second moment of area. In addition, the use of high reinforcement areas can cause problems in consolidation as the aggregates can be trapped between the reinforcement. In the American Concrete Institute (2008) code the size of aggregate should not exceed three-quarters of the clear spacing between reinforcement. This limitation is to avoid honeycombs or voids. With steel reinforcement minimum clear spacing can be achieved by using larger bar size and decreasing the number of bars in the section. With bamboo, it is harder to control the size of strips because of the thickness of the culm is harder to control. One solution is to flatten the reinforcement to and bundle the reinforcement as shown in Figure 7.36. Another solution is to use engineered bamboo the size of the reinforcement can be controlled in addition to the MOE. In addition, the use of bamboo species which have a higher MOE such as Guadua can help in reducing the required reinforcement area.

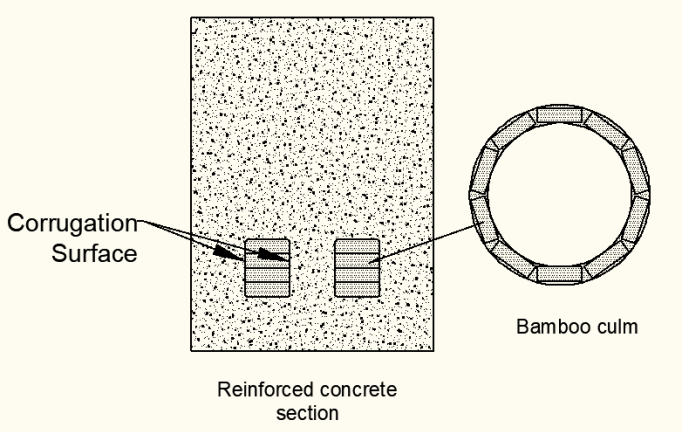

Figure 7.36 Illustration of corrugated bundled bamboo reinforcement inside the concrete at $\rho = 8\%$

7.5 Sustainability credentials of bamboo reinforcement

One of the main arguments for the use of bamboo as reinforcement is its low carbon footprint when compared to steel. However, this claim was never proved. Archila *et al.* (2018) life cycle assessment (LCA) was the first to test the sustainability claim. As a result of increased concrete usage, Archila *et al.* (2018) showed that bamboo reinforced structures with the following characteristics have a higher carbon footprint relative to steel reinforced concrete:

1. 3-4% bamboo reinforcement of the gross section;
2. use of Cox and McDonald (1970) design method where the section is conservatively assumed to be un-cracked to avoid excessive deflection and cracking;
3. use of bamboo compression reinforcement in beams and columns.

Another comparison can be carried here based on the limit state design method proposed in the current research. In Archila *et al.* (2018) analysis, the carbon footprint for medium carbon steel was 2.2–2.8 $kgCO_2/kg$ while that of bamboo is equal to 0.25 $kgCO_2/kg$. However, steel is denser than bamboo; 7,750 kg/m^3 for steel and 500 to 800 kg/m^3 for

bamboo (Kumar *et al.*, 1994). Therefore, the section area of bamboo that would have the same carbon footprint is equal to (2.6*7750)/(0.25*650)=124 times the steel area. Much lower bamboo is needed to achieve similar stiffness against deflection and cracking. For example, the area section of bamboo with 13.9 GPa MOE needed to achieve the same stiffness as 0.5% steel reinforcement is 6%. Since an equal area of concrete is used in this comparison, only the reinforcement carbon footprint needs to be considered. Therefore, the reinforcement carbon footprint with steel is 12 to 15 times (124/10) that of bamboo for equal beam stiffness.

Furthermore, if the carbon stored in the bamboo is included in the calculation, bamboo and composite bamboo can be considered carbon negative. INBAR issued a technical report by Lugt and Vogtländer (2015) to report on the environmental impact of industrial bamboo products. The report argued that the carbon footprint of industrial bamboo products (e.g. strand woven bamboo), is negative due to the sequestration of carbon from the atmosphere during the growth of bamboo.

7.6 Discussion

This chapter answers research questions 5-8. It proposed a deflection model for bamboo reinforced concrete and validated the model using the experimental results in the literature and the current research. A model for bond failure was developed and validated using the experimental results in the literature and the current research. This chapter investigated the use of two cracking models to predict the cracking in bamboo reinforced concrete. Depending on the MOE of bamboo reinforcement, up to 1% of steel reinforcement can be replaced with bamboo reinforcement for equal stiffness and cracking behaviour with a lower carbon footprint. It should be noted that 1% of steel reinforcement is commonly used in normal applications and considered to be the most economical steel percentage (McCormac and Brown, 2014).

7.6.1 Discussion of serviceability of bamboo reinforced concrete

Serviceability is the critical design criteria for bamboo reinforced concrete. The lower MOE of bamboo relative to steel and GFRP requires the use of a higher reinforcement area to achieve similar stiffness in deflection. The stiffness achieved using bamboo, FRP, and steel reinforcement is on a continuum because the stiffness of the reinforcement is the product of area and MOE. Bamboo can replace steel in applications where the required steel reinforcement for deflection is less than 1%. However, with higher design load and span lengths, higher steel reinforcement needs to be used to control deflection.

A limitation of the current research is that it focused on the simpler case of a simply supported beam while in real life flexural elements can have multiple spans. At which steel have and advantage of moment redistribution where the benefit of steel reinforcement is to achieve a more economical design. However, as this chapter argued the critical design criteria for bamboo reinforced concrete is the serviceability limits. For equal section stiffness, the flexural moment capacity of a bamboo reinforced concrete member is much higher relative to a steel-reinforced member.

Another concern with using high reinforcement area is the difficulties with achieving an adequate bond. However, in the case of corrugated bamboo, it is possible to bundle the reinforcement without an excessive loss of bond because the reinforcement is corrugated on the thickness side. There are other solutions to improve the serviceability of bamboo reinforced concrete without increasing the reinforcement area. Cambering and pre-stressing the bamboo can improve the serviceability of bamboo reinforced concrete. However, while cambering can limit deflection, it cannot limit cracking. On the other hand, pre-stressing bamboo can mitigate both deflection and cracking problems; however, pre-stressing is likely to be prohibitively impractical and expensive.

7.6.2 Discussion of sustainability of bamboo reinforced concrete

This investigation shows that replacing steel with bamboo can reduce the carbon footprint for beams reinforced with less than 1% steel reinforcement. The current research focused on limiting the comparison to steel and bamboo by using an equal amount of concrete. The width of the flexural element is kept constant while the depth is adjusted to account for the reinforcement displaced concrete. While replacing up to 1% steel reinforcement in slabs with bamboo reinforcement is feasible, in beams, higher reinforcement areas are commonly used. Therefore, the benefit of bamboo reinforcement in beams is very limited from a sustainability point of view. In addition, it should be considered that increasing the amount of concrete in the slab has an additional effect on the size of the columns and foundation and their carbon footprint. Therefore, the overall carbon footprint should be considered in sustainability evaluation. Replacing steel with bamboo reinforcement could result in an overall higher carbon footprint as a result of the need for more concrete in the section. Another limitation of this research that it has not investigated the use of bamboo reinforcement with lower carbon concrete. Using bamboo reinforcement with low carbon concrete may prove to be a more attractive prospect because the carbon footprint of the concrete as shown by Archila *et al.* (2018) is a considerable part of the total carbon footprint.

7.7 Conclusion

Deflection and crack control are the critical limitations in the design of bamboo reinforced concrete. The effect of the low MOE of bamboo can be partly mitigated by the use of a higher reinforcement percentage. It is difficult to achieve the same bond strength with bamboo reinforcement relative to steel and FRP bars. However, in this chapter a model was developed that can account for the effect of bond on the deflection behaviour of bamboo reinforced concrete beams. Two models were validated for the estimation cracking. Concerning sustainability, it is possible to achieve a better carbon footprint with bamboo if the equivalent steel-reinforced concrete has less than 1% reinforcement. The percentage of bamboo that can be used in the section is limited by the workability of the section. In the case of corrugated bamboo, it is possible to bundle the reinforcement to increase the reinforcement in the section without an excessive loss of bond.

Chapter 8

8. Conclusions & Future Work

This chapter provides a summary of the conclusions made during this summary. In addition, it identifies relevant areas of for future research.

8.1 The bond of bamboo to concrete

Corrugating bamboo significantly improves the bamboo bond with the concrete through mechanical interlock. The bond strength of corrugated bamboo can be estimated under low embedment lengths (100 mm) based on the shear strength of bamboo and the shear-friction of concrete. The slip corresponding 80% of the maximum bond is equal to 1.11 mm. The bond achieved using waterproofed corrugated bamboo splints is comparable to the bond achieved using splints treated with expensive epoxy treatments. 2 mm projection is adequate for achieving adequate mechanical interlock and utilising the full shear strength of the bamboo in bond. The stiffness of the reinforcement affects the bond at long embedment length (over 100 mm) and needs to be taken into account when estimating the average bond. A model was presented that can estimate the bond of bamboo in uncracked concrete at any embedment length using the bond-slip model under small embedment length, the modulus of elasticity, and the area of reinforcement as inputs.

8.2 Flexural and shear capacities of bamboo reinforced concrete

This research showed that the brittle behaviour of bamboo makes its flexural design analogous to FRP reinforced concrete. Similarly, the low modulus of elasticity of bamboo makes the shear design of bamboo analogous to FRP reinforced concrete where only the uncracked concrete can transfer shear. However, the weaker bond of bamboo in comparison with steel and FRP reinforcement can result in bonding failure. A bond failure model was presented and validated in the current research.

8.3 Deflection and cracking estimation of bamboo reinforced concrete

The current research showed that deflection and cracking are the critical limits in the design of bamboo reinforced concrete beams and slabs. An adjustment was made to Bischoff's (2005) model to account for the effect of bond on stiffness. It is difficult to achieve the same bond strength with bamboo reinforcement relative to steel and FRP bars. However, in this thesis, a model was developed that can account for the effect of bond on the deflection behaviour of bamboo reinforced concrete beams.

The spacing of cracks in bamboo reinforced concrete is larger in comparison with steel-reinforced concrete. This due to the weaker bond with concrete and the lower stiffness of bamboo reinforcement. The models of Frosch (1999) and CEB-FIB (1993) after adjustment for bamboo reinforced concrete produced similar correlation strength with the experimental cracking results.

8.4 Comparing bamboo reinforcement to steel and FRP

Bundling of the reinforcement is sufficient to achieve a stiffness similar to that obtained using GFRP reinforcement and in applications where less than 1% of steel reinforcement

can be used. Using a conservative estimate of the bamboo carbon footprint, the reinforcement carbon footprint with steel is 12 to 15 times that of bamboo for equal beam stiffness. It is possible to achieve a superior carbon footprint with bamboo reinforcement relative to steel by using a higher reinforcement area of bamboo without increasing the concrete in the section. However, 1% is the upper limit of steel reinforcement that can be replaced with bamboo due to the workability of the section problem.

8.5 Limitations of using bamboo as reinforcement

The use of bamboo as reinforcement in concrete still faces serious challenges including durability and creep. Another limitation of bamboo reinforced concrete is that, unlike in steel-reinforced concrete, moment redistribution cannot be achieved. In steel-reinforced concrete, moment redistribution helps in achieving a more efficient design. In addition, the ductility of steel allows for an overall higher margin of safety. Moreover, the ductility of steel help in dissipating the energy of seismic loading. The energy of the seismic loading is partly absorbed by the plastic deformation of steel. Brittle and elastic materials such as FRP and bamboo cannot absorb energy into plastic deformation which means that the concrete has to absorb all the energy of the seismic loading. Therefore, it is not advisable for bamboo to be used as reinforcement in seismic active locations. Another limitation is the shrinkage problem in concrete. Steel reinforcement in compression and tension can resist shrinkage and creep stresses in concrete. However, it is not clear whether bamboo reinforcement can be beneficial in resisting shrinkage.

The high bamboo reinforcement area required to replace steel and the workability of the section problem limits its use as reinforcement in beams. While replacing up to 1% steel reinforcement in slabs with bamboo reinforcement is feasible, higher reinforcement areas are commonly used in beams. Therefore, the benefit of bamboo reinforcement in beams is very limited from a sustainability point of view.

In addition, the use of bamboo requires special considerations. For example, the low density of bamboo can make the bamboo float in the concrete. Therefore, the reinforcement needs to be tied to the formwork. Furthermore, corrugating the bamboo requires special machines to provide corrugation without excessive labour. Another limitation is that there is currently no research on fire resistance of bamboo reinforced concrete. Concrete protects the steel and FRP reinforcement against fire. While the strength and MOE of FRP are reduced by 50% at 250^{o} C (Nanni, De Luca and Jawaheri Zadeh, 2014), after ninety minutes of heat treatment at 220^{o} C the strength of bamboo is reduced only by 24% (Wahab *et al.*, 2005). However, it is not known if the heat affects the strength of bamboo during heat exposure more severely. The use of higher reinforcement percentage to replace steel can limit the efficacy of splicing the reinforcement. In addition, the connection between the reinforcement and the supports can be complicated by the high reinforcement area.

A practical limitation in the design of bamboo reinforced concrete is the lack of a grading system. For design purposes, the characteristic strength of the reinforcement should be used in the design. While there have been attempts to provide non-destructive tests for standardizing bamboo, a grading system similar to that in wood has not arrived.

8.6 Future work

The research that currently exists on the long-term behaviour of bamboo is scarce. More research is needed on durability treatments and creep before bamboo can be safely used as reinforcement in concrete. More research is needed on the behaviour of bamboo shear reinforcement. The behaviour of bamboo reinforced concrete in indeterminate structures has not been investigated and further investigation is needed. More research is needed on engineered bamboo materials to provide a high reinforcement MOE. More research is needed on the combination of bamboo and low carbon concrete to lower the carbon

footprint of the structure. Other structural shapes should be investigated such as vaults and arches as they are likely to be more effective in comparison with beams and slabs because they put less pressure on the bamboo reinforcement.

References

Acha Navarro, E.H. (2011) Bamboo: High Tech Material for Concrete Reinforcement. PhD, Pontifical Catholic University of Rio de Janeiro.

ACI Committee 446.1R (1991) Fracture Mechanics of Concrete: Concepts, Models and Determination of Material Properties. In: Bazant, Z.P. First International Conference on Fracture Mechanics of Concrete Structures. Breckenridge Colorado, 1-5 June 1992. London: Elsevier, 1-140.

Adewuyi, A.P., Otukoya, A.A., Olaniyi, O.A. and Olafusi, O.S. (2015) Comparative Studies of Steel, Bamboo and Rattan as Reinforcing Bars in Concrete: Tensile and Flexural Characteristics. Open Journal of Civil Engineering. 5 (2), pp. 228-238.

Adom-Asamoah, M. and Osei, J.B. (2018) Shear performance of bamboo reinforced self-compacting concrete beams without stirrups. ARPN Journal of Engineering and Applied Sciences. 13 (10), pp. 3312-3324.

Adom-Asamoah, M. and Russell, A.O. (2011) A comparative study of Bamboo reinforced concrete beams using different stirrup materials for rural construction. International Journal of Civil & Structural Engineering. 2 (2), pp. 407–423.

Agarwal, A., Nanda, B. and Maity, D. (2014) Experimental investigation on chemically treated bamboo reinforced concrete beams and columns. Construction and Building Materials. 71 pp. 610–617.

Aktas, M. and Sumer, Y. (2014) Nonlinear finite element analysis of damaged and strengthened reinforced concrete beams. Journal of Civil Engineering and Management. 20 (2), pp. 201–210.

Altalmas, A., El Refai, A. and Abed, F. (2015) Bond degradation of basalt fiber-reinforced polymer (BFRP) bars exposed to accelerated aging conditions. Construction and Building Materials. 81 pp. 162–171.

American Concrete Institute (2008) ACI 318-08 Building code requirements for structural concrete and commentary. Farmington Hills: American Concrete Institute.

American Concrete Institute (2003) ACI 440.1R-03 Guide for the Design and Construction of Concrete Reinforced with FRP Bars. Farmington Hills: American Concrete Institute.

American Concrete Institute (2015) ACI 440.1R Guide for the Design and Construction of Structural Concrete Reinforced with FRP Bars. Farmington Hills: American Concrete Institute.

American Concrete Institute (1997) Finite Element Analysis of Fracture in Concrete Structures: State-of-the-Art. Farmington Hills: American Concrete Institute.

American Wood Council (2018) National Design Specifications for Wood Construction. Leesburg: American Wood Council.

An, F. (2015) Modelling of FRP-concrete interfacial bond behaviour. PhD, The University of Edinburgh.

Archila, H., Kaminski, S., Trujillo, D., Zea Escamilla, E. and Harries, K.A. (2018) Bamboo reinforced concrete: a critical review. Materials and Structures. 51 (102), pp. 1-18.

Arel, H.S. and Yazici, S. (2012) Concrete–reinforcement bond in different concrete classes. Construction and Building Materials. 36 pp. 78–83.

Ascione, L., Berardi, V.P. and D'Aponte, A. (2012) Creep phenomena in FRP materials. Mechanics Research Communications. 43 pp. 15-21.

ASTM (2015) D6815-09 Standard Specification for Evaluation of Duration of Load and Creep Effects of Wood and Wood-Based Products. West Conshohocken: ASTM International.

ASTM (2014) D7913 Standard Test Method for Bond Strength of Fiber-Reinforced Polymer Matrix Composite Bars to Concrete by Pullout Testing. West Conshohocken: ASTM International.

Austin, P.C. and Steyerberg, E.W. (2015) The number of subjects per variable required in linear regression analyses. Journal of clinical epidemiology. 68 (6), pp. 627–636.

Azadeh, A. and Kazemi, H.H. (2014) New Approaches to Bond between Bamboo and Concrete. Key Engineering Materials. 600 pp. 69–77.

Baena, M., Torres, L., Turon, A. and Barris, C. (2009) Experimental study of bond behaviour between concrete and FRP bars using a pull-out test. Composites Part B: Engineering. 40 (8) pp. 784–797.

Bahçecitapar, M.K., Karadağ, O and Aktas, S. (2016) Estimation of sample size and power for general full factorial designs. Journal of Statisticians: Statistics and Actuarial Sciences. 9 (2), pp. 79-86.

Bažant, Z.P. and Becq-Giraudon, E. (2002) Statistical prediction of fracture parameters of concrete and implications for choice of testing standard. Cement and Concrete Research. 32 (4), pp. 529–556.

Bažant, Z.P. and Oh, B.H. (1983) Crack band theory for fracture of concrete. Materials and Structures. 16 (3), pp. 155–177.

Bentz, E.C. (2005) Explaining the Riddle of Tension Stiffening Models for Shear Panel Experiments. Journal of Structural Engineering. 131 (9), pp. 1422–1425.

Bijen, J. (2003) Durability of engineering structures: design, repair and maintenance. Cambridge: Woodhead.

Bischoff, P.H. (2005) Reevaluation of Deflection Prediction for Concrete Beams Reinforced with Steel and Fiber Reinforced Polymer Bars. Journal of Structural Engineering. 131 (5), pp. 752-767.

Borst, D.R., Remmers, J.J., Needleman, A. and Abellan, M.A. (2004) Discrete vs smeared crack models for concrete fracture: bridging the gap. International Journal for Numerical and Analytical Methods in Geomechanics. 28 (7–8), pp. 583–607.

Branson, D. and Metz, G.A. (1963) Instantaneous and time-dependent deflections of simple and continuous reinforced concrete beams. Auburn: Bureau of Research and Development.

Brink, F.E. and Rush, P.J. (1966) Bamboo reinforced concrete construction. Port Hueneme: US Naval Civil Engineering Laboratory.

British Srandards Institution (2002) BS EN 1990 Eurocode - Basis of structural design. London: British Srandards Institution.

British Standards Institution (2009) BS EN 338 Structural timber - strength classes. London: British Standards Institution.

British Standards Institution (2013) BS EN 335 Durability of wood and wood-based products- Use classes: definitions, application to solid wood and wood-based products. London: British Standards Institution.

Bui, Q.B., Grillet, A.C. and Tran, H.D. (2017) A Bamboo Treatment Procedure: Effects on the Durability and Mechanical Performance. Sustainability. 9 (9).

Burgoyne, C. and Balafas, I. (2007) Why is FRP not a Financial Success? 8th International Symposium on Fiber Reinforces Polymer Reinforcement for Concrete Structures. 16-18 July 2007 Patras: University of Patras.

CEB-FIB (1993) Model Code 1990. London: Thomas Telford.

CEB-FIB (2007) Bulletin 40 FRP reinforcement in RC structures. Lausanne: International Federation for Structural Concrete.

Chen, G.-M. (2010) Behaviour and strength of RC beams shear-strengthened with externally bonded FRP reinforcement. PhD, The Hong Kong Polytechnic University.

Chen, G.M., Chen, J.F. and Teng, J.G. (2012) On the finite element modelling of RC beams shear-strengthened with FRP. Construction and Building Materials. 32 pp. 13–26.

Chen, W.F. and Saleeb, A.F. (1994) Constitutive Equations for Engineering Materials. Volume 1: Elasticity and Modeling. 2nd ed. Amsterdam: Elsevier.

Chen, W. (2007) Plasticity in reinforced concrete. 2nd ed. Fort Lauderdale: J. Ross Publication.

Chow, H.K. (1914) Bamboo As A Material for Reinforcing Concrete. Master, Massachusetts Institute of Technology.

Cohen, J. (1989) Statistical Power Analysis for the Behavioral Sciences. 2nd ed. New York: Lawrence Erlbaum Associates.

Coronado, C.A. and Lopez, M.M. (2006) Sensitivity analysis of reinforced concrete beams strengthened with FRP laminates. Cement and Concrete Composites. 28 (1), pp. 102–114.

Cox, F.B. and Geymayer, H.G. (1969) Expedient Reinforcement for Concrete for Use in Southeast Asia: Preliminary Tests of Bamboo. Report number: 1. Vicksburg: US Army Engineer Waterways Experiment Station.

Cox, F.B. and McDonald, J.E. (1970) Expedient Reinforcement for Concrete for Use in Southeast Asia: Additional Tests of Bamboo. Report number: 3. Vicksburg: US Army Engineer Waterways Experiment Station.

Crisfield, M.A. (1981) A fast incremental/iterative solution procedure that handles "snap-through". Computers & Structures. 13 (1–3), pp. 55–62.

Crisfield, M.A. (1986) Snap-through and snap-back response in concrete structures and the dangers of under-integration. International Journal for Numerical Methods in Engineering. 22 (3), pp. 751–767.

Curtis, P.T. (2000) Durability Testing of Polymer Composites. In: Kelly, A. and Zweben, C. (2000) Comprehensive Composite Materials. Oxford: Pergamon.

D'Agostino, R.B. (1971) An omnibus test of normality for moderate and large size samples. Biometrika. 58 (2), pp. 341–348.

Dey, A. and Chetia, N. (2018) Experimental study of Bamboo Reinforced Concrete beams having various frictional properties. Materials Today: Proceedings. 5 (1), pp. 436–444.

El-Mogy, M., El-Ragaby, A. and El-Salakawy, E. (2011) Behavior of continuous concrete beams reinforced with FRP bars. In: Advances in FRP Composites in Civil Engineering

- Proceedings of the 5th International Conference on FRP Composites in Civil Engineering, Beijing, 27-29 Septemper 2010. Berlin: Springer, pp. 283–286.

European Committee for Standardization (2004) EN 1992-1-1 Eurocode 2: Design of Concrete Structures - Part 1: General rules and rules for buildings. Brussels: European Committee for Standardization.

Feng, J., Chen, J., Chen, M., Su, X. and Shi, Q. (2017) Effects of biocide treatments on durability of wood and bamboo/high density polyethylene composites against algal and fungal decay. Journal of Applied Polymer Science. 134 (31).

Focacci, F., Nanni, A. and Bakis, C.E. (2000) Local bond-slip relationship for FRP reinforcement in concrete. Journal of Composites for Construction. 4 (1), pp. 24-31.

Fox, J. (2016) Applied regression analysis and generalized linear models. 3rd edition. London: SAGE Publications.

Frosch, R.J. (1999) Another look at cracking and crack control in reinforced concrete. ACI Structural Journal, 96 (3), pp. 437-442.

Geymayer, H.G. and Cox, F.B. (1970) Bamboo reinforced concrete. ACI Journal Proceedings. 67 (10), pp. 841–846.

Ghasemi, A. and Zahediasl, S. (2012) Normality tests for statistical analysis: A guide for non-statisticians. International Journal of Endocrinology and Metabolism. 10 (2), pp. 486-489.

Ghavami, K. (2005) Bamboo as reinforcement in structural concrete elements. Cement and concrete composites. 27 (6), pp. 637–649.

Ghavami, K. (1995) Ultimate load behaviour of bamboo-reinforced lightweight concrete beams. Cement and concrete composites. 17 (4), pp. 281–288.

Gottron, J., Harries, K.A. and Xu, Q. (2014) Creep behaviour of bamboo. Construction and Building Materials. 66, pp. 79–88.

Gravina, R.J. and Smith, S.T. (2008) Flexural behaviour of indeterminate concrete beams reinforced with FRP bars. Engineering Structures. 30 (9), pp. 2370–2380.

Hawileh, R.A. (2012) Nonlinear finite element modeling of RC beams strengthened with NSM FRP rods. Construction and Building Materials. 27 (1), pp. 461-471.

Hawileh, R.A., Naser, M.Z. and Abdalla, J.A. (2013) Finite element simulation of reinforced concrete beams externally strengthened with short-length CFRP plates. Composites Part B: Engineering. 45 (1), pp. 1722–1730.

Hillerborg, A., Modéer, M. and Petersson, P.E. (1976) Analysis of crack formation and crack growth in concrete by means of fracture mechanics and finite elements. Cement and Concrete Research. 6 (6), pp. 773–781.

Hognestad, E., Hanson, N. and McHenry, D. (1955) Concrete stress distribution in ultimate strength design. ACI Journal Proceedings. 52 (12), pp. 455–480.

Humar, M. and Lesar, B. (2013) Efficacy of linseed- and tung-oil-treated wood against wood-decay fungi and water uptake. International Biodeterioration and Biodegradation. 85, pp. 223-227.

IBM Knowledge Center (2019) Covariance Structures. Available from: https://www.ibm.com/support/knowledgecenter/en/SSLVMB_23.0.0/spss/advanced/covariance_structures.html [Accessed 15 January 2019].

ISIS Canada (2007) Reinforcing Concrete Structures with Fibre Reinforced Polymers (Design Manual No. 3). Manitoba: ISIS Canada.

International Organization for Standardization (2004) ISO 22157 Determination of physical and mechanical properties of bamboo. Geneva: International Organization for Standardization

Janssen, J.A. (2000) Designing and Building with Bamboo. Report number: 20. Beijing: INBAR.

Jason, L., Torre-Casanova, A., Davenne, L. and Pinelli, X. (2013) Cracking behavior of reinforced concrete beams: experiment and simulations on the numerical influence of the steel-concrete bond. International Journal of Fracture. 180 (2), pp. 243-260.

Javadian, A., Wielopolski, M., Smith, I.F.C. and Hebel, D.E. (2016) Bond-behavior study of newly developed bamboo-composite reinforcement in concrete. Construction and Building Materials. 122 pp. 110-117.

Jiang, Z., Wang, H., Tian, G., Liu, X. and Yu, Y. (2012) Sensitivity of several selected mechanical properties of moso bamboo to moisture content change under the fibre saturation point. BioResources. 7 (4), pp. 5048-5058.

Kankam, C.K. (1997) Relationship of Bond Stress, Steel Stress, and Slip in Reinforced Concrete. Journal of Structural Engineering. 123 (1), pp. 79–85.

Kelchner, S.A. and Group, B.P. (2013) Higher level phylogenetic relationships within the bamboos (Poaceae: Bambusoideae) based on five plastid markers. Molecular phylogenetics and evolution. 67 (2), pp. 404-413.

Khatib, A. and Nounu, G. (2017) Corrugated bamboo as reinforcement in concrete. Proceedings of the Institution of Civil Engineers. 170 (4), pp. 311-318.

Khatib, J.M. (2009) Sustainability of construction materials. Oxford: Woodhead.

Kim, N.H. (2014) Introduction to nonlinear finite element analysis. Boston: Springer.

Kriker, A., Bali, A., Debicki, G., Bouziane, M. and Chabannet, M. (2008) Durability of date palm fibres and their use as reinforcement in hot dry climates. Cement and Concrete Composites. 30 (7), pp. 639-648.

Kumar, S., Shukla, K.S., Dev, T. and Dobriyal, P.B. (1994) Bamboo Preservation Techniques: a review. INBAR & ICRFE.

Kute, S.Y. and Wakchaure, M.R. (2013) Performance Evaluation for Enhancement of Some of the Engineering Properties of Bamboo as Reinforcement in Concrete. Journal of The Institution of Engineers (India): Series A. 94 (4), pp. 235–242.

Landau, S. and Everitt, B.S. (2003) A Handbook of Statistical Analyses Using SPSS. Boca Raton: Chapman & Hall/CRC Press.

Leelatanon, S., Srivaro, S. and Matan, N. (2010) Compressive strength and ductility of short concrete columns reinforced by bamboo. Sonklanakarin Journal of Science and Technology. 32 (4), pp. 419-424.

Li, H. and Shen, S. (2011) The mechanical properties of bamboo and vascular bundles. Journal of Materials Research. 26 (21), pp. 2749–2756.

Li, T., Zhu, H., Wang, Q., Li, J. and Wu, T. (2018) Experimental study on the enhancement of additional ribs to the bond performance of FRP bars in concrete. Construction and Building Materials. 185, pp. 545–554.

Lima Jr, H.C., Willrich, F.L., Barbosa, N.P., Rosa, M.A. and Cunha, B.S. (2008) Durability analysis of bamboo as concrete reinforcement. Materials and Structures. 41 (5), pp. 981–989.

Lobovikov, M., Paudel, S., Piazza, M., Ren, H. and Wu, J. (2007) World bamboo resources: a thematic study prepared in the framework of the Global Forest Resources Assessment 2005. Rome: Food and Agriculture Organization of the United Nations.

Lobovikov, M., Schoene, D. and Yping, L. (2012) Bamboo in climate change and rural livelihoods. Mitigation and Adaptation Strategies for Global Change. 17 (3), pp. 261–276.

Logan, D.L. (2011) A first course in the finite element method. 4th edition. USA: Cengage Learning.

Lozhechnikova, A., Vahtikari, K., Hughes, M. and Österberg, M. (2015) Toward energy efficiency through an optimized use of wood: The development of natural hydrophobic coatings that retain moisture-buffering ability. Energy and Buildings. 105, pp. 37-42.

Lubliner, J., Oliver, J., Oller, S. and Onate, E. (1989) A plastic-damage model for concrete. International Journal of Solids and Structures. 25 (3), pp. 299–326.

Lugt, P. van der and Vogtländer, J.G. (2015) The Environmental Impact of Industrial Bamboo Products: Life-Cycle assessment and Carbon Sequestration. Report nomber 35. Beijing: INBAR.

Ma, X., Liu, X., Jiang, Z., Fei, B. and Wang, G. (2016) Flexural creep behavior of bamboo culm (Phyllostachys pubescens) in its radial direction. Journal of Wood Science. 62 (6), pp. 487–491.

Ma, X., Shi, S.Q., Wang, G., Fei, B. and Jiang, Z. (2018) Long creep-recovery behavior of bamboo-based products. Journal of Wood Science. 64 (2), pp. 119–125.

Maggi, Y.I., Gonçalves, R.M., Leon, R.T. and Ribeiro, L.F.L. (2005) Parametric analysis of steel bolted end plate connections using finite element modeling. Journal of Constructional Steel Research. 61 (5), pp. 689-708.

Masmoudi, R., Thériault, M. and Benmokrane, B. (1998) Flexural behavior of concrete beams reinforced with deformed fiber reinforced plastic reinforcing rods. ACI Structural Journal. 95 (6), 665-676.

McCormac, J.C. and Brown, R.H. (2014) Design of Reinforced Concrete. 9th edition. USA: Wiley & Sons.

Mercan, B., Stolarski, H.K. and Schultz, A.E. (2016) Arc-length and explicit methods for static analysis of prestressed concrete members. Computers and Concrete. 18 (1), pp. 17–37.

Metwally, I.M. (2017) Three-dimensional nonlinear finite element analysis of concrete deep beam reinforced with GFRP bars. HBRC Journal. 13 (1), pp. 25–38.

Mias, C., Torres, L., Guadagnini, M. and Turon, A. (2015) Short and long-term cracking behaviour of GFRP reinforced concrete beams. Composites Part B: Engineering. 77, pp. 223–231.

Montgomery, D.C. (2003) Applied Statistics and Probability for Engineers. 3rd ed. Danvers: John Wiley & Sons.

Nanni, A., De Luca, A. and Jawaheri Zadeh, H. (2014) Reinforced concrete with FRP bars : mechanics and design. Boca Raton: CRC Press.

Ngo, D. and Scordelis, A.C. (1967) Finite element analysis of reinforced concrete beams. Journal Proceedings. 64 (3), pp. 152–163.

Orangun, C.O., Jirsa, J.O. and Breen, J.E. (1977) A Reevaluation of Test Data on Development Length and Splices. ACI Journal Proceedings. 74 (3), pp. 114-122.

Pacheco-Torgal, F. and Labrincha, J.A. (2013) The future of construction materials research and the seventh UN Millennium Development Goal: A few insights. Construction and Building Materials. 40, pp. 729–737.

Potisuk, T., Higgins, C.C., Miller, T.H. and Yim, S.C. (2011) Finite Element Analysis of Reinforced Concrete Beams with Corrosion Subjected to Shear. Advances in Civil Engineering. 2011, pp. 1–14.

Ramakrishna, G. and Sundararajan, T. (2005) Studies on the durability of natural fibres and the effect of corroded fibres on the strength of mortar. Cement and Concrete Composites. 27 (5), pp. 575-582.

Rami Hamad, J.A., Megat Johari, M.A. and Haddad, R.H. (2017) Mechanical properties and bond characteristics of different fiber reinforced polymer rebars at elevated temperatures. Construction and Building Materials. 142 pp. 521–535.

Richard, M.J. (2013) Assessing the performance of bamboo structural components. PhD: University of Pittsburgh.

Rolland, A., Quiertant, M., Khadour, A., Chataigner, S., Benzarti, K. and Argoul, P. (2018) Experimental investigations on the bond behavior between concrete and FRP reinforcing bars. Construction and Building Materials. 173 pp. 136–148.

Rots, J.G. (1988) Computational modeling of concrete fracture. PhD, Delft University of Technology.

Schneider, N., Pang, W. and Gu, M. (2014) Application of bamboo for flexural and shear reinforcement in concrete beams. In: Bell, G.R. and Card, M.A., Structures Congress 2014. Boston, 3-5 April 2014. Reston: ASCE, pp. 1025-1035.

Sharma, A. (1990) Bamboo-reinforced concrete beams. In: Vandepitte, D. Mixed Structures, including New Materials. Brussels, 1990. Zurich: International Association for Bridge and Structural Engineering. pp. 677–682.

Sun, F., Bao, B., Ma, L., Chen, A. and Duan, X. (2012) Mould-resistance of bamboo treated with the compound of chitosan-copper complex and organic fungicides. Journal of Wood Science. 58 (1), pp. 51–56.

Terai, M. and Minami, K. (2012) Research and Development on Bamboo Reinforced Concrete Structure. In: 15th World Conference on Earthquake Engineering, International Association for Earthquake Engineering. Lisbon, 24-28 Septemper 2012. Lisbon: Sociedade Portuguesa de Engenharia Sismica.

Tolêdo Filho, R.D., Scrivener, K., England, G.L. and Ghavami, K. (2000) Durability of alkali-sensitive sisal and coconut fibres in cement mortar composites. Cement and Concrete Composites. 22 (2), pp. 127–143.

Trujillo, D., Jangra, S. and Gibson, J.M. (2017) Flexural properties as a basis for bamboo strength grading. Structures and Buildings. 170 (4), pp. 284-294.

Tsavdaridis, K.D. and Papadopoulos, T. (2016) A FE parametric study of RWS beam-to-column bolted connections with cellular beams. Journal of Constructional Steel Research. 116, pp. 92-113.

Tureyen, A.K. and Frosch, R.J. (2002) Shear tests of FRP-reinforced concrete beams without stirrups. ACI Structural Journal. 99 (4), pp. 427-434.

USGS (2015) Mineral Commodity Summaries 2015. Reston: U.S. Geological Survey.

USGS (2019) Mineral Commodity Summaries 2019. Reston: U.S. Geological Survey.

Vasiliev, V. V and Morozov, E. V (2013) Advanced mechanics of composite materials and structural elements. 3rd ed. Amsterdam: Elsevier.

Verma, C.S., Chariar, V.M. and Purohit, R. (2012) Tensile strength analysis of bamboo and layered laminate bamboo composites. International Journal of Engineering Research and Applications. 2 (2), pp. 1253–1264.

Wahab, Samsi, Mohamad and Sulaiman (2005) Effect of heat treatment using palm oil on properties and durability of Semantan bamboo. Journal of Bamboo and Rattan. 4 (3), pp. 211–220.

Wambeke, B.W. and Shield, C.K. (2006) Development Length of Glass Fiber-Reinforced Polymer Bars in Concrete. ACI Structural Journal. 103 (1), pp. 11.

Wang, H. and Belarbi, A. (2010) Static and fatigue bond characteristics of FRP rebars embedded in fiber-reinforced concrete. Journal of Composite Materials. 44 (13), pp. 1605-1622.

Wei, D., Schmidt, O. and Liese, W. (2013) Durability test of bamboo against fungi according to EN standards. European Journal of Wood and Wood Products. 71 (5), pp. 551–556.

Wight, J.K. and MacGregor, J.G. (2012) Reinforced concrete: mechanics and design. 6th ed. Harlow: Pearson Education.

World Agroforestry Centre (2006) Case Study on Bamboo Marketing in Lao P.D.R. Nairobi. World Agroforestry Centre.

Wu, W., Liu, Q., Zhu, Z. and Shen, Y. (2015) Managing Bamboo for Carbon Sequestration, Bamboo Stem and Bamboo Shoots. Small-scale Forestry. 14 (2), pp. 233-243.

Yamaguchi, M., Murakami, K. and Takeda, K. (2013) Flexural Performance of Bamboo-Reinforced-Concrete Beams using Bamboo as Main Rebars and Stirrups. In: 3rd International Conference on Sustainable Construction. Kyoto, 18-21 August 2013. Kyoto: Japan Concrete Institute.

Yao, J., Teng, J.G. and Chen, J.F. (2005) Experimental study on FRP-to-concrete bonded joints. Composites Part B: Engineering. 36 (2), pp. 99-113.

Yellishetty, M., Ranjith, P.G. and Tharumarajah, A. (2010) Iron ore and steel production trends and material flows in the world: Is this really sustainable? Resources, Conservation and Recycling. 54 (12), pp. 1084–1094.

Ziari, A. and Kianoush, M.R. (2014) Finite-element parametric study of bond and splitting stresses in reinforced concrete tie members. Journal of Structural Engineering. 140 (5).

Appendix A

Table A.1 FE models of reinforced concrete in literature

Fracture energy model		-	CEB-FIP (1993) model
Control of test & solution procedure		Load & static	Displacement & dynamic
Concrete dilatation angle (ψ) and Poisson's ratio (ν)	ψ	-	35
	ν	-	0.2
Tension Softening		No model	Hordijk softening model
Prediction of cracks		No prediction	A good prediction of the pattern and widths of the cracks
Software package		-	ABAQUS
Concrete and reinforcement elements		Triangular plane elements for concrete and reinforcement	Plane elements (CPS4) for concrete and T2D2 truss elements for reinforcement
Cracking model		Predefined discrete cracks	Smeared crack band model with Rot's recommended width and Rot's model for shear retention
Bond model		Used springs at 6 in intervals to model a linear bond	CEB-FIP equation using interfacial element (COH2D4)
Concrete uniaxial stress-strain relationship		Linear	Saenz's stress-strain equation
Concrete constitutive model		Linear elastic	Plastic model
Research Paper		Ngo and Scordelis (1967)	Chen (2010) and Chen, Chen and Teng (2012)

Fracture energy model		-	Bažant and Becq-Giraudon (2002)
Control of test & solution procedure		-	-
Concrete dilatation angle (ψ) and Poisson's ratio (ν)	ψ	-	30
	ν	0.2	0.2
Tension Softening		-	Linear and bilinear softening models as shown in figure (4)
Prediction of cracks		-	No prediction

Software package	ANSYS	ABAQUS
Concrete and reinforcement elements	3D 8-node brick elements (SOLID65) for concrete and bar elements for reinforcement (LINK8)	CPE4R reduced integration plane elements for concrete and T2D2 truss elements for reinforcement
Cracking model	Smeared crack model	Smeared crack model within the damaged plasticity model
Bond model	CEB-FIP equation using COMBIN14 spring elements	Perfect bond
Concrete uniaxial stress-strain relationship	Hognestad, Hanson, and McHenry (1955)	The researchers investigated three relationships as shown in figure (2)
Concrete constitutive model	Plastic model	The damaged plasticity model
Research Paper	Hawileh, Naser and Abdalla (2013)	Coronado and Lopez (2006)

Fracture energy model		-	CEB-FIP (1993) equation
Control of test & solution procedure		N/M	Displacement controlled
Concrete dilatation angle (ψ) and Poisson's ratio (ν)	ψ	-	30
	ν	-	*
Tension Softening		The model parameters were adjusted to comply with Hillerborg *et al.* (1976)	linear softening models as shown in figure (4)
Prediction of cracks		Good prediction of cracks using the bond model	No prediction
Software package		Cast3m 2012 finite element code	ABAQUS
Concrete and reinforcement elements		8-node brick elements (15 mm side) for concrete and 2-node truss elements for reinforcement	CPE4R reduced integration plane elements for concrete and T2D2 truss elements for reinforcement
Cracking model		-	Smeared crack model within the damaged plasticity model
Bond model		The hardening part of the Harajli bond-slip model	Perfect bond
Concrete uniaxial stress-strain relationship		N/M	Hognestad model
Concrete constitutive model		Damage constitutive model	The damaged plasticity model
Research Paper		Jason *et al.* (2013)	Aktas and Sumer (2014)

Fracture energy model		-	-	CEB-FIP (1993) equation
Control of test & solution procedure		Quasi-displacement controlled by using springs to apply the load	Load controlled with 10 N load increments	N/M
Concrete dilatation angle (ψ) and Poisson's ratio (ν)	ψ	N/M	N/M	N/M
	ν	0.2	0.2	0.2
Tension Softening		N/M	-	N/M
Prediction of cracks		Prediction of location but no prediction of crack widths	Prediction of location but no prediction of crack widths	Prediction of location but no prediction of crack widths
Software package		ANSYS	ANSYS	ABAQUS
Concrete and reinforcement elements		SOLID65 8-node brick elements (15 mm side) for concrete and LINK8 2-node truss elements for reinforcement	SOLID65 8-node brick elements (15 mm side) for concrete and LINK8 2-node truss elements for reinforcement	C3D8 8-node brick elements for concrete and T3D2 truss elements for reinforcement
Cracking model		Smeared crack model	Smeared crack model	N/M
Bond model		No bond models.	CEB-FIP equation using COMBIN14 spring elements	Perfect bond (The researcher justified this by the strong bond due to sand coating)
Concrete uniaxial stress-strain relationship		Todeschini stress-strain relationship	Hognestad, Hanson and McHenry model and William and Warnke concrete failure criterion	N/M
Concrete constitutive model		Plastic model	Plastic model	The damaged plasticity model
Research Paper		Potisuk *et al.* (2011)	Hawileh (2012)	Metwally (2017)

Appendix B

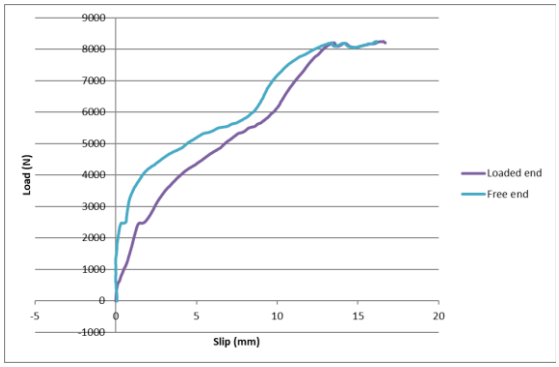

B.1 Plot of pull-out VS slip of 1mm 1:1 A specimen (maximum load achieved at exceedingly high slippage)

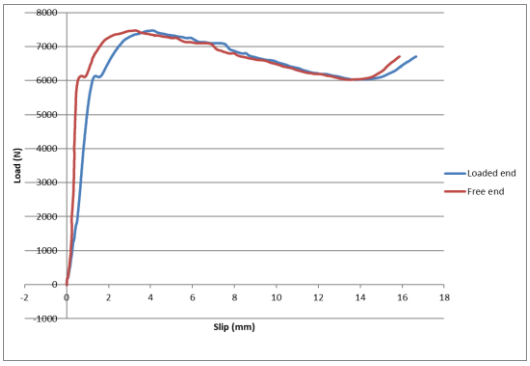

B.2 Plot of pull-out VS slip of 1mm 1:1 B specimen

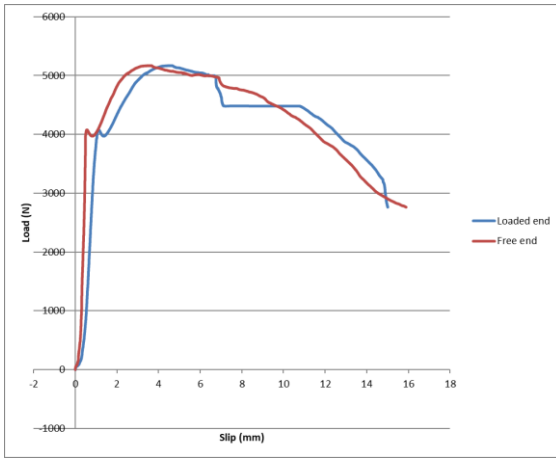

B.3 Plot of pull-out VS slip of 1mm 1:1 C specimen

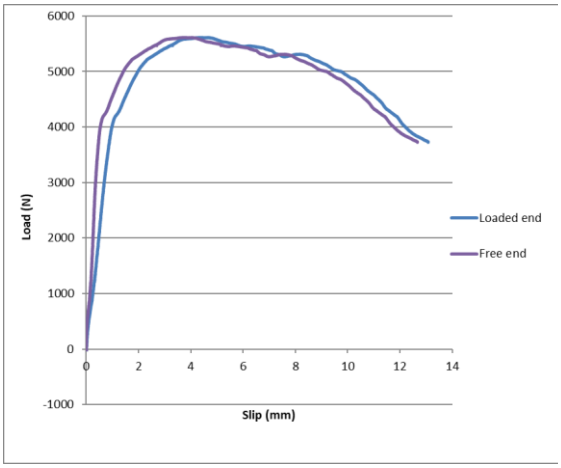

B.4 Plot of pull-out VS slip of 2mm 1:1 A specimen

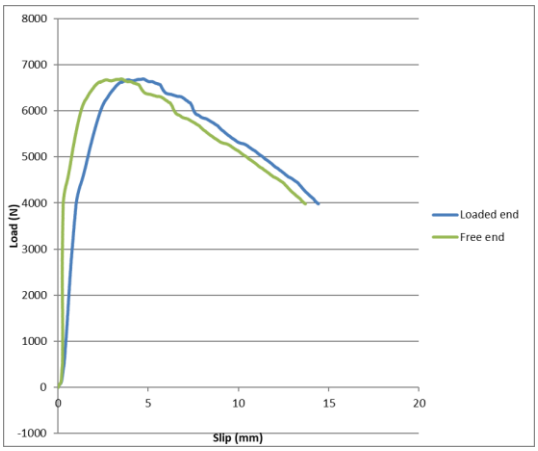

B.5 Plot of pull-out VS slip of 2 mm 1:1 B specimen

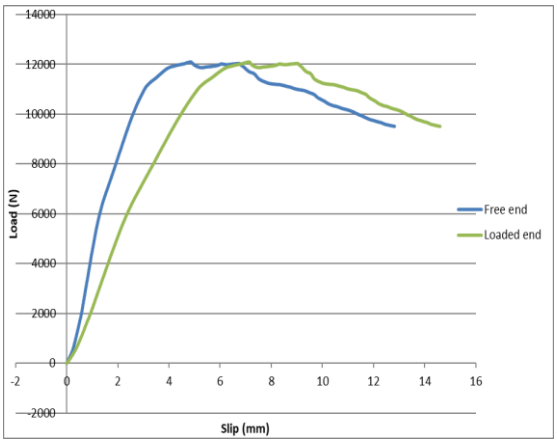

B.6 Plot of pull-out VS slip of 2mm 1:1 C specimen

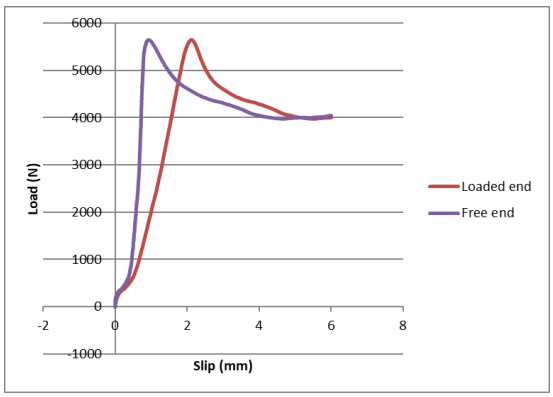

B.7 Plot of pull-out VS slip of A specimen

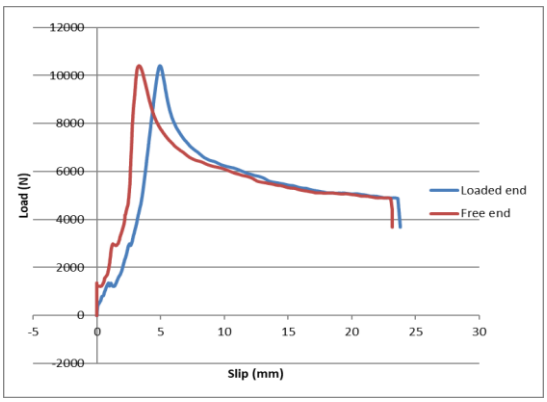

B.8 Plot of pull-out VS slip of B specimen (technical error in setting the rate of pull-out to 10mm/min instead of 1 mm/min)

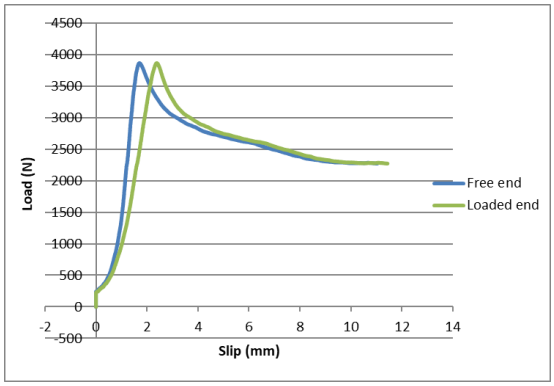

B.9 Plot of pull-out VS slip of C specimen

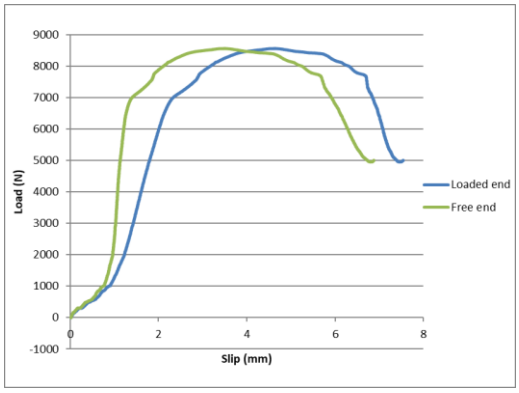

B.10 Plot of pull-out VS slip of Tr 1mm 1:1 A specimen

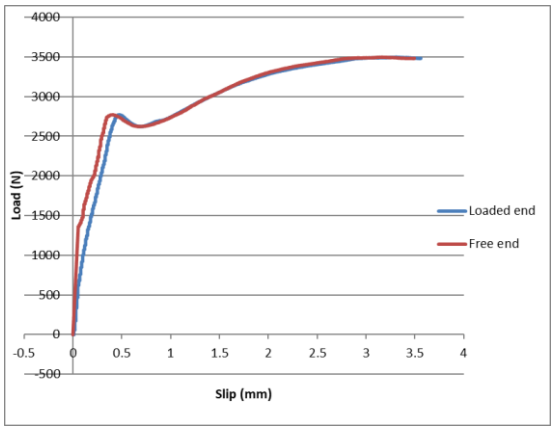

B.11 Plot of pull-out VS slip of Tr 1mm 1:1 B specimen

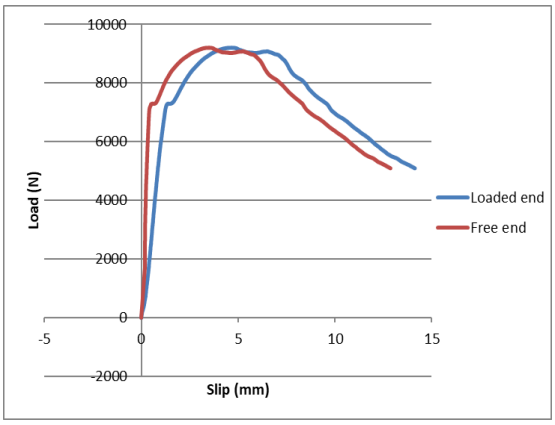

B.12 Plot of pull-out VS slip of Tr 1mm 1:1 C specimen

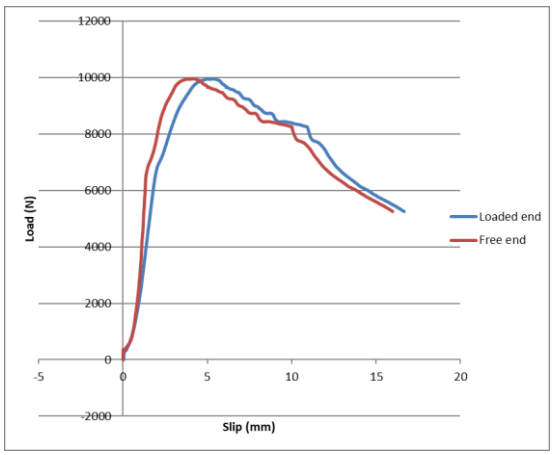

B.13 Plot of pull-out VS slip of Tr 2mm 1.5:1 A specimen

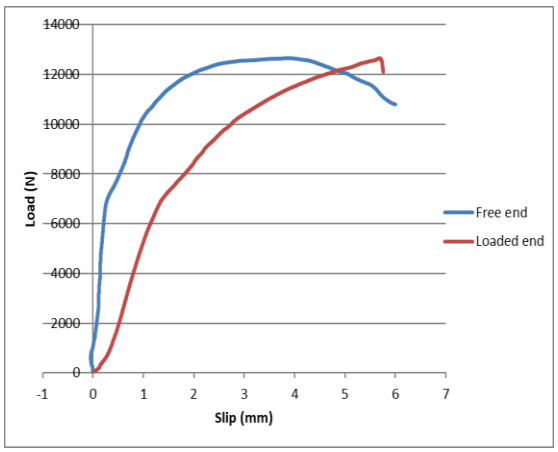

B.14 Plot of pull-out VS slip of Tr 2mm 1.5:1 B specimen

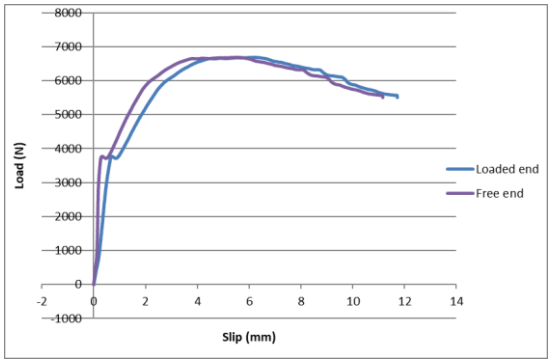

B.15 Plot of pull-out VS slip of Tr 2mm 1.5:1 C specimen

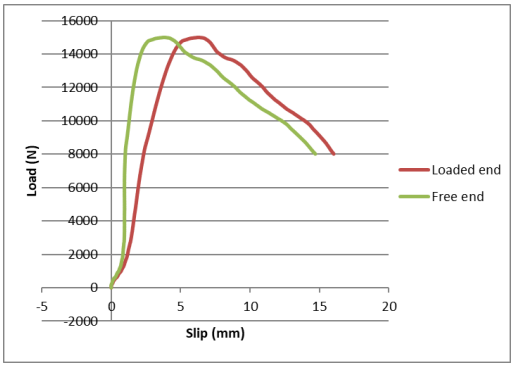

B.16 Plot of pull-out VS slip of Tr 2mm 1:1 A specimen

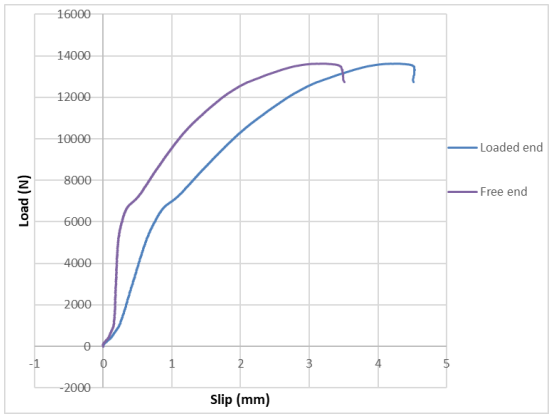

B.17 Plot of pull-out VS slip of Tr 2mm 1:1 B specimen

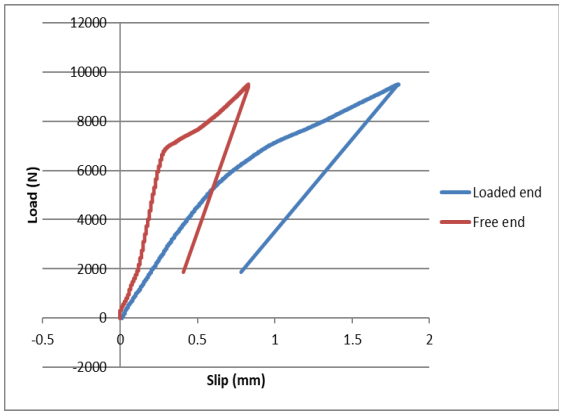

B.18 Plot of pull-out VS slip of Tr 2mm 1:1 C specimen (Tensile failure in the specimen)

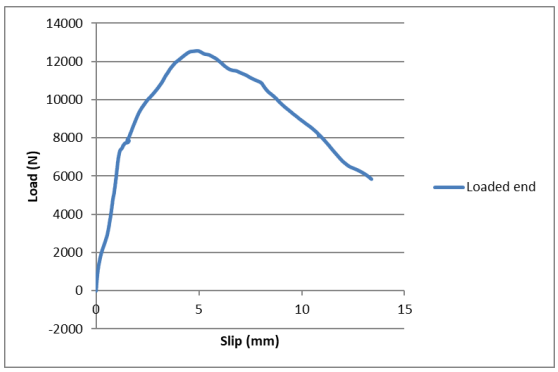

B.19 Plot of pull-out VS slip of Tr 2mm 1:1.5 A specimen (The free end slippage reading is lost due to technical error)

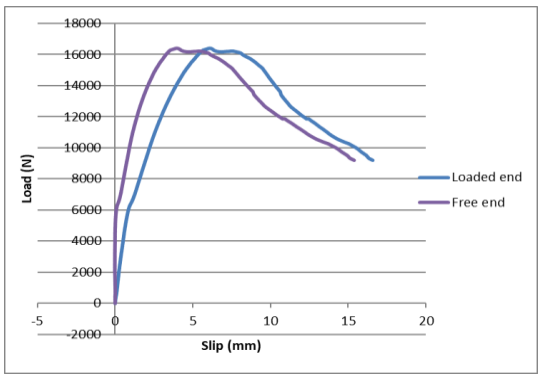

B.20 Plot of pull-out VS slip of Tr 2mm 1:1.5 B specimen

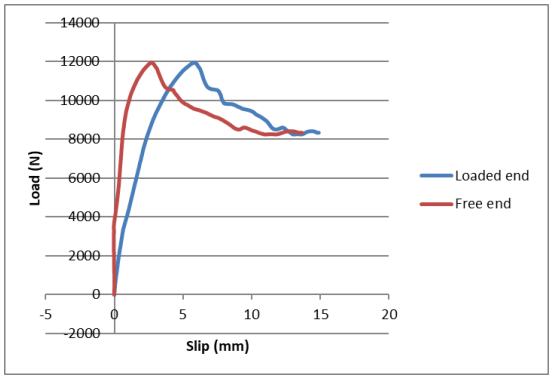

B.21 Plot of pull-out VS slip of Tr 2mm 1:1.5 C specimen

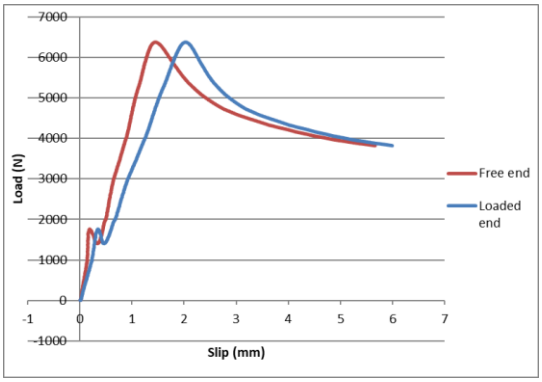

B.22 Plot of pull-out VS slip of Tr A specimen

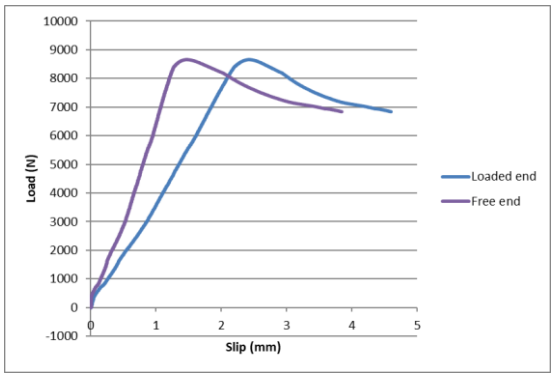

B.23 Plot of pull-out VS slip of Tr B specimen

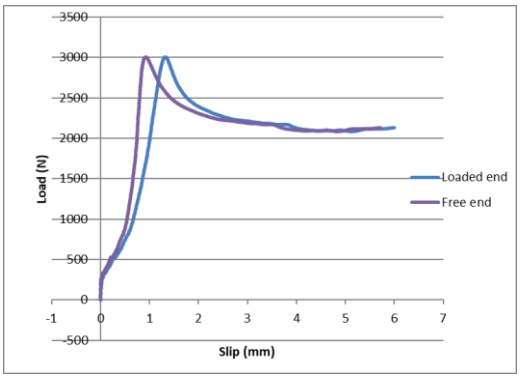

B.24 Plot of pull-out VS slip of Tr C specimen

Table B.1 Details of the tensile specimens

Specimen	Width (mm)	Thickness (mm)
1mm 1:1 A	16.9	7.8
1mm 1:1 B	13.8	9.6
1mm 1:1 C	15.4	8.1
2mm 1:1 A	16.2	8.1
2mm 1:1 B	16.7	7.4
2mm 1:1 C	17.1	9.4
A	18.8	8.4
B	18.8	9.1
C	18.5	7.1
Tr 1mm 1:1 A	16	7.7
Tr 1mm 1:1 B	15.7	7.6
Tr 1mm 1:1 C	14.8	9.5
Tr 2mm 1.5:1 A	13.5	8.7
Tr 2mm 1.5:1 B	15.6	8.9
Tr 2mm 1.5:1 C	12.8	8.3
Tr 2mm 1:1 A	15.1	9.3
Tr 2mm 1:1 B	16.8	10.4
Tr 2mm 1:1 C	15.8	9.1
Tr 2mm 1:1.5 A	12.6	10.6
Tr 2mm 1:1.5 B	14.7	9
Tr 2mm 1:1.5 C	15.3	7.7
Tr A	19.3	7.8
Tr B	19	8.2
Tr C	19.6	7.7

Example solution for the estimation of the bond at high embedment length

Since S_{max} is not known in Geymayer and Cox (1970), it is assumed that S_{max} is equal to the average value found in the current research at 1.383 mm and it drops to zero at 2.766 mm. At 150 mm the average maximum bond achieved by Geymayer and Cox (1970) is 4.13 Kg/cm^2= 0.405 MPa. The reinforcement area is 34.3, the and the maximum longitudinal bond is 13.8 N/mm and the MOE is 18 GPa.

The first step is to determine the maximum length at which there is a transfer of shear between the reinforcement and the concrete. Taking the bond at 150 mm as a reasonable representation of bond at short embedment length L_1 and L_2 can be calculated a follows:

$$L_1 = \sqrt{S_{max} \times 4EA/\tau_{l,max}} = \sqrt{1.383 \times 4 \times 18000 \times 34.3/13.8} = 497\ mm$$

$$F_1 = \frac{1}{2}\tau_{l,max} L_1 = 0.5 \times 13.8 \times 497 = 3433\ N$$

$$L_2 = \sqrt{3((S_0 - S_{max})EA - F_1 L_2)/\tau_{l,max}}$$

$$= \sqrt{\frac{3\left((2.766 - 1.383) \times 18000 \times 34.3 - 3433 L_2\right)}{13.8}}$$

Solving for L_2, $L_2 = 196.8\, mm$

As an example here the average bond with 400 mm is found as follows:

$$f_1 = \tau_{l,max} B l \left(1 - B\frac{l}{2L_1}\right) = 13.8 \times 0.7 \times 400 \left(1 - 0.7\frac{400}{2 \times 497}\right) = 2776\ N$$

$$f_2 = \tau_{l,max}(1 - B)\left(l - (1 - B)\frac{l^2}{2L_2}\right)$$

$$= 13.8(1 - 0.7)\left(400 - (1 - 0.7)\frac{400^2}{2 * 196.8}\right) = 1151\ N$$

The average bond τ_{avg} along the embedment can be found now as following:

$$\tau_{avg} = \frac{f_1 + f_2}{2lw} = \frac{2776 + 1151}{2 * 400 * 17} = 0.289\ MPa$$

Appendix C

Table C.1 Tensile MOE and strength of bamboo used as reinforcement in beams

Specimen	Pole	Thickness (mm)	Width (mm)	MOE (Mpa)	Tensile strength (MPa)
1A	1	8.60	8.32	12042	69.1
1B	1	7.81	10.46	12321	51.6
1C	1	9.53	7.65	11287	74.6
2A	2	8.75	7.98	13783	139.7
2B	2	8.36	7.57	9973	86.0
2C	2	8.53	7.58	14503	141.2
3A	3	7.90	10.43	11458	94.9
3B	3	6.78	7.57	15247	107.4
3C	3	7.67	11.37	14116	97.6
4A	4	6.95	8.42	13062	128.0
4B	4	7.57	7.85	14071	105.2
4C	4	8.05	9.71	10331	120.2
5A	5	7.01	9.36	20527	146.8
5B	5	7.18	9.51	17493	121.7
5C	5	7.19	9.79	17882	150.2
6A	7	7.74	11.88	17983	114.4
6B	7	7.47	8.41	10676	118.0
6C	7	6.73	7.65	14214	125.1
7A	8	8.36	10.57	13422	119.7
7B	8	8.76	11.78	18765	121.2
7C	8	8.61	8.88	9718	141.3

Table C.2 Tensile MOE and strength of Moso and Guadua bamboo using different testing methods

Grip width : Gauge width ratio	Specimen ends treatment	Species	Width	Thichness	Tensile strength (MPa)	MOE (GPa)
1:2	-	Guadua	7.67	10.20	134	22.5
1:2	-	Guadua	8.40	10.53	133	19.6
1:2	-	Guadua	8.27	10.23	150	21.5
1:3	-	Guadua	7.47	8.80	157	18.6
1:3	-	Guadua	8.03	8.70	150	17.7
1:3	-	Guadua	7.77	8.93	163	21.8
1:4	-	Guadua	5.97	8.93	158	23.3
1:4	-	Guadua	6.07	8.97	165	21.0
1:4	-	Guadua	5.97	9.03	170	20.1
1:4	-	Guadua	6.17	9.80	124	22.8
1:4	-	Guadua	5.77	9.45	112	26.0
1:4	-	Guadua	5.90	9.35	142	24.3
1:2	-	Moso	9.40	10.07	133	14.1
1:2	-	Moso	9.23	9.30	130	13.3
1:2	-	Moso	8.20	9.83	137	14.0
1:2	Aluminium tabs + epoxy	Moso	9.87	9.30	130	12.4
1:2	Aluminium tabs + epoxy	Moso	8.80	8.50	138	13.4
1:2	Aluminium tabs + epoxy	Moso	9.47	10.00	114	11.7
1:2	Flattened	Moso	9.97	7.67	143	12.0
1:2	Flattened	Moso	9.43	8.07	153	10.2
1:2	Flattened	Moso	9.33	8.17	112	11.0
1:3	-	Moso	6.43	7.70	177	14.6
1:3	-	Moso	6.30	9.47	165	10.9
1:3	-	Moso	6.00	9.73	169	11.8
1:3	-	Moso	6.10	8.87	126	12.6
1:3	-	Moso	6.17	9.20	137	12.9
1:3	-	Moso	5.67	8.87	127	14.6

Appendix D

Example of solution for CG19 is provided here to help the reader understand how the bond, shear, and flexural capacity models were applied as follows:

1. Flexural capacity assuming no bond failure

Cox and Geymayer (1969) reinforced their beams with split culms in two vertical planes with the concave side facing sideways and tied to vertical splints. They provided the exact depth of the reinforcement only for one beam (CG4) as shown in Figure D.1. Since they reported that the culms they used had an average outside diameter of 17 mm and thickness of 2.8 mm, the number of splints used can be estimated and then the depth of the reinforcement can be found.

For CG4 the number of splints can be found using $\frac{A_b}{17\times2.8\times\pi/2} = 6$

$d = h - cover - 3 \times 17 = 171\ mm$

$cover = 30\ mm$

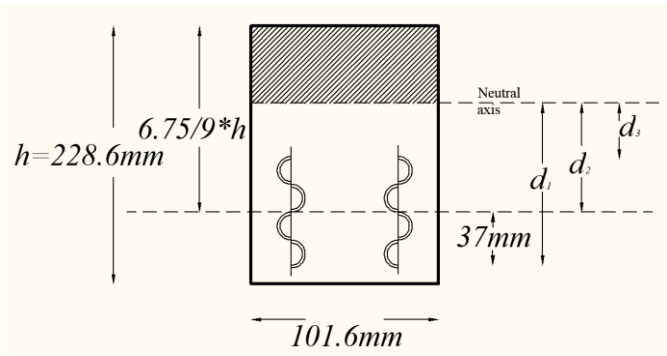

Figure D.1 Section in a typical beam

For beam CG19, the number of splints was found equal to 5.4 making the effective depth of the reinforcement equal to 152 mm.

Determining the balanced section requires knowing the stress at which the reinforcement reaches failure. Cox and Geymayer (1969) reported the tensile strength of their reinforcement at 108.3. However, their distribution of reinforcement would result in the bottom reinforcement failure before the top reinforcement (Figure D.1). The strain is maximal at the bamboo half culm furthest from the neutral axis and when it reaches maximum stress the other bamboo splints achieve stress in proportion to their distance from the neutral axis. Therefore, the average reinforcement stress should be used to calculate strength. The weighted value for the overall behaviour was calculated using three points as shown in Figure D.1 and $\frac{\frac{d_1}{d_1}+\frac{2d_2}{d_1}+\frac{d_3}{d_1}}{4}$. However, to find this averaged stress requires determining the depth of the neutral axis. Therefore, an iterative procedure is used to solve the problem. The first iteration is calculated based on a balanced section.

$$c_b{}^{1st} = \frac{\varepsilon_{cu}}{\varepsilon_{cu} + \varepsilon_{bu}} d = \frac{0.003}{0.003 + \sigma_{bu}/E} d = \frac{0.003}{0.003 + 108.3/18000} d_1 = 66.0\ mm$$

$$\sigma_{b,avg}{}^{1st} = \sigma_{bu} \frac{\frac{d_1}{d_1} + \frac{2d_2}{d_1} + \frac{d_3}{d_1}}{4} = 70.18\ MPa$$

Now the depth of the neutral axis can be estimated by equalising the tension and compression in the section by taking f'_c to be the average prism strength (the purpose here is analysis; not design) as follows:

$$C = \alpha_1 f'_c \beta_1 b c^{2nd} = T = \sigma_{b,avg}{}^{1st} \times A_b$$

$$c^{2nd} = 34.5\ mm$$

After updating the values of $d_1, d_2, and\ d_3$, the averaged tensile strength for the reinforcement in the second iteration can be found

$$\sigma_{b,avg}{}^{2nd} = \sigma_{bu}\frac{\frac{d_1}{d_1}+\frac{2d_2}{d_1}+\frac{d_3}{d_1}}{4} = 77.5\ MPa$$

$$C = \alpha_1 f'_c \beta_1 b c^{3rd} = T = \sigma_{b,avg}{}^{2nd} \times A_b$$

$$c^{3rd} = 38.1\ mm$$

$$\sigma_{b,avg}{}^{3rd} = \sigma_{bu}\frac{\frac{d_1}{d_1}+\frac{2d_2}{d_1}+\frac{d_3}{d_1}}{4} = 76.8\ MPa$$

The difference between the second and third iteration is about 1%. Therefore, the third iteration used to find the flexural strength. The member is under-reinforced because $c < c_b$ and the flexural capacity assuming perfect bond (M_f) can be found as follows:

$$M_f = T\left(d - \frac{\beta_1 c_b}{2}\right) = 76.8 \times 813 \times (152 - 0.85 \times \frac{66}{2}) = 7.8\ Kn.M$$

2. Flexural capacity at bond failure

The longitudinal bond is calculated using the bond test and the specimen's details. Cox and Geymayer (1969) used half culms to reinforce CG19 with 0.808 MPa bond using polyester and sand treatment. The maximum longitudinal bond can be found as follows:

$$\tau_{l,max} = \frac{A_b}{17 \times 2.8} \times 17 \times 2 \times 0.808 = 469\ N/mm$$

Now to calculate the maximum stress that can be achieved in the reinforcement without bond failure.

$$\sigma_{max} = 0.654 \times \tau_{l,max} l_{cr} / A_b$$

Before calculating the cracking moment and the cracked length l_{cr}, the average tensile strength of the concrete (f_t) need to be found. l^{1st} is the first shear span between the

support and the load. The average tensile strength of the concrete (f_t) can be found as follows:

$$f_t = 0.6{f'_c}^{0.5} = 2.84\ MPa$$

$$l_{cr} = l^{1st} - \frac{M_{cr}}{M_f} l^{1st} = 600 - \frac{M_{cr}}{7.8} \times 600$$

$$M_{cr} = \frac{I_g f_t}{h/2} = \frac{bh^3 f_t}{12 \times h/2} = 2.52\ KN.M$$

l_{cr}= 407 mm

$$\sigma_{max} = 0.654 \times 469 \times \frac{407}{882} = 154 \text{ MPa}$$

To calculate the tensile stress at bond failure (σ_τ) the following equation is used:

$$\sigma_\tau = \left(\frac{\rho E_b}{1177}\right)^{1.246} \times \sigma_{max} + \left[1 - \left(\frac{\rho E_b}{1177}\right)^{1.246}\right] \times \sigma_{min} \leq \sigma_{max}$$

σ_{min} was evaluated using the same approach shown in appendix B. Since its value exceeded σ_{bu}, there is no bond failure in the section.

3. Shear capacity

Since Cox and Geymayer (1969) used no stirrups, the shear stress is only resisted by the concrete. The average prism strength is used here because the purpose is to find whether the model conservatively predicts the shear strength. In design, however, the characteristic (or the specified) strength should be used.

$$V = V_c + V_s = 0.4\sqrt{f'_c}bc + 0 = 0.4 \times 22.5^{0.5} \times 101.6 \times c$$

Since shear failure can occur before the concrete reach ultimate strength, c is evaluated using elastic analysis where ρ is the reinforcement area percentage and n is the ratio of reinforcement and the concrete modulus of elasticities (The concrete MOE is evaluated using the formula $E_c = 4700 f'^{0.5}_c$) as following:

$$n = \frac{E_b}{E_c} = \frac{18}{18.96}$$

$$c^e = (\sqrt{2\rho n + (\rho n)^2} - \rho n)d = 41.0\ mm$$

$$V = V_c = 0.4 \times 22.5^{0.5} \times 41 \times 101.6 = 7904\ N$$

The moment corresponding the maximum shear strength (M_v) can be found for a beam loaded at third points by the following:

$$M_v = l^v \times \frac{7904}{1000} = 0.6 \times 7.904 = 4.74\ KN.M$$

Since the moment achieved at shear capacity is the lowest moment, shear is the critical failure mechanism.

Table D.1 provides a summary of the details of the bamboo reinforced beams used in this investigation.

Table D.1 Summary of bamboo reinforced beams details

Beam	A_b	$\tau_{l,max}$	Maximum stress in the reinforcement based on bond	Span (mm)	W (mm)	H (mm)	D (mm)	Prisim compressive strength
CG1	455	63.6	36.6	2000	101.6	228.6	185	25.5
CG2	687	96.1	42.1	2000	101.6	228.6	178	25.5
CG3	1052	147.1	44.8	2000	101.6	228.6	168	25.5
CG4	455	94.4	54.8	2000	101.6	228.6	172	20.0
CG5	687	142.6	60.9	2000	101.6	228.6	159	20.0
CG6	1052	285.1	74.2	2000	101.6	228.6	138	26.0
CG7	455	123.4	66.7	2000	101.6	228.6	172	26.0
CG8	1052	285.1	74.2	2000	101.6	228.6	138	26.0
CG9	455	123.4	72.4	2000	101.6	228.6	172	19.0
CG10	687	186.3	79.4	2000	101.6	228.6	159	19.0
CG11	1052	285.1	72.1	2000	101.6	228.6	138	19.0
CG12	465	-	-	2000	101.6	228.6	172	19.0
CG13	455	123.4	69.4	2000	101.6	228.6	172	22.5
CG14	687	186.3	78.9	2000	101.6	228.6	159	22.5
CG15	1052	285.1	73.3	2000	101.6	228.6	138	22.5
CG16	813	380.1	134.8	2000	101.6	228.6	152	21.0
CG17	813	538.5	191.0	2000	101.6	228.6	152	21.0
CG18	813	538.5	191.8	2000	101.6	228.6	152	22.5
CG19	813	380.1	135.4	2000	101.6	228.6	152	22.5
CG20	813	-	-	2000	101.6	228.6	152	27.5
A2	881	-	-	1800	150	225	175	29.6
A3	893	-	-	1800	150	225	175	23.2
B4	1273	-	-	1800	150	225	175	32.8
B5	1302	-	-	1800	150	225	175	29.6
C6	1362	-	-	1800	150	225	175	24.0
C7	1361	-	-	1800	150	225	175	28.0
D8	1374	-	-	1800	150	225	175	23.2
D9	1367	-	-	1800	150	225	175	24.8
BBR1	1031	-	-	1800	110	165	135	22.7
BBR5	1421	-	-	2000	110	230	200	23.4
BB1	1093	-	-	1800	110	165	135	14.9
BB5	983	-	-	1800	110	230	200	19.3
BBR2	1163	-	-	1800	110	165	135	22.7
BBR6	1382	-	-	2000	110	230	200	23.4
BB2	1050	-	-	1800	110	165	135	14.9
BB6	1032	-	-	2000	110	230	200	19.3
BBR3	1072	-	-	1800	110	165	135	22.7
BBR7	1208	-	-	2000	110	230	200	23.4
BB3	1019	-	-	1800	110	165	135	14.9
BB7	1078	-	-	2000	110	230	200	19.3
BBR4	1045	-	-	1800	110	165	135	22.7
BBR8	1364	-	-	2000	110	230	200	23.4

Beam	A_b	$\tau_{l,max}$	Maximum stress in the reinforcement based on bond	Span (mm)	W (mm)	H (mm)	D (mm)	Prisim compressive strength
BB4	1010	-	-	1800	110	165	135	14.9
BB8	917	-	-	2000	110	230	200	19.3
YA	1200	180	61.5	2000	150	250	207.5	29.8
YB	1200	180	61.5	2000	150	250	207.5	29.8
1.5SCC150	206	-	-	850	110	150	125	21.16
1.5VC150	206	-	-	850	110	150	125	26.12
3.0SCC150	413	-	-	850	110	150	125	21.16
3.0VC150	413	-	-	850	110	150	125	26.12
1.5SCC250	371	-	-	1000	110	250	225	21.16
1.5VC250	371	-	-	1000	110	250	225	26.12
3.0SCC250	743	-	-	1000	110	250	225	21.16
3.0VC250	743	-	-	1000	110	250	225	26.12
1.5SCC275	413	-	-	1800	110	275	250	21.16
1.5VC275	413	-	-	1800	110	275	250	26.12
3.0SCC275	825	-	-	1800	110	275	250	21.16
3.0VC275	825	-	-	1800	110	275	250	26.12
B6	680	433.9	444.0	2400	135	185	145	37.3
B7	743	406.5	378.4	2400	135	185	145	37.3
B8	792	430.5	376.1	2400	135	185	145	37.3
B9	743	418.4	378.3	2400	135	185	145	37.3
B10	388	263.2	445.5	2400	135	185	145	37.3
B11	393	267.4	448.8	2400	135	185	145	37.3
B12	371	259.1	437.3	2400	135	185	145	37.3
B13	478	296.1	414.9	2400	135	185	145	37.3
B14	449	287.0	417.6	2400	135	185	145	37.3
B15	441	286.6	426.4	2400	135	185	145	37.3

Appendix E

An example provided here to help the reader understand how the proposed deflection model is applied. The deflection for beam 8 is estimated at 20000 N total load applied at third points as shown in Figure E.1.

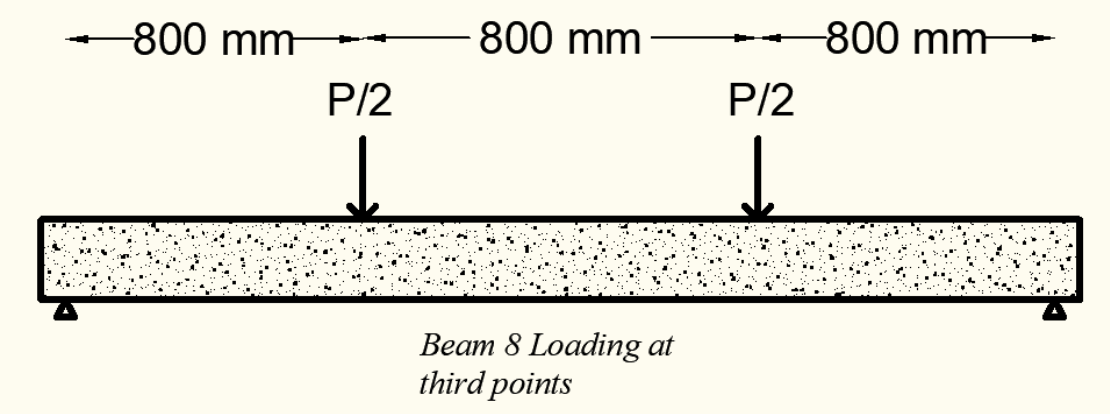

Figure E.1 Plot of the loading arrangement for B8 at third points

$$I_{e,b} = \frac{I_{cr}}{1 - y\left(\frac{M_{cr}}{M_a}\right)^2\left(1 - \frac{I_{cr}}{I_g}\right)} \times \left(\frac{13.9\tau_{l,max}}{E_b A_b}\right)^{0.096} \leq I_e$$

To estimate I_{cr}, we need to estimate c^e where $\rho = \frac{A_b}{bd} = \frac{792}{135\times140} = 0.0419$ and $n = E_b/E_c$.

The MOE is linked to the specified concrete strength where $f'_c = Avg\ prisim - 8.3\ MPa$ for $20.7 < f'_c < 34.5\ MPa$ (American Concrete Institute, 2008).

$E_c = 4700\sqrt{f'_c} = 25400\ MPa$

$$c^e = \left(\sqrt{2\rho n + (\rho n)^2} - \rho n\right) d$$

$$= \left(\sqrt{2 \times 0.0419 \times 0.546 + (0.0419 \times 0.546)^2} - 0.0419 \times 0.546\right)$$

$$\times 140 = 26.9\ mm$$

$$I_{cr} = \frac{bc^{e\,3}}{3} + A_b n(d - c^e)^2 = 6.41 \times 10^6\ mm^4$$

$$I_g = \frac{bh^3}{12} + A_b(n-1)\left(d - \frac{h}{2}\right)^2 = 70.4 \times 10^6\ mm^4$$

$M_{cr} = \frac{2I_g f_t}{h} = 2.47 \times 10^6\ N.mm$ where $f_t = 0.61f'_c$.

$$M_a = \frac{P}{2} \times 800 = 8 \times 10^6 N.mm$$

$$y = 1.72 - 0.72\left(\frac{M_a}{M_{cr}}\right) = 1.50$$

$$I_{e,b} = \frac{6.41 \times 10^6}{1 - 1.5\left(\frac{2.47 \times 10^6}{8 \times 10^6}\right)^2\left(1 - \frac{6.41 \times 10^6}{70.4 \times 10^6}\right)} \times \left(\frac{13.9 \times 430.5}{13.9 \times 792}\right)^{0.096}$$

$$= 6.95 \times 10^6\ mm^4$$

Deflection (Δ) can now be estimated by double integration over the span (L) or by simply using the following formula for beams' mid-span deflection when loaded at third points:

$$\Delta = \frac{23L^2\ M_a}{216E_c I_{e,b}} = \frac{23 \times 2400^2 \times 8 \times 10^6}{216 \times 25400 \times 6.95 \times 10^6} = 27.8\ mm$$

Appendix F

Table F.1 Cracking measurements during the flexural testing of beams

Beam	Deflection (mm)	Total load (KN)	Moment (KN.M)	Crack 1 (mm)	Crack 2 (mm)	Crack 3 (mm)	Crack 4 (mm)	Crack 5 (mm)	Crack 6 (mm)
5	23.95	14.78	5.91	0.46	0.6	0.76	1.29	1	
5	38.04	21.75	8.70	1.11	1.4	2.34	2.28	2.1	
6	63.694	37.14	14.86	4.22	2.34	2.06	3.45		
7	5.67	7.68	3.07	0.64	0.5				
7	8.91	8.78	3.51			0.44	0.54		
7	10.35	9.36	3.75	0.48	0.97				
7	17.3	13.44	5.38			0.84	0.95		
7	24.33	17.41	6.96	1.02	1.72				
7	28.44	19.64	7.86			1.64	1.32		
7	41.21	26.56	10.62	2.39	2.93				
7	46.34	29.35	11.74			2.42	2.06		
8	10.51	10.62	4.25	0.42	0.71				
8	14.24	12.15	4.86			0.67	0.45	0.43	
8	21.65	15.62	6.25	0.51	0.41				
8	27.08	18.55	7.42			0.79	0.98	0.82	
8	36.18	22.74	9.09	1.32	0.84				
8	42.91	25.88	10.35			1.7	1.68	1.61	
9	11.05	10.11	4.04	0.51	0.38	0.46			
9	15.23	12.31	4.92				0.55	0.4	0.54
9	21.11	15.18	6.07	1.09	0.88	1			
9	27.11	17.63	7.05				0.98	1.04	1.1
9	37.53	22.17	8.87	1.94	1.39	1.58			
9	45.45	25.55	10.22				1.2	1.34	1.57
10	10.23	6.98	2.79	0.5	0.64				
10	13.58	7.95	3.18			0.73	0.5		
10	19.68	10.60	4.24	1.01	1.18				
10	23.73	12.37	4.95			1.45	1.27		
10	32.51	15.15	6.06	1.87	2.11				
10	37.4	16.38	6.55			2.66	2.16		
11	9.89	7.73	3.09	0.75	0.79	0.74			
11	14.45	9.56	3.83				0.58	0.44	
11	19.74	11.70	4.68	1.27	1.13				
11	24.98	13.92	5.57				0.96	0.6	
11	31.1	16.77	6.71	1.94	1.61	1.7			
11	37.33	18.79	7.52				1.17	1.1	
12	9.12	6.26	2.50	1.35					
12	12.89	6.74	2.69		1.08	0.8			
12	17.29	7.43	2.97	1.22					
12	21.73	8.84	3.53		1.6	1.43	0.79		
12	30.95	11.71	4.68	2.17					
12	35.59	12.93	5.17		2.74	2.58	2.1		

Beam	Deflection (mm)	Total load (KN)	Moment (KN.M)	Crack 1 (mm)	Crack 2 (mm)	Crack 3 (mm)	Crack 4 (mm)	Crack 5 (mm)	Crack 6 (mm)
12	43.38	14.92	5.97	2.88					
12	49.32	16.65	6.66			3.32	2.63		
13	11.42	7.93	3.17	0.4	0.43	0.4			
13	15.86	9.44	3.78				0.65	0.71	0.56
13	23.47	13.10	5.24	0.77	0.81	0.81			
13	28.73	15.35	6.14				1.44	1.35	1.09
13	39.06	20.66	8.26	1.38	1.22	1.3			
13	45.83	23.71	9.49				2.15	2.43	1.37
14	11.33	10.09	4.04	0.45	0.59				
14	15.93	11.25	4.50				0.98	1.15	
14	19.94	12.73	5.09	0.84	0.82				
14	24.71	14.60	5.84				1.46	1.58	
14	35.94	18.45	7.38	1.2	1.37	1.33			
14	42	20.69	8.28				2.11	2.19	
15	15.4	11.34	4.54	0.36	0.27	0.7			
15	19.9	12.64	5.06				1.35	1.19	
15	24.76	14.61	5.84	0.83	0.69	0.88			
15	31.82	17.14	6.86					1.28	0.56
15	37.84	19.16	7.66	1.43	0.88	1.55			
15	44.33	21.70	8.68					1.81	0.95